Cell Journal (Yakhteh)

Guide for Authors

Aims and Scope: Cell Journal (Yakhteh) is a quarterly English publication of Royan Institute of Iran**.** The aim of the journal is to disseminate information through publishing the most recent scientific research studies on exclusively Cellular, Molecular and other related topics. **Cell J**, has been certified by Ministry of Culture and Islamic Guidance since 1999 and also accredited as a scientific and research journal by HBI (Health and Biomedical Information) Journal Accreditation Commission since 2000. **This journal holds the membership of the Committee on Publication Ethics (COPE).**

1. Types of articles

The articles in the field of Fertility and Sterility can be considered for publications in **Cell J**. These articles are as below:

A. Original articles are scientific reports of the original research studies. The article consists of English Abstract (structured), Introduction, Materials and Methods, Results, Discussion, Conclusion, Acknowledgements, Author's Contributions, and References **(Up to 40).**

B. Review articles are the articles written by well experienced authors and those who have excellence in the related fields. The corresponding author of the review article must be one of the authors of at least three published articles appearing in the references. The review article consists of English Abstract (unstructured), Introduction, Conclusion, Author's Contributions, and References **(Up to 70).**

C. Systematic Reviews

Systematic reviews are a type of literature review that collect and critically analyzes multiple research studies or papers. The Systematic reviews consist of English Abstract (unstructured), Introduction, Materials and Methods, Results, Discussion, Conclusion, Acknowledgements, Author's Contributions, and References **(Up to 70).**

D. Short communications are the articles containing new findings. Submissions should be brief reports of ongoing researches. The short communication consists of English Abstract (unstructured), the body of the manuscript (should not hold heading or subheading), Acknowledgements, Author's Contributions, and References **(Up to 30)**.

E. Case reports are short discussions of a case or case series with unique features not previously described which make an important teaching point or scientific observation. They may describe novel techniques or use equipment, or new information on diseases of importance. It consists of English Abstracts (Unstructured), Introduction, Case Report, Discussion, Acknowledgements, Author's Contributions, and References **(Up to 30)**.

F. Editorial should be written by either the editor in chief or the editorial board.

G. Imaging in biology should focus on a single case with an interesting illustration such as a photograph, histological specimen or investigation. Color images are welcomed. The text should be brief and informative.

H. Letter to the editors are welcome in response to previously published **Cell J** articles, and may also include interesting cases that do not meet the requirement of being truly exceptional, as well as other brief technical or clinical notes of general interest.

I. Debate.

2. Submission Process

It is recommended to see the guidelines for reporting different kinds of manuscripts here. This guide explains how to prepare the manuscript for submission. Before submitting, we suggest authors familiarize themselves with **Cell J** format and content by reading the journal via website (www.celljournal.org). The corresponding author ensures that all authors are included in the author list and agree with its order, and they must be aware of the manuscript submission.

A. Author contributions statements

It is essential for authors to include a statement of responsibility in the manuscript that specifies the contribution of every one of them. This participation must include conception and design of the manuscript, data acquisition or data analysis and interpretation, drafting of the manuscript and/or revising it for critically important intellectual content, revision and final approval of the manuscript and statistical analysis, obtaining funding, administrative, technical, or material support, or supervision. Authors who do not meet the above criteria should be acknowledged in the **Acknowledgements Section.**

B. Cover letter

Each article should be accompanied by a cover letter, signed by all authors specifying the following statement: "The manuscript has been seen and approved by all authors and is not under active consideration for publication. It has neither been accepted for publication nor published in another journal fully or partially (except in abstract form). I hereby assign the copyright of the enclosed manuscript to **Cell J.** Corresponding author must confirm the proof of the manuscript before online publishing. Also, is it needed to suggest three peer reviewers in the field of their manuscript.

C. Manuscript preparation

Authors whose first language is not English encouraged to consult a native English speaker in order to confirm his manuscripts to US or British (not a mixture) English usage and grammar. The manuscript should be prepared in accordance with the "International Committee of Medical Journal Editors (ICMJE)". Please send your manuscript in two formats (word and Pdf). The abstract and text pages should have consecutive line numbers in the left margin beginning with title page and continuing through the last page of the written text. Each abbreviation must be defined in the abstract and text when they are mentioned for the first time. Avoid using abbreviation in title. Please use the

international and standard abbreviations and symbols.

It should be added that an essential step toward the integration and linking of scientific information reported in published literature is using standardized nomenclature in all fields of science and medicine. Species names must be italicized (e.g., *Homo sapiens*) and also the full genus and species written out in full, both in the title of the manuscript and at the first mention of an organism in a paper.

It is necessary to mention that genes, mutations, genotypes, and alleles must be indicated in italics. Please use the recommended name by consulting the appropriate genetic nomenclature database, e.g., HUGO for human genes. In another words; if it is a human gene, you must write all the letters in capital and italic (e.g., *OCT4, c-MYC*). If not, only write the first letter in capital and italic (e.g., *Oct4, c-Myc*). **In addition, protein designations are the same as the gene symbol but are not italicized.**

Of note, Cell J will only consider publishing genetic association study papers that are novel and statistically robust. Authors are advised to adhere to the recommendations outlined in the STREGA statement (http://www.strega-statement.org). The following criteria must be met for all submissions:

1. Hardy-Weinberg Equilibrium (HWE) calculations must be carried out and reported along with the P-values if applicable [see Namipashaki et al. 2015 (Cell J, Vol 17, N 2, Pages: 187-192) for a discussion].

2. Linkage disequilibrium (LD) structure between SNPs (if multiple SNPs are reported) must be presented.

3. Appropriate multiple testing correction (if multiple independent SNPs are reported) must be included.

Submissions that fail to meet the above criteria will be rejected before being sent out for review.

Each of the following manuscript components should begin in the following sequence:

Authors' names and order of them must be carefully considered (full name(s), highest awarded academic degree(s), email(s), and institutional affiliation(s) of all the authors in English. Also, you must send mobile number and full postal address of the corresponding author).

Changes to Authorship such as addition, deletion or rearrangement of author names must be made only before the manuscript has been accepted in the case of approving by the journal editor. In this case, the corresponding author must explain the reason of changing and confirm them (which has been signed by all authors of the manuscript). If the manuscript has already been published in an online issue, an erratum is needed.

Title is providing the full title of the research (do not use abbreviations in title).

Running title is providing a maximum of 7 words (no more than 50 characters).

Abstract must include Background, Materials and Methods, Results, and Conclusion (no more than **300** words).

Keywords, three to five, must be supplied by the authors at the foot of the abstract chosen from the Medical Subject Heading (MeSH). Therefore; they must be specific and relevant to the paper.

The following components should be identified after the abstract:

Introduction: The Introduction should provide a brief background to the subject of the paper, explain the importance of the study, and state a precise study question or purpose.

Materials and Methods: It includes the exact methods or observations of experiments. If an apparatus is used, its manufacturer's name and address should be stipulated in parenthesis. If the method is established, give reference but if the method is new, give enough information so that another author can perform it. If a drug is used, its generic name, dose, and route of administration must be given. Standard units of measurements and chemical symbols of elements do not need to be defined.
Statistical analysis: Type of study and statistical methods should be mentioned and specified by any general computer program used.

Ethical considerations: Please state that informed consent was obtained from all human adult participants and from the parents or legal guardians of minors and include the name of the appropriate institutional review board that approved the project. It is necessary to indicate in the text that the maintenance and care of experimental animals complies with National Institutes of Health guidelines for the humane use of laboratory animals, or those of your Institute or agency.

Clinical trial registration: All of the Clinical Trials performing in Iran must be registered in Iranian Registry of Clinical Trials (www.irct.ir). The clinical trials performed abroad, could be considered for publication if they register in a registration site approved by WHO or www.clinicaltrials.gov. If you are reporting phase II or phase III randomized controlled trials, you must refer to the CONSORT Statement for recommendations to facilitate the complete and transparent reporting of trial findings. Reports that do not conform to the CONSORT guidelines may need to be revised before peer reviewing.

Results: They must be presented in the form of text, tables, and figures. Take care that the text does not repeat data that are presented in tables and/or figures. Only emphasize and summarize the essential features of the main results. Tables and figures must be numbered consecutively as appeared in the text and should be organized in separate pages at the end of article while their location should be mentioned in the main text.

Tables and figures: Tables should have a short descriptive heading above them and also any footnotes. Figure's legend should contain a brief title for the whole figure and continue with a short explanation of each part and also the symbols used (no more than 100 words). All figures must be prepared based on cell journal's guideline in color (no more than **6** Figures and Tables) and also in GIF or JPEG format with 300 dpi resolutions.

Supplementary materials would be published on the online version of the journal. This material is important to the understanding

and interpretation of the report and should not repeat material within the print article. The amount of supplementary material should be limited. Supplementary material should be original and not previously published and will undergo editorial and peer review with the main manuscript. Also, they must be cited in the manuscript text in parentheses, in a similar way as when citing a figure or a table. Provide a legend for each supplementary material submitted.

Discussion: It should emphasize the present findings and the variations or similarities with other researches done by other researchers. The detailed results should not be repeated in the discussion again. It must emphasize the new and important aspects of the study.

Conclusion: It emphasizes the new and important aspects of the study. All conclusions are justified by the results of the study.

Acknowledgements: This part includes a statement thanking those who contributed substantially with work relevant to the study but does not have authorship criteria. It includes those who provided technical help, writing assistance and name of departments that provided only general support. You must mention financial support in the study. Otherwise; write this sentence "There is no financial support in this study".

Conflict of Interest: Any conflict of interest (financial or otherwise) and sources of financial support must be listed in the Acknowledgements. It includes providers of supplies and services from a commercial organization. Any commercial affiliation must be disclosed, regardless of providing the funding or not.

References: The references must be written based on the Vancouver style. Thus the references are cited numerically in the text and listed in the bibliography by the order of their appearance. The titles of journals must be abbreviated according to the style used in the list of Journals Indexed in PubMed. Write surname and initials of all authors when there are six or less. In the case of seven or more authors, the names of first six authors followed by "et al." must be listed. The reference of information must be based on the following order:

Article:

Surname(s) and first letter of name & middle name(s) of author(s). Manuscript title. Journal title (abbr).publication date (year); Volume

(Issue): Page number.

Example: Manicardi GC, Bianchi PG, Pantano S, Azzoni P, Bizzaro D, Bianchi U, et al. Presence of endogenous nicks in DNA of ejaculated human spermatozoa and its relationship to chromomycin A3 accessibility. Biol Reprod. 1995; 52(4): 864-867.

Book:

Surname(s) and first letter of name & middle name(s) of author(s). Book title. Edition. Publication place: publisher name; publication date (year); Page number.

Example: Edelman CL, Mandle CL. Health promotion throughout the life span. 2nd ed.ST Louis: Mosby; 1998; 145-163.

Chapter of book:

Surname(s) and first letter of name & middle name(s) of author(s). Chapter title. In: Surname(s) and first letter of name &middle name(s) of editor(s), editors. Book title. Edition. Publication place: publisher name; publication date (year); Page number.

Example: Phillips SJ, Whisnant JP. Hypertension and stroke. In: Laragh JH, Brenner BM, editors. Hypertension: pathophysiology, diagnosis, and management. 2nd ed. New York: Raven Press; 1995; 465-478.

Abstract book:

Example: Nabavi SM. Stem cell therapy for multiple sclerosis. Cell J. 2013; 5 Suppl 1: Os-13.

Thesis:

Name of author. Thesis title. Degree. City name. University. Publication date (year).

Example: Eftekhari Yazdi P. Comparison of fragment removal and co-culture with Vero cell monolayer's on development of human fragmented embryos. Presented for the Ph.D., Tehran. Tarbiyat Modarres University. 2004.

Internet References

Article:

Surname(s) and first letter of name & middle name(s) of author(s). Manuscript title. Journal title (abbr). Publication date (year); Volume (Issue): Page number. Available from: URL link. (Observation date).

Example: Jahanshahi A, Mirnajafi-Zadeh J, Javan M, Mohammad-Zadeh M, Rohani M. Effect of low-frequency stimulation on adenosineA1 and A2A receptors gene expression in dentate gyrus of perforant path kindled rats. Cell J. 2008; 10 (2): 87-92. Available from: http://www.celljournal.org. (20 Oct 2008).

Book:

Example: Anderson SC, Poulsen KB. Anderson's electronic atlas of hematology.[CD-ROM]. Philadelphia: Lippincott Williams & Wilkins; 2002.

Law:

Example: Embryo donation law. Iran Judicature, Official Gazette of the Islamic Republic of Iran. Available from: http://www.dastour.ir/Brows/?lid=245069.(20 Jul 2013).

D. Proofs are sent by email as PDF files and should be checked and returned within 72 hours of receipt. It is the authors' responsibility to check that all the text and data as contained in the page proofs are correct and suitable for publication. **We are requested to pay particular attention to author's names and affiliations as it is essential that these details be accurate when the article is published.**

E. Pay for publication: Authors do not have to pay any Manuscript Processing Charge or Open Access Publication Fee. **Before publishing author's article, it would be the author's responsibility to pay for the expenses, if the editor feels the level of English used in the manuscript requires editing.**

F. Ethics of scientific publication: Manuscripts that have been published elsewhere with the same intellectual material will refer to duplicate publication. If authors have used their own previously published work or work that is currently under review, as the basis for a submitted manuscript, they are required to cite the previous work and indicate how their submitted manuscript offers novel contributions beyond those of the previous work. Research and publication misconduct is considered a serious breach of ethics. The Journal systematically employs iThenticate, a plagiarism detection and prevention software designed to ensure the originality of written work before publication.

Plagiarism of text from a previously published manuscript by the same or another author is a serious publication offence. Some parts of text may be used, only where the source of the quoted material is clearly acknowledged.

3. General information

A. You can send your article via online submission system which is available at our website: **http://www.celljournal.org.** If the article is not prepared according to the format of **Cell J**, it will be returned to authors.

B. The order of article appearance in the Journal is not demonstrating the scientific characters of the authors.

C. Cell J has authority to accept or reject the articles.

D. The received articles will be evaluated by one epidemiologist. Then associate editor will determine its reviewers. If three reviewers pass their judgments on the article, it will be presented to the editorial board of **Cell J.** If the editorial board has a positive judgment about the article, reviewers' comments will be presented to the corresponding author (the identification of the reviewers will not be revealed). The executive member of journal will contact the corresponding author directly within 7-8 weeks by email. If authors do not receive any reply from journal office after the specified time, they can contact journal office. Executive manager will respond promptly to authors' message.

The Final Checklist

The authors must ensure that before submitting the manuscript for publication, they have to consider the following parts:

1. Title page should contain title, name of the author/coauthors, their academic qualifications, designation & institutions they are affiliated with, mailing address for future correspondence, email address, phone, and fax number.

2. Text of manuscript and References prepared as stated in the "guide for authors" section.

3. Tables should be in a separate page. Figures must be sent in color and also in GIF or JPEG format with 300 dpi resolutions.

4. Covering Letter.

The Editor-in-Chief: Ahmad Hosseini, Ph.D.

Cell Journal (Yakhteh),

P.O. Box: 16635-148, Iran

Tel/Fax: + 98-21-22510895

Emails: Celljournal@royaninstitute.org

info@celljournal.org

Dr. Saeed Kazemi Ashtiani

IN THE NAME OF GOD

Gone But not Forgotten

In the memory of the late Director of Royan Institute, Founder of Stem Cells Research in Iran and Chairman of ***Cell Journal*** *(Yakhteh)*. May he rest in peace.

PUBLISHED & SPONSORED BY:
Publication of Royan Institute (ACECR)

Indexed in:
1. Thomson Reuters (ISI); *Impact Factor: 2.046*
2. PubMed
3. PubMed Central (PMC)
4. National Library Medicine (NLM)
5. Biosis Preview
6. Index Medicus for the Eastern Mediterranean Region (IMEMR)
7. Index Copernicus International
8. Cambridge Scientific Abstract (CSA)
9. EMBASE
10. Scopus
11. Cinahl Database
12. Google Scholar
13. Chemical Abstract Service (CAS)
14. Proquest
15. Directory of Open Access Journals (DOAJ)
16. Open Academic Journals Index (OAJI)
17. Directory of Research Journals Indexing (DRJI)
18. Scientific Information Database (SID)
19. Iranmedex
20. Regional Information Center for Sciences and Technology (RICeST)
21. Islamic World Science Citation Center (ISC)
22. Magiran
23. Science Library Index

ACECR

Editorial Office Address (Dr. Ahmad Hosseini):
Royan Institute, P.O.Box: 16635-148,
Tehran, Iran
Tel & Fax: (+9821)22510895
Website: www.celljournal.org
Emails: info@celljournal.org
celljournal@royaninstitute.org

Printing Company:
Jurband Ghaemprint Co.
NO. 5, Jalil khoob alley, Niroo Havaei Street,
Tehran, Iran

Cell Journal (Yakhteh), Vol 22, No 1, April-June (Spring) 2020, Serial Number: 85, Pages: 1-132

CONTENTS

Original Articles

Ethics, Legal, Social, Counseling Article

Case Report

• **Front page of Cell Journal$_{(Yakhteh)}$: Figure 2, Page: 100**

Original Article

The Effect of Radiation Emitted by Cell Phone on The Gelatinolytic Activity of Matrix Metalloproteinase-2 and -9 of Mouse Pre-Antral Follicles during *In Vitro* Culture

Fariba Azimipour, M.Sc.[1], Saeed Zavareh, Ph.D.[1, 2*], Taghi Lashkarbolouki, Ph.D.[1, 2]

1. School of Biology, Damghan University, Damghan, Iran
2. Institute of Biological Sciences, Damghan University, Damghan, Iran

Corresponding Address: P.O.Box: 3671641167, School of Biology, Damghan University, Damghan, Iran
Email: zavareh.s@du.ac.ir

Received: 17/November/2018, Accepted: 20/February/2019

Abstract

Objective: The unfavorable effects of electromagnetic radiation (EMR) emitted by the cell phone on reproduction health are controversial. Metalloproteinases play a vital role in ovarian follicle development. This study was designed to investigate the effects of exposure to the cell phone on the gelatinolytic activity of *in vitro* cultured mouse pre-antral follicle.

Materials and Methods: In this experimental study, pre-antral follicles were isolated from ovaries of immature mice (n=16) and cultured with or without exposure to the cell phone in talking mode for 60 minutes. The gelatinolytic activity was evaluated through the zymography method, as well as the gene expression of matrix metalloproteinases (MMPs) namely *MMP-2* and -9 and tissue inhibitors of metalloproteinases (TIMPs) namely, *TIMP-1* and -2 by the real-time polymerase chain reaction (PCR) method. Also, in parallel, the development of pre-antral follicles was assessed.

Results: The maturation parameters of the cell phone-exposed pre-antral follicles were significantly lower compared with the control group ($P<0.05$). The gelatinolytic activity was significantly decreased in the cell phone-exposed pre-antral follicles compared with the control group ($P<0.05$). The relative mRNA expression of the *MMP-2* gene was significantly ($P<0.05$) increased in the cell phone-exposed pre-antral follicles whereas the expression rate of the *MMP-9* gene was considerably ($P<0.05$) reduced when compared with the control group. Conversely, the relative expression of the *TIMP-1* was markedly ($P<0.05$) increased in the cell phone-exposed pre-antral follicles while the expression of the *TIMP-2* was ($P<0.05$) significantly diminished in comparison with the control group.

Conclusion: Exposure to the cell phone alters the growth and maturation rate of murine ovarian follicle through the changing in the expression of the *MMP-2* and *-9* genes, as well as the gelatinolytic activity.

Keywords: Cell Phone, Gelatinase, Ovarian Follicles, Radiation

Cell Journal(Yakhteh), Vol 22, No 1, April-June (Spring) 2020, Pages: 1-8

Citation: **Azimipour F, Zavareh S, Lashkarbolouki T. The effect of radiation emitted by cell phone on the gelatinolytic activity of matrix metalloproteinase-2 and -9 of mouse pre-antral follicles during in vitro culture. Cell J. 2020; 22(1): 1-8. doi: 10.22074/cellj.2020.6548.**

Introduction

Nowadays, the usage of mobile phone and exposure to its electromagnetic radiation (EMR) raised some concerns about the dangerous effects on health. EMR affect the cells and organs through thermal and non-thermal mechanisms (1). However, there are some controversial reports, indicating EMR may increase the free radical production, mitochondrial dysfunction, heat shock proteins, apoptosis, and DNA damage (2-5). Besides, EMR may target the plasma membrane and disturb various enzymatic activities and the receptor functions (6). It is also shown that exposure to EMR increases the NADH oxidase activity of the plasma membrane which subsequently changes the activation of matrix metalloproteinase (MMPs) (7) b¿. The interaction of MMPs and tissue inhibitor of metalloproteinases (TIMPs) regulates the extracellular matrix (ECM) remodeling in many physiological processes (8) which could subsequently maintain cellular homeostasis (9).

The development of ovarian follicle is accompanied by immense cellular turnover and remodeling of ovarian tissue. The essential part of this remodeling is the modification of the ECM constituents and provision of the structural support for the follicle formation and maturation. Among MMPs, gelatinase A (MMP-2) and B (MMP-9) play significant roles in follicle development and ovulation (10). Furthermore, TIMP-1 and TIMP-2 bind to MMP-9 and MMP-2, respectively, and regulate their activations. TIMP-1 regulates the rate of proteolysis within the granulosa cells through the ovulatory process. By contrast, TIMP-2, in the thecal cells, promotes the proteolysis process via the localization of pro-gelatinase A on the cell surface which may be used as biomarkers of the normal follicle development (10, 11).

There is limited information about the effect of EMR, emitted from the cell phone on female reproductive tissue. However, no report is available about the effect of EMR on different aspects of folliculogenesis. The present study aimed to investigate whether exposure to cell phone radiation affects the gelatinolytic activity of MMP-2 and MMP-9, as well as the mRNA expression of *MMP-2* and

-9 along with their inhibitors *TIMP-1* and *-2* in mouse pre-antral follicles during *in vitro* culture.

Materials and Methods

Reagents

Unless otherwise specified, all reagents and chemical were obtained from Sigma Aldrich (UK). Water used for the preparation of the culture medium was purified by the Milli-Q system.

Animals

In this experimental study, all experiments were conducted using female Naval Medical Research Institute (NMRI) mice which were obtained from the Razi Vaccine and Serum Research Institute. Female offspring with age range of 14-16 days was used for all experiments. Animal experiments were performed based on the ethical principles of the Declaration of Helsinki as revised in Tokyo 2004 and was approved by the Ethics Committee of Damghan University. The animals were kept and bred under the standard conditions with a circadian rhythm of 12 hours of light/12 hours of darkness and at an ambient temperature of 22 ± 2˚C with adequate food and water.

Experimental design

Mice were sacrificed through cervical dislocation, and their ovarian tissues were aseptically removed using scissors and forceps and put into 100 µl of the alpha-minimum essential medium (α-MEM) containing 25 mM HEPES, 70 µg/mL streptomycin, 100 IU/ml penicillin, 10% fetal bovine serum (FBS, Gibco, UK), and 2.2 g/l sodium bicarbonate. The pre-antral follicles with the diameter of 140-160 µm were mechanically isolated and selected based on the previously described criteria (intact with at least two to three granulosa cell layers and a centrally located oocyte) (12). The pre-antral follicles were randomly grouped into control (n=240) and cell phone-exposed groups (n=240). Exposed pre-antral follicles were kept in close to the commercial cell phone (Sony Ericsson K800) in the talking mode at 5 cm distance for 60 minutes. After that, the cell phone was removed, and pre-antral follicles were cultured for up to 12 days. The same protocols were applied for the control group except they were not exposed to the cell phone radiation. Some of the cultured pre-antral follicles were used for the assessment of the growth rate, and the remained cells were used for the molecular analyses.

In vitro maturation of pre-antral follicles

Cultivation of pre-antral follicles were performed in which the cells were covered with embryo-tested mineral oil in 25-µL drops of the α-MEM medium containing 100 mU/ml recombinant human follicle stimulating hormone (rhFSH), 5% FBS, 20 ng/ml recombinant epidermal growth factor (rEGF), and 1% insulin-transferring-selenium (ITS), in an incubator at 37˚C in 5% CO_2 for 10 days, as previously described (12). The fresh maturation medium was replaced every two days. During the cultivation period, pre-antral follicles diameter was calculated under an inverted microscope at ×400 magnification by calculating the average of two perpendicular diameters with a pre-calibrated ocular micrometer in 2nd and 4th days of the culture period. The antrum cavity was defined as every lucent area between the granulosa cells and degenerated pre-antral follicles were detected with the darkness surrounding the cumulus cells and follicles without oocytes or denuded oocytes. In the 10th days of the cultivation period, ovulation was induced by the addition of 1.5 IU/ml human chorionic gonadotropin (hCG, Choriomon, IBSA, Switzerland). After 24-48 hours, oocytes were categorized based on the maturation status [germinal vesicle (GV), germinal vesicle breakdown (GVBD), and metaphase II oocytes (MII)].

Gelatin zymography

The gelatinase activity of MMP-2 and -9 was assessed using zymography on polyacrylamide gels containing gelatin, as described previously with some modifications (13). An equal amount of the culture medium was harvested during the culture period (days of 2, 4, 6, 8, 10, and 12). The medium was mixed and homogenized with an equal volume of non-reducing buffer containing 2% sodium dodecyl sulfate (SDS); Tris-HCl, (125 mM, pH=6.8), glycerol (10% v/v), and bromophenol blue (0.001% v/v). Afterward, the mixture was electrophoresed in 10% SDS page supplemented with gelatin (0.05% w/v). The gel was then washed twice in Triton X-100 (2%) for 20 minutes at room temperature and incubated in digestion buffer supplemented with Tris-HCl (50 mM), $CaCl_2$ (2.5 mM,) NaCl (200 mM), and $ZnCl_2$ (1 mM) in pH=7.4 at 37˚C overnight. Finally, the gel was stained with 0.5% Coomassie Brilliant Blue (Bio-Rad, Canada), and the destaining process was performed in glacial acetic acid (10% v/v) and methanol (30% v/v) dissolved in H_2O for five hours at room temperate. The gelatinase activity was characterized based on unstained bands, and the quantification was performed using a computerized image analysis program (Image J) which, in turn, quantified the intensity and surface of unstained bands.

Reverse transcription-quantitative polymerase chain reaction

Real-time polymerase chain reaction (PCR) was performed to evaluate the relative mRNA expressions of the *MMP-2* and *-9* genes, as well as the *TIMP-1* and *-2* genes in pre-antral follicles during the cultivation period

at the initial time and days of 6 and 12.

RNA extraction

Total RNA extraction was carried out, as described previously on the basis of using acid guanidinium thiocyanate-phenol-chloroform (14, 15). In brief, pre-antral follicles (n=15 for each replicate) were placed in a 500 µl solution consisted of guanidine thiocyanate (4 M), sodium citrate (25 mM, pH=7.0), N-lauroylsarcosine (0.5% w/v), and 2-Mercaptoethanol (3.6 µl), and it was homogenized at room temperature. The homogenate was mixed with sodium acetate (50 µl), phenol (500 µl), and chloroform (200 µl) at 4˚C and centrifuged at 12,000 g at 4˚C for 20 minutes. Cold isopropanol was added to the resultant supernatants and placed at -20˚C for 20 minutes and centrifuged (12,000 g) for 20 minutes. The resultant pellet was rinsed with 75% ethanol and diluted in RNase-free water. DNase was used to remove any DNA contamination. The RNA quality and quantity were evaluated using a density ratio of 28S to 18S rRNA bands and the measurement of its absorbance at A260 nm with the spectrophotometer. An A260 of 1.0 was considered 40 µg/mL of the extracted RNA. Also, the ratio of A260 to A280 nm was measured, and the samples with an A260 to A280 ratio of 1.8 to 2.0 were acceptable and used for reverse transcription.

Real-time polymerase chain reaction

The gene-specific primer sets were designed to span introns or cross exon/exon junctions, using the Oligo software version 7 (DBA Oligo, Inc., USA). All primer pairs were specific for the corresponding mRNAs and were tested for no amplification of genomic DNA. The contamination of genomic DNA in the sample was evaluated by performing a control reaction possessing no reverse transcribed RNA. Real-time PCR primer sequences and the thermal conditions are shown in Table 1, based on the MIQE (Minimum Information for Publication of Quantitative Real-Time RT-PCR Experiments) (16). The process of reverse transcription was accomplished by the synthesis of the first-strand cDNA using 1 µg of total RNA, Random Hexamer Primers (Fermentas, USA), Ribolock RNase Inhibitor, dNTP mix (Fermentas, USA), RevertAid M-Mul V reverse transcriptase (Fermentas, USA), 5X reaction buffer (Fermentas, USA), and RNase-free water according to the manufacturer's instructions. The reaction was run in a thermocycler (Eppendorf, USA) with a thermal profile of 65˚C for 5 minutes and one cycle of 42˚C for 1 hour. Real-time RT-qPCR was performed on an ABI Step One machine (Applied Biosystems, ABI, USA) using the RT-PCR Kit (SYBR Green, Amplicon, Denmark).

The thermal profile was adjusted to denaturation at 95˚C for 15 minutes, followed by 40 cycles of denaturation at 95˚C for 60 seconds, annealing and extension at 60˚C for 60 seconds. The relative expression of the target genes was normalized against *GAPDH*. The $2^{-\Delta\Delta Ct}$ method was used to assess the relative gene expression for each gene. The specificity of real-time PCR was assessed through the melting curve analysis.

Statistical analysis

The SPSS software (version 24, Chicago, IL, USA) was used for the analysis of the data. Experiments were repeated at least four times. All data were expressed as the mean ± SD. Independent samples t test was applied for the determination of differences between groups. A $P<0.05$ was considered statistically significant.

Table 1: Oligonucleotide primer sequences for real time polymerase chain reaction

Gene	Primer sequence (5´-3´)	Length (bp)	Product size
MMP9	F: CTGTCCAGACCAAGGGTACAG	20	247
	R: CATAGTGGGAGGTGCTGTCG	21	
MMP2	F: GAGAAGGACAAGTGGTCCGC	20	265
	R: CTGTTGTAGGAGGTGCCCTG	20	
TIMP1	F: GGGTGTGCACAGTGTTTCCC	22	202
	R: TTCAGTTTTTCCTGGGGGAAGG	20	
TIMP2	F: GCAGACGTAGTGATCAGAGCC	20	281
	R: TCCCAGGGCACAATGAAGTC	21	
GAPDH	F: TGACATCAAGAAGGTGGTGAAGC	22	203
	R: CCCTGTTGCTGTAGCCGTATTC	23	

Results

Effect of electromagnetic radiation on the maturation parameters of pre-antral follicles

Pre-antral follicles were monitored and evaluated morphologically every other day during the *in vitro* culture period. On the first day of the culture, there was no significant difference between the diameter of pre-antral follicles in the control group and the cell phone-exposed group (P>0.05, Fig.1). Whereas, at day 2 and 4 of the culture period, the diameter of the cultured pre-antral follicle in the cell phone-exposed group was significantly decreased compared with the control group (P<0.05, Fig.1).

Additionally, the results revealed that the survival rate of follicles was significantly higher in the control group compared with the cell phone-exposed group (P<0.05, Fig.2). The antral formation rate of cultured pre-antral follicles in the cell phone-exposed group was significantly decreased compared with the control group (P<0.05, Fig.2). After 12 days of the culture period and induction of ovulation, the rate of ovulation in pre-antral follicle exposed to the cell phone was statistically decreased in comparison with the control group (P<0.05, Fig.2). Also, the rates of MII and GVBD oocytes were significantly lower in the cell phone-exposed group than the control group (P<0.05, Fig.3), while, the GV rate of the cell phone-exposed group was increased significantly compared with the control group (P<0.05, Fig.3).

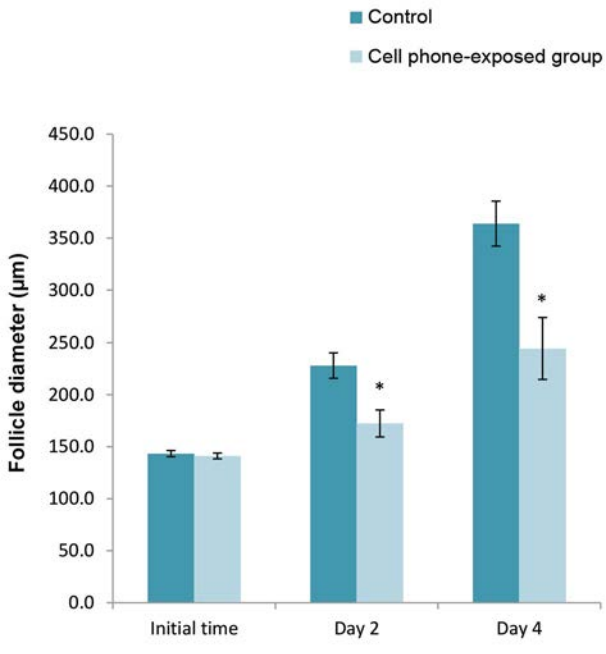

Fig.1: The diameter of pre-antral follicles at the initial time, days 2 and 4 of culturing. Data are expressed as the mean ± SD. *; Indicates a significant difference compared with the control (P<0.05).

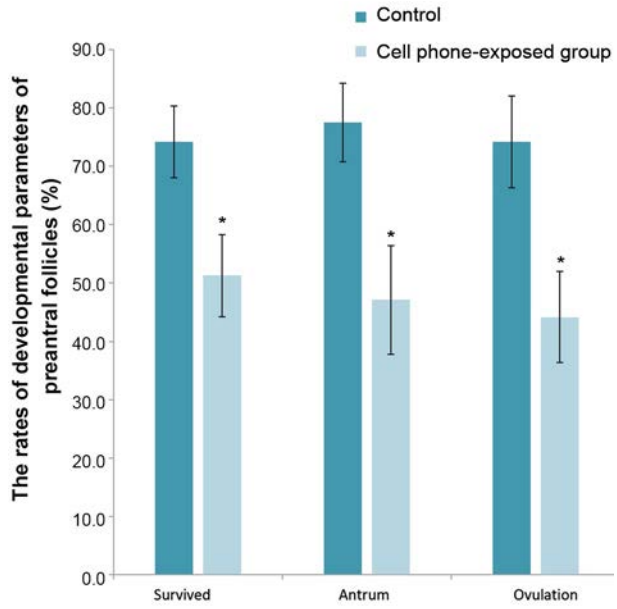

Fig.2: The rate of developmental parameters of pre-antral follicles. Data are expressed as the mean ± SD. *; Indicates a significant difference compared with the control (P<0.05).

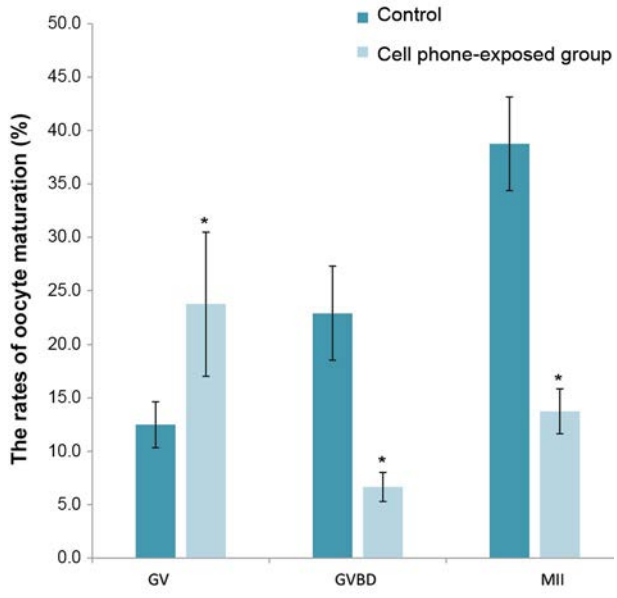

Fig.3: The rates of the oocyte maturation. Data are expressed as the mean ± SD. *; Indicates a significant difference compared with control (P<0.05), GV; Germinal vesicle, GVBD; Germinal vesicle breakdown, and MII; Metaphase II oocytes.

Effect of electromagnetic radiation on the gelatinase activity of pre-antral follicles

The gelatinase activity of both MMP-2 and -9 was evaluated in cultured pre-antral follicles through gelatin zymography. The gelatin activity of both MMP-2 and -9 was decreased during the culture period in pre-antral follicles of the control and cell phone-exposed groups, whereas in the 12th days of the culture period, the activity was increased upon the addition of human chorion gonadotrophin (hCG) to the culture medium (P<0.05, Fig.4). Additionally, as shown in Figure 5, it was

found that the *MMP-2* activity in the pre-antral follicles of the cell phone-exposed group was significantly lower in comparison with the control group (P<0.05). Similar conditions were found for the MMP-9 activity, and thus, the activity of MMP-9 in pre-antral follicles of the cell phone-exposed was significantly lower than the control group during culture period (P< 0.05, Fig.4).

Effect of electromagnetic radiation on the gene expression of *MMP-2* and *-9*, as well as *TIMP-1* and *-2*

The expression of the *MMP-2* and *-9*, as well as the *TIMP-1* and *-2* genes are shown in Figure 5. The results show that the gene expression of the *MMP-2* gene was significantly increased in pre-antral follicles of the cell phone-exposed group compared with the control group during *in vitro* culture (P<0.05). Inversely, the gene expression of the *MMP-9* gene was markedly decreased in pre-antral follicles of the cell phone-exposed group compared with the control group during *in vitro* culture. Furthermore, the gene expression of *TIMP-1* showed a significant increase in pre-antral follicles of the cell phone-exposed group compared with the corresponding values in the control group during culture period (P<0.05), whereas, the *TIMP-2* expression in pre-antral follicles of the cell phone-exposed group was significantly reduced during the culture period compared with the control groups (P<0.05).

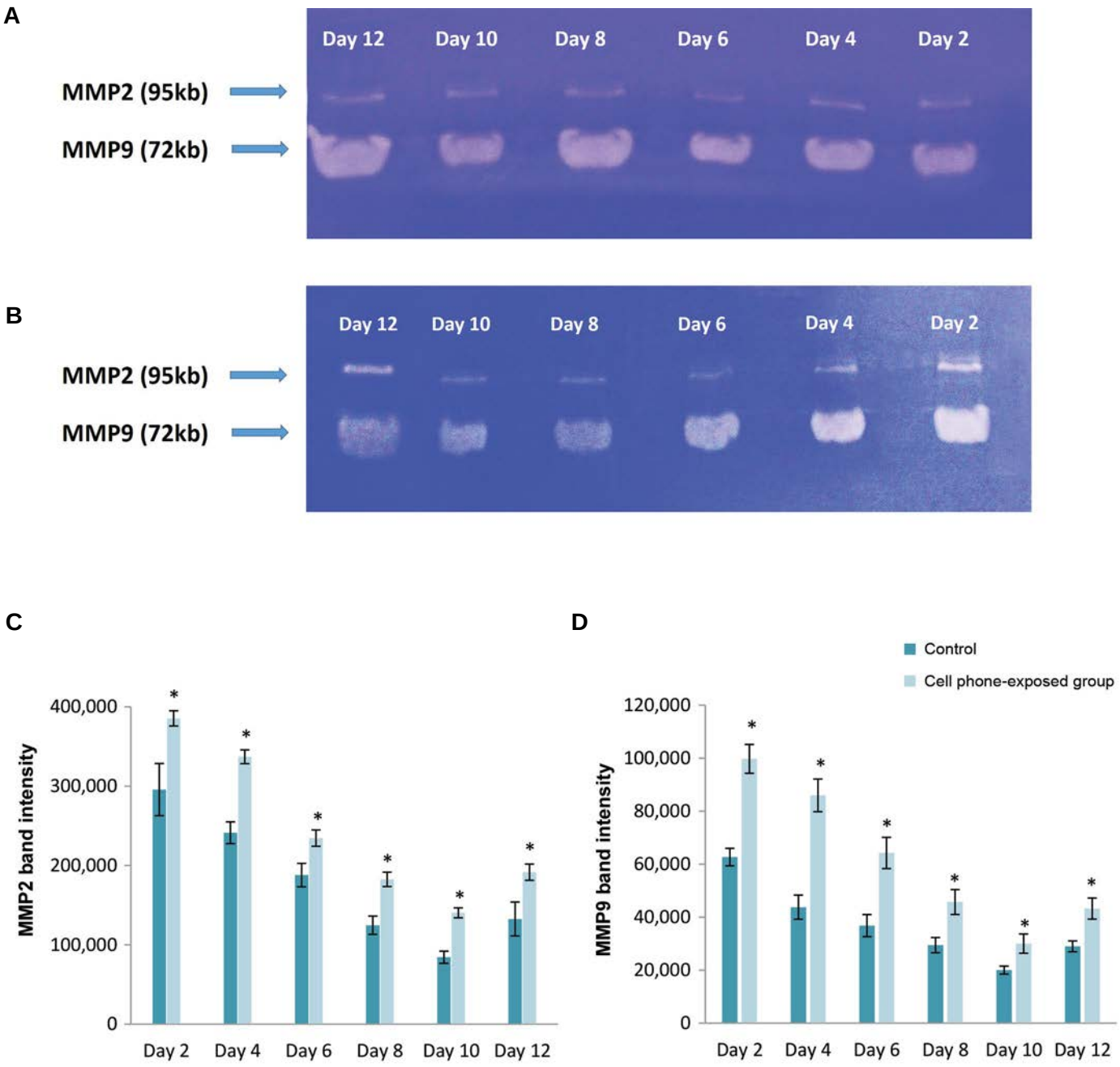

Fig.4: MMP-2 and-9 activities of *in vitro* cultured pre-antral follicles with or without cell phone exposure determined by zymography as described in the text. **A.** Gelatin zymography of the control group, **B.** Gelatin zymography of cell phone-exposed group, **C.** Relative optical density of MMP-2, and **D.** Relative optical density of MMP-9. Data are expressed as the mean ± SD. *; Indicates significant a difference compared with control (P<0.05).

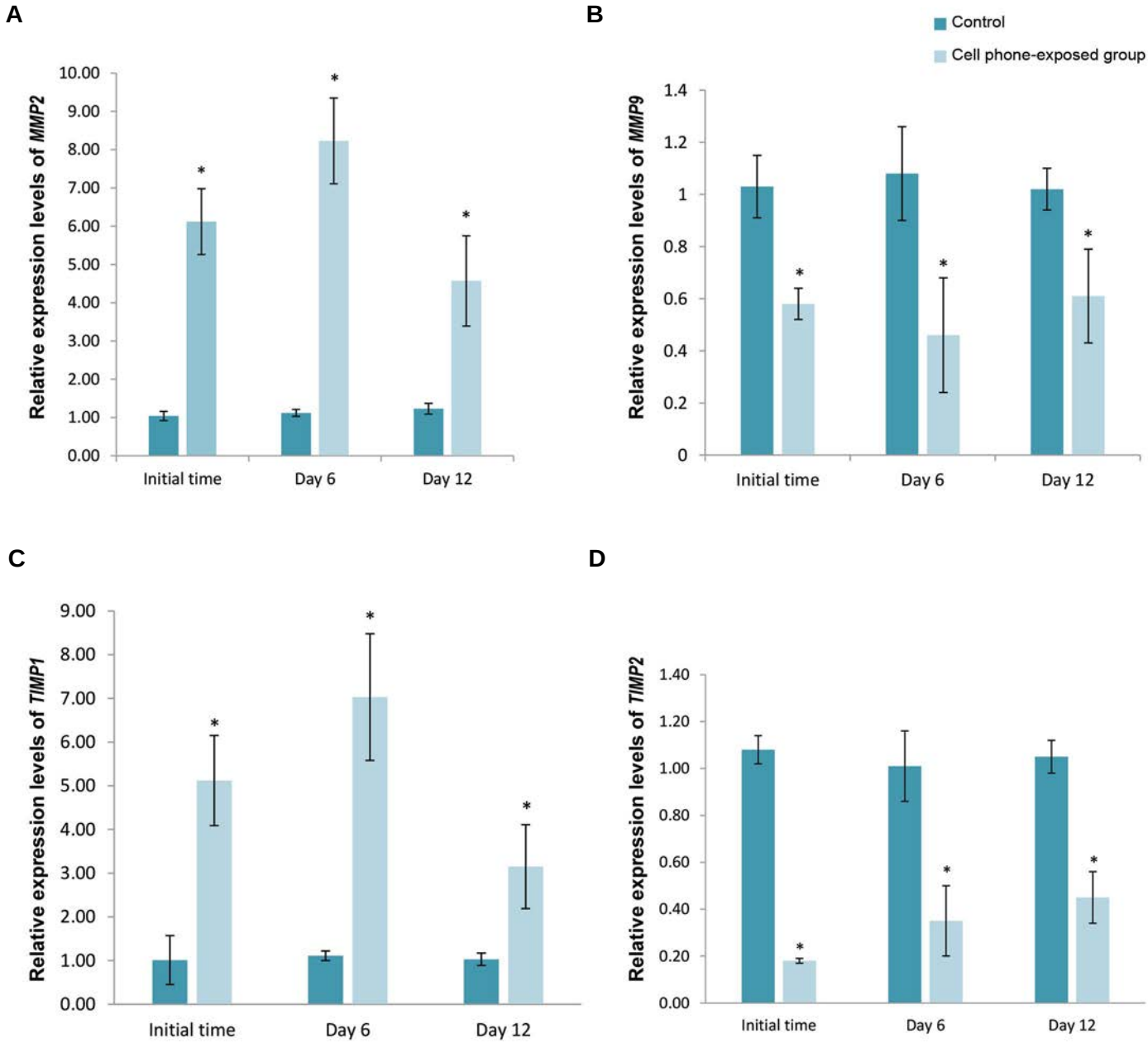

Fig.5: The mRNA expression levels of *MMP-2, MMP-9, TIMP-1*, and *TIMP-2* in pre-antral follicles during *in vitro* culture with or without (control) cell phone exposure. **A.** The mRNA expression levels of *MMP-2*, **B.** The mRNA expression levels of *MMP-9,* **C.** The mRNA expression levels of *TIMP1*, and **D.** The mRNA expression levels of *TIMP2*. Data are expressed as the mean ± SD. *; Indicate a significant difference compared with control (P<0.05).

Discussion

To date, there are a lot of conflicting reports on the adverse effects of mobile phones on human health. These contradictory reports have been attributed to the difference in exposure time, variable frequencies, types of tissue, etc. (17-19). The mechanism of EMR, emitted by mobile phone has not been well understood. Nevertheless, it has been shown that EMR cause changes in the cell membrane integrity and activity of different enzymes (17, 18).

In the present study, we showed that exposure to the mobile phone could damage the development of pre-antral follicles, decrease the number of ovulated oocytes, and increase the number of arrested GV oocytes. The regulated interplay between different cells, hormones, and various macromolecules are necessary for ovarian folliculogenesis (20). In the present study, incomplete oocyte nuclear maturation, at least to some extent, could be explained by EMR-induced apoptosis in somatic cells of pre-antral follicles, particularly the granulosa cells and reduced proliferation as shown previously (21). Although the precise mechanism of EMR is unknown, another explanation might be the inhibition of cell growth, protein misfolding, and detrimental effects on cellular signaling (18). Furthermore, in the *in vivo* condition, mobile phone radiation could induce oxidative stress (OS) via an increase in the reactive oxygen species (ROS) production and a reduction in antioxidant activity of enzymes (22).

In this regard, Mao et al. (23) showed that EMR increases ROS production and decreases the activity of enzymatic antioxidants. Also, Agarwal et al. (24) indicated that cell phone radiation increases the generation of ROS and MDA, while, it can decrease the antioxidant enzyme activity in semen plasma, suggesting that exposure to the cell phone has unfavorable effects on the fertility potential of spermatozoa (6). It has also been shown that cell phone radiation induces apoptosis and OS and it is capable of reducing the total antioxidants capacity in follicular granulosa cells (25) which, in turn, led to the reduced number of ovarian pre-antral follicles (26).

It has been also demonstrated that the induction of oxidative stress, as a result of the mobile phone exposure may damage the ECM (27). The results of the current study showed that exposure to mobile phone altered the MMPs activity and their inhibitors in cultured pre-antral follicles. The activity of MMPs in the ovarian cycle is pre-requisite for the ECM remodeling and follicular development. MMPs and TIMPs have critical roles in this process such as theca cells differentiation, proliferation/differentiation of the granulosa cells, antrum formation, the formation of the basement membrane, and ovulation (28). Thus, any change in the normal ECM remodeling and the activity of MMPs could interrupt the process of folliculogenesis. This confirms the results of the present study because the gelatinase activity and expression levels of *MMP-2* and *-9* and their tissue inhibitors changed upon exposure to cell phone radiation which, in turn, led to the impairment in the development of cultured pre-antral follicles.

Gelatinase (MMP-2 and 9) plays a crucial role in the membrane destruction in the ovulation process, which separates granulosa and thecal layers and it can hydrolyze collagen fibers. Hence, dysregulation in gelatinase function leads to the perturbations in the folliculogenesis and ovulation processes. This finding is in agreement with our results, wherein changes in the expression of *MMP-2* and *-9*, as well as the gelatinase activity significantly reduced the follicle development and ovulation. It has been suggested that MMPs play a significant role in follicular atresia; so, increased activities of *MMP-2* and *-9* in the follicular fluid is associated with the induction of atresia (10). These observations confirm the findings of the present study indicating that a higher degeneration rate in cell phone-exposed pre-antral follicles is associated with increased activity of both *MMP-2* and *-9*. The results of the present study demonstrated that the activity of *MMP-2* and *-9* is increased in day 12 of the cultivation period followed by the administration of hCG in both cell phone-exposed and untreated pre-antral follicles. This change appears to be due to the addition of hCG to the culture medium that causes the induction of ovulation. In the *in vivo* condition, ovulation is a dynamic process initiated with the luteinizing hormone (LH) surge, follicular wall rupture, and oocyte release (20). Pre-ovulatory LH surge is an endocrine signal for ovulation. The LH surge along with biochemical events involved in the synthesis and secretion of prostaglandins, progesterone, cytokines, and growth factors is closely related to proteolytic enzyme activities, such as MMPs. Evidence suggests that proteolytic destruction of the ECM at the apex of pre-ovulatory follicles before the ovulation process is the essential stage in the onset of the LH surge, whereas the synthesis of MMP inhibitors inhibit the ovulation process (29). Therefore, LH-induced proteolysis activity plays a vital role in the ovulation process. In this regard, the activity of gelatinase A in ovine follicles is increased followed by the LH surge (30). This situation was also found in rats (31), which was similar to the results of our study. The supplemented culture medium with hCG increased the activities of MMP-2 and -9. The activity of TIMPs was also concomitantly regulated with MMPs. Therefore, the activity of TIMPs is negatively correlated with the activity of MMPs.

Conclusion

The results of the present study demonstrated that cell phone radiation changes gelatinolytic activity linked to MMP-2 and -9, leading to decreased developmental competence of mouse pre-antral follicles. However, in the *in vivo* condition, ovarian tissue and cell phone are separated by several tissue layers; therefore, further studies are warranted to mimic the *in vivo* condition for cultured pre-antral follicles to evaluate the effect of cell phone radiation.

Acknowledgements

This study was funded by Damghan University, Damghan, Iran. The authors are grateful to Mr. Abutaleb Koosha for providing technical assistance. There is no conflict of interest in this study.

Authors' Contributions

F.A.; Performed experiments and collected data. S.Z.; Developed the concept and designed experiments, analyzed data and wrote the manuscript. T.L.; Gave technical support and conceptual advice. All authors performed the edition and approved the final version of this manuscript.

References

1. Wyde ME, Horn TL, Capstick MH, Ladbury JM, Koepke G, Wilson PF, et al. Effect of cell phone radiofrequency radiation on body temperature in rodents: Pilot studies of the National Toxicology Program's reverberation chamber exposure system. Bioelectromagnetics. 2018; 39(3): 190-199.
2. Ayata A, Mollaoglu H, Yilmaz HR, Akturk O, Ozguner F, Altuntas I. Oxidative stress-mediated skin damage in an experimental mobile phone model can be prevented by melatonin. J Dermatol. 2004; 31(11): 878-883.
3. Oyewopo AO, Olaniyi SK, Oyewopo CI, Jimoh AT. Radiofrequency electromagnetic radiation from cell phone causes defective testicular function in male Wistar rats. Andrologia. 2017; 49(10).
4. Rao VS, Titushkin IA, Moros EG, Pickard WF, Thatte HS, Cho MR. Nonthermal effects of radiofrequency-field exposure on calcium dynamics in stem cell-derived neuronal cells: elucidation of calcium pathways. Radiat Res. 2008; 169(3): 319-329.
5. Remondini D, Nylund R, Reivinen J, Poulletier de Gannes F, Veyret B, Lagroye I, et al. Gene expression changes in human cells after exposure to mobile phone microwaves. Proteomics. 2006; 6(17):

4745-4754.
6. Desai NR, Kesari KK, Agarwal A. Pathophysiology of cell phone radiation: oxidative stress and carcinogenesis with focus on male reproductive system. Reprod Biol Endocrinol. 2009; 7: 114.
7. Friedman J, Kraus S, Hauptman Y, Schiff Y, Seger R. Mechanism of short-term ERK activation by electromagnetic fields at mobile phone frequencies. Biochem J. 2007; 405(3): 559-568.
8. Sternlicht MD, Werb Z. How matrix metalloproteinases regulate cell behavior. Annu Rev Cell Dev Biol. 2001; 17: 463-516.
9. Singh D, Srivastava SK, Chaudhuri TK, Upadhyay G. Multifaceted role of matrix metalloproteinases (MMPs). Front Mol Biosci. 2015; 2 :19.
10. Goldman S, Shalev E. MMPS and TIMPS in ovarian physiology and pathophysiology. Front Biosci. 2004; 9: 2474-2483.
11. Baka S, Zourla K, Kouskouni E, Makrakis E, Demeridou S, Tzanakaki D, et al. Matrix metalloproteinases 2 and 9 and their tissue inhibitors in the follicular fluid of patients with polycystic ovaries undergoing in vitro fertilisation. In Vivo. 2010; 24(3): 293-296.
12. Hatami S, Zavareh S, Salehnia M, Lashkarbolouki T, Ghorbanian MT, Karimi I. The impact of alpha lipoic acid on developmental competence of mouse vitrified pre-antral follicles in comparison to those isolated from vitrified ovaries. Iran J Reprod Med. 2014; 12(1): 57-64.
13. Toth M, Fridman R. Assessment of gelatinases (MMP-2 and MMP-9 by gelatin zymography. Methods Mol Med. 2001; 57: 163-174.
14. Chomczynski P, Sacchi N. Single-step method of RNA isolation by acid guanidinium thiocyanate-phenol-chloroform extraction. Anal Biochem. 1987; 162(1): 156-159.
15. Bagheri F, Goudarzi I, Lashkarbolouki T, Salmani ME. Melatonin prevents oxidative damage induced by maternal ethanol administration and reduces homocysteine in the cerebellum of rat pups. Behav Brain Res. 2015; 287: 215-225.
16. Bustin SA, Benes V, Garson JA, Hellemans J, Huggett J, Kubista M, et al. The MIQE guidelines: minimum information for publication of quantitative real-time PCR experiments. Clin Chem. 2009; 55(4): 611-622.
17. Merhi ZO. Challenging cell phone impact on reproduction: a review. J Assist Reprod Genet. 2012; 29(4): 293-297.
18. Gye MC, Park CJ. Effect of electromagnetic field exposure on the reproductive system. Clin Exp Reprod Med. 2012; 39(1): 1-9.
19. Suzuki S, Okutsu M, Suganuma R, Komiya H, Nakatani-Enomoto S, Kobayashi S, et al. Influence of radiofrequency–electromagnetic waves from 3rd-generation cellular phones on fertilization and embryo development in mice. Bioelectromagnetics. 2017; 38(6): 466-473.
20. Baerwald AR, Adams GP, Pierson RA. Ovarian antral folliculogenesis during the human menstrual cycle: a review. Hum Reprod Update. 2012; 18(1): 73-91.
21. Cecconi S, Gualtieri G, Di Bartolomeo A, Troiani G, Cifone MG, Canipari R. Evaluation of the effects of extremely low frequency electromagnetic fields on mammalian follicle development. Hum Reprod. 2000; 15(11): 2319-2325.
22. Balci M, Devrim E, Durak I. Effects of mobile phones on oxidant/antioxidant balance in cornea and lens of rats. Curr Eye Res. 2007; 32(1): 21-25.
23. Mao XW, Mekonnen T, Kennedy AR, Gridley DS. Differential expression of oxidative stress and extracellular matrix remodeling genes in low- or high-dose-rate photon-irradiated skin. Radiat Res. 2011; 176(2): 187-197.
24. Agarwal A, Desai NR, Makker K, Varghese A, Mouradi R, Sabanegh E, et al. Effects of radiofrequency electromagnetic waves (RF-EMW) from cellular phones on human ejaculated semen: an in vitro pilot study. Fertil Steril. 2009; 92(4): 1318-1325.
25. Merhi ZO. Challenging cell phone impact on reproduction: a review. J Assist Reprod Genet. 2012; 29(4): 293-297.
26. Bakacak M, Bostancı MS, Attar R, Yıldırım ÖK, Yıldırım G, Bakacak Z, et al. The effects of electromagnetic fields on the number of ovarian primordial follicles: an experimental study. Kaohsiung J Med Sci. 2015; 31(6): 287-292.
27. Alge-Priglinger CS, Kreutzer T, Obholzer K, Wolf A, Mempel M, Kernt M, et al. Oxidative Stress-Mediated Induction of MMP-1 and MMP-3 in Human RPE Cells. Invest Ophthalmol Vis Sci. 2009; 50(11): 5495-5503.
28. Smith MF, Ricke WA, Bakke LJ, Dow MP, Smith GW. Ovarian tissue remodeling: role of matrix metalloproteinases and their inhibitors. Mol Cell Endocrinol. 2002; 191(1): 45-56.
29. Gottsch ML, Van Kirk EA, Murdoch WJ. Role of matrix metalloproteinase 2 in the ovulatory folliculo-luteal transition of ewes. Reproduction. 2002; 124(3): 347-352.
30. Gottsch ML, Van Kirk EA, Murdoch WJ. Tumour necrosis factor alpha up-regulates matrix metalloproteinase-2 activity in periovulatory ovine follicles: metamorphic and endocrine implications. Reprod Fertil Dev. 2000; 12(1-2): 75-80.
31. Robker RL, Russell DL, Espey LL, Lydon JP, O'Malley BW, Richards JS. Progesterone-regulated genes in the ovulation process: ADAMTS-1 and cathepsin L proteases. Proc Natl Acad Sci USA. 2000; 97(9): 4689-4694.

Original Article

The Effect of Melatonin on Mitochondrial Function and Autophagy in *In Vitro* Matured Oocytes of Aged Mice

Zahraa Nasheed Hamad Almohammed, M.D., Ph.D.[1, 2], Fatemeh Moghani-Ghoroghi, Ph.D.[3], Iraj Ragerdi-Kashani, Ph.D.[3], Rouhollah Fathi, Ph.D.[4], Leila Sadat Tahaei, M.Sc.[4], Mohamad Naji, Ph.D.[5], Parichehr Pasbakhsh, Ph.D.[3]*

1. Department of Anatomy, School of Medicine, Tehran University of Medical Sciences, International Campus, Tehran, Iran
2. Department of Gynecology, Alshatra Hospital, Thiqar Health Office, Health Ministry of Iraq
3. Department of Anatomy, School of Medicine, Tehran University of Medical Science, Tehran, Iran
4. Department of Embryology, Reproductive Biomedicine Research Center, Royan Institute for Reproductive Biomedicine, ACECR, Tehran, Iran
5. Urology and Nephrology Research Center, Shahid Beheshti University of Medical Sciences, Tehran, Iran

Corresponding Address: P.O.Box: 14155-6447, Department of Anatomy, School of Medicine, Tehran University of Medical Sciences, Tehran, Iran
Email: pasbakhsh@hotmail.com

Received: 17/August/2018, Accepted: 26/December/2018

Abstract

Objective: This study examined the *in vitro* effect of melatonin on the protein synthesis of mitochondria, as well as autophagy in matured oocytes of aged mice.

Materials and Methods: In this experimental study, germinal vesicles (GV) oocytes were collected from aged (with the age of six-months-old) and young mice (with age range of 6-8 weeks old) and then cultured in the *in vitro* culture medium (IVM) for 24 hours to each metaphase II (MII) oocytes and then supplemented with melatonin at a concentration of 10 μM. The culture medium of MII oocytes was devoid of melatonin. Afterward, the expression of the SIRT-1 and LC3 was assessed by immunocytochemistry. ATP-dependent luciferin-luciferase bioluminescence assay was employed for the measurement of the ATP contents. Intracellular reactive oxygen specious (ROS) was detected by DCFH-DA, and the total antioxidant capacity (TAC) level was determined by TAC assay.

Results: The expression of SIRT-1 and LC3, as well as the measurement of the ATP content, was significantly increased in oocytes treated with melatonin compared with the oocytes receiving no treatment. Moreover, TAC was considerably higher in melatonin-treated oocytes than oocytes receiving no treatment. On the other hand, the level of ROS was significantly decreased in oocytes treated with melatonin in comparison with the untreated oocytes. The results indicated that melatonin considerably improved the development of oocytes as well.

Conclusion: According to the data, melatonin increased mitochondrial function and autophagy via an increase in the expression of SIRT1 and LC3, as well as the ATP contents while it decreased the levels of ROS and increased TAC in oocytes derived from aged mice.

Keywords: Aged Mice, Autophagy, Melatonin, Mitochondria

Cell Journal(Yakhteh), Vol 22, No 1, April-June (Spring) 2020, Pages: 9-16

Citation: **Nasheed Hamad Almohammed Z, Moghani-Ghoroghi F, Ragerdi-Kashani I, Fathi R, Tahaei LS, Naji M, Pasbakhsh P. The effect of melatonin on mitochondrial function and autophagy in in vitro matured oocytes of aged mice. Cell J. 2020; 22(1): 9-16. doi: 10.22074/cellj.2020.6302.**

Introduction

Age-related infertility is one of the significant concerns of female individuals (1). In 1975, only 5% of pregnant women were over 30 years old, whereas this percentage was increased up to 26% in 2010 (2). Although aging influences all features of female reproduction, most studies have focused on oocytes (3). Several lines of evidence demonstrated that aging alters both the quality and quantity of oocytes (4). The precise mechanism underlying age-induced reproductive disorders is still unclear; however, hormonal imbalance, reduced ovarian follicle reserve, increased oocyte aneuploidy, and mitochondrial dysfunction in oocytes are involved in this scenario (5). The main factor restricting the success rate of assisted reproduction techniques (ART) is oocyte competence. Although ART has been widely improved, the percentage of successful pregnancies and alive babies are 47.7 % for women younger than 35 and less than 30% for women older than 35 (6, 7).

Several studies have reported a relationship between oocyte quality and mitochondrial function (8). The number of mitochondria and their function are regulated through the organized processes of mitochondrial biosynthesis and degradation in the cells (9). SIRT is a vital mitochondrial deacetylase, which regulates biological mitochondrial functions (10).

SIRT-1 is associated with the regulation of autophagy and mitochondrial function in the cells which can increase the ATP contents within the cells and protect them from excessive reactive oxygen species (ROS) and oxidative damage (11).

Autophagy is a cellular process that leads to the degradation and removal of damaged organelles mediated by lysosomes. It has been implicated that melatonin improves mitochondrial functions (12).

LC3 is a protein marker, located on the membrane of the autophagosome (9). Mitochondrial functions in oocytes can be affected by excessive ROS. So, the ROS concentration should be counterbalanced by the activity of antioxidant agents (13).

Melatonin (N-acetyl-5 methoxytryptamine) has been

introduced as a free radical scavenger and could be indirectly considered an antioxidant molecule (14). Hence, the use of melatonin for the decrease of age-related mitochondrial oxidative stress in oocytes could be a point of view. Since aging is associated with low oocyte competence and infertility, the current study was designed to evaluate whether melatonin can improve the quality of aged oocytes thereby increasing the mitochondrial number and protein synthesis, as well as the ATP contents of aged murine oocytes during *in vitro* culture medium (IVM). Our results provide influential perceptions into the mechanisms of aging and mitochondrial regulation in oocytes.

Materials and Methods

All chemicals in this experimental study were purchased from Sigma (St Louis, MO, USA) except for fetal calf serum (FCS) which was obtained from Invitrogen (Carlsbad, CA, USA). Human chorionic gonadotropin (hCG) and follitropin alfa (Gonal-F) were procured from Organon (Oss, Netherlands).

Animal procedures

NMRI mice (purchased from the Pasteur Institute of Iran) were housed in an air-conditioned room under a 12 hours light: 12 hours dark cycle (7 AM to 7 PM) and temperature 20-25˚C with free access to food and water. All animal experiments were carried out according to the guidelines of the Iranian Council for Use and Care of Animals and approved by the Animal Research Ethical Committee of Tehran University of Medical Sciences (Ethical Committee code: IR. TUMS.VCR. REC.1397.4954).

Experimental groups

All experiments were carried out in two main groups as follows; the first group consisted of young mice with age range of 6-8 weeks (15-17) and the second group included old mice with the age of six months (18). Female NMRI mice received an intraperitoneal injection of 5 IU pregnant mare serum gonadotropin (PMSG). Then mice were sacrificed by cervical dislocation 48 hours after the injection of PMSG and ovaries were collected and transferred to a petri dish containing the α-MEM culture medium supplemented with 5% fetal bovine serum (FBS) and a mixture of antibiotics (penicillin, streptomycin). Oocytes at the germinal vesicle (GV) stage were mechanically isolated from ovaries and collected under a stereomicroscope (Nikon SMZ- 2T, Japan).

In vitro maturation of germinal vesicle oocyte

The *in vitro* maturation medium consisted of the α-Minimum Essential Medium (α-MEM, Sigma, USA) supplemented with 5 mg/ml streptomycin, 6 mg/ml penicillin, 5% fetal calf serum (FCS, Invitrogen, USA), 100 mIU/ml recombinant human follicle stimulating hormone (rhFSH), and 7.5 IU/ml human chorionic gonadotropin (hCG, Sigma, USA) . The GV stage oocytes (n=6-8) were cultured with 0 or 10 µM melatonin (19) at 37˚C, 5% CO_2 and 95% humidity in a 20-µl drop of the IVM medium for 24 hours in both old and young groups. After 24 hours of the culture period, the maturity of the oocytes in the above groups was assessed under an inverted microscope (Labamed, USA). Oocytes which reached to the MII stage were selected for further experiments.

Detection of SIRT1 and LC3 by fluorescence immunostaining

After 24 hours of the culture period in the IVM medium with 0 or 10 µM melatonin, five MII stage oocytes were randomly chosen from each young and old groups and then the immunofluorescence experiments were performed (20). After removal of zona pellucida by Tyrod's acid solution (Sigma-Aldrich, USA), oocytes were fixed and permeabilized with 4% paraformaldehyde with 0.1% Triton X-100 in phosphate-buffered saline (PBS, Sigma, USA) for 20 minutes at room temperature, then washed with 0.3% Triton X-100 in PBS for 5 minutes. Afterward, oocytes were blocked in a 10% bovine serum albumin (BSA, Sigma, USA)/PBS drop for 30 minutes. Finally, they were incubated with a primary antibody containing anti-LC3 and anti-Sirt1 [rabbit polyclonal, 1:100 (Abcam, USA)] in 2% BSA/PBS at 4˚C overnight. In the next day, oocytes were washed three times in 2% BSA/PBS and incubated with fluorescein-conjugated goat anti-rabbit IgG (1:200; Abcam, USA) as a secondary antibody for at 37˚C for 40 minutes. After three times washing by PBS, oocytes were mounted on glass slides using an anti-fade reagent containing 6-Diamidino-2-phenylindole (DAPI, Sigma-Aldrich, USA). The expression of SIRT1 and LC3 was evaluated using a fluorescence microscope (Labamed, USA) at 488-excitation wavelengths. The images of individual oocytes in each group were captured by a digital camera (DeltaPix, Denmark). The fluorescence intensity of each marker was quantified using the Image J (1.48. version) software (National Institutes of Health, Bethesda).

ATP quantification

The measurement of the ATP content of oocytes was carried out using the luminescence (Berthold LB 9501 illuminometer) generated in an ATP-dependent luciferin-luciferase bioluminescence assay. A commercial ATP assay kit (ATP bioluminescence assay kit HS II Roche) was used following the procedure defined by the manufacturer's recommendations. A total of 35-50 MII stage oocytes from each group was mixed with 50 ml of lysis solution and vortexed for one minute on ice for the lysis process. Then, the mixture was centrifuged at 12,000 g at 4˚C for 10 minutes, and the supernatant was applied for further assessments. A six-point standard curve (0-5 pmol) was deliberated in each series of an assay. The standard curves were generated, and the ATP content

was calculated using the formula derived from the linear regression of the standard curve.

Determination of Intracellular reactive oxygen species

To quantify of ROS levels, 40-50 MII stage oocytes from each group were incubated with 2 μM of 2',7'-dichlorofluorescein diacetate (DCFH-DA, Sigma, USA) at 37˚C for 30 minutes in the αMEM medium in a dark place (21). After 3 times washing with αMEM, oocytes were analyzed under a fluorescence microscope (Olympus BX51, Japan) equipped with UV filters (450-490 nm (excitation) and 520 nm (emission) filters. The fluorescence intensity of oocytes was assessed by the ImageJ (1.48. version) software (National Institutes of Health, Bethesda).

Measurement of total antioxidant capacity content

Oocytes at the GV stage were cultured in the IVM culture medium for 24 hours. After 24 hours, 50 μL of the culture medium from each group was collected for the measurement of the TAC content. A commercial kit (Zell Bio GmbH, Germany) was used for the quantitative assay of TAC by the oxidation-reduction colorimetric assay. All of the procedures were performed according to the manufacturer's instruction. Then, the TAC concentration (mM) in samples was calculated based on the standard curve drawn using the standard optic density absorbance against the standard concentration. TAC concentration was determined in the range of 0.125-2 mM.

Statistical analysis

All experiments were performed in triplicate, and the data were expressed as the mean ± standard deviation (SD). The statistical analysis was carried out using one-way analysis of variance (ANOVA) followed by Tukey's post hoc tests using the SPSS 16 version. The $P<0.05$ was considered statistically significant.

Results

Effect of Melatonin on SIRT-1 expression

The immunostaining analysis was performed to evaluate the effects of melatonin on the expression of SIRT-1 in oocytes. The results of immunostaining following the treatment with melatonin showed that 10 μM melatonin upregulated the SIRT-1 expression in the aged MII oocyte+melatonin group versus the aged MII oocyte group (42.2 ± 0.99% vs. 11.9 ± 0.54% respectively, $P<0.01$). Moreover, a higher expression of SIRT-1 was observed in the young MII oocyte+melatonin group compared with the young MII oocyte group (54.4 ± 1.65% vs. 42.8 ± 3.34, respectively, $P<0.05$). As shown in Figure 1, there was no significant difference between the aged MII oocyte+melatonin group and young MII oocyte group (42.2 ± 0.99% vs. 42.8 ± 3.34%, respectively, $P=0.84$).

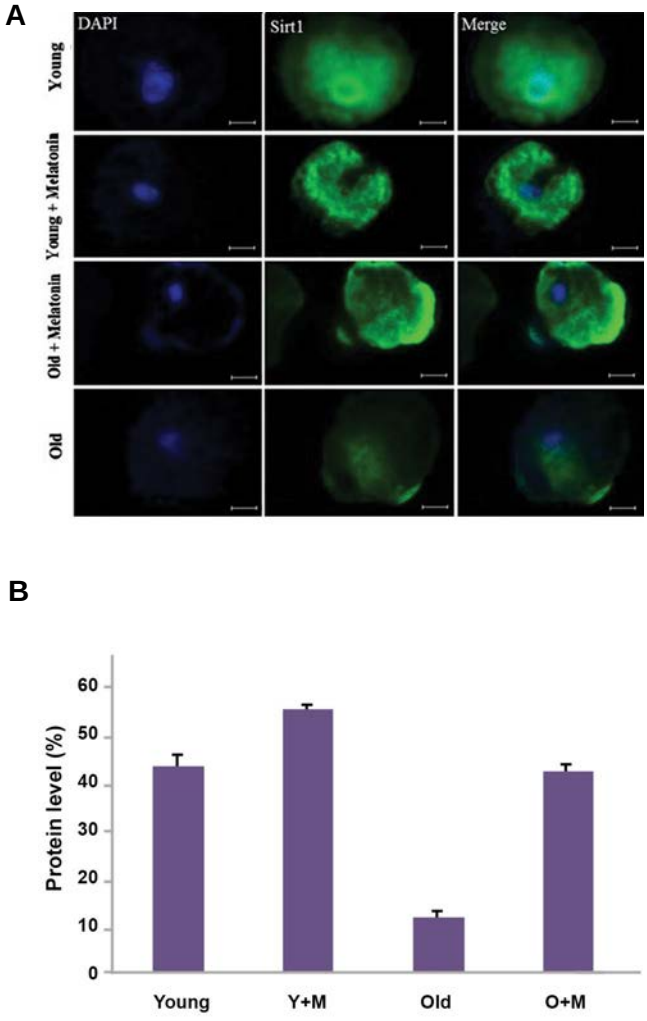

Fig.1: The expression of SIRT-1 at the MII stage of *in vitro* matured oocytes, isolated from young and aged mice was evaluated using immunofluorescence staining. **A.** The micrograph represents the intensity of the SIRT-1 expression among the young MII oocyte, young MII oocyte+melatonin, aged MII oocyte+melatonin, and aged MII oocyte groups. The nuclei were stained by DAPI. The secondary antibody was conjugated with FITC and **B.** The expression of SIRT-1 in the aged MII oocyte+melatonin group was significantly higher than the aged MII oocyte ($P<0.01$). Accordingly, the SIRT-1 expression was elevated in the young MII oocyte+melatonin group compared with the young MII oocyte group ($P<0.05$) (magnification × 400, scale bars: 20 μm). Y+M; Young MII oocyte+melatonin and O+M; Aged MII oocyte+melatonin.

Effect of melatonin on autophagy in oocytes

We examined the expression of the LC3 protein (the marker of autophagosomes) in oocytes by the immunostaining method to assess the effect of melatonin on autophagy.

The expression of the LC3 protein in oocytes has been shown in Figure 2. The results indicated that LC3 was significantly upregulated in the aged oocyte+melatonin group versus the aged oocyte group (24.1 ± 0.37% vs. 11.05 ± 1.25%, respectively, $P<0.01$). Also, significantly higher expression of the LC3 protein was observed in young oocyte+melatonin group versus the young MII oocyte group (42.06 ± 0.26% vs. 24.81 ± 0.7%, respectively, $P<0.01$). As depicted in Figure 2, our data showed that there was no significant difference between the aged MII oocyte+melatonin group and young MII oocyte group (24.1 ± 0.37% vs. 24.81 ± 0.7%, respectively, $P=0.36$).

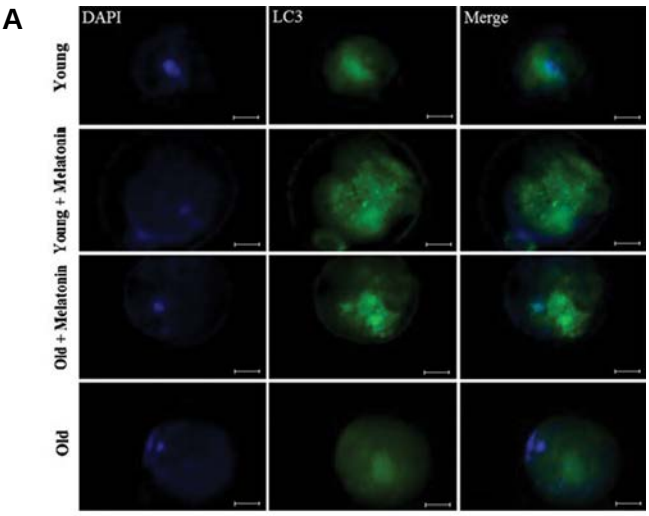

Fig.2: The expression of the LC3 protein in *in vitro* matured MII oocytes, isolated from aged and young mice was determined by the Immunofluorescence staining. **A.** The micrograph represents a significant difference in intensity of the LC3 expression between the young MII oocyte, young MII oocyte+melatonin, aged MII oocyte+melatonin, and aged MII oocyte groups. The nuclei were stained by DAPI. The secondary antibody was conjugated with FITC (magnification ×400, scale bars: 20 µm) and **B.** Significantly higher levels of LC3 were found in the aged MII oocyte+melatonin compared with the aged MII oocyte groups (P<0.01). The expression of the LC3 was significantly higher in the young MII oocyte+melatonin than the young MII oocyte groups (P<0.01). Y+M; Young MII oocyte+melatonin and O+M; Aged MII oocyte+melatonin.

Effect of Melatonin on the ATP content of *in vitro* matured oocytes

The effect of melatonin on the ATP content of in-vitro matured oocytes was assessed by ATP-dependent luciferin-luciferase bioluminescence assay. The levels of ATP were compared among different groups in Figure 3. The data showed that the ATP levels were significantly increased in the aged MII oocyte+melatonin group in comparison with the aged MII oocyte group (2.7 ± 0.1 vs. 1.9 ± 0.07 pmol, respectively, P<0.001).

Moreover, the ATP contents of the young MII oocyte+melatonin group were significantly higher than the young MII oocyte group (3.5 ± 0.1 vs. 3.1 ± 0.1 pmol, P<0.05). As indicated in Figure 3, there was a significant difference between the aged MII oocyte+melatonin and young MII oocyte group as well (2.7 ± 0.1 vs. 3.1 ± 0.1 pmol, respectively, P<0.01).

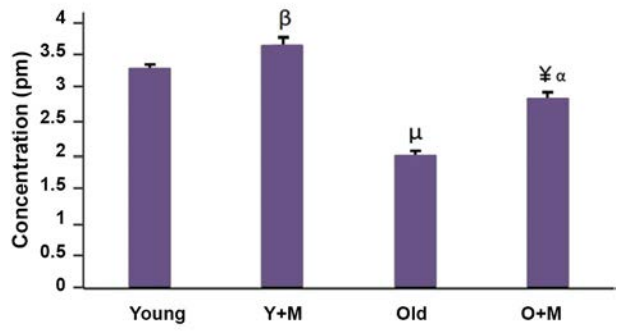

Fig.3: The levels of the ATP contents of *in vitro* matured MII oocytes in all experimental groups, namely aged MII oocyte, young MII oocyte, aged MII oocyte+10 µM melatonin, and young MII oocyte+10 µM melatonin. Each group consisted of 35-50 MII oocytes. The obtained data were represented as mean ± SD. ¥; P<0.001 vs. aged group, β; P<0.05 vs. young group, α; P<0.01 vs. young group, µ; P< 0.001 vs. young group, Y+M; Young+melatonin, and O+M; Aged+melatonin.

Melatonin increased total antioxidant capacity in culture media of *in vitro* matured oocytes

TAC was measured in culture media of *in vitro* matured oocytes to monitor the efficacy of melatonin in antioxidant capacity of oocytes. The results of TAC levels in different groups are shown in Figure 4. As demonstrated in Figure 4, the level of TAC was increased in the aged MII oocyte+melatonin group in comparison with the aged MII oocyte group (0.35 ± 0.06 vs. 0.11 ± 0.05 mM), but there was no significant difference between them (P=0.07). The TAC level was also significantly higher in the young MII oocyte+melatonin group compared with the young group (0.79 ± 0.14 vs. 0.51 ± 0.00, respectively, P<0.05). Moreover, the results demonstrated that there was no significant difference between the aged MII oocyte+melatonin and young MII oocyte group (P=0.31).

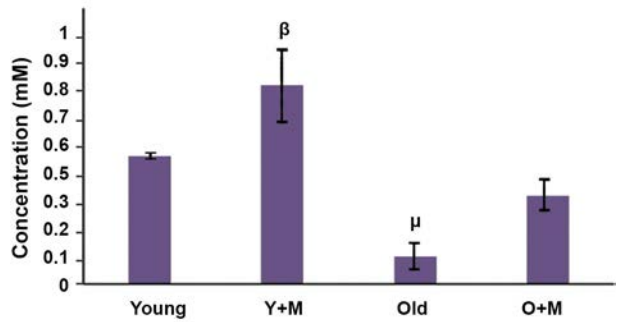

Fig.4: The total antioxidant capacity (TAC) of MII stage *in vitro* matured mouse oocytes in four groups: old and young or old and young supplemented by 10 µM melatonin. 50 µL of culture media of each group were used for TAC content measurement. The data was represented based on mean ± SD. Although TAC level increased in aged MII oocyte+melatonin in comparison to the aged MII oocyte group, (0.35 ± 0.06 vs. 0.11 ± 0.05 mM) but there is no significant difference between them (P=0.07). The result shows that there is no significant difference between aged MII oocyte+melatonin and Young groups as well (P=0.31). It also shows a significant difference between young MII oocyte+melatonin vs. young MII oocyte group. µ; P<0.01, β; P<0.05, Y+M; Young MII oocyte+melatonin, and O+M; Aged MII oocyte+melatonin.

Melatonin decreased the reactive oxygen species level in *in vitro* matured MII oocytes

The rate of oxidative stress in oocytes was evaluated by the measurement of intracellular ROS using DCFH-DA. The levels of ROS in different groups are illustrated in Figures 5 and 6. The increased production of ROS was markedly reversed upon the treatment with melatonin. The results show that the fluorescence intensity of stained oocytes with DCFH-DA in the aged MII oocyte+melatonin group was significantly lower than the aged MII oocyte group (47 ± 3.09 vs. 79 ± 6.18, respectively, P<0.05). Although the ROS level was decreased in the young MII oocyte+melatonin compared with the young MII oocyte group, the difference was not statistically significant (4 ± 0.81 vs. 17 ± 3.09, respectively, P=0.71). Moreover, there was no significant difference between the aged MII oocyte+melatonin and young MII oocyte groups (P=0.10).

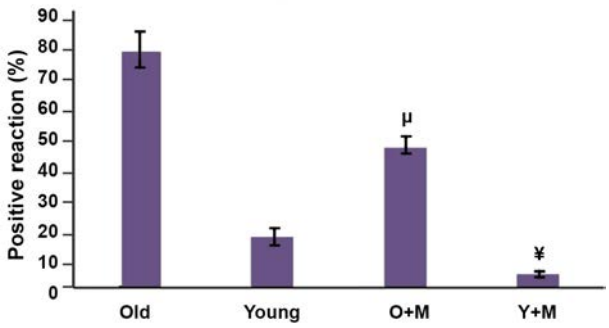

Fig.5: Intracellular reactive oxygen specious (ROS) levels of MII *in vitro* matured oocytes were measured by immunofluorescence dye (DCFH-DA) in all experimental groups, namely aged MII oocyte, young MII oocyte, aged MII oocyte+10 µM melatonin, and young MII oocyte+10 µM melatonin and they were quantified by the ImageJ software. Each group consisted of 40-50 MII oocytes. The results were expressed as mean ± SD. The different symbols represent a significant difference between the two experimental groups. Although the ROS level was decreased in young MII oocyte+melatonin group compared with the young MII oocyte group, the difference was not statistically significant (4 ± 0.81 vs. 17 ± 3.09, P=0.71). The results also showed that there was no significant difference between the aged MII oocytes+melatonin and young MII oocytes groups (P=0.10). ¥; P< 0.05 vs. aged group, µ; P<0.001 vs. young group, Y+M; Young+melatonin, and O+M; Aged+melatonin.

Melatonin improved the development of *in vitro* matured oocytes

A total of 680 oocytes at the GV stage were used for *in vitro* maturation. Meiotic competency of oocytes among the different groups was determined after 24 hours of the *in vitro* maturation process. Percentage of MII oocytes in the aged MII oocyte+melatonin group was 80.12%, which was significantly higher than the aged MII oocyte group (63.63%, P<0.001). There was a significant difference between the young MII oocyte+melatonin and young MII oocyte groups (92.34 and 70.17% respectively, P<0.0001). The results also showed that there was a significant difference between the aged MII oocyte+melatonin and young MII oocyte groups (P<0.05).

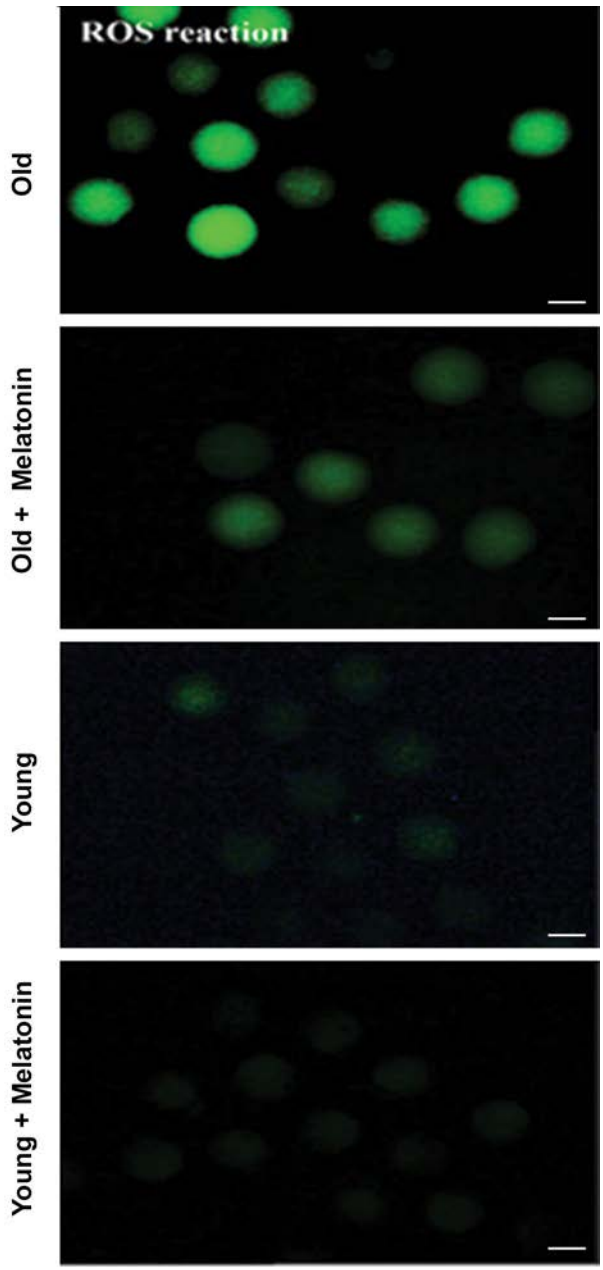

Fig.6: The levels of DCFH-DA representing the reactive oxygen specious (ROS) production in MII *in vitro* matured oocytes, isolated from young and aged mice. The micrograph depicts the different intensity of ROS among the young MII oocytes, young MII oocytes+10 µM melatonin, aged MII oocytes, and aged MII oocytes+10 µM melatonin groups. The phase contrast of each group shows the morphology of oocytes. The fluorescence intensity of DCFH-DA was applied to probe ROS within the cytoplasm of oocytes (magnification: ×200, scale bars: 100 µm).

Discussion

Reproductive senescence has been introduced as a major health problem over the world. Female fertility is promptly decreased after age of 35 years. A decline in ovarian follicle reserve and oocyte pool, as well as an increase in the number of low-quality oocytes, are featured characteristics of ovarian aging (22). Perhaps,

diminished mitochondrial biogenesis has been regarded as a significant factor related to poor oocyte quality as a result of aging (23). Although the mechanisms underlying age-induced decreased oocyte quality is still unknown, mitochondrial dysfunction is thought to be involved in this process (3). Various antioxidants such as resveratrol were found to improve mitochondrial function through the activation of SIRT-1 (24, 25).

Melatonin is an effective antioxidant and free-radical scavenger which has a central role in the improvement of ovarian function and oocyte quality (26). It has been reported that melatonin supplementation significantly postpones postovulatory aging of murine oocytes through the upregulation of the expression of SIRT-1. It has been reported that melatonin could reverse age-induced reproduction damage caused by postovulatory aging through the regulation of the SIRT-1 expression (27). Our results also showed that the culture of oocytes, which were at the GV stage, with melatonin for 24 hours considerably enhanced the expression level of SIRT-1 in oocytes in both aged and young mice. Melatonin could increase the SIRT-1 expression in aged MII oocyte+melatonin as much as the young MII oocyte group, implying the improvement of mitochondrial function.

It has been reported that SIRT-1 is also associated with the regulation of autophagy, a cellular process that ends with lysosomal degradation, and mitochondrial activities in cells upon oxidative stress (28, 29). Autophagy is a process that degrades misfolded and long-lived proteins and damaged organelles such as mitochondria, endoplasmic reticulum, as well as intracellular pathogens, to maintain cellular homeostasis (12, 29).

The LC3 protein which is generally localized on autophagosome membranes can be considered a biomarker of autophagy. In a previous study, it has been reported that resveratrol significantly increased autophagosomes in oocytes of aged cows and enhanced oocyte competence (9). On the other hand, the results of another research showed that melatonin attenuated autophagy in postovulatory oocytes (27).

Our results demonstrated that melatonin could significantly increase the LC3 expression in oocytes of aged mice, indicating an increase in the number of autophagosomes. Moreover, the LC3 expression in aged MII oocyte+melatonin group had no significant difference when compared with the young MII oocyte group, showing that melatonin could increase the number of autophagosomes similar to that of the young MII oocyte group.

Mitochondrial involvement in the aging process is also attributed to the energy production and regulation of the different cellular signaling pathways (30). Adenosine triphosphate is mainly produced in mitochondria, and it is essential for oocytes. The ATP generation is one of the major tasks of mitochondria, and the amount of ATP in mature oocytes represents the quality of oocytes (31). The level of ATP in oocytes could be considered an indicator of the developmental potential of mammalian oocytes (26). According to the literature, poor oocyte quality and failure in embryonic development could be directly associated with the sub-normal production of ATP (32).

Although increased ROS production in aged oocytes has been shown to result in a decrease in the concentrations of intracellular ATP (26), other scientists believe that SIRT could increase the ATP level and thus protecting the cells from ROS-mediated oxidative damage (11). Melatonin can improve mitochondrial function by an increase in the ATP production within oocytes (33).

In the present study, it has been found that *in vitro* matured melatonin-treated oocytes of old and young mice exhibited a significant increase in ATP content compared with those untreated oocytes. It is suggesting that melatonin could enhance mitochondrial function.

Notably, the comparison between melatonin-treated and untreated oocytes revealed that there was a significant increase (1.4 fold) in the ATP content in the aged MII oocyte+melatonin group as compared with the young MII oocyte group (increased by 1.1 fold). A significant difference observed between the aged MII oocyte+melatonin and young MII oocyte groups indicated that although melatonin increased the ATP content in the aged MII oocyte+melatonin group, such an increase did not reach to that of the young MII oocyte group.

Considering the primary source of ROS production is placed in mitochondria, the aging process increases the rate of mitochondrial ROS (mROS) and weakens antioxidant defense systems (22, 34). Scientists believe that mitochondria have a critical role in cellular events associated with the aging process, through an accumulation of mitochondrial ROS and oxidative damage to mitochondrial and cytoplasmic components. According to various theories, mitochondrial respiratory activity and mitochondrial membrane potential are diminished during the aging process and endogenous antioxidant system function, denoting that these phenomena are decreased in an age-dependent manner (22). Therefore, to reduce the adverse effects of excessive ROS and improve the maturation process of oocytes, antioxidants are widely used in *in vitro* culture systems (35). Melatonin is an effective modulator of mitochondrial DNA damage. It has been implicated that an increase in the electron transport efficiency within mitochondria prevents ROS formation and protects DNA mutation in response to oxidative damage (36).

Some reports have indicated that melatonin and its metabolic derivatives can consecutively detoxify ROS and regulate different antioxidant enzymes through their receptors to halt radical-mediated damages, leading to preservation of the quality of oocytes (37). Melatonin could also dramatically decrease the ROS level in porcine oocytes and improve the quality of oocytes (38).

In this study, we found that the addition of melatonin to the culture medium significantly reduced the ROS level

in oocytes and increased TAC in the culture media. Based on above statements, it would be plausible that melatonin not only reduces ROS level via its direct ROS-scavenging ability but also improves the mitochondrial function by the enhancement of autophagy which maintains cellular homeostasis and oocyte quality.

Previous studies demonstrated that melatonin supplementation during the in-vitro culture significantly reduced ROS production and augmented the glutathione (GSH) contents (39). Our findings were inconsistent with other studies which report that melatonin has a direct protective effect against oxidative stress for mammalian oocytes. Although our data showed that melatonin increased TAC levels in the aged MII oocyte+melatonin group in comparison with the aged MII oocyte group, there was no significant difference between the two groups. On the other hand, the TAC level was increased significantly in the young MII oocyte+melatonin group compared with young oocyte group. It has also been observed that there was no significant difference between the aged oocyte+melatonin and young oocyte groups, implying that melatonin improved the ability of aged MII oocytes to increase the level of TAC in comparison with the ability of the young MII oocytes.

Melatonin also improved the oocyte maturation rate and consequently the embryo development thereby the reduction of ROS during the *in vitro* maturation process of the porcine oocyte (39). Our results showed a significant increase in meiotic competency of melatonin-treated MII oocytes in comparison with non-treated oocytes.

Conclusion

The present study demonstrated that the treatment of *in vitro* matured MII oocytes, isolated from aged mice with melatonin could improve the mitochondrial function by an increase in the SIRT-1 expression, the ATP content, and autophagy, ultimately resulting in the improvement of the quality of mitochondria in cells. Melatonin also decreased intracellular ROS and increased TAC production. As the final point, melatonin could improve the oocyte maturation rate.

Acknowledgements

This research was financially supported by a research grant (ID: 36762) from International Campus of the Tehran University of Medical Sciences, Tehran, Iran. The authors wish to thank all staffs of the embryology laboratory of Royan Institute for their kind cooperation during this project. There is no conflict of interest in this study.

Authors' Contributions

Z.N.H.A.; Contributed to all part of experimental work. P.P.; Participated in study design, responsible for overall supervision and contributed acquisition of data and interpretation of the data and the conclusion. I.R.-K.; Contributed for ATP experiment and interpretation of the data and participated in statistical analysis performed editing and approving the final version of this manuscript for submission. F.M.-G.; Contributed in collecting of data of the ROS and TAC experiment. R.F.; Participated in intracellular ROS experiment and ordered ATP assay kit. L.S.T.; Participated in oocytes collection and prepared GV oocytes for IVM pertaining to this component of the study. M.N.; Contributed in immunostaining experiment for lC3 and SIT1. All authors read and approved the final manuscript.

References

1. Takeo S, Kawahara-Miki R, Goto H, Cao F, Kimura K, Monji Y, et al. Age-associated changes in gene expression and developmental competence of bovine oocytes, and a possible countermeasure against age-associated events. Mol Reprod Dev. 2013; 80(7): 508-521.
2. Vitale SG, Rossetti P, Corrado F, Rapisarda AM, La Vignera S, Condorelli RA, et al. How to achieve high-quality oocytes? The key role of myo-Inositol and melatonin. Int J Endocrinol. 2016; 2016: 4987436.
3. Iwata H. Age-associated events in bovine oocytes and possible countermeasures. Reprod Med Biol. 2016; 15(3): 155-164.
4. Yamamoto T, Iwata H, Goto H, Shiratuki S, Tanaka H, Monji Y, et al. Effect of maternal age on the developmental competence and progression of nuclear maturation in bovine oocytes. Mol Reprod Dev. 2010; 77(7): 595-604.
5. Linnane AW, Zhang C, Baumer A, Nagley P. Mitochondrial DNA mutation and the ageing process: bioenergy and pharmacological intervention. Mutat Res. 1992; 275(3-6): 195-208.
6. Cetinkaya MB, Siano LJ, Benadiva C, Sakkas D, Patrizio P. Reproductive outcome of women 43 years and beyond undergoing ART treatment with their own oocytes in two connecticut university programs. J Assist Reprod Genet. 2013; 30(5): 673-678.
7. Kim HO, Sung N, Song IO. Predictors of live birth and pregnancy success after in vitro fertilization in infertile women aged 40 and over. Clin Exp Reprod Med. 2017; 44(2): 111-117.
8. Iwata H, Goto H, Tanaka H, Sakaguchi Y, Kimura K, Kuwayama T, et al. Effect of maternal age on mitochondrial DNA copy number, ATP content and IVF outcome of bovine oocytes. Reprod Fertil Dev. 2011; 23(3): 424-432.
9. Sugiyama M, Kawahara-Miki R, Kawana H, Shirasuna K, Kuwayama T, Iwata H. Resveratrol-induced mitochondrial synthesis and autophagy in oocytes derived from early antral follicles of aged cows. J Reprod Dev. 2015; 61(4): 251-259.
10. Pi H, Xu S, Reiter RJ, Guo P, Zhang L, Li Y, et al. SIRT3-SOD2-mROS-dependent autophagy in cadmium-induced hepatotoxicity and salvage by melatonin. Autophagy. 2015; 11(7): 1037-1051.
11. Ahn BH, Kim HS, Song S, Lee IH, Liu J, Vassilopoulos A, et al. A role for the mitochondrial deacetylase Sirt3 in regulating energy homeostasis. Proc Natl Acad Sci USA. 2008; 105(38): 14447-14452.
12. Nasheehamad Almohammed Z, Kiros Bitsue Z, Ragerdi Kashani I, Pasbakhsh P. The effect of autophagy in regulation of ROS, mitochondria damage, aging, inflammation and metabolic control and protects against genome instability and necrosis as a potential target in cancer and autoimmunity treatment and prevention. International Journal of Scientific and Engineering Research. 2017; 8(5): 370-393.
13. Ruder EH, Hartman TJ, Goldman MB. Impact of oxidative stress on female fertility. Curr Opin Obstet Gynecol. 2009; 21(3): 219-222.
14. Reiter RJ, Tan DX, Rosales-Corral S, Galano A, Zhou XJ, Xu B. Mitochondria: central organelles for melatonin's antioxidant and anti-aging actions. Molecules. 2018; 23(2): 509.
15. Bahadori MH, Ghasemian F, Ramezani M, Asgari Z. Melatonin effect during different maturation stages of oocyte and subsequent embryo development in mice. Iran J Reprod Med. 2013; 11(1): 11-18.
16. Andreollo NA, Santos EF, Araújo MR, Lopes LR. Rat's age versus human's age: what is the relationship? Arq Bras Cir Dig. 2012; 25(1): 49-51.
17. Caligioni CS. Assessing reproductive status/stages in mice. Curr Protoc Neurosci. 2009; Appendix 4: Appendix 4I.
18. Dutta S, Sengupta P. Men and mice: relating their ages. Life Sci. 2016; 152: 244-248.

19. Adriaens I, Jacquet P, Cortvrindt R, Janssen K, Smitz J. Melatonin has dose-dependent effects on folliculogenesis, oocyte maturation capacity and steroidogenesis. Toxicology. 2006; 228(2-3): 333-343.
20. Tatone C, Amicarelli F, Carbone MC, Monteleone P, Caserta D, Marci R, et al. Cellular and molecular aspects of ovarian follicle ageing. Hum Reprod Update. 2008; 14(2): 131-142.
21. Park S-H, Yu I-J. Effect of dibutyryl cyclic adenosine monophosphate on reactive oxygen species and glutathione of porcine oocytes, apoptosis of cumulus cells, and embryonic development. Zygote. 2013; 21(3): 305-313.
22. Song C, Peng W, Yin S, Zhao J, Fu B, Zhang J, et al. Melatonin improves age-induced fertility decline and attenuates ovarian mitochondrial oxidative stress in mice. Sci Rep. 2016; 6: 35165.
23. Woods DC, Khrapko K, Tilly JL. Influence of Maternal aging on mitochondrial heterogeneity, inheritance, and function in oocytes and preimplantation embryos. Genes (Basel). 2018; 9(5). pii: E265.24
24. Li Y, Wang J, Zhang Z, Yi J, He C, Wang F, et al. Resveratrol compares with melatonin in improving in vitro porcine oocyte maturation under heat stress. J Anim Sci Biotechnol. 2016; 7: 33.
25. Liu MJ, Sun AG, Zhao SG, Liu H, Ma SY, Li M, et al. Resveratrol improves in vitro maturation of oocytes in aged mice and humans. Fertil Steril. 2018; 109(5): 900-907.
26. Liang S, Guo J, Choi JW, Kim NH, Cui XS. Effect and possible mechanisms of melatonin treatment on the quality and developmental potential of aged bovine oocytes. Reprod Fertil Dev. 2017; 29(9): 1821-1831.
27. Yang Q, Dai S, Luo X, Zhu J, Li F, Liu J, et al. Melatonin attenuates postovulatory oocyte dysfunction by regulating SIRT1 expression. Reproduction. 2018; 156(1): 81-92.
28. Ou X, Lee MR, Huang X, Messina-Graham S, Broxmeyer HE. SIRT1 positively regulates autophagy and mitochondria function in embryonic stem cells under oxidative stress. Stem Cells. 2014; 32(5): 1183-1194.
29. Chen Z, Zuo X, Li H, Hong R, Ding B, Liu C, et al. Effects of melatonin on maturation, histone acetylation, autophagy of porcine oocytes and subsequent embryonic development. Anim Sci J. 2017; 88(9): 1298-1310.
30. May-Panloup P, Boucret L, Chao de la Barca JM, Desquiret-Dumas V, Ferré-L'Hotellier V, Morinière C, et al. Ovarian ageing: the role of mitochondria in oocytes and follicles. Hum Reprod Update. 2016; 22(6): 725-743.
31. Cantó C, Gerhart-Hines Z, Feige JN, Lagouge M, Noriega L, Milne JC, et al. AMPK regulates energy expenditure by modulating NAD+ metabolism and SIRT1 activity. Nature. 2009; 458(7241): 1056-1060.
32. Gonzalez-Freire M, de Cabo R, Bernier M, Sollott SJ, Fabbri E, Navas P, et al. Reconsidering the role of mitochondria in aging. J Gerontol A Biol Sci Med Sci. 2015; 70(11): 1334-1342.
33. He C, Wang J, Zhang Z, Yang M, Li Y, Tian X, et al. Mitochondria synthesize melatonin to ameliorate its function and improve mice oocyte's quality under in vitro conditions. Int J Mol Sci. 2016; 17(6). pii: E939.
34. Reiter RJ, Tan DX, Rosales-Corral S, Galano A, Zhou XJ, Xu B. Mitochondria: central organelles for melatonin′ s antioxidant and anti-aging actions. Molecules. 2018; 23(2). pii: E509.
35. Wang F, Tian X, Zhang L, He C, Ji P, Li Y, et al. Beneficial effect of resveratrol on bovine oocyte maturation and subsequent embryonic development after in vitro fertilization. Fertil Steril. 2014; 101(2): 577-586.
36. Hardeland R. Antioxidative protection by melatonin: multiplicity of mechanisms from radical detoxification to radical avoidance. Endocrine. 2005; 27(2): 119-130.
37. Pang Yw, Jiang Xl, Zhao Sj, Huang Zq, Zhu Hb. Beneficial role of melatonin in protecting mammalian gametes and embryos from oxidative damage. J Integr Agric. 2018; 17(10): 2320-2335.
38. Wang T, Gao YY, Chen L, Nie ZW, Cheng W, Liu X, et al. Melatonin prevents postovulatory oocyte aging and promotes subsequent embryonic development in the pig. Aging (Albany NY). 2017; 9(6): 1552-1564.
39. Li Y, Zhang Z, He C, Zhu K, Xu Z, Ma T, et al. Melatonin protects porcine oocyte in vitro maturation from heat stress. J Pineal Res. 2015; 59(3): 365-375.

Original Article

Elevated Expression of Cytosolic Phospholipase A_2 Delta Is Associated with Lipid Metabolism Dysregulation during Hepatocellular Carcinoma Progression

Maryam Ranjpour, Ph.D.[1], Saima Wajid, Ph.D.[1], Swatantra Kumar Jain, Ph.D.[2*]

1. Department of Biotechnology, School of Chemical and Life Sciences, Jamia Hamdard, New Delhi, India
2. Department of Medical Biochemistry, HIMSR, Jamia Hamdard, New Delhi, India

Corresponding Address: Department of Medical Biochemistry, HIMSR, Jamia Hamdard, New Delhi, India
Email: skjain@jamiahamdard.ac.in

Received: 6/November/2018, Accepted: 4/February/2019

Abstract

Objective: Liver cancer is the third rank amongst the common malignancies, causing maximum death in the patients diagnosed with cancers. Currently available biomarkers are not enough sensitive for early diagnosis of hepatocellular carcinoma (HCC). This makes difficult management of HCC. With the aim of finding new generation of proteomic-based biomarkers, the represented study was designed to characterize the differentially expressed proteins at different stages of HCC initiation and at progression. This could lead to find potential biomarkers for early detection of HCC.

Materials and Methods: In this experimental study, we report induction of HCC by administrating chemical carcinogens in male Wistar rats. Disease progression was monitored by histological evaluation. Serum proteomic analyses such as 2 dimensional (2D)-electrophoresis, MALDI-TOF-MS/MS and Western blot have been used to analyze and characterize the differentially expressed proteins during HCC development.

Results: HCC initiation and tumorigenesis were observed at one and four months post carcinogen treatment, respectively. One of the differentially-expressed proteins, namely, cytosolic phospholipase A_2 delta was significantly up-regulated at very early stage of HCC development. Its expression continued to increase during cancer progression and hepatotumorigenesis stages. Its elevated expression has been confirmed by Western blot analysis. Consistent to this, analyses of the sera in the clinically confirmed liver cancer patients showed elevated expression of this protein, further validating our experimental results.

Conclusion: This study suggests that elevation in the expression of cytosolic phospholipase A_2 delta is associated with progression of HCC.

Keywords: Chemical Carcinogens, Cytosolic Phospholipase A_2 Delta, Hepatocellular Carcinoma, MALDI-TOF-MS/MS, Western Blot Analysis

Cell Journal(Yakhteh), Vol 22, No 1, April-June (Spring) 2020, Pages: 17-22

Citation: **Ranjpour M, Wajid S, Jain SK. Elevated expression of cytosolic phospholipase A_2 delta Is associated with lipid metabolism dysregulation during hepatocellular carcinoma progression. Cell J. 2020; 22(1): 17-22. doi: 10.22074/cellj.2020.6527.**

Introduction

Hepatocellular carcinoma (HCC) is globally the fifth most common cancer with a high rate of morbidity and the third type of cancer causing maximum death among the patients diagnosed with cancers (1, 2). Etiological influences such as hepatitis B virus (HBV) and hepatitis C virus (HCV) infections, alcohol abuse, metabolic diseases and carcinogen exposure lead to chronic inflammation of liver and mutation causing heterogeneous HCC (3). Lack of clear symptoms, numerous relapse and inefficient therapy lead to poor prognosis and high mortality in patients diagnosed with HCC (2). Finding new generation noninvasive biomarkers to detect HCC at early stage would help reduce the rate of cancer-related mortality (4). Currently available markers, such as alpha-fetoprotein, do not have high sensitivity and search for novel markers is mandatory. Effective treatment and patient survival rate are dependent on the early diagnosis of HCC which can be provided based on the novel prognostic and diagnostic biomarkers (5).

In the present study, using animal model, we aimed to find out differentially expressed proteins that are associated with HCC initiation and progression to introduce as potential biomarker(s) or to target as therapeutic agent at very early stage of liver cancer initiation.

Materials and Methods

The experimental study involves analysis of rodent model *in vivo* which has previously been developed in our laboratory to study HCC. Further, the obtained data are validated with sera of clinically approved liver cancer patients.

Liver cancer induction and development of the rodent model

Liver cancer was chemically induced in 4-6 weeks old male Wistar rats weighing 80-100 g, by administrating chemical carcinogens DEN and 2-AAF as reported by our group earlier. Animal experimentation was performed following approval from Jamia Hamdard (New Delhi, India) Institutional Animal Ethics Committee formed for the Purpose of Control and Supervision of Experiments on Animals (project number 908). The protocol for HCC development in rats was

essentially the same as previously described instruction (6). Briefly, the rats were kept in polypropylene cages while temperature was maintained at 25 ± 2˚C with 12 hours cycle of light/dark in the animal house of Jamia Hamdard. These were fed ad libitum with free access to standard laboratory food (Amrut Laboratory, rat and mice feed, Navmaharashtra Chakan Oil Mills Ltd., India) and water daily. DEN (200 mg/kg body weight) and 2-AAF dissolved in 1% carboxymethyl cellulose (150 mg/kg body weight) were used as the initiator and promoter of HCC, respectively. Animals were randomly split up into two groups namely control and treated groups. Treated groups were further divided into two different groups namely, 1 M (sacrificed after one month) and 4 M (sacrificed after four months). The carcinogen treated animals were given a single high dose intraperitoneally (I.P.) of DEN, and after one week recovery period, the rats were administered with 2-AAF. Three doses of 2-AAF were orally administered on three alternative days among the first week of each month for entire study period (four months). Therefore, a total of 3 and 12 doses of 2-AAF were administered to the animals in the 1 M and 4M treated groups, respectively. The rats in control group received normal saline at the same schedule. The rats in the 1 M and 4 M groups were kept in a glass chamber containing cotton soaked with diethyl ether to be anesthetized and sacrificed at respectively one and four months after carcinogen treatment, respectively. At the time of sacrificing, the animals were perfused transcardially with saline and after their death they were dissected to excise livers for further analysis.

Histological examination

Livers were fixed in 10% formalin, sliced, dried out and buried in paraffin. Cross-sections were taken and stained with Hematoxylin and Eosin. Sections were mounted with DPX mountant (Sigma-Aldrich, USA) and checked employing light microscope for histological changes.

Proteomic analysis of differentially expressed proteins

The Bradford's method was used to measure protein concentration (7). Depletion of albumin in serum samples and their preparation, 2 dimensional (2D)-electrophoresis of the total serum proteins and their analysis with PD-Quest software and ultimately MALDI-TOF-MS/MS characterization were performed as previously described (8, 9).

Validation of protein expression by Western blot analysis

30 µg of total serum protein was fractionated on 10% poly acrylamide gel at 80 V and it was transferred to polyvinylidene difluoride (PVDF) membrane employing Hoefer Western blotting apparatus (Hoefer Inc, USA, 4˚C, 150 mA for three hours). Immuno-detection was performed using 1:500 diluted primary antibody (Sigma-Aldrich, USA) in Tris-buffered saline (TBS) overnight at 4˚C and 1:4000 diluted HRP conjugated anti-rabbit secondary antibody (Sigma-Aldrich, USA) for three hours. The protein expression was visualized with diaminobenzidine (DAB, Sigma-Aldrich, USA) and Luminata™ Forte Western HRP Substrate (Millipore, USA) system. Analyses of clinically approved liver cancer patients sera (including two male patients aged 35 and 73 years used for the analyses) and controls (including two matched age healthy males with liver cancer patients used for the analyses) were carried out after receiving the approval of Jamia Hamdard Institutional Ethics Committee (JHIEC). The informed consent was obtained from all participating subjects. The HCC patients were clinically approved and were under various therapies.

Statistical analysis

The experiments were carried out in triplicate and data are revealed as means ± standard error of the mean (SEM). The significance of differences (control vs. treated groups) was analyzed employing One-way ANOVA pursued by Dunnett test and they were considered statistically significant when $P<0.05$.

Results

Development of hepatocellular carcinoma model and serum analysis of carcinogen treated rats and controls

HCC was induced by administrating chemical carcinogens (DEN and 2-AAF) in male Wistar rats, as previously reported by us (6). Histological analysis revealed disease initiation at one month and development of cancer and tumorigenesis at four months after carcinogen treatment (Fig.1) (8).

Reproducible results were obtained following repeatedly performing 2D-electrophoresis analyses. The analyses of 2D gels using PD-Quest were assigned unique sample spot protein (SSP) numbers to protein spots and compared differentially expressed proteins (8-10). One of these proteins, up-regulating at one month (initiation stage of HCC) and four months (tumorigenesis stage) after carcinogen treatment, was selected for further analysis. Detailed expression analysis of this protein following carcinogen administration has been illustrated in Figure 2. Changes in the levels of protein expression were statistically significant ($P<0.05$). The protein spot was excised from 2D gels, digested and the mass fingerprinting of its peptides was obtained by MALDI-TOF-MS/MS characterization. The protein was characterized as orthologue of cytosolic phospholipase A_2 delta, gi|109470683, [*Rattus norvegicus*], using NCBI database search by MASCOT software (Fig.3A, B). Detailed analysis and characterization of cytosolic phospholipase A_2 delta have been shown in Table 1.

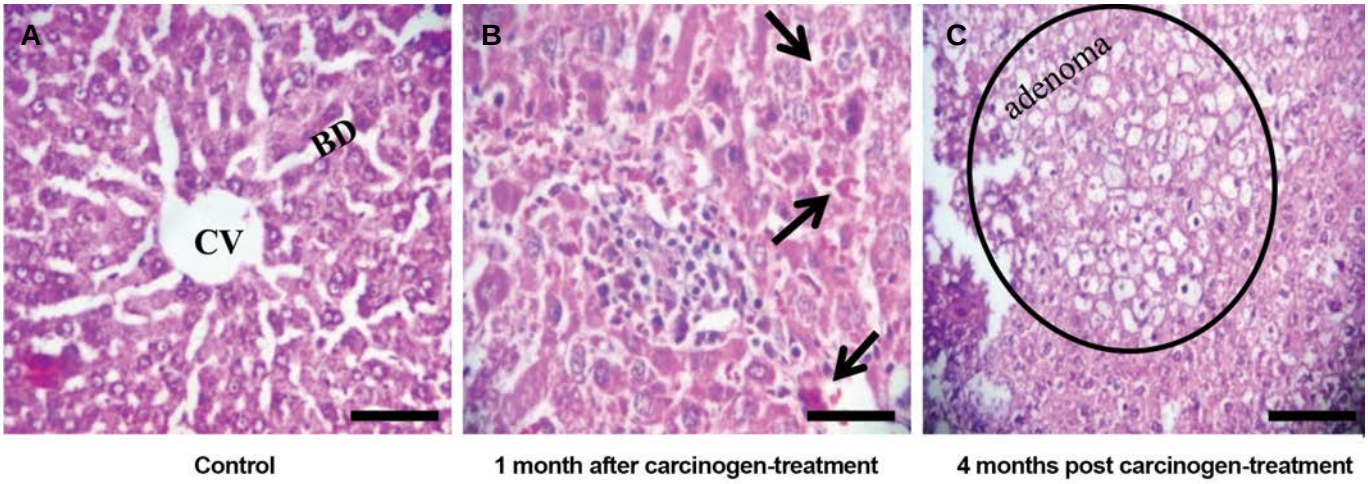

Fig.1: Histological analysis of liver tissue. Photomicrographs show histological changes in liver at high power. **A.** Normal architecture of central vein (CV) and bile duct (BD) are shown in the control liver (each treated group has its own control to be compared), **B.** One month post carcinogen treatment, inflammation and hemorrhage leading to HCC initiation are shown, using the arrows, and **C.** Development of adenoma (within the circle) was observed at four months after carcinogen treatment. Cystic degeneration of hepatocytes has been shown at tumors within the circle (scale bar: 20 µm at ×400 magnifications).

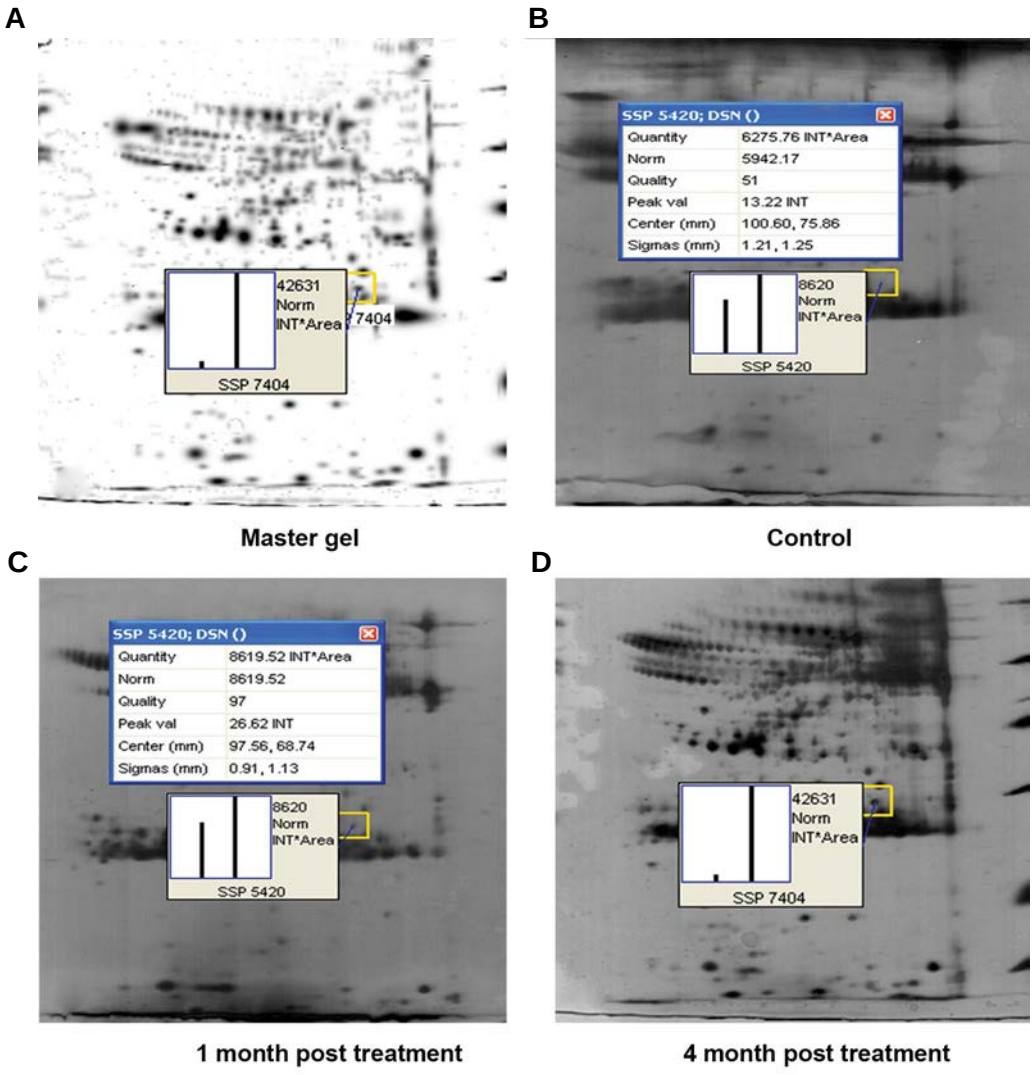

Fig.2: PD-Quest analysis of serum protein on 2D gels. The master gel represents protein spots from both control and treated groups, with pop up graph for protein of interest. The protein expression has been quantified based on intensity (INT) × area. **A.** The protein of interest quantification for the SSP 7404 master gel has been calculated based on the protein intensity of four months post carcinogen-treatment group. The protein spots were quantified and compared to **B.** SSP 5420 in control, **C.** SSP 5420 in one month post treatment groups, and **D.** SSP 7404 in the four months after carcinogen-treatment group. The expression intensity showed significant elevation of target protein level. SSP; Stands for sample spot protein and each spot protein has a unique SSP number.

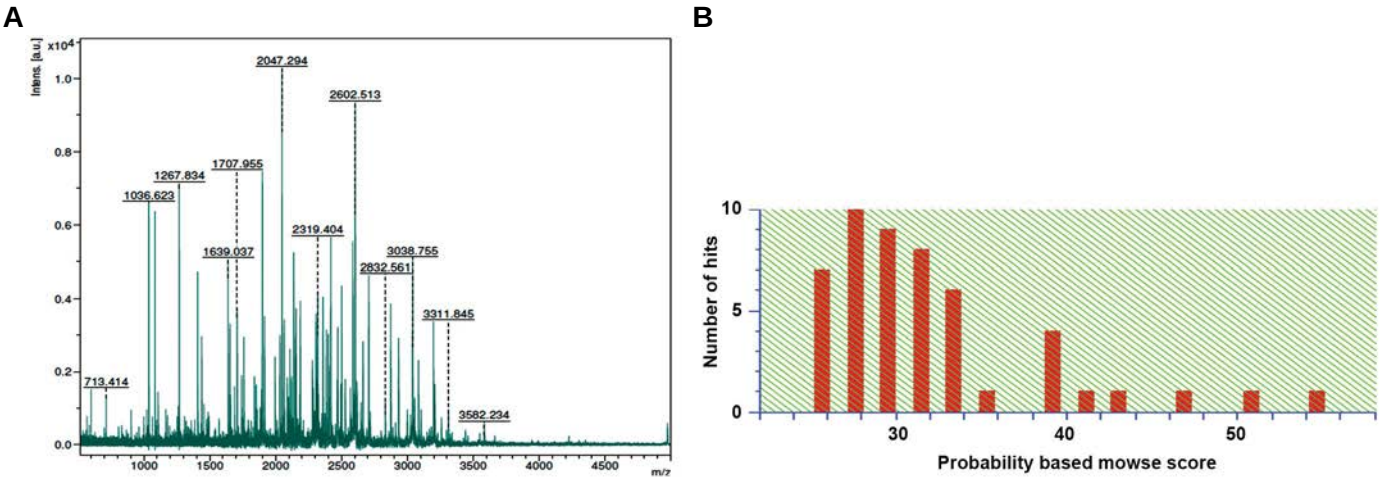

Fig.3: MALDI-TOF-MS/MS characterization of target spot. **A.** Spectra for the target spot were shown by MALDI-TOF-MS/MS characterization and **B.** MASOT histogram analysis: probability based on MOWSE score is defined as −10×log (P), where P is probability of the observed match with a random event. Individual protein scores, greater than 59, indicate identity or extensive homology (P<0.05).

Table 1: MALDI-TOF-MS/MS characterization of cytosolic phospholipase A_2 delta

Observed	Mr (Expt)	Mr (Calc)	ppm	Start-End	Miss	Peptide
1094.6700	1093.6627	1093.5516	102	389-398	0	K.DLEGPISHAR.E
1267.8339	1266.8267	1266.6357	151	478-487	0	K.ENHLETLHFK.E
1639.0371	1638.0298	1637.8485	111	445-458	1	K.LHGQVTDQKLSEQR.A
1740.0199	1739.0126	1738.8348	102	291-305	0	R.LSYGLCPEEQAFLGR.R
1839.1123	1838.1051	1838.0513	29.3	309-325	1	K.LVAAALKQALQLDEDLK.E
1994.2330	1993.2257	1992.9840	121	689-706	1	K.GLQQSGKYCSAQGLPFPR.V
2047.2940	2046.2867	2046.0745	104	791-808	0	R.LSEYNIQNNQGTILQALK.T
2107.4134	2106.4061	2106.0700	160	180-199	1	R.AGSTTMAAGQDKLELELMLK.G
2121.3561	2120.3488	2120.0936	120	24-41	1	R.QEEASVFCQLTVKILEAR.S
2319.4037	2318.3964	2318.1430	109	132-151	0	K.TFSLNPQGPEELDVEFLVER.T
2324.3359	2323.3286	2323.1630	71.3	286-305	1	K.ELSVRLSYGLCPEEQAFLGR.R
2399.2732	2398.2659	2398.1490	48.8	502-522	1	K.YGGFVPSELFGSEFFMGRLMK.R
2418.4232	2417.4159	2417.1493	110	169-191	1	R.ELSHLDVSLDRAGSTTMAAGQDK. L+Oxidation (M)
2832.5611	2831.5539	2831.3775	62.3	357-381	0	K.LGLLDCVTYFSGISGATWTMAHLYR.D
3023.9028	3022.8955	3022.4634	143	755-781	1	R.SPDELKAGQVDLTGVASPYFLYNMTYK. N+Oxidation (M)
3257.9532	3256.9459	3256.6616	87.3	425-453	1	R.EEQGYTVTIADLWGLVLESKLHGQVTDQK.L

Mr; Average molecular mass of the peptide in kilodalton, Expt; Experimentally determined molecular mass, Calc; Theoretically calculated mass of peptide based on atomic mass of the component, and Ppm; Parts per million.

Western blot analysis revealed up-regulation of cytosolic phospholipase A_2 delta expression in the serum of carcinogen treated rats vis-a-vis age-matched controls. Expression of cytosolic phospholipase A_2 delta was elevated at one month after carcinogen treatment and it was continued to increase during cancer progression until tumor stage at four months post carcinogen treatment. Expression of β-actin was considered as internal control (Fig.4A).

Moreover, Western blot analyses of clinically confirmed liver cancer patients' sera showed elevation of cytosolic phospholipase A_2 delta expression compared to the controls (Fig.4B). This observation validated our experimental results.

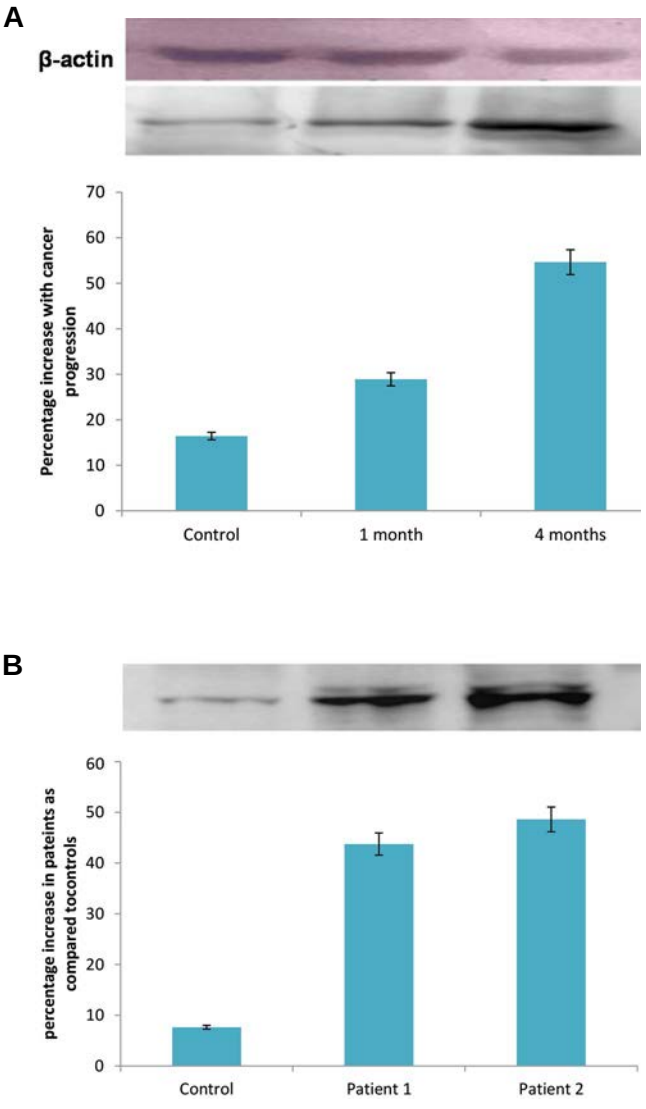

Fig.4: Expression analysis of cytosolic phospholipase A_2 delta by Western blotting. **A.** β-actin was used as internal control. Analyses showed time and dose dependent elevation in the expression of protein of interest, in rats belong to carcinogen treated groups, by liver cancer progression. Consistent increase in protein expression has been shown during liver cancer progression and **B.** Significant elevation in expression of cytosolic phospholipase A_2 delta has been shown in sera of clinically confirmed liver cancer patients as compared to the healthy controls ($P<0.001$, n=3, serum samples were taken from two male patients at age 35 and 73 for the analyses. Sear of healthy control was drawn from the same age group). The Image j software was used to quantify the intensity of protein bands. Fold change in expression of cytosolic phospholipase A_2 delta was normalized over the age-matched controls. Data are presented as mean ± SEM (n=3), using one way ANOVA followed by Dunnett test.

Discussion

Neoplastic cell induction served as implication of cancer initiation in liver tissue of rats. Our method for animal model development is novel, as it neither requires carcinogen doses causing necrosis nor partial hepatectomy (6, 10). The serum protein profile of carcinogen treated rats and controls were compared and differentially expressed proteins were identified. However, one of these proteins was further characterized as cytosolic phospholipase A_2 delta. Changes taking place in the expression of HCC-related proteins have been systematically monitored during various stages of HCC development, from the initiation of cancer to hepatotumorigenesis, when fully grown tumors were observed.

The importance of cytosolic phospholipase A enzymes in cancer progression is of the considerable interests, as these enzymes play important role in the pathways associated with progression of cancer. This enzyme family controls cell proliferation, differentiation, survival and motility in almost all tissues. Their increased expression results in dysregulation and facilitates unlimited growth of tumors and metastasis for cancer cells. Significant role of this family members has been implicated in tumor progression and tumorigenesis (11). This family is composed of six intracellular enzymes simply indicated as cytosolic phospholipase A_2-α, -β, -γ, -δ, -ε and –ζ (12). Cytosolic phospholipase A_2 family mediates biologically active fatty acids release from the pool of phospholipids located in membranes (13) of virtually all cells in humans and rodents (12). Aberrant expression of cytosolic phospholipase A_2 family has been linked to progression of malignancies such as prostate, liver (13) and colon cancers (14). A study has reported that elevating cytosolic phospholipase A_2 expression has been taken place through pathways associated with ERK1/2 and p38 MAPK. The study reported that cytosolic phospholipase A_2 expression is significantly associated with vascular endothelial growth factor expression; however, its expression was not related to any clinico-pathological specification (14). No much information is available about the function of cytosolic phospholipase A_2 family *in vivo* (12). Among three main classes of cytosolic phospholipase A_2 family in mammals, cytosolic phospholipase A_2-α has gained the most attention, regarding that is widely expressed in virtually all mammalian cells (14). Cytosolic phospholipase A_2-α is activated by transforming growth factor beta (TGF-β) regulating growth of primary and transformed hepatocytes. The inter-relationship among cytosolic phospholipase A_2-α and TGF-β signaling pathways has been reported in primary hepatocytes of rats and human HCC; thus cytosolic phospholipase A_2-α is an important factor regulating TGF-β signaling pathway and controlling proliferation of hepatocytes and hepatocarcinogenesis (15). Cytosolic phospholipase A_2-α regulates biosynthesis of prostaglandins through arachidonic acid cleavage, from

membrane phospholipids (12), through cyclooxigenase (COX) (16). The prostaglandins increase storage of triglycerides in hepatocytes leading to liver damage and cirrhosis (12). This pathway is activated in variety of cancers including HCC (15). Arachidonic acid, as a substrate for COXs and lipoxygenases (14), is a necessary factor that producing bioactive eicosanoids and platelet activating factor which, in turn, regulate inflammation (17), tumor cell proliferation and motility, differentiation, survival, invasion, angiogenesis and metastasis in HCC (13, 15). We observed elevated levels of cytosolic phospholipase A_2 delta in the serum of HCC rats and in human patients with liver cancer. This suggests that is one of the important factors associated with HCC initiation and progression leading to hepatotumorigenesis. Elevation of cytosolic phospholipase A_2 delta expression in liver cancer might be associated with dysregulation of lipid metabolism and liver damage, causing cancer initiation in tissue at precancerous stage, while the epithelial cells are actively proliferating.

Conclusion

Taken together, the present study suggests that evaluation of cytosolic phospholipase A_2 delta concentration, alone or in consolidation with other conventional markers, may provide critical knowledge for the early noninvasive disclosure of HCC. Moreover, cytosolic phospholipase A_2 delta might also be served as a potential target to find out the status and progression of liver cancer.

Acknowledgements

The authors would like to thank Dr. Tiwari (Animal House, Jamia Hamdard, New Delhi, India) for his contribution in histological analysis**.** The work was supported by a MRP grant from UGC to S.K. Jain [Grant #40-155/2011(SR)], New Delhi, India. There is no conflict of interest in this study.

Authors' Contributions

S.K.J.; Is principal investigator of the project, designed and supervised the entire study, interpreted the data, provided financial support for carrying out the research and finalized the manuscript. M.R.; Carried out all the experiments and has written the manuscript which was further corrected by S.K.J. S.W.; Has contributed in interpretation of the results. All authors have contributed equally, read, and approved the final manuscript.

References

1. Kornberg A, Witt U, Schernhammer M, Kornberg J, Ceyhan GO, Mueller K, et al. Combining ^{18}F-FDG positron emission tomography with Up-to-seven criteria for selecting suitable liver transplant patients with advanced hepatocellular carcinoma. Sci Rep. 2017; 7(1): 14176.
2. Bao H, Su H. Long noncoding RNAs act as novel biomarkers for hepatocellular carcinoma: progress and prospects. Biomed Res Int. 2017; 2017: 6049480.
3. Ashida R, Okamura Y, Ohshima K, Kakuda Y, Uesaka K, Sugiura T, et al. CYP3A4 gene is a novel biomarker for predicting a poor prognosis in hepatocellular carcinoma. Cancer Genomics Proteomics. 2017; 14(6): 445-453.
4. Wang M, Sanda M, Comunale MA, Herrera H, Swindell C, Kono Y, et al. Changes in the glycosylation of kininogen and the development of a kininogen-based algorithm for the early detection of HCC. Cancer Epidemiol Biomarkers Prev. 2017; 26(5): 795-803.
5. Gonzalez SA. Novel biomarkers for hepatocellular carcinoma surveillance: has the future arrived? Hepatobiliary Surg Nutr. 2014; 3(6): 410-414.
6. Malik S, Bhatnagar S, Chaudhary N, Katare DP, Jain SK. DEN+ 2-AAF-induced multistep hepatotumorigenesis in Wistar rats: supportive evidence and insights. Protoplasma. 2013; 250(1): 175-183.
7. Bradford MM. A rapid and sensitive method for the quantitation of microgram quantities of protein utilizing the principle of protein-dye binding. Anal Biochem. 1976; 72: 248-254.
8. Ranjpour M, Katare DP, Wajid S, Jain SK. HCC specific protein network involving interactions of EGFR with A-Raf and transthyretin: experimental analysis and computational biology correlates. Anticancer Agents Med Chem. 2018; 18(8): 1163-1176.
9. Ranjpour M, Wajid S, Jain SK. Elevated expression of A-Raf and FA2H in hepatocellular carcinoma is associated with lipid metabolism dysregulation and cancer progression. Anticancer Agents Med Chem. 2018 (ahead of print).
10. P Katare D, Malik S, J Mani R, Ranjpour M, Jain SK. Novel Mutations in transthyretin gene associated with hepatocellular carcinoma. Mol Carcinog. 2018; 57(1): 70-77.
11. Scott KF, Sajinovic M, Hein J, Nixdorf S, Galettis P, Liauw W, et al. Emerging roles for phospholipase A2 enzymes in cancer. Biochimie. 2010; 92(6): 601-610.
12. Leslie CC. Cytosolic phospholipase A_2: physiological function and role in disease. J Lipid Res. 2015; 56(8): 1386-1402.
13. Scott KF, Sajinovic M, Hein J, Nixdorf S, Galettis P, Liauw W, et al. Emerging roles for phospholipase A2 enzymes in cancer. Biochimie. 2010; 92(6): 601-610.
14. Sun GY, Chuang DY, Zong Y, Jiang J, Lee JC, Gu Z, et al. Role of cytosolic phospholipase A2 in oxidative and inflammatory signaling pathways in different cell types in the central nervous system. Mol Neurobiol. 2014; 50(1): 6-14.
15. Han C, Bowen WC, Li G, Demetris AJ, Michalopoulos GK, Wu T. Cytosolic phospholipase A2alpha and peroxisome proliferator-activated receptor gamma signaling pathway counteracts transforming growth factor beta-mediated inhibition of primary and transformed hepatocyte growth. Hepatology. 2010; 52(2): 644-655.
16. Xu L, Han C, Lim K, Wu T. Cross-talk between peroxisome proliferator-activated receptor delta and cytosolic phospholipase A(2) alpha/cyclooxygenase-2/prostaglandin E(2) signaling pathways in human hepatocellular carcinoma cells. Cancer Res. 2006; 66(24): 11859-11868.
17. Haq S, Kilter H, Michael A, Tao J, O'Leary E, Sun XM, et al. Deletion of cytosolic phospholipase A2 promotes striated muscle growth. Nat Med. 2003; 9(7): 944-951.

Original Article

Indirect Tumor Inhibitory Effects of MicroRNA-124 through Targeting *EZH2* in The Multiple Myeloma Cell Line

Javid Sabour Takanlu, M.Sc.[1, 2#], Arad Aghaie Fard, M.Sc.[1#], Saeed Mohammdi, Ph.D.[2, 3], Seyed Mohammad Ali Hosseini Rad, M.Sc.[4], Saeid Abroun, Ph.D.[1*], Mohsen Nikbakht, Ph.D.[2, 3*]

1. Department of Hematology, Faculty of Medical Sciences, Tarbiat Modares University, Tehran, Iran
2. Hematology, Oncology and Stem Cell Transplantation Research Center, Tehran University of Medical Sciences, Tehran, Iran
3. Hematologic Malignancies Research Center, Tehran University of Medical Sciences, Tehran, Iran
4. Department of Microbiology and Immunology, University of Otago, Dunedin, New Zealand

#The first two authors equally contributed to this work.

**Corresponding Addresses: P.O.Box: 1411713131, Department of Hematology, Faculty of Medical Sciences, Tarbiat Modares University, Tehran, Iran*
P.O.Box: 14115111, Hematology, Oncology and Stem Cell Transplantation Research Center, Tehran University of Medical Sciences, Tehran, Iran
Emails: abroun@modres.ac.ir, m-nikbakht@sina.tums.ac.ir

Received: 25/October/2018, Accepted: 19/January/2019

Abstract

Objective: Multiple myeloma (MM) is an incurable plasma cell malignancy. Several genetic and epigenetic changes affect numerous critical genes expression status in this disorder. *CDKN2A* gene is expressed at low level in almost all cases with MM disease. The mechanism of this gene down-regulation has remained controversial. In the present study, we targeted *EZH2* by microRNA-124 (miR-124) in L-363 cells and assessed following possible impact on *CDKN2A* gene expression and phenotypic changes.

Materials and Methods: In this experimental study, growth inhibitory effects of miR-124 were measured by MTT assay in L-363 cell line. Likewise, cell cycle assay was measured by flowcytometery. The expression levels of *EZH2* and *CDKN2A* were evaluated by real-time quantitative reverse-transcription polymerase chain reaction (qRT-PCR).

Results: qRT-PCR results showed induction of *EZH2* gene expression after transduction of cells with lentivector expressing miR-124. The expression of *CDKN2A* was also upregulated as the result of EZH2 supression. Coincide with gene expression changes, cell cycle analysis by flow-cytometry indicated slightly increased G1-arrest in miR-transduced cells ($P<0.05$). MTT assay results also showed a significant decrease in viability and proliferation of miR-transduced cells ($P<0.05$).

Conclusion: It seems that assembling of H3K27me3 mark mediated by EZH2 is one of the key mechanisms of suppressing *CDKN2A* gene expression in MM disease. However, this suppressive function is applied by a multi-factor mechanism. In other words, targeting EZH2, as the core functional subunit of PRC2 complex, can increase expression of the downstream suppressive genes. Consequently, by increasing expression of tumor suppressor genes, myeloma cells are stopped from aberrant expansions and they become susceptible to regulated cellular death.

Keywords: Cyclin-Dependent Kinase Inhibitor 2A, Enhancer of Zeste Homolog 2, Multiple Myeloma, MicroRNA

Cell Journal(Yakhteh), Vol 22, No 1, April-June (Spring) 2020, Pages: 23-29

Citation: **Sabour Takanlu J, Aghaie Fard A, Mohammdi S, Hosseini Rad SMA, Abroun S, Nikbakht M. Indirect tumor inhibitory effects of microRNA-124 through targeting EZH2 in the multiple myeloma cell line. Cell J. 2020; 22(1): 23-29. doi: 10.22074/cellj.2020.6492.**

Introduction

Multiple myeloma (MM) is a malignant proliferation of monoclonal plasma cells characterized by clinical complications including hyper-calcaemia, renal dysfunction, anemia, and bone disease (CRAB) (1). MM is an intricate disease driven by the accumulation of several genetic and epigenetic changes. Whole oncogenomic studies of MM showed the presence of many highly recurrent and pivotal amplifications and/or deletions in genomic regions including the genes that are proposed to be involved in MM pathogenesis and progression (2).

Aberrations in G1/S checkpoint of the cell cycle caused by either loss of tumor suppressor genes -such as retinoblastoma (Rb) and P16- or enhanced activity of cyclin D1 or CDK4/6 in the cell-cycle machinery, lead to neoplastic progression. One of the most frequently affected components of this pathway is P16. *CDKN2A* gene, encoding P16 tumor suppressor and located at 9p21, has been shown to be dysregulated in several neoplasias by deletions, point mutations and promoter hyper-methylation (3, 4). Additionally, this tumor suppressor gene defective performance may be imperative for transformed phenotype commencement and maintenance in numerous neoplasms (5). Hence, it seems this gene has a crucial role in the initiation and progression of different malignancies, such as MM.

In the recent years, there has been an increasing interest in epigenetic impacts on cancer which can be described as a disease with gene expression alterations. DNA methylation, histone modifications and noncoding RNAs are examples of epigenetic elements contributing to the pathobiology of MM through gene expression changes (6).

Different DNA related procedures, such as transcription and replication, are affected by post-translational histone modifications (7). Several kinds of histone modifications

-methylation, acetylation, phosphorylation, etc. based on the type and particularly affected residue, have a distinct influence on genes expression profile (8). In this study, we focused on a histone silencing mark -trimethylation of lysine on position 27 of histone 3 (H3K27me3)- which is mediated by polycomb repressive complex 2 (PRC2) catalytic subunit, EZH2 (9).

Altered expression of EZH2 has been reported in various cancers. EZH2 overexpression frequently occurs in solid tumors whereas its down-regulation happens in hematological malignancies (10). Hence, depending on the type of malignancies and its role in cancer progression, EZH2 can be considered as onco/tumor suppressor gene. The mechanisms of these misregulations are different. For example in MM, interleukin-6 (IL-6) and c-Myc activation can mediated EZH2 up-regulation (11, 12). Different subsets of genes, having important roles in MM pathogenesis, are affected by EZH2 silencing impact.

microRNAs (miRNAs) are non-coding RNAs that have a crucial role in the regulation of gene expressions, particularly at the post-transcriptional level. These tiny gene regulators play an important role in carcinogenesis. Several studies have shown down-regulation of miR-124 in different types of cancers including hematological malignant disorders (13, 14).

miR-124 was previously introduced as a direct repressor of *EZH2* and its expression is decreased in 50% of myeloma cell lines (14-16). This study aims to reveal the positive effect of miR-124 on *CDKN2A* gene expression through targeting *EZH2* gene and also evaluate phenotypic changes in myeloma cell line.

Materials and Methods

Bacterial culture and plasmid extraction

E. Coli (DH5α) containing Lenti-miR-GFP-has-miR-124, pLenti-III-GFP-mir-control, psPAX2 and pMD2G plasmids (abm Inc., Canada) were cultured in LB-ampicillin broth and LB-kanamycin broth (Merck Darmstadt, Germany), respectively and incubated in shaker-incubator at 37˚C at 120 rpm. After that, plasmid extraction was done using a DNA purification kit (NucleoBond^{R} Xtra Midi, MACHERY-NAGEL, Germany) according to the manufacturer's instructions.

Transfection and virus packaging

In this experimental study, for virus packaging, HEK293T cells were grown in DMEM cell culture media (Gibco, USA) supplemented with 10% fetal bovine serum (FBS), 100 units/ml penicillin (Pen), 100 mg/ml streptomycin (Strep, all from Gibco, USA) and incubated in 37˚C with 5% CO_2. To passage, HEK293T cells were separated from flask by Trypsin-EDTA (Gibco, USA) and after two passages, HEK293T cells with confluency of about 70-80% were used for virus packaging. PsPAX2 plasmid comprising of the gag/pol packaging genes and pMD2.G plasmid composed of VSV-G were co-transfected with pLenti-III-miR-GFP-has-miR-124 (also pLenti-III-GFP-mir-control vector) by calcium phosphate transfection method, as previously described (Fig.1A, B) (17). Viral supernatant was collected every 12 hours post-transfection until 72 hours, and it also was centrifuged (3000×g for 10 minutes at 4˚C) to remove cell debris. Finally, viruses were concentrated using ultracentrifugation at 21000 rpm at 4˚C for 3 hours. Viral titration was performed on HEK293T cells with a serial dilution of the viral stock. Virus stock was aliquoted and it was frozen at -70˚C for further use.

Cell culture and transduction

HEK293T and L-363 myeloma cell lines were purchased from Pasture Institute (Iran). L-363 cells were cultured in RPMI-1640 (Gibco, USA) supplemented with 10% FBS and 1% Pen/Strep. They were then cultured at 37˚C in a 5% CO_2 incubator. For stable expression of miR-124, L-363 cells were transducted with lentiviruses by spinoculation protocol which increases transduction efficiency in the presence of 6 mg/ml polybrene (Sigma-Aldrich, USA) (Fig.1C, D).

RNA extraction, cDNA synthesis and quantitative reverse-transcription polymerase chain reaction

Total RNA was extracted using QIAzol Reagent (Qiagen, USA) according to the manufacturer's instructions. Total RNA-including miRNAs and mRNAs were used for cDNA synthesis following the manufacturer's protocol (Thermo Scientific, USA). For miRNA, reverse transcription was performed using a miRNA 1st-Strand cDNA Synthesis Kit (Stratagene, Agilent Technologies Inc., USA). The cDNA samples were subjected to quantitative reverse-transcription polymerase chain reaction (qRT-PCR, EvaGreen-based qRT-PCR, USA) using High-Specificity miRNA qRT-PCR Detection Kit (Stratagene, Agilent Technologies Inc., USA). Relative expression levels of miRNAs were normalized to SNORD-47 as an endogenous control. For mRNAs, *β-ACTIN* was used as reference gene in the qRT-PCR reaction. In the next step, PCR and qRTPCR were done in order to evaluate miR-124, *EZH2* and *CDCN2A* expression levels. Taq DNA polymerase 2x Master Mix Red and Real Q-PCR 2x Master Mix Kit (Amplicon, Denmark) was used for PCR and qRT-PCR, respectively. Relative expression levels of miRNA and other genes were calculated using the $2^{-\Delta\Delta Ct}$ method. The primer sequences are provided in Table 1.

Flow cytometric analysis

Flow cytometry was used for both evaluations of GFP-expressing transduced cells and cell cycle analysis.48 hours post-transduction, L-363 cells were checked to find GFP-positive cells (Fig.2). In order to analyze cell cycle, the L-363 cells were fixed with cold (-20˚C) 70% ethanol. Afterward, the cells were washed in phosphate buffered saline with tween-20 (PBST). They were suspended again in 0.5 ml PBST, comprising 20 µg/ml RNase, and incubated at 37˚C for 40 minutes. Then, the cells were stained with 20 µg/ml propidium iodide (PI) for 30 minutes at 37˚C. DNA quantity was measured using a Flow-cytometry (BD Biosciences, USA).

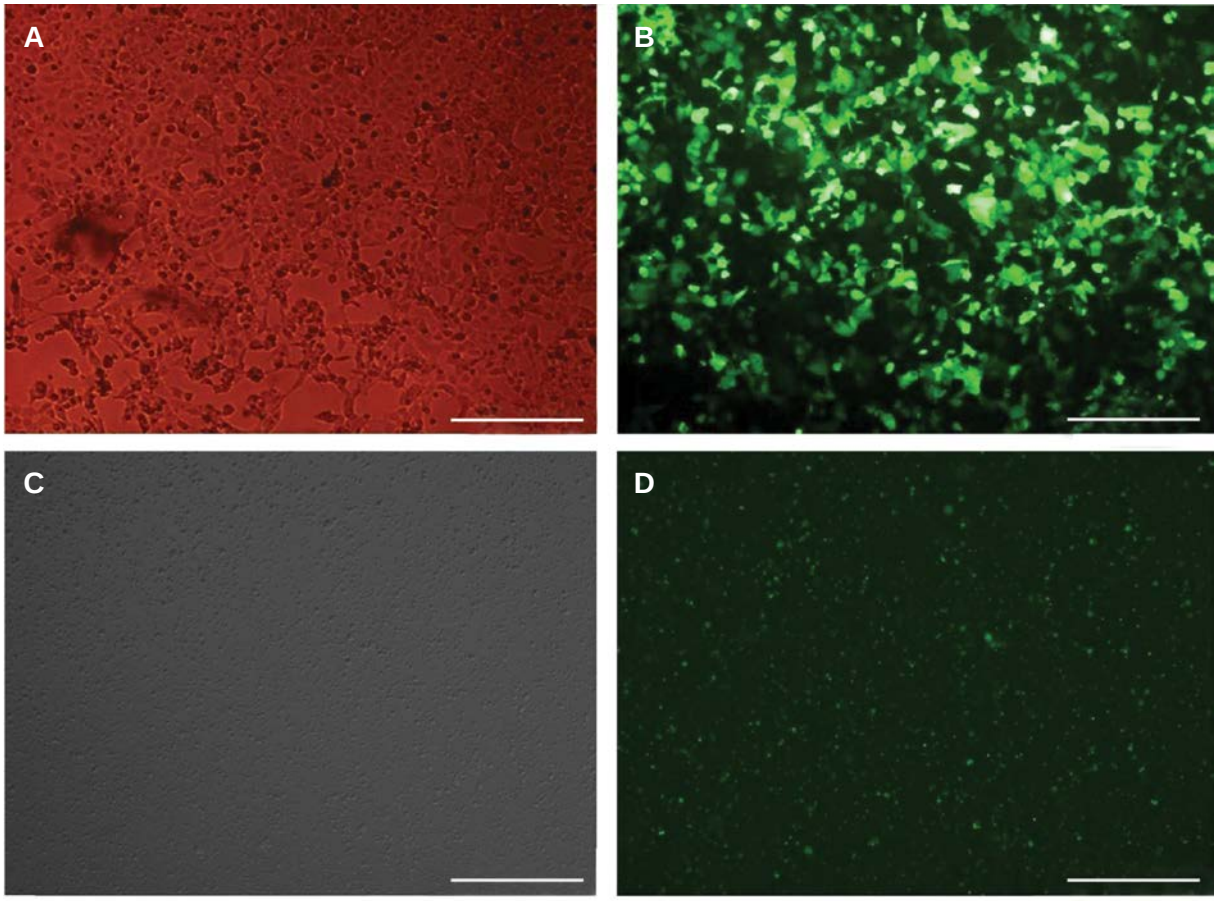

Fig.1: Light and fluorescent microscopic pictures of HEK293T and L-363 cells 48 hours post-transfection (×10). **A.** Light microscopic picture of the HEK cells (scale bar: 100 µm), **B.** The HEK cells transfected with pLenti-III-mir-GFP-124 (scale bar: 100 µm), **C.** Light microscopic picture of the L-363 cells, 48 hours post-transduction (×4), and **D.** The L-363 cells transduced with pLenti-III-miR-GFP-has-miR-124 (scale bar: 200 µm).

Table 1: List of the primers used in quantitative reverse-transcription polymerase chain reaction (qRT-PCR) analyses

Genes	Primer type	Primer sequence (5´-3´)
hsa-miR124-3p	stem-loop RT primer (For cDNA synthesis)	GTC GTA TCG AGA GCA GGG TCC GAG GTA TTC GCA CTC GAT ACG ACG GCA TT
	Forward	GCT AAG GCA AGC GGT G
	Reverse (Common for both miR and Snord)	GAG CAG GGT CCG AGG T
SNORD-47	RT	GTC GTA TGC AGA GCA GGG TCC GAG GTA TTC GCA CTG CAT ACG ACA ACC TC
	Forward	ATC ACT GTA AAA CCG TTC CA
EZH2	Forward	TAC TTG TGG AGC CGC TGA C
	Reverse	CTG CCA CGT CAG ATG GTG
CDKN2A	Forward	CCC AAC GCA CCG AAT AGT TA
	Reverse	ACC AGC GTG TCC AGG AAG
B-ACTIN	Forward	CTG GAA CGG TGA AGG TGA CA
	Reverse	AAG GGA CTT CCT GTA ACA ATG CA

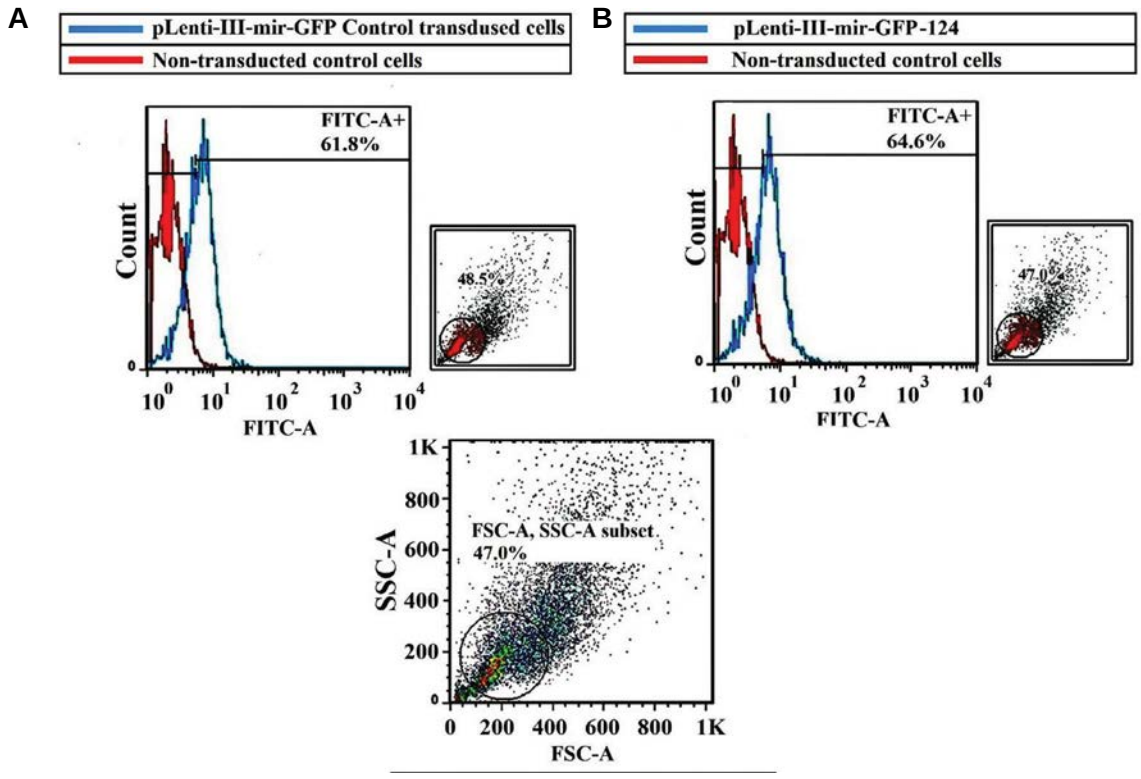

Fig.2: Flow cytometric data of virus transduced L-363 cells 48 hours post-transduction. **A.** PLenti-III-GFP-mir-control transduced cells and **B.** PLenti-III-miR-GFP-has-miR-124 transduced cells. Results show 61.8% and 64.6% GFP-expressing cells for control and miR-transduced cells, respectively.

Proliferation assay

MTT assay was done in 96-well plates for evaluating cell proliferation. Briefly, the L-363 cells (5×10^3 per well) were seeded in 100 µl culture medium in a 96-well plate. Then, 10 µl MTT (5 mg/ml in PBS, Sigma-Aldrich, USA) was added to each well and incubated at 37˚C for 3 hours. At the end, the supernatant was changed with 100 µl dimethyl sulfoxide (DMSO, Sigma-Aldrich, USA) and absorption of viable cells were measured at 570 nm using a microplate ELISA reader (Labomed, USA). The wells containing only DMSO (without cells) have been used as a blank.

Statistical analysis

The obtained data were analyzed by SPSS 18.0. Student's t test was used to compare the results. All data are presented as means ± standard error (SE) of triplicate determinant. $P<0.05$ was considered statistically significant in all experiments.

Results

Expression level of miR-124 in L-363 cells after transduction

To evaluate up-regulation of miR-124 after transduction, expression level of this microRNA was assessed by qRT-PCR in transduced (as well as non-transduced) L-363 cell line after 72 hours post-transduction. Comparing the results of pLenti-III-miR-GFP-has-miR-124 and pLenti-III-GFP-mir-control vector-transduced cells with non-transduced L-363 cells, relatively showed respectively about 2.8 ± 0.2 and 87.4 ± 2.4 fold expression changes (Fig.3A).

Gene expression analyses of *EZH2* and *CDKN2A*

EZH2 and *CDKN2A* gene expressions were evaluated after 72 hours and 96 hours post-transduction. *EZH2* gene expression in pLenti-III-mir-GFPcontrol vector and pLenti-III-miR-GFP-has-miR-124 transduced cells showed about 2.3 ± 0.13 and 1.3 ± 0.08 fold after 72 hours ($P<0.01$) and also about 0.4 ± 0.04 and 1.3 ± 0.01 fold after 96 hours ($P<0.001$), respectively (Fig.3B). These changes showed down-regulated status of *EZH2* in the miR-transduced cells compared to the control group. Fold changes were calculated in comparison with the non-transduced cells. qRT-PCR analysis of *CDKN2A* gene showed interesting results, including no detectable expression in none of the non-transduced and transduced cells, except the cells evaluated 96 hours after transduction. The expression level of *CDKN2A* was changed with a delay. Thus, 96 hours after forced expression of miR-124, *CDKN2A* level showed up-regulation.

miR124- overexpression effect on cell cycle

Similar to the gene expression analysis, three groups were studied for cell cycle analysis. Flow-cytometric data showed perturbations in pLenti-III-miR-GFP-has-miR-124 transduced cells in comparison with pLenti-III-GFP-mir-control vector and non-transduced cells. It seems that miR-124 overexpression increases the percentage of cells in G1 phase with a concomitant reduction in the percentage of cells in the S phase. About 34.72% ± 1.2% of L-363 cells expressing miR-124 were arrested in G1 phase, in comparison with 28.76% ± 0.5% and 30.73% ± 0.54% for pLenti-III-GFP-mir-control vector and non-transduced cells, respectively ($P<0.05$, Fig.4).

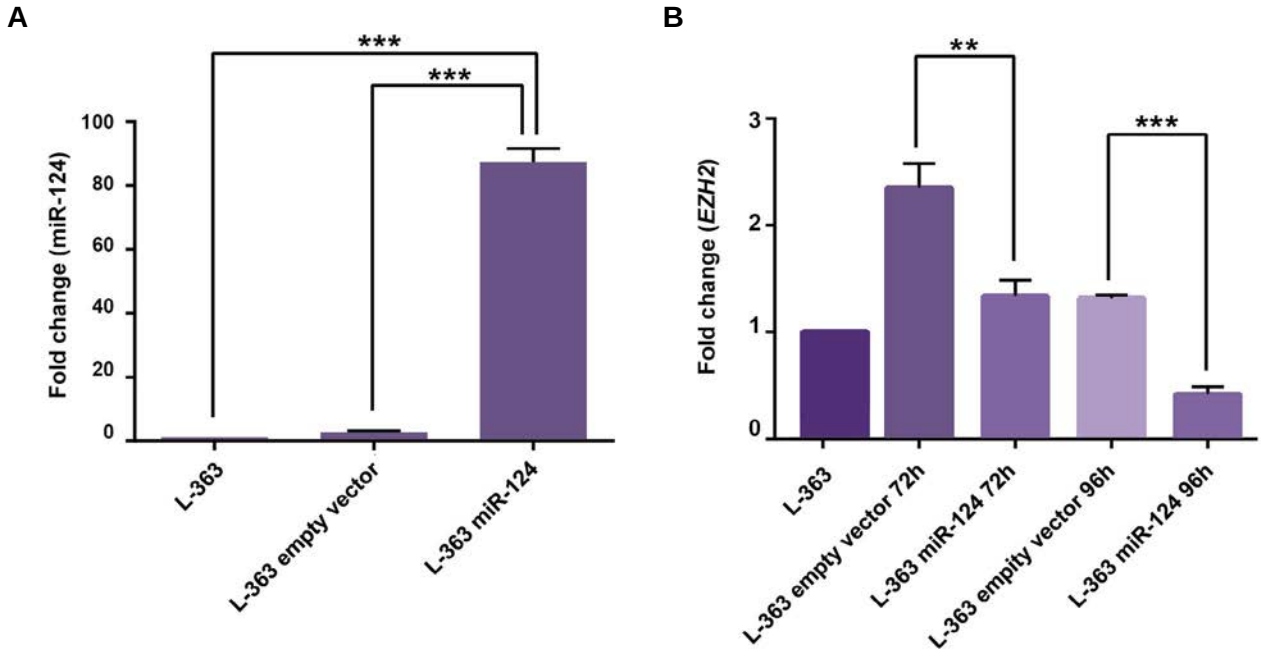

Fig.3: miR-124 and *EZH2* expression fold changes before and after transduction. **A.** Expression levels of miR-124 evaluated by quantitative reverse-transcription polymerase chain reaction (qRT-PCR) in the transduced L-363 cells with miR-124 in comparison with the empty vector group and the cells without transduction (after 72 hours) and **B.** Expression levels of *EZH2* evaluated by qRT-PCR in L-363 cells transduced with miR-124 in comparison with the empty vector transduced group and the cells without transduction (after 72 and 96 hours). **; P<0.01 and ***; P<0.001. Experiments were performed at least three times, independently.

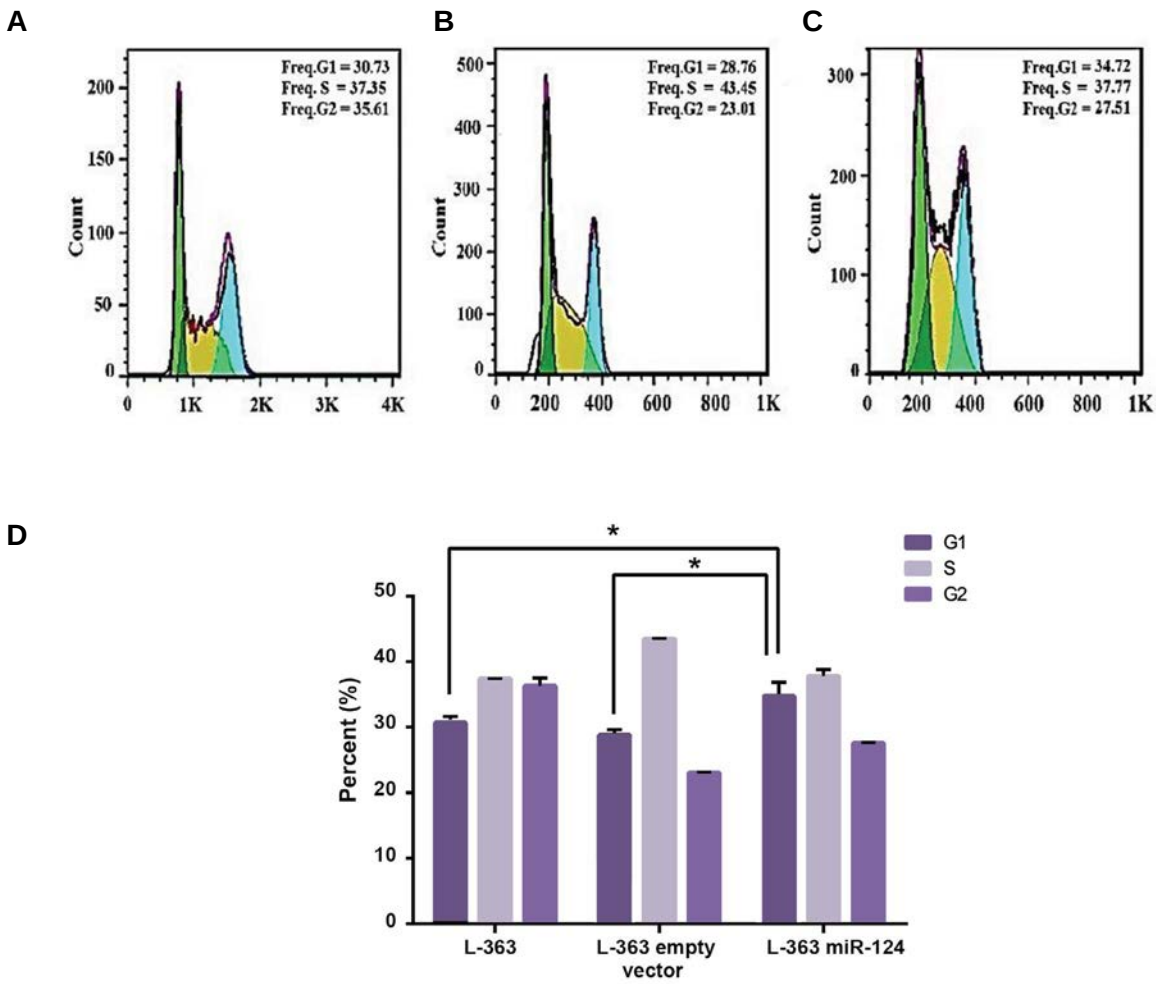

Fig.4: Cell cycle analysis of L-363 cells before and after transduction of miR-124. **A.** L-363 cells before transduction, **B.** Empty vector-transduced L-363 cells, **C.** miR-124 transduced-L-363 cells (means ±SE), and **D.** Representative bar graph of the L-363 cells cycle before and after transduction. *; P<0.05.

Cellular viability and proliferation rate change after miR-124 induction

We used MTT assay to estimate cell viability and proliferation. In line with cell cycle results, MTT assay showed a significant decline in the viability and proliferation of cells with an elevation of miR-124 level (Fig.5).

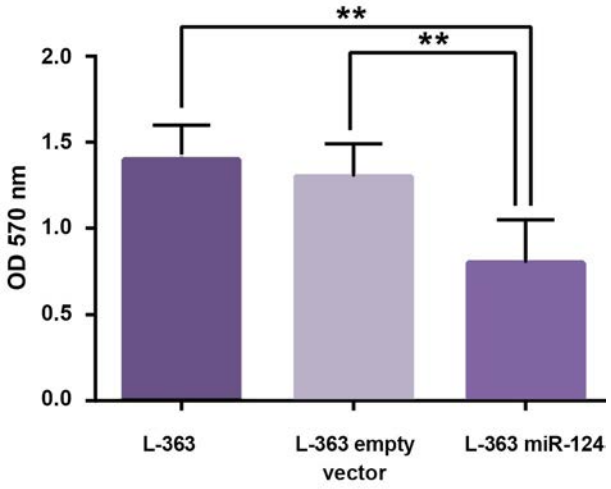

Fig.5: MTT assay results in 96 hours post-transduction. L-363 cells transduced with miR-124 show decreased absorbance in 570 nm compared to the control groups. **; P<0.01.

Discussion

Accumulating data showed changing epigenome in malignancies. So this area of research could be considered as a promising approach for the treatment of various cancers (18, 19). Without direct changing of DNA sequences, epigenetic mechanisms have the robust capability to control different genes expression status. In this study, we attempted to reveal another role of miR-124 in epigenetic of MM disease, through modulation of core enzymatic subunit of PRC2, EZH2, in gene expression status of *CDKN2A* locus. Previously Zhan et al. (20) showed that EZH2 level along with 30 other genes has different expression status in normal and malignant plasma cells. Moreover, a straight correlation between EZH2 level with cancer progression has been detected (9).

miR-124 was recognized to be down-regulated in many types of cancer. It has also been reported as tumor suppressor microRNA. It has been shown that the miR-124 expression is decreased in leukemic cell lines e.g. MM cell (14). Among 9217 target genes predicted for miR-124 in microRNA.org (http://www.microrna.org), 3′-UTR of *EZH2* has been shown to have a complementary sequence for binding to miR-124. In line with the previous studies, our results confirmed that *EZH2* is a target gene of miR-124 (15, 16).

Numerous studies have reported down-regulation of *CDKN2A* in almost all MM cases, despite infrequent genetic aberrations of the related gene. Promoter hyper-methylation of the *CDKN2A* occurs only in 40% of patient with MM (21-23). Additionally, promoter methylation of *CDKN2A* does not seems to be the sole or at least the main element of silencing this locus, since even the cases without promoter methylation status express low level of *CDKN2A* gene (3, 22). Through specific inhibiting *EZH2* expression, mediated by miR-124, we suggested that this histone modifying enzyme can be among the key elements causing *CDKN2A* low expression in MM. We showed that inhibition of PRC2 complex through targeting *EZH2* by miR-124 would lead to increased expression level of *CDKN2A* gene. This result was consistent to Overhoff et al. (24) who found a positive feedback loop between senescence-associated miRNAs targeting *EZH2* and inducing *CDKN2A* gene in both human epithelial cells and fibroblasts. These findings suggest a potential approach for recovery of *CDKN2A* expression level by targeting epigenetic suppressor complexes in MM disease.

There are several cell cycle studies showing that G1 controlling proteins which are suppressed in most MM cases. This suggests the critical role of negative cell cycle checkpoint regulators, such as P16 in MM's pathogenesis (3, 21, 25). By inhibiting EZH2, through overexpression of a miRNA, we proposed a simple and efficient strategy to increase *CDKN2A* expression. This resulted in a decrease of proliferation and viability of myeloma cell line. We showed that indirect up-regulation of *CDKN2A* gene, through exogenous expression of miR-124, resulted in increasing the number of cells accumulated in the G1 phase of the cell cycle. Moreover, it was shown that prolonged G1 arrest would diminish anti-apoptotic proteins like IRF4, which protecting myeloma cells from apoptosis or decreasing chemo-resistance (26).

It has been previously determined that *INK4b-ARF-CDKN2A* locus encoding three important tumor suppressors, $P15^{INK4b}$, $P14^{ARF}$, and $P16^{INK4a}$ is tightly controlled (27). Different factors participate in the regulation of this locus along with PRCs (PRC1 and PRC2), including long non-coding RNAs (lncRNAs), specially ANRIL (28). So, for sufficient elevation of gene expression levels in this locus, targeting two or more molecules could likely reinforce arbitrary impacts on *CDKN2A*.

Conclusion

Collectively, *CDKN2A* is a vital controller of the cell cycle in malignant plasma cells. It is negatively affected by suppressive histone marks, through PRC complexes. miR-124 is able to eliminate adverse impacts on the expression level of *INK4b-ARF-CDKN2A* locus through targeting EZH2. However, multiple factors are involved in PRC2-mediated histone changes; therefore, other factors like structural subunits of PRC complex as well as ANRIL, working as an scaffold for PRC complexes, can be targeted along with EZH2. It can also be recommended

for future researches that miR-targeted cells can be treated with chemotherapeutical agents coincidently and following analysis can reveal efficiency of this anti-cancer strategy.

Acknowledgements

This study was performed and funded by Department of Hematology, Faculty of Medical Sciences, Tarbiat Modares University (Tehran, Iran) and Hematology, Oncology and Stem Cell Transplantation Research Center, Tehran University of Medical Sciences (Tehran, Iran). The authors declare no competing interests in this study.

Authors' Contributions

J.S.T., A.A.F.; Participated in study design, data collection and evaluation, drafting and statistical analysis, and performed the research. S.A., J.S.T., M.N., S.M.; Contributed to conception and design. J.S.T., A.A.F., S.M.A.H.R.; Statistical and data analyzing. All authors performed editing and approving the final version of this manuscript for submission, also participated in the finalization of the manuscript and approved the final draft.

References

1. Rajkumar SV. Multiple myeloma: 2018 update on diagnosis, risk-stratification, and management. Am J Hematol. 2018; 93(8): 981-1114.
2. Hoang PH, Dobbins SE, Cornish AJ, Chubb D, Law PJ, Kaiser M, et al. Whole-genome sequencing of multiple myeloma reveals oncogenic pathways are targeted somatically through multiple mechanisms. Leukemia. 2018; 32(11): 2459-2470.
3. Gonzalez-Paz N, Chng WJ, McClure RF, Blood E, Oken MM, Van Ness B, et al. Tumor suppressor p16 methylation in multiple myeloma: biological and clinical implications. Blood. 2007; 109(3): 1228-1232.
4. Sherborne AL, Hosking FJ, Prasad RB, Kumar R, Koehler R, Vijayakrishnan J, et al. Variation in CDKN2A at 9p21. 3 influences childhood acute lymphoblastic leukemia risk. Nat Genet. 2010; 42(6): 492-494.
5. Yu H, Yang L, Fu Y, Gao M, Tian L. Clinicopathological significance of the p16 hypermethylation in multiple myeloma, a systematic review and meta-analysis. Oncotarget. 2017; 8(47): 83270-83279.
6. Dimopoulos K, Gimsing P, Grønbæk K. The role of epigenetics in the biology of multiple myeloma. Blood Cancer J. 2014; 4: e207.
7. Tessarz P, Kouzarides T. Histone core modifications regulating nucleosome structure and dynamics. Nat Rev Mol Cell Biol. 2014; 15(11): 703-708.
8. Audia JE, Campbell RM. Histone modifications and cancer. Cold Spring Harb Perspect Biol. 2016; 8(4): a019521.
9. Kim KH, Roberts CW. Targeting EZH2 in cancer. Nat Med. 2016; 22(2): 128-134.
10. Völkel P, Dupret B, Le Bourhis X, Angrand PO. Diverse involvement of EZH2 in cancer epigenetics. Am J Transl Res. 2015; 7(2): 175-193. eCollection 2015.
11. Anreddy N, Hazlehurst LA. Targeting intrinsic and extrinsic vulnerabilities for the treatment of multiple myeloma. J Cell Biochem. 2017; 118(1): 15-25.
12. Croonquist PA, Van Ness B. The polycomb group protein enhancer of zeste homolog 2 (EZH2) is an oncogene that influences myeloma cell growth and the mutant ras phenotype. Oncogene. 2005; 24(41): 6269-6280.
13. Liz J, Esteller M. lncRNAs and microRNAs with a role in cancer development. Biochim Biophys Acta. 2016; 1859(1): 169-176.
14. Wong KY, So CC, Loong F, Chung LP, Lam W, Liang R, et al. Epigenetic inactivation of the miR-124-1 in haematological malignancies. PLoS One. 2011; 6(4): e19027.
15. Xie L, Zhang Z, Tan Z, He R, Zeng X, Xie Y, et al. microRNA-124 inhibits proliferation and induces apoptosis by directly repressing EZH2 in gastric cancer. Mol Cell Biochem. 2014; 392(1-2): 153-159.
16. Neo WH, Yap K, Lee SH, Looi LS, Khandelia P, Neo SX, et al. MicroRNA miR-124 controls the choice between neuronal and astrocyte differentiation by fine-tuning Ezh2 expression. J Biol Chem. 2014; 289(30): 20788-20801.
17. Langroudi L, Jamshidi-Adegani F, Shafiee A, Rad SM, Keramati F, Azadmanesh K, et al. MiR-371-373 cluster acts as a tumor-suppressor-miR and promotes cell cycle arrest in unrestricted somatic stem cells. Tumour Biol. 2015; 36(10): 7765-7774.
18. Dawson MA, Kouzarides T. Cancer epigenetics: from mechanism to therapy. Cell. 2012; 150(1): 12-27.
19. Jones PA, Issa JP, Baylin S. Targeting the cancer epigenome for therapy. Nat Rev Genet. 2016; 17(10): 630-641.
20. Zhan F, Hardin J, Kordsmeier B, Bumm K, Zheng M, Tian E, et al. Global gene expression profiling of multiple myeloma, monoclonal gammopathy of undetermined significance, and normal bone marrow plasma cells. Blood. 2002; 99(5): 1745-1757.
21. Mateos MV, García-Sanz R, López-Pérez R, Moro MJ, Ocio E, Hernández J, et al. Methylation is an inactivating mechanism of the p16 gene in multiple myeloma associated with high plasma cell proliferation and short survival. Br J Haematol. 2002; 118(4): 1034-1040.
22. Hatzimichael E, Benetatos L, Dasoula A, Dranitsaris G, Tsiara S, Georgiou I, et al. Absence of methylation-dependent transcriptional silencing in TP73 irrespective of the methylation status of the CDKN2A CpG island in plasma cell neoplasia. Leuk Res. 2009; 33(9): 1272-1275.
23. Stanganelli C, Arbelbide J, Fantl DB, Corrado C, Slavutsky I. DNA methylation analysis of tumor suppressor genes in monoclonal gammopathy of undetermined significance. Ann Hematol. 2010; 89(2): 191-199.
24. Overhoff MG, Garbe JC, Koh J, Stampfer MR, Beach DH, Bishop CL. Cellular senescence mediated by p16INK4A-coupled miRNA pathways. Nucleic Acids Res. 2014; 42(3): 1606-1618.
25. Wang X, Zhu YB, Cui HP, Yu TT. Aberrant promoter methylation of p15 INK4b and p16 INK4a genes may contribute to the pathogenesis of multiple myeloma: a meta-analysis. Tumour Biol. 2014; 35(9): 9035-9043.
26. Huang X, Di Liberto M, Jayabalan D, Liang J, Ely S, Bretz J, et al. Prolonged early G(1) arrest by selective CDK4/CDK6 inhibition sensitizes myeloma cells to cytotoxic killing through cell cycle-coupled loss of IRF4. Blood. 2012; 120(5): 1095-1106.
27. Gil J, Peters G. Regulation of the INK4b–ARF–INK4a tumour suppressor locus: all for one or one for all. Nat Rev Mol Cell Biol. 2006; 7(9): 667-677.
28. Kotake Y, Nakagawa T, Kitagawa K, Suzuki S, Liu N, Kitagawa M, et al. Long non-coding RNA ANRIL is required for the PRC2 recruitment to and silencing of p15(INK4B) tumor suppressor gene. Oncogene. 2011; 30(16): 1956-1962.

Original Article

Phospholipase-Cγ1 Signaling Protein Down-Regulation by Oligoclonal-VHHs based Immuno-Liposome: A Potent Metastasis Deterrent in HER2 Positive Breast Cancer Cells

Ommolbanin Asadpour, Ph.D.[1], Fatemeh Rahbarizadeh, Ph.D.[1, 2*]

1. Department of Medical Biotechnology, Faculty of Medical Sciences, Tarbiat Modares University, Tehran, Iran
2. Research and Development Center of Biotechnology, Tarbiat Modares University, Tehran, Iran

Corresponding Address: P.O.Box: 14115-331, Department of Medical Biotechnology, School of Medical Sciences, Tarbiat Modares University, Tehran, Iran
Email: rahbarif@modares.ac.ir

Received: 7/January/2019, Accepted: 23/February/2019

Abstract

Objective: The purpose of this study was to develop multivalent antibody constructs via grafting anti-HER2 antibodies, including Herceptin and oligoclonal-variable domain of heavy chain antibodies (VHHs), onto liposome membranes to enhance antibody activity and compare their effect on phospholipase C (PLC) signaling pathway with control.

Materials and Methods: In this experimental study, SKBR3 and BT-474 cell lines as HER2 positive and MCF10A cell line as normal cell were screened with anti-HER2 antibodies, including constructs of multivalent liposomal antibody developed with Herceptin and anti-HER2 oligoclonal-VHHs. To confirm the accuracy of the study, immunofluorescent assay, migration assay and immuno-liposome binding ability to HER2 were evaluated. Finally, the antibodies effect on PLCγ1 protein level was measured by an immunoassay method (ELISA).

Results: In the present study, by using multivalent form of antibodies, we were able to significantly inhibit the PLCγ1 protein level. Interestingly, the results of migration assay, used for study the motility of different types of cell, shows correspondingly decreased number of immigrated cells in SKBR3 and BT-474 cell lines. Since MCF10A cells show no overexpression of HER2, as expected, the result did not show any change in PLCγ1 level. Moreover, immunofluorescent assay has confirmed high expression of HER2 in SKBR3 and BT-474 cell lines and low HER2 expression on MCF10A cell line. High binding of immuno-liposome to SKBR3 and BT-474 cells and low binding to MCF10A confirmed that in this study anti-HER2 antibodies have conserved binding ability to HER2 even after conjugation with liposome.

Conclusion: PLCγ1 protein levels did indeed decrease after treatment with immuno-liposome form of compounds in both two tested cell lines, verifying the inhibition ability of them. Moreover, an elevated antibody activity is associated with liposomes conjugation suggesting that immuno-liposome may be a potential target for enhancing the antibody activity.

Keywords: HER2, Liposome, Oligoclonal, Phospholipase Cγ1, VHHs

Cell Journal(Yakhteh), Vol 22, No 1, April-June (Spring) 2020, Pages: 30-39

Citation: **Asadpour O, Rahbarizadeh F. Phospholipase-Cγ1 signaling protein down-regulation by oligoclonal-VHHs based immuno-Liposome: a potent metastasis deterrent in HER2 positive breast cancer cells. Cell J. 2020; 22(1): 30-39. doi: 10.22074/cellj.2020.6704.**

Introduction

Breast cancer is a well-known cancer among women worldwide (1, 2). Amplification of HER2 oncogene, as a member of the epidermal growth factor receptor (EFGR, also knwon as HER) family in human, leads to expansion and progression of the defined offensive types of breast cancer. Moreover, it has been known that HER2 plays a critical role in uncontrolled propagation of cancer cells in breast cancer through dysregulation of HER2-mediated signaling pathways. Hence, in the last decades, HER2 targeting has been applied as a strategy for curing this type of cancer (3). The previous studies showed that HER2 has no specific ligand and activated by homo- or hetero-dimerization with other family members such as HER1 and HER3. In addition, HER2 dimerization results in auto-phosphorylation on tyrosine and cytoplasmic domain residues of the receptors result in a variety of signaling pathways including phospholipase C (PLC) initiates (4, 5).

PLC, which belongs to membrane-associated enzyme family, plays a remarkable role in signal transduction pathways in response to hormones, growth factors and neurotransmitters. PLC hydrolyzes phospholipid phosphatidylinositol 4 and 5-bisphosphate (PIP2) to produce 1,2-diacylglycerol (DAG) and inositol 1,4,5-trisphosphate (IP3). Therefore, DAG and IP_3 act as significant secondary messengers in initiating various cellular processes as well as substrating the synthesis of some important signaling molecules. Based on PLC similarities in their conserved core structure and its different act in the specific domains of each family, they are classified into six isotypes, including PLCβ, PLCγ, PLCδ, PLCε, PLCζ and PLCη in mammals (6). The γ1 isoform of PLC is one of the popular signaling proteins, with a molecular weight of 145-kDa, encoded by *PLCγ1* gene in humans. it is activated in response to growth factors or integrin receptors-dependent pathways (7, 8). Phosphorylation on tyrosine residue 783 of PLCγ1 activates this enzyme to contribute critical roles in cell migration, invasion and spreading in cancers (7, 9, 10).

By studying PLCγ1 and the corresponding role in tumors like breast carcinomas, it was clarified that extreme expression of PLCγ1 facilitates cancer metastasis, while blocking this protein will halt the cancer expansion (7, 11). Consequently, PLCγ1 can be considered as a key regulator in cell migration upon RTK signaling and the development of new anti-cancer drugs could be an ongoing research field around this protein (12).

Recombinant antibody technologies, generating novel drug formats, honored the Nobel Prize in 1970 and considered as a revolution in Immunology (13, 14). A variable domain of heavy chain antibodies (VHH), as the novel member of recombinant antibodies which is found in Camelidae, consists of a single monomeric variable antibody domain, applying selective binding to a specific antigen. Molecular weight of this extraordinary fragment is 15 kDa and it is characterized by 4 nm height and a 2.5 nm diameter and with desirable properties such as convenient cloning, affordable manufacturing, supreme stability and invisible epitopes binding that make it an attractive option in cancer treatment (15-18).

Monoclonal antibody (mAb) has a monovalent affinity for the same epitope on an antigen which may lead to certain limitations such as resistance and limited efficacy in therapy. In contrast, oligoclonal antibodies, as the new model of this era, mimics the natural immune system and consist of a mixture of mAb clones. Altogether, they show specificity of monoclonal antibodies as well as sensitivity and affinity of polyclonal antibodies. Therefore, a combination of monoclonal antibodies with an oligoclonal-based approach might be more effective than monotherapy (19).

Multivalent antibody constructs, as a novel product in therapeutic purposes, attracted more attention within the last few years. This structure consists of a suitable surface to bind into 10s-100s of molecules in order to increase the efficiency of the antibody/target complex. When multivalent constructs of antibody subjects tumor antigens, capacity and avidity of the structure culminates due to target/antibody gathering (20). Consequently, they may form the fundamental aspects of developing a cancer therapy in pharmaceuticals. One way to formulate the structure is through the conjugation of antibodies on the surface of a liposome. Liposomes consist of the lipid bilayer membrane surrounding an aqueous core and attaching multiple copies of antibodies on each liposome could provide multi-valency to them (21, 22).

The present study explores an alternative strategy to enhance therapeutic activity of anti-HER2 antibodies, namely combining three distinct VHHs. The next challenge is to develop a multivalent constructs of antibodies that can effectively decrease PLCγ1 protein level compared to the control.

Materials and Methods

Cell lines and culture conditions

In this experimental study, as two HER2-overexpressing breast cancer cell lines, SKBR3 (adenocarcinoma epithelial cells) and BT-474 (ductal carcinoma epithelial cells) were purchased from DMSZ (Braunschweig, Germany). SKBR3 cells were grown in Dulbecco's Modified Eagle Medium (DMEM, Thermo Fisher Scientific, USA) enriched with 15% fetal bovine serum (FBS, Thermo Fisher Scientific, USA), 10 mg/ml insulin (Sigma-Aldrich, USA) and 1x penicillin-streptomycin (100x solutions, Thermo Fisher Scientific, USA). BT-474 cells were cultured in RPMI-1640 (Thermo Fisher Scientific, USA) supplemented with 10 mg/ml insulin, 20% FBS and 1x penicillin-streptomycin. Moreover, MCF10A (human breast fibrocystic disease/normal epithelial cells) as a HER2-negative model were grown in DMEM/Nutrient Mixture F-12 (DMEM/F12, Thermo Fisher Scientific, USA) completed with 0.001 mg/ml insulin, 20 ng/ml epidermal growth factor (EGF, Peprotech, USA), 5% horse serum (Thermo Fisher Scientific, USA), 500 ng/ml hydrocortisone (Sigma-Aldrich, USA) and 1x penicillin-streptomycin.

Purification of anti-HER2 VHHs

The anti-HER2 VHHs clones (RR4, RR3 and RR13) were isolated using phage display technique and transformed in shuffle T7 competent *E. coli* (NEB, USA) (15, 23). Luria-Bertani (LB) broth containing 100 mg/ml Kanamycin was used to produce a starter culture at 37˚C. Then, it was inoculated at a 1:1000 dilution rate into Terrific Broth (TB) contained Kanamycin and incubated at 37˚C until optical density $(OD)_{600\,nm}$ was reached to 0.5. In the next step, 0.25 mM isopropyl-ß-D-thio-galactoside (IPTG, MW 238g/mol, Sigma-Aldrich, USA) was used to induce protein expression at 18˚C overnight. After centrifugation at 5000×g for 15 minutes (4˚C), 5 ml lysis buffer (including 50 mM Na_2HP_4, 300 mM NaCl, 15 mM imidazole, 1 mM phenylmethane sulfonyl fluoride as a serine protease inhibitor from Sigma-Aldrich, 1% Triton X-100 and 100 mg/ml lysozyme, pH=8.0) was added to each gram of pellet and incubated for 30 minutes at room temperature (RT), followed by sonication (60% power, 2 cycles: 5 minutes with 5 minutes interval on ice). The yield of suspension was centrifuged at 5200×g for 30 minutes (4˚C) and the supernatant containing proteins was passed through a 0.45 µm filter immediately before applying to the column. Then, it was applied to pre-equilibrated nickel-nitrilotriacetic acid column (Ni-NTA, Qiagen, Germany) with adsorption buffer (500 mM NaCl, 50 mM NaH_2PO_4, 20 mM imidazole, pH=8.0) at 4˚C. Next, the column was washed with adsorption buffer (500 mM NaCl, 50 mM NaH_2PO_4, 20 mM imidazole, pH=7.5) five column volumes (CV). The adsorbed VHHs were eluted using the imidazole buffer (500 mM NaCl, 50 mM NaH_2PO_4, 500 mM imidazole, pH=8.0) two CVs. Purified VHHs were collected with a flow rate of 1 ml/minute, followed by de-saltation and concentration by Amicon filter (EMD Millipore, Germany) using 3 kDa cut-off. Total protein concentration was measured by Bradford assay (24) and finally analyzed by sodium dodecyl sulfate-polyacrylamide gel electrophoresis (SDS-

PAGE) (25). Purified VHHs confirmation was approved by western blotting assay (Abcam protocol, UK) using 6x-histidine tag IgG and anti-mouse-HRP antibodies with 3,3′-Diaminobenzidine (DAB, Sigma-Aldrich, USA).

Liposome preparation and characterization

Liposomes were composed of dipalmitoylphosphatidylcholine (DPPC), DSPE-PEG (2000) maleimide, cholesterol, 1.2-distearoyl-sn-glycero-3-phosphoethanolamine-N-(amino(polyethylene glycol)-2000) (DSPE-PEG2000) with respectively 7, 0.1, 2.5 and 0.4 µmol volume, obtaining from Avanti Polar Lipids (USA). After dissolving in chloroform and methanol solutions (rate of 9:1 v/v, both from Sigma-Aldrich, USA), thin biofilm was formed in a round-bottom flask. After evaporation of the resulting suspension, a rotary evaporator under low pressure (45˚C, 70 rpm) was used up to completely removing the solvents. In continue, the produced biofilm was hydrated in 1.2 ml sodium phosphate buffer (including 50 mM NaH_2PO_4, 0.15 mM NaCl and 1 mM EDTA, pH=7.0) at 70˚C resulting in spontaneously organized multi-lamellar vesicles (MLVs). Finally, the MLVs were extruded 21 times at 65˚C through 0.1 µm pore sized polycarbonate membranes (Avanti Polar Lipids, USA) using an Avanti's mini-extruder (Avanti Polar Lipids) to form small uni-lamellar vesicles. After incubation of the liposomes at RT to cool-down, they were stored at 4˚C. Produced liposome diameters were defined by a Zetasizer Nano APS (Malvern Instruments Ltd, UK) at 25˚C following the appropriate dilution with phosphate buffered saline (PBS).

Synthesis of immuno-liposomes

Anti-HER2 oligoclonal-VHHs and Herceptin (a mAb against HER2) were thiolated using 2-iminothiolane hydrochloride (Traut's reagent, Sigma-Aldrich, USA) in sodium borate buffer (composed of 0.15 M H_3BO_3 and 1 mM EDTA, pH=8.3) by incubating for 60 minutes at RT. The buffer was next concentrated and exchanged with sodium phosphatase buffer (including 50 mM NaH_2PO_4, 0.15 mM NaCl, 1 mM EDTA, pH=7.0) using appropriate Amicon filters (EMD Millipore, USA) with respectively 3 and 100 kDa cut-off. Thiolated antibodies were used in conjugation with liposomes at a molar ratio of 10:1 (2-iminothiolane: antibody). In order to do this, 50 mg of the prepared liposomes containing maleimide-terminated linker was mixed with 1.7 mg/ml of thiolated VHHs and 1 mg/ml of thiolated Herceptin under constant gentle shaking for 1 hour at RT, following unconjugated antibodies elimination by ultra-centrifugation at 30000×g for 1 hour. The sample volumes were adjusted to 1 ml with the mentioned sodium phosphate buffer and PEGylated immuno-liposomes were sterilized by transmission through a 0.22 mm sterile filter and stored at 4˚C. In continue, SDS-PAGE following on silver staining was used for confirmation of conjugation (26). The zeta potential and average size of PEGylated immuno-liposome were calculated using a dynamic light scattering technique (DLS) at maximum 830 nm laser sources and a scattering angle of 90° at RT. Three different tests were done for each estimation. The amount of bounded antibodies to liposome was calculated as described by Allen et al. (27) considering that the diameter of 17 kDa VHH molecule was around 14.2 A° and sum of the area of a cholesterol molecule and phospholipid in liposome was 81 A° for a DPPC:cholesterol, in 1:1 molar ratio (the area of polar head for phospholipid and cholesterol were respectively 72 A° and around 19 A°).

In vitro fluorescent imaging of liposomes

In order to determine binding ability of anti-HER2 antibodies, the liposomes were labeled by PKH67 green fluorescent cell linker kit (Sigma-Aldrich, USA) as described in the manufacturer's handbook with some modifications. Briefly, 1 mg liposomes was washed twice in PBS and centrifuged at 400×g for 5 minutes to obtain a loose pellet. The supernatant was then carefully aspirated and liposome was suspended in 1 ml diluent C staining vehicle (included in the kit; it is a solution to maximize dye solubility and efficiency) via gentle pipetting. After preparing 2x Dye solution (4×10^{-6} M in diluent C) immediately and before staining, liposome suspension was mixed with the dye solution (1:1) and incubated for 5 minutes with periodic mixing. The staining was stopped by adding an equal volume of 1% bovine serum albomine (BSA) for one minute. Then, the suspension was centrifuged at 400×g for 10 minutes (RT) in order to omit excess dies. Finally, the supernatant was removed and washed liposome was suspended in 10 ml PBS. 48 hours prior to preparing fluorescent-labeled liposome, SKBR3 and MCF10A cells were cultured in a 24-well plate (10000 cells per well). The growth medium was replaced with fresh medium containing 500 µg/ml of each labeled non-conjugated liposome, labeled Herceptin-conjugated liposome and labeled oligoclonal-VHHs-conjugated liposome. After 15 minutes, the cells were rinsed with PBS (pH=7.4) once and visualized using fluorescence microscopy at 635 nm wavelength.

Immunofluorscent studies of the fixed cultured SK-BR-3, BT-474 and MCF10A cells

Immunofluorscent protocol (Abcam, UK) was used to quantitate HER2 amplification on SKBR3, BT-474 and MCF10A cell lines. Briefly, the cells were grown on chambered cell culture slides (Green Bio Research, USA) to a density of 10000 cells/cm^2 in the aforesaid medium. The monolayer cells were fixed in 4% paraformaldehyde (PFA, Merck, Germany) in PBS (pH=7.3) for 20 minutes on ice. The fixed monolayer cells were blocked and permeabilized by incubation in 3% BSA, 0.1% Triton X-100 in PBS (pH=7.3) at RT for 20 minutes. Then, the cells were reacted with rabbit Anti-ErbB2 mAb (EP1045Y; final concentration of 1:250) primary antibodies (Abcam, UK) for 60 minutes at RT. Finally, 4′,6-diamidino-2-phenylindole (DAPI, 1:10000, Sigma-Aldrich, USA) was added and incubated for five minutes. The fluorescence was detected by fluorescence microscopy at 635 nm wavelength.

Cell migration assay

Cell migration assay was done in transwell polycarbonate membrane inserts (tissue-culture-treated, 24 well format, 8 µm pores, Sigma-Aldrich, USA) coated with 40 µg/ml collagen I (Sigma-Aldrich, USA). SKBR3 and BT-474 cells were pretreated with the mentioned amount of different treatments for 30 minutes and they were subsequently detached. The cells were then suspended in DMEM and RPMI-1640 containing the treatments, added (20000 cells/100 µl) to the top of each migration chamber, and allowed to migrate. After 2 and 24 hours, the membrane drained out. The cells, which had not migrated, were removed with a cotton swab. The cells on the insert filter were fixed with 4% paraformaldehyde, stained with 1% crystal violet and then counted.

Total PLCγ1 protein expression assay

To determine total PLCγ1 protein content by western blotting (Abcam, UK), the membranes were blotted with anti-PLCγ1 mouse primary mAb (Merk, Germany) visualized with anti-rabbit horseradish peroxidase (HRP)-conjugated goat secondary antibody (Elabscience, China). The protein bands were detected using the enhanced chemiluminescence (ECL) western detection system (Amersham Pharmacia Biotech, USA). B-actin antibody (Cell Signaling Technology, USA) was used as housekeeping protein.

PLCγ1 protein immunoassay

Antigen binding ability of the prepared immuno-liposomes was immediately studied after labeling. 500000 cells from each BT-474, SKBR3 and MCF10A line were seeded in T25 flasks and incubated for 24 hours. Then, the cells were subjected to 7.37 µg/ml, 19.61 µg/ml, 26.12 µg/ml, 10 µg/ml and 38.7 µg/ml of respectively RR3, RR4, RR13, Herceptin and oligoclonal-VHHs final concentration. In addition, 50 mg/ml of non-conjugated liposome, Herceptin-conjugated liposome and oligoclonal-VHHs-conjugated liposome were added to each flask. Herceptin concentration was chosen based upon the previously reported data (28)þ , and VHH concentrations were based upon the mass ratio between Herceptin (160 kDa) and VHHs (RR3, 16.9 kDa; RR4, 15.7 kDa and RR13, 16.9 kDa) and the cells were approximately at the same viability and confluence on the day of treatment. After 2 and 24 hours, the medium was discarded and the cells were washed with PBS (pH=7.4). Then, the washed cells were lysed with RIPA Buffer 10X (Cell Signaling Technology). Total protein concentration was determined by Bradford method. To detect PLCγ1 protein an enzyme-linked immunosorbent assay (ELISA) kit was used for human specific PLC gamma 1 (PLCΓ1, Cloud-Clone Corp., USA) relying on a sandwich enzyme immunoassay for *in vitro* quantitative measurement of PLCγ1 in some biological fluids. The procedure was done according to the kit handbook (SEA269hu 96 Tests). The standards or samples were added to microtiter the plate containing biotin-conjugated PLCγ1antibody. Then, HRP conjugated avidin solutions were added to each well and incubated for 30 minutes at 37˚C. Only the color of those wells that contained PLCγ1 protein was changed. The reaction was stopped using 0.2 M sulphuric acid. Finally, the level of color changing was measured spectrophotometrically at $OD_{450\ nm}$. The concentrations of PLCγ1 in the samples were determined comparing to the used standard curve.

Statistical analysis

Statistical analysis was carried out using SPSS for windows, version 16.0 (SPSS Inc., USA). A one-way ANOVA, followed by the least significant difference (LSD) test was used to compare different groups. Levels of $P<0.05$, $P<0.01$ and $P<0.001$ were considered statistically significant. Data are expressed as mean ± SD.

Results

Anti-HER2 VHHs expression and purification

A single protein band was obtained for each VHH with the expected molecular mass, as shown in the figure obtained from 12% SDS-PAGE (Fig.1A) using Coomassie blue staining. The Bradford assay results indicated obtaining almost 2.13 mg/ml, 1.95 mg/ml and 1.35 mg/ml protein for respectively RR3, RR4 and RR13 per 250 ml of bacterial culture. The validity of VHHs purification was confirmed by Immunoblot detection using mouse anti-6x his-tag IgG and anti-mouse-HRP antibodies, showing the bands around 17 kDa. This confirms successful expression and purification of the soluble VHHs (Fig.1B-E).

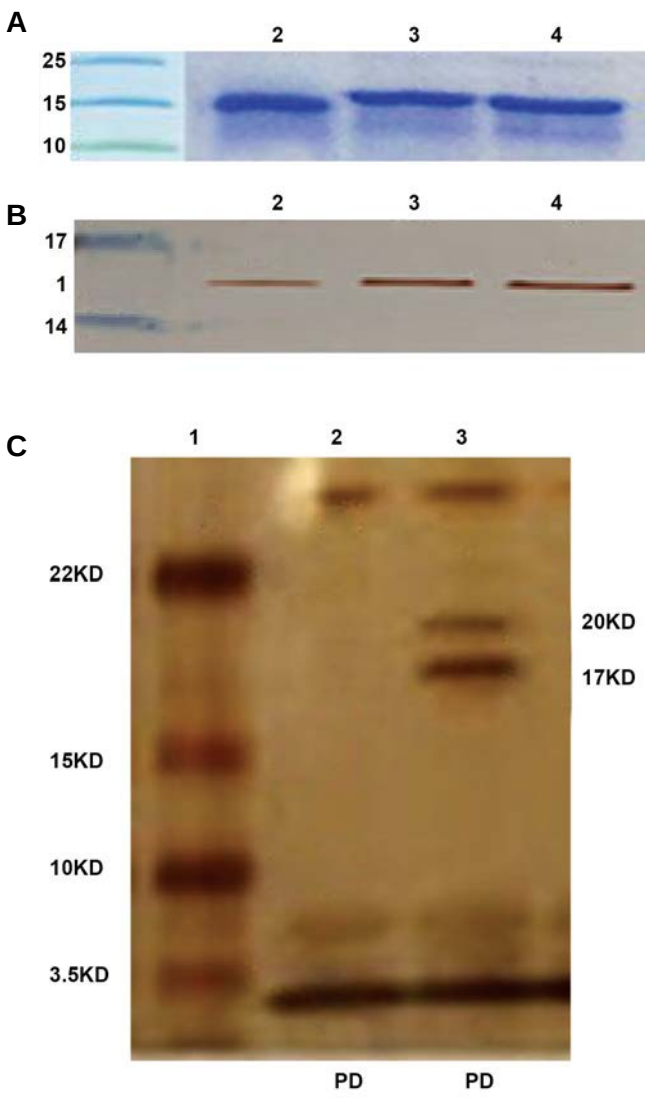

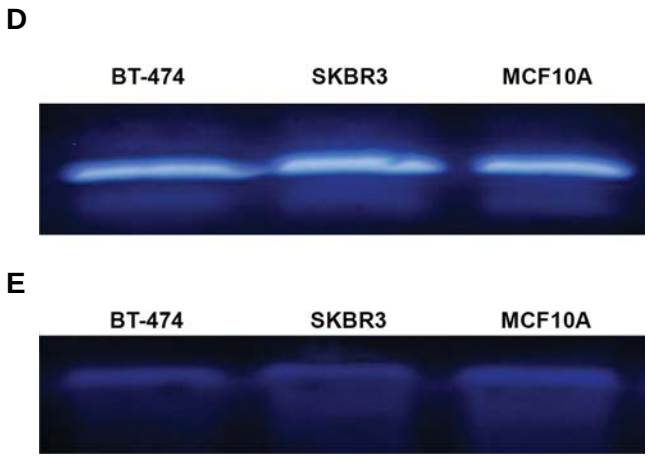

Fig.1: Expression and purification of VHHs and confirmation of its conjugation to liposome. **A.** SDS-PAGE analysis of anti-HER2 VHHs purification using nickel affinity chromatography. Lane 1; Molecular weight of protein markers, Lane 2; RR3, Lane 3; RR4, and Lane 4; RR 13, **B.** Western blotting analysis of anti-HER2 VHHs using 6x-histidine tag IgG and anti-mouse-HRP antibodies with DAB. Lane 1; Protein molecular weight marker, Lane 2; RR3, Lane 3; RR4, Lane 4; RR13, **C.** Confirmation of anti-HER2 VHHs conjugation on the surface of liposome by SDS-PAGE silver staining. Lane 1; Protein molecular weight marker, Lane 2; Non-conjugated liposome, Lane 3; VHHs-conjugated liposome and phospholipid debris, **D.** Detection of B-actin, and **E.** Total PLCγ1 expression in different breast cancer cell lines by western blotting. SDS-PAGE; Sodium dodecyl sulphate-polyacrylamide gel electrophoresis and VHH; Variable domain of heavy chain antibodies.

Characterization of liposomes

Zeta potential and particle size

Zeta potential and particle size, as two most important characterization parameters, help predict the stability and act of liposomes. Both of the size and zeta potential results showed excellent reproducibility after three times repetition (Fig.2). The results indicated a monodisperse system for the naked PEG derived liposome with the size below 100 ± 10 nm, corresponding to the diameter of polycarbonate filter, but the particle size of antibody conjugated liposome was in a mean size of 110 ± 10 nm. This confirmed VHHs conjugation with PEGylated liposomes.

Zeta potential measures the protein electrophoretic mobility that is defined by the overall charge of a particle in a particular medium. So, any subsequent modification of the liposome surface can be monitored through its measurement. While working with the cell lines, it is preferable to have a ZP which should not be too much negative, since the cell membrane is already negatively charged; thus, it causes more interactions between nano-carrier and the cell. In this study, the mean zeta potential of the naked PEG derived liposome was 0.42 ± 0.1 mV which is close to neutral range. However, it was decreased into -5 mv after liposomes modification by VHHs indicating that the VHHs induce a negative charge on the surface of liposomes to minimize nonspecific interaction with cell membrane.

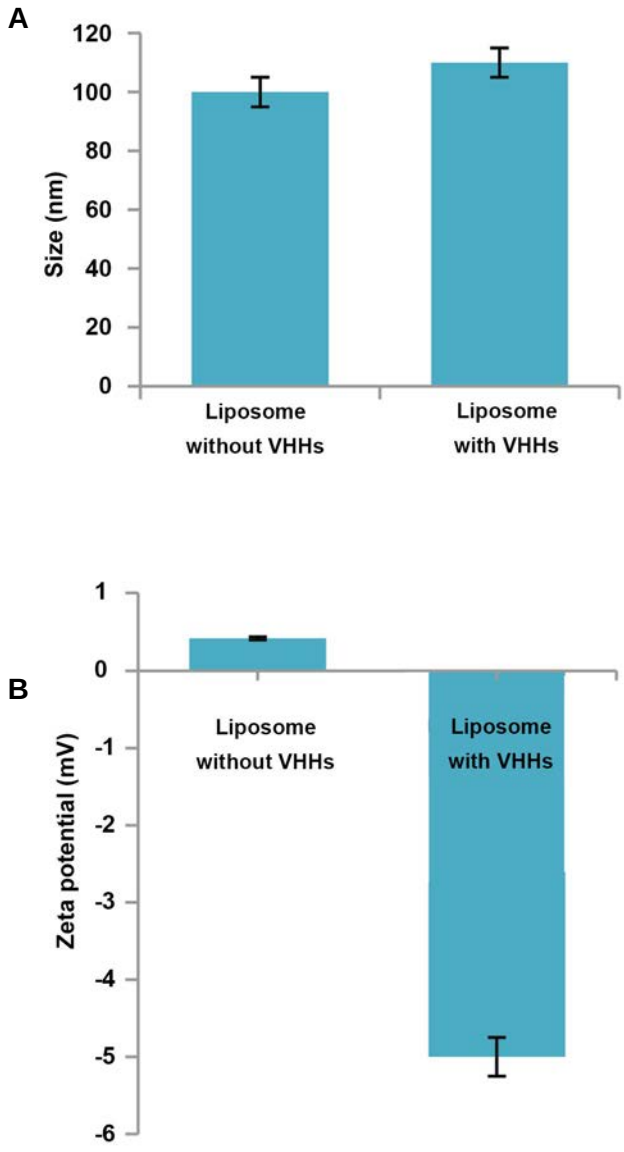

Fig.2: Physicochemical characterization of PEGylated liposome and PEGylated immuno-liposome. **A.** Mean size and **B.** Zeta potential. Data are expressed as the mean ± SD (n=3).

Determination of oligoclonal-VHHs liposome conjugation

Integrity of VHHs on liposome was confirmed by SDS-PAGE, followed by silver staining (Fig.1). The conjugated VHHs molecular weight of the band was around 20 kDa which was larger than free VHHs molecular weight (16.9 kDa). VHHs molecular weight was approximately increased 3kDa, due to the ligation of VHHs to Mal-PEG2000-DSPE. This finding showed that intact form of the VHHs was efficiently incorporated into the liposome.

In vitro fluorescent imaging of liposomes

Fluorescence-labeled liposomes were prepared from a homogeneous population of uni-lamellar liposomes by incorporating PKH67 green fluorescent dye into the liposomal phospholipid bilayer. By using a fluorescence microscopy, it was shown that cultured cells were labeled with fluorescent liposomes and a clear shine was observed (Fig.3). The results indicated strong observation of fluorescence in SKBR3 cells,

despite MCF10A cells confirmed specific binding ability of immuno-liposomes. Moreover, obtaining the similar fluorescence by Herceptin and VHHs showed comparable HER2 binding ability of VHHs against Herceptin.

Immunofluorescent analysis of the fixed cultured cells

In the preparation of the fixed cells, Immunofluorescent experiments with anti-ErbB2 antibody [EP1045Y] detected high levels of HER2 protein in SKBR3 and BT-474 as HER2 positive cell lines, compared to the MCF10A as a normal cell line (Fig.4). A notably high-strength of HER2 fluorescence signal were localized to the cell membrane in SKBR3 and BT-474 cell lines, whereas only low signal levels were found in the MCF10A control.

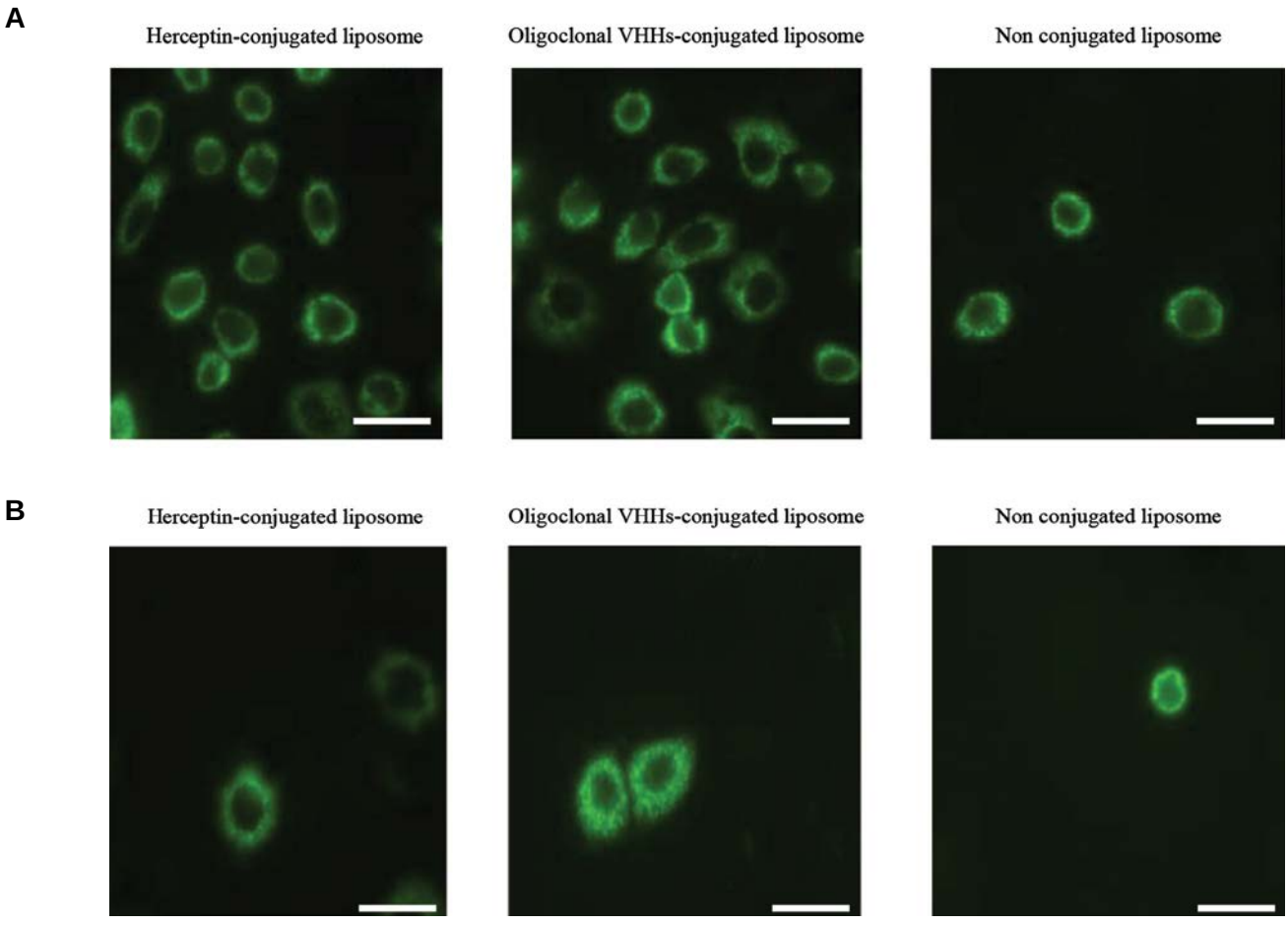

Fig.3: Representation of binding ability of PKH67 labeled Herceptin-conjugated liposome, oligoclonal VHHs-conjugated liposome and non-conjugated liposome on HER2-positive and HER2-negative cells using Nikon EcliPSE Ti fluorescence microscopy (Nikon, Japan), on **A.** SKBR3 and **B.** MCF10A cells (scale bar: 0.1 μm).

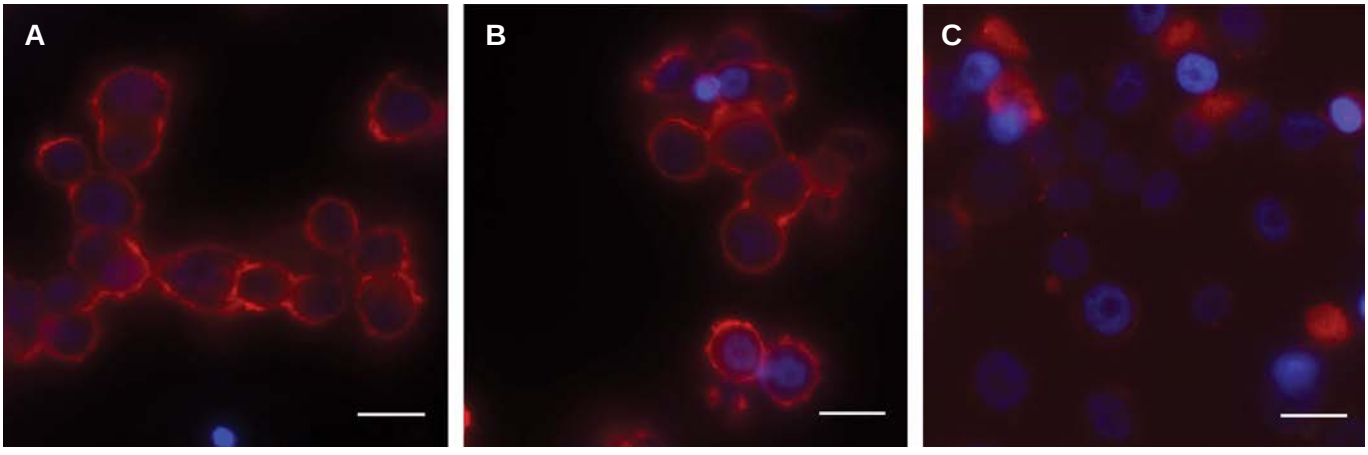

Fig.4: Immuno-fluorescent analyses of HER2 production using fluorescent anti-ErbB2 antibody [EP1045Y] ,on the fixed cultured cells of **A.** SK-BR-3, **B.** BT-474, and **C.** MCF-7 cell lines by Nikon EcliPSE Ti fluorescence microscopy. The results of this test shows high-expression of HER2 on the surface of SKBR3 cells and BT-474 cells, cells, and Very low-expression for MCF10A cells.

Immuno-liposomes detracted cell migration

We next tested the effect of different anti-HER2 antibodies on cell migration in SKBR3 and BT-474 cell lines. Treatment with Immuno-liposomes specifically reduced the cell migration as well as Herceptin and oligoclonal-VHHs in both cell lines (Fig.5). No inhibition was observed when the other treatments were used in comparison with the control.

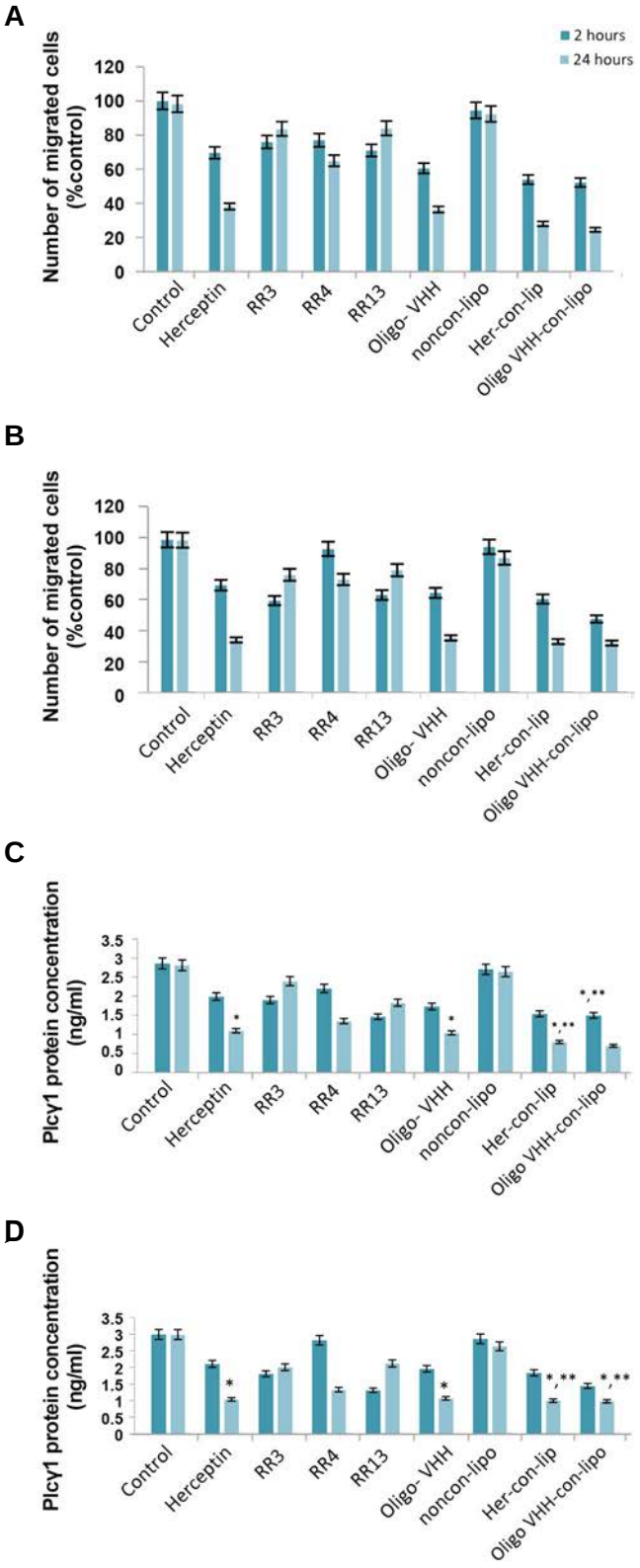

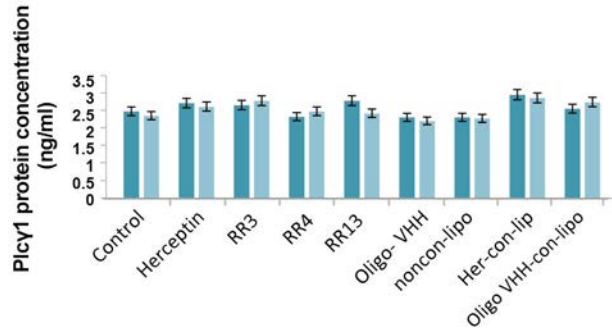

Fig.5: Functional characterization of immunoliposomes. **A.** Cell migration assay in BT-474 cells, **B.** Cell migration assay in SKBR3 cells. *In vitro* treatment of cancer cells with monovalent or liposomal antibody constructs including Herceptin, RR3, RR4, RR13, oligoclonal-VHHs (oligo-VHH), non-conjugated liposome (non-con-lipo), Herceptin conjugated liposome (Her-con-lip) and oligoclonal-VHHs conjugated liposome (oligo VHH-con-lip) in **C.** BT-474, **D.** SKBR3, as HER2 positive cell lines, and **E.** MCF10A, as a normal cell line. The total cell numbers, migrated cells and plcγ1 protein concentration were quantitated after 2 and 24 hours of different treatments. *; P<0.05 and **; P<0.01 shows the significant decrease after treatment by Herceptin and oligoclonal-VHHs individually or in conjugation with liposome against control. Data show mean ± SD.

Total PLCγ1 protein expression

High levels of PLCγ1 protein expression were detected in the SKBR3 and BT-474 positive cells for HER2 whereas the corresponding bands in the MCF10A control cells were very low (Fig.1E). All cell lines expressed clear and distinct bands of B-actin (Fig.1D) indicating integrity of the assay.

PLCγ1 protein immunoassay

The effects of free and liposome conjugated anti-HER2 antibodies on PLC pathway were studied in SKBR3, BT-474 and MCF10A cells via PLCγ1 protein level, as PLC pathway downstream target introduced as an essential factor for metastasis development and cancer progression (6). As the results showed (Fig.5), in both of HER2 positive cells, oligoclonal-VHHs and Herceptin individually or in liposome conjugated form, decreased PLCγ1 protein level in comparison with the untreated cells (SKBR3: Herceptin P=0.028, oligoconal-VHHs P=0.031, Herceptin conjugated liposome P=0.026 and oligoclonal-VHHs conjugated liposome P=0.025, BT-474: Herceptin P=0.04, oligoconal-VHHs P=0.034, Herceptin conjugated liposome P=0.011, and oligoclonal-VHHs conjugated liposome P=0.018). The result did not show any change in PLCγ1 level of MCF10A cells, since these cells showed no overexpression of HER2. In addition, activity of immuno-liposomes was magnified. In this case, the liposome form which antibodies were cumulated on its surface, increased the effect of the antibodies.

The charts represent results of different treatments in the three indicated cell lines (Fig.5). This observation collaborates with the fact that free antibodies induced a decline in the quantity of PLCγ1 protein in HER2 positive cells, emphasizing that liposomal conjugated antibodies decreased it even more significantly. It is worthy to say

that differences in the ability of individual antibody and immuno-liposomes in PLC cell signaling pathway modulation could be therapeutically important (29, 30).

Discussion

Previous studies suggested that overexpression of PLCγ1 protein is one of the key factors in cellular migration and invasion. It can be proposed as a vital enzyme in the development and maintenance of tumor metastasis (11). Despite it has been shown that PLCγ1 is activated by HER2 (1), in practice, no dedicated HER2 target has been introduced to control the activity of PLCγ1 protein (3) and it seems urgent to consider this issue.

The present study has investigated the effect of multi-capacity immuno-suppressive agents carrying anti-HER2 compounds *in vitro*. As observed, oligoclonal-VHHs and Herceptin can decrease the level of the PLCγ1 protein and immuno-liposomal application also intensifies this effect. Finding similar results in BT-474 and SKBR3 cancer cells can confirm the ability to strengthen antibody-based therapies using immuno-liposomal technology. One of the most important advantages of the multiplicity structure antibody is the increased binding reliability compared to single antibodies (31). Although clinical trials of mAb therapy have provided the best hope for increasing the clinical benefits of antibodies, especially for inhibiting signaling via tyrosine kinase receptors (32), enhancing their performance in some features such as stability, affinity, specificity and size as well as their pharmacokinetic properties are still being studied and the demand for introducing suitable alternatives has become a challenge. In this case, discovery of heavy chain antibodies in camel species has created a new opportunity (33). In comparison with conventional antibodies, heavy chain antibodies have been completely evolved in the absence of light chains, while their unique biophysical and pharmacologic properties have categorized these molecules as a new member of antibody-based therapy agents enabling them to gradually make obsolute commonly used therapeutic antibodies (34). Additionally, improvement in the expression and purification of oligoclonal antibody mixtures in the field of therapeutic agent productions provides an opportunity for imitation of the natural immune system and oligoclonal VHHs are suggested as a good tool for improving overall response. Recently, a clinical trial combined Pertuzumab and Trastuzumab with high affinity against different subdomains of the HER2 extracellular domain and reported a 24.2% response rate in HER2-positive breast cancer patients (15). Moreover, other clinical trial showed that non-overlapping binding of two anti-EGFR monoclonal antibodies promoted reduction of receptor expression on the cell surface. Furthermore, combination of Pertuzumab and Trastuzumab oligoclonal antibodies blocked HER2-dependent signals much more efficiently compared to its individual components (35).

In recent years, several strategies have been established to improve the efficiency of antibody-based therapies, among which immuno-liposomes, as a strong approach, have potential to produce multi-dose antibodies to enhance the action of antibody-based therapies. They have also been appeared as a common thread for a broad range of biological processes which can mediate the multiplicative interactions of cellular signaling by developing the cross-linking of antibody/target complex (6). Chiu et al. (21) examined the potency of free and liposomal form of Trastuzumab to detract the expression levels of HER2 and Akt, as respectively a target and downstream molecule. She demonstrated that multiplicity of liposomal Trastuzumab can reduce active regulation of the Akt phosphorylated form.

One of the remarkable cases in this study is the observation of different behavior of individual VHHs in HER2-positive cells. As the results show, RR3 and RR13 showed a decrease after two hours, followed by slightly increase in the amount of PLCγ1 protein level after 24 hours. This could strongly suggest different epitopes diagnosis and their effect on PLCγ1 protein in these two VHHs, while the effect of oligoclonal VHHs showed an increase in 2 and 24 hours. The challenge of differences in their behavior might be answered by considering the overall synergistic effect of oligoclonal-VHHs.

Prior to investigating the therapeutic effect of immuno-liposomes, it was necessary to clarify some characteristics of experiment material, including: i. The ability of immuno-liposome binding after conjugation with antibodies. Since using fluorescence microscope is considered as an effective tool for assessing the cumulative effect of liposomes (36), preparation of the labeled immuno-liposomes was performed using a PKH67 fluorescence label, which specifically affects the lipid profile of membrane, and the liposome lipid structure allows application of this fluorescent (37). According to the results, observing stronger fluorescence in SKBR3 compared to MCF10A cells confirmed successful attachment of the antibodies to the liposomal surface (8, 38). ii. Immunofluorescent method was used to study HER2 protein level on two breast carcinoma cell lines: SK-BR-3 and BT-474 compared to MCF10A, as a normal cell line. The first two cell lines were characterized in terms of higher HER2 protein content, whereas MCF10A cells have a very low HER2 protein content. The method presented here compares high and low protein content by analyzing relative intensity of signals.

iii. One of the considerable experiments was to determine total PLCγ1 protein in cell lysates by western blotting method, when an internal calibrator is included in the assay systems. B-actin antibody showed a band with the same intensity in different treatments providing accurateness in the sample quantification among different assays. Using this antibody provides a good reference for confirming the correctness of total PLCγ1 protein level estimation in different samples. By comparing the results of total and phosphorylated form of PLCγ1 protein level, it is suggested that the inhibitory effect of this protein might not be due to the inhibition of total PLCγ1 synthesis, but

it happens after the protein phosphorylation.

iv. In terms of cell migration, some studies showed a relation between PLCγ1 protein and cell migration indicating the importance of considering immigration ability, in presence of HER2.

Therefore, considering the above indications, immunoliposome has been proposed as a construct of multicapacity antibody and it can be considered as a demanding intermediary in signaling pathways associated with cell metastasis.

Conclusion

These observations are along with previous studies and prepare a stimulating prospect for improving the avidity of antibodies by enhancing the quantity of binding of antibodies to antigens, especially in oligoclonal form, in comparison with single antibodies. Oligoclonal-VHHs-conjugated liposome showed a significant elevated affinity in comparison with oligoclonal-VHHs itself. It indicates the effectiveness of these nanoparticles in targeting the HER2 receptor. Furthermore, the observation of similar results between conjugated liposomes with oligoconal-VHHs and conjugated liposomes with Herceptin suggests the possibility of comparative effects of these two antibodies on HER2 positive cancer cells. Based on the results, this study might lead to the expansion of a clinically relevant nanomaterial, whereby PLCγ1, as an effective metastasis factor, is a suitable candidate for targeting. In addition, similar effect of oligoclonal-VHHs and Herceptin in liposome conjugation form remarkably brings new hopes to treat breast cancer with higher efficiency potential by using this approach.

Acknowledgements

This article is part of a Ph.D. thesis financial supported by Department of Medical Biotechnology, Faculty of Medical Sciences, Tarbiat Modares University. This research was supported in part by Research and Development Center of Biotechnology, Tarbiat Modares University, Tehran, Iran. The authors declare no conflict of interest.

Authors' Contributions

O.A.; Contributed to all experimental work, data and statistical analysis. F.R.; Conducted all experimental work and statistical analysis and was responsible for overall supervision, preparation of the final manuscript. All authors read and approved the final manuscript.

References

1. Ferlay J, Soerjomataram I, Dikshit R, Eser S, Mathers C, Rebelo M, et al. Cancer incidence and mortality worldwide: sources, methods and major patterns in GLOBOCAN 2012. Int J Cancer. 2015; 136(5): E359-E386.
2. Salouti M. Radioimmunoscintigraphy of breast cancer. J Immun Serum Biol. 2017; 3(1): 1-2.
3. Mitri Z, Constantine T, O'Regan R. The HER2 receptor in breast cancer: pathophysiology, clinical use, and new advances in therapy. Chemother Res Pract. 2012; 2012: 743193.
4. Li SG, Li L. Targeted therapy in HER2positive breast cancer. Biomed Rep. 2013; 1(4): 499-505.
5. Tai W, Mahato R, Cheng K. The role of HER2 in cancer therapy and targeted drug delivery. J Control Release. 2010; 146(3): 264-275.
6. Falkenburger BH, Jensen JB, Dickson EJ, Suh BC, Hille B. Symposium review: phosphoinositides: lipid regulators of membrane proteins. J Physiol. 2010; 588(Pt 17): 3179-3185.
7. Burgess WH, Dionne CA, Kaplow J, Mudd R, Friesel R, Zilberstein A, et al. Characterization and cDNA cloning of phospholipase C-gamma, a major substrate for heparin-binding growth factor 1 (acidic fibroblast growth factor)-activated tyrosine kinase. Mol Cell Biol. 1990; 10(9): 4770-4777.
8. Bristol A, Hall SM, Kriz RW, Stahl ML, Fan YS, Byers MG, et al. Phospholipase C-148: chromosomal location and deletion mapping of functional domains. Cold Spring Harb Symp Quant Biol. 1988; 53 Pt 2: 915-920.
9. Seidman A, Hudis C, Pierri MK, Shak S, Paton V, Ashby M, et al. Cardiac dysfunction in the trastuzumab clinical trials experience. J Clin Oncol. 2002; 20(5): 1215-1221.
10. Walker K, Boyd NH, Anderson JC, Willey CD, Hjelmeland AB. Kinomic profiling of glioblastoma cells reveals PLCG1 as a target in restricted glucose. Biomark Res. 2018; 6: 22.
11. Sala G, Dituri F, Raimondi C, Previdi S, Maffucci T, Mazzoletti M, et al. Phospholipase Cgamma1 is required for metastasis development and progression. Cancer Res. 2008; 68(24): 10187-10196.
12. Kang DS, Yang YR, Lee C, Park B, Park KI, Seo JK, et al. Netrin-1/DCC-mediated PLCγ1 activation is required for axon guidance and brain structure development. EMBO Rep. 2018; 19(11). pii: e46250.
13. Koch J, Tesar M. Recombinant antibodies to arm cytotoxic lymphocytes in cancer immunotherapy. Transfus Med Hemother. 2017; 44(5): 337-350.
14. Cha SW, Bonissone S, Na S, Pevzner PA, Bafna V. The antibody repertoire of colorectal cancer. Mol Cell Proteomics. 2017; 16(12): 2111-2124.
15. Jamnani FR, Rahbarizadeh F, Shokrgozar MA, Ahmadvand D, Mahboudi F, Sharifzadeh Z. Targeting high affinity and epitope-distinct oligoclonal nanobodies to HER2 over-expressing tumor cells. Exp Cell Res. 2012; 318(10): 1112-1124.
16. Heidari Z, Salouti M. Targeting molecular imaging of breast cancer by radioimmunodetection method in nuclear medicine. Current Molecular Imaging. 2012; 1(1): 26-43.
17. Van Audenhove I, Gettemans J. Nanobodies as versatile tools to understand, diagnose, visualize and treat cancer. EBioMedicine. 2016; 8: 40-48.
18. Bannas P, Hambach J, Koch-Nolte F. Nanobodies and nanobody-based human heavy chain antibodies as antitumor therapeutics. Front Immunol. 2017; 8: 1603.
19. Gupta RK, Glassy MC. Oligoclonal and polyclonal antibody preparations. In: Dübel S, Reichert JM, editors. Handbook of therapeutic antibodies. Germany: Wiley-VCH Verlag GmbH & Co. KGaA; 2014; 1289-1308.
20. Saeed M, van Brakel M, Zalba S, Schooten E, Rens JA, Koning GA, et al. Targeting melanoma with immunoliposomes coupled to anti-MAGE A1 TCR-like single-chain antibody. Int J Nanomedicine. 2016; 11: 955-975.
21. Chiu GN, Edwards LA, Kapanen AI, Malinen MM, Dragowska WH, Warburton C, et al. Modulation of cancer cell survival pathways using multivalent liposomal therapeutic antibody constructs. Mol Cancer Ther. 2007; 6(3): 844-855.
22. Kontermann R. Immunoliposomes for cancer therapy. Curr Opin Mol Ther. 2006; 8(1): 39-45.
23. Nikkhoi SK, Rahbarizadeh F, Ahmadvand D. Oligo-clonal nanobodies as an innovative targeting agent for cancer therapy: new biology and novel targeting systems. Protein Expr Purif. 2017; 129: 115-121.
24. Bradford MM. A rapid and sensitive method for the quantitation of microgram quantities of protein utilizing the principle of protein-dye binding. Anal Biochem. 1976; 72: 248-254.
25. Laemmli UK. Cleavage of structural proteins during the assembly of the head of bacteriophage T4. Nature. 1970; 227(5259): 680-685.
26. Chevallet M, Luche S, Rabilloud T. Silver staining of proteins in polyacrylamide gels. Nat Protoc. 2006; 1(4): 1852-1858.
27. Allen LG, Hovey T, Love MS, Smith JTW. The life history of the spotted sand bass (Paralabrax maculatofasciatus) within the Southern California Bight. CalCOFI Rep. 1995: 36: 193-203.
28. Yakes FM, Chinratanalab W, Ritter CA, King W, Seelig S, Arteaga CL. Herceptin-induced inhibition of phosphatidylinositol-3 kinase

and Akt Is required for antibody-mediated effects on p27, cyclin D1, and antitumor action. Cancer Res. 2002; 62(14): 4132-4141.
29. Wilson CH, Ali ES, Scrimgeour N, Martin AM, Hua J, Tallis GA, et al. Steatosis inhibits liver cell store-operated Ca2+ entry and reduces ER Ca2+ through a protein kinase C-dependent mechanism. Biochem J. 2015; 466(2): 379-390.
30. Burgess WH, Dionne CA, Kaplow J, Mudd R, Friesel R, Zilberstein A, et al. Characterization and cDNA cloning of phospholipase C-gamma, a major substrate for heparin-binding growth factor 1 (acidic fibroblast growth factor)-activated tyrosine kinase. Mol Cell Biol. 1990; 10(9): 4770-4777.
31. Niwa T, Kasuya Y, Suzuki Y, Ichikawa K, Yoshida H, Kurimoto A, et al. Novel immunoliposome technology for enhancing the activity of the agonistic antibody against the tumor necrosis factor receptor superfamily. Mol Pharm. 2018; 15(9): 3729-3740.
32. Shuptrine CW, Surana R, Weiner LM. Monoclonal antibodies for the treatment of cancer. Semin Cancer Biol. 2012; 22(1): 3-13.
33. Cortez-Retamozo V, Backmann N, Senter PD, Wernery U, De Baetselier P, Muyldermans S, et al. Efficient cancer therapy with a nanobody-based conjugate. Cancer Res. 2004; 64(8): 2853-2857.
34. Moghimi SM, Rahbarizadeh F, Ahmadvand D, Parhamifar L. Heavy chain only antibodies: a new paradigm in personalized HER2+ breast cancer therapy. Bioimpacts. 2013; 3(1): 1-4.
35. D'souza JW, Robinson MK. Oligoclonal antibodies to target the ErbB family. Expert Opin Biol Ther. 2015; 15(7): 1015-1021.
36. Kamaly N, Kalber T, Ahmad A, Oliver MH, So P-W, Herlihy AH, et al. Bimodal paramagnetic and fluorescent liposomes for cellular and tumor magnetic resonance imaging. Bioconjug Chem. 2008; 19(1): 118-129.
37. Dean-Colomb W, Esteva FJ. Her2-positive breast cancer: herceptin and beyond. Eur J Cancer. 2008; 44(18): 2806-2812.
38. Shi C, Gao F, Gao X, Liu Y. A novel anti-VEGF165 monoclonal antibody-conjugated liposomal nanocarrier system: Physical characterization and cellular uptake evaluation in vitro and in vivo. Biomed Pharmacother. 2015; 69: 191-200.

Original Article

Effect of Plasma-Derived Exosomes of Refractory/Relapsed or Responsive Patients with Diffuse Large B-Cell Lymphoma on Natural Killer Cells Functions

Nasrin Zare, Ph.D.[1], Shaghayegh Haghjooy Javanmard, M.D, Ph.D.[2], Valiollah Mehrzad, M.D.[3], Nahid Eskandari, M.D, Ph.D.[1]*, Alireza Andalib, Ph.D.[1]

1. Department of Immunology, School of Medicine, Isfahan University of Medical Sciences, Isfahan, Iran
2. Department of Physiology, School of Medicine and Applied Physiology Research Center, Cardiovascular Research Institute, Isfahan University of Medical Sciences, Isfahan, Iran
3. Department of Hematology and Medical Oncology, Isfahan University of Medical Sciences, Isfahan, Iran

Corresponding Address: P.O.Box: 81746-73461, Department of Immunology, School of Medicine, Isfahan University of Medical Sciences, Isfahan, Iran
Email: neskandari@med.mui.ac.ir

Received: 18/November/2018, Accepted: 20/February/2019

Abstract

Objective: The purpose of this study was to investigate effect of plasma-derived exosomes of refractory/relapsed or responsive diffuse large B-cell lymphoma (DLBCL) patients on natural killer (NK) cell functions.

Materials and Methods: In this cross-sectional and experimental study, NK cells were purified from responsive patients (n=10) or refractory/relapsed patients (n=12) and healthy donors (n=12). NK cells were treated with plasma-derived exosomes of responsive or refractory/relapsed patients. We examined the expression levels of *hsa-miR-155-5p, hsa-let-7g-5p, INPP5D (SHIP-1)* and *SOCS-1* in NK cells quantitative reverse transcription-polymerase chain reaction (qRT-PCR). Percentages of NK cells expressing CD69, NKG2D and CD16, NK cell cytotoxicity and NK cell proliferation (using flow-cytometry) as well as interferon-gamma (IFN-γ) level in the supernatant of NK cells using ELISA were also investigated.

Results: We observed an increased level of *hsa-miR-155-5p* and a decreased level of *SOCS-1* in NK cells treated with exosomes compared to untreated NK cell in healthy donors and DLBCL patients. An increase in *hsa-miR-155-5p* level was associated with an increased level of IFN-γ in healthy donors. The decreased levels of *hsa-let-7g-5p* were observed in NK cells treated with exosomes in comparison with untreated NK cells in DLBCL patients ($P<0.05$). There was no significant difference in the percentage of $CD69^+$ NK cells and $NKG2D^+$ NK cells in the absence or presence of exosomes of DLBCL patients in each group. Furthermore, we observed significant reduction of NK cell proliferation in DLBCL patients and healthy donors in the presence of exosomes of refractory/relapsed patients ($P<0.05$). A significant decrease was observed in cytotoxicity of NK cell in patients with DLBCL treated with exosomes of responsive patients.

Conclusion: Our findings demonstrated adverse effect of plasma-derived exosomes of DLBCL patients on some functions of NK cell. It was also determined that low NK cell count might be associated with impaired response to R-CHOP and an increased recurrence risk of cancer.

Keywords: Cytotoxicity, Diffuse Large B-Cell Lymphoma, *hsa-miR-155-5p*, Interferon-Gamma, Proliferation

Cell Journal(Yakhteh), Vol 22, No 1, April-June (Spring) 2020, Pages: 40-54

Citation: **Zare N, Haghjooy Javanmard Sh, Mehrzad V, Eskandari N, Andalib AR. Effect of plasma-derived exosomes of refractory/relapsed or responsive patients with diffuse large B-cell lymphoma on natural killer cells functions. Cell J. 2020; 22(1): 40-54. doi: 10.22074/cellj.2020.6550.**

Introduction

The most common high-grade form of non-hodgkin lymphoma (NHL) is diffuse large B-cell lymphoma (DLBCL) accounting for more than 30-40% of new cases. B-cells are divided into either indolent (prolonged survival but generally incurable) or aggressive (rapid growth but potentially curable). DLBCL is an aggressive type of lymphoma which can be cured with rituximab, cyclophosphamide, doxorubicin hydrochloride (hydroxydaunomycin), vincristine sulfate (oncovin) and prednisone (R-CHOP). More than half of patients experience complete responses (CRs) and approximately 30% have partial responses (PRs). Despite the advance in treatment, relapsed and refractory disease represent a major treatment challenge; thus, about one-third of patients are either refractory to the treatment or experience relapse (1). Hence, it is necessary to optimize front-line therapy, investigate the physiologic and immunologic circumstances of the patients and develop more effectively salvage strategies (2).

Natural killer (NK) cells are differentiated from bone marrow and include 5-15% of all peripheral blood mononuclear cells (PBMC). NK cells are defined as large granular lymphocytes expressing $CD3^-CD19^-CD56^+$. NK cells contribute to immune surveillance without prior immunization or major histocompatibility complex (MHC) restriction, as a major component of innate immunity. They induce cytotoxicity or secretion of cytokine/chemokine against infected cells, malignant cells and stressed cells (3). Interferon-gamma (IFN-γ) produced by NK cells is a critical cytokine for the clearance of infectious pathogens and tumor surveillance. Efficient elimination of tumor cell generally requires collaboration between activating

and inhibitory receptors. These receptors, including NKp30, NKp46, NKG2D, DNAM-1 and the inducible co-stimulatory molecule CD137 (4-1BB), contribute to antitumor immunity (4). NK cells also express CD16 (FcγRIIIA), a low-affinity Fcγ receptor which can eliminate tumor cells bound to antibodies. CD16 marker is expressed on the cytotoxic $CD56^{dim}$ NK-cell subset, which constitutes about 90% of peripheral NK cells (5). NK cells express activating type of IIIA Fc receptor (FcRYIIIa; CD16a) on their surface. Thus, NK cell-mediated antibody-dependent cellular cytotoxicity (ADCC) occurs through binding to Antibody-coated target cells, leading to NK-cell activation and degranulation (6).

Previous studies have shown that NK cell activation by IL-2, IL-12, IL-15 and IL-18 leads to an increase in the expression levels of *hsa-miR-155-5p* and *hsa-let-7g-5p*. These cytokines activate signal transducer and activator of transcription (STATS). Then, activation of JAK/STATs triggers the suppressor of cytokine signaling (SOCS) proteins, especially SOCS-1, which is a negative regulator of this pathway and it inhibits activation of STATs. Additionally, *hsa-miR-155-5p* directly inhibits SOCS-1 expression. It seems that *hsa-miR-155-5p* could regulate activation of the NK cells by inhibiting *SOCS-1* (7).

Furthermore, NK cells stimulated by CD16 or IL-12 and IL-18 induces an increase in the *hsa-miR-155-5p* expression. Overexpression of *hsa-miR-155-5p* targets Src homology 2 domain-containing Inositol 5′-phosphatase (SHIP-1) as a negative regulator, consequently up-regulating phosphatidylinositol-3 kinase and enhancing IFN-γ production (8). IFN-γ is a critical cytokine for tumor surveillance. Therefore, understanding molecular pathways of IFN-γ expression could lead to identifying potential therapeutic targets for chronic inflammation and/or cancer. In this regard, *miR-155* could play an important role in NK cell activation, NK cell cytotoxicity and NK cell immunotherapy (9).

NKG2D is a member of CD94/NKG2 family of C-type lectin-like receptors. NKG2D is expressed by NK cells and connected to the MHC class I-related chain (MIC) A, MICB, and UL16-binding proteins (ULBPs). These proteins are expressed in the conditions of stress and disease, like cancer. Therefore, NKG2D with its ligands plays a critical role in immunosurveillance of cancer. A reduction of NKG2D ligands results in an impaired susceptibility to NKG2D-mediated cytotoxicity and systemic down-regulation of NKG2D in NK cells of cancer patients (10).

Exosomes are membrane nano-vesicles (30-100 nm) released by most of the cell types in biological fluids such as urine, serum and plasma. Exosomes are involved in both physiological and pathophysiological processes such as coagulation, immune stimulation or suppression, delivery of proteins and genetic material, cell-free viral infection, tumorigenesis and tumor immune escape. Exosomes from different sources contain various types of proteins, lipid classes and nucleic acids. On the other hand, due to the endosomal origin, they have similar protein and lipid combinations. Interestingly, molecular content of exosomes in the sera of cancer patients is different from other exosomes and this profile can induce or suppress immune responses. Exosomes carry genetic information in the form of DNA, mRNA and microRNA; therefore, they can potentially induce genetic changes in target cells (11).

microRNAs (miRs) including *hsa-miR-155-5p* play significant regulatory roles in proliferation, differentiation, signal transduction, immune responses and carcinogenesis (8). Some evidences showed that elevated expression levels of *hsa-miR-155-5p* in the serum and exosomes isolated from the patients can increase the occurrence of lymphoma, such as DLBCL (12, 13). Furthermore, studies showed an increased expression levels of *hsa-miR-155-5p* and *hsa-let-7g-5p* in plasma-derived exosomes of patients with chronic lymphoblastic leukemia (CLL) (14).

Let-7 family exerts effective anti-tumor and anti-proliferative activities by repressing several oncogenes and key regulators of the cell cycle, cell differentiation and apoptotic pathways. This family is down-regulated in a number of human cancers such as lung, colon, ovarian and breast cancers. Therefore the restoration of *let-7* expression might inhibit cancer growth (15, 16). *Let-7* family contributes to development, muscle formation, cell adhesion and gene regulation in physiological condition. A number of studies have shown that *let-7* family is down-regulated in several types of cancer, including lung cancer, colon cancer and Burkitt's lymphoma (17). Recent studies have indicated that *hsa-let-7g-5p* can prevent cell invasion and metastasis in gastric and breast cancers. A high *hsa-let-7g-5p* expression might correlate with a lower risk of cancer recurrence in patients with advanced pathological stage (18).

The purpose of this study was to determine whether exosomes isolated from plasma of patients with DLBCL contribute to NK cell activation or suppression. Therefore, we evaluated their effects on some phenotypical and functional attributes of NK cells from DLBCL patients.

Materials and Methods

Subjects

This investigation was a cross-sectional and experimental study. Patients were consecutively selected from the Cancer Referral Centers (Isfahan, Iran). Samples of peripheral blood were obtained from responsive patients with DLBCL (response to R-CHOP, n=10), refractory/relapsed patients with DLBCL (resistant to R-CHOP, n=12) and healthy people (n=12). The mean age of patients was 43.15 ± 11.76 years (mean ± SD); 54.54% of patients were male and 45.45% were female.

The responsive patients were those who achieved

complete remission for 6-12 months after completion of the R-CHOP therapy. The refractory patients were those who failed to respond to six cycles of R-CHOP, as the first-line treatment (n=7). Relapsed patients with DLBCL were those who experienced a relapse at least over a year period after R-CHOP therapy (n=5). The patients who received other chemotherapies, or they had a low-grade DLBCL and/or other different types of NHL, were excluded from the study.

All subjects signed an informed consent form approved by the Isfahan University of Medical Sciences (Isfahan, Iran). The clinical files and laboratory findings of the patients were reviewed to obtain different characteristics such as age, sex, disease stage, performance statue, nodal/extra-nodal disease, international prognostic index (IPI) score, serum lactate dehydrogenase (LDH) level, Ki-67 proliferation index (Ki-67 PI) and response to treatment. Immunohistochemically, all patients with DLBCL were non-germinal center B-cell (GCB)-like subtype ($CD20^+CD10^-$ $BCL\text{-}6^-$). The demographic and clinical data of patients with DLBCL were recorded. The samples were carried to the laboratory and used for experiments immediately after processing.

Peripheral blood specimen

Blood was drawn into EDTA-containing tubes (10 ml). Peripheral blood mono-nuclear cells (PBMCs) were separated in a Ficoll-Hypaque gradient and they were immediately used for the experiments. Plasma aliquots were either processed for exosomes isolation or stored at -70˚C.

Preparation of plasma and isolation of exosomes using ExoSpin Exosome purification Kit

Plasma was diluted with an equal volume of sterile phosphate buffered saline (PBS) to decrease viscosity. Since some exosomes might be trapped within the clot when the serum is prepared, EDTA-plasma samples were used rather than serum samples. On the other hand, heparin-plasma samples could facilitate formation of exosome-heparin complexes and aggregation of exosomes, as previously reported (19).

Then plasma was centrifuged at 300 g, 4˚C for 10 minutes. It was transferred to the new tube without pellet contamination and centrifuged for 30 minutes at 2000 g, 4˚C. The resulting supernatant was centrifuged for a further 30 minutes at 16500 g, 4˚C. Plasma was centrifuged by differential centrifugations at increasing speed (300-16500 g) to eliminate large dead cells, large cell debris, platelets, subcellular fragments and larger microvesicles (20).

The supernatant was passed through a 0.22 μm filter and collected in a fresh tube. Ultrafiltration using 0.2 μm filter was performed to remove larger vesicles (above 200 nm) and thrombocytes (about 1-2 μm) remaining in plasma even after differential centrifugation. Apart from thrombocytes and microvesicles, other "contaminating" elements such as lysosomes, mitochondria, nucleic acid-protein aggregates and even bacteria may be present in plasma as seen by by transmission electron microscopy (TEM) (Fig.1A). Ultrafiltration removes the majority of these contaminants.

Two milliliter aliquots of plasma were processed according to the manufacturer's instructions (Cell Guidance Systems, USA). Briefly, the 1 ml volume of Buffer A was added to each sample and the sample was vortexed. Samples were incubated at 4˚C for 1 hour and they were next centrifuged for 1 hour at 16500 g. Then, the supernatant was discarded and each pellet was resuspended in 200 μl PBS. The resuspended pellets were applied to ExoSpin columns and centrifuged at 50 g for 60 seconds. The elution was discarded and a further 200 μl of PBS was applied to each column. It was centrifuged at 50 g for 60 seconds and the elution containing exosomes was stored at -80˚C.

Size determination of plasma-derived exosomes

Size of the isolated exosomes was determined using a Zetasizer (Malvern Zen 3600 Instruments, UK) according to the manufacturer's instructions. The exosomes isolated by the ExoSpin kit were diluted 1:100 in PBS to determine their size.

Transmission electron microscopy

Morphology of the exosomes was evaluated by TEM using negative staining. Carbon-coated copper grids were placed on top of 5-10 μl sample drops for 20 minutes and they were fixed by 2% paraformaldehyde. The grids were then washed in the distilled water drops three times for 5 minutes, stained with 1% uranyl acetate in 50% alcohol for 15 minutes and washed in drops of distilled water three times for 5 minutes. The last drops of water were removed from the grids. The stained grids were air-dried. Images were obtained using an FEI/Philips TEM 208S microscope (Eindhoven, Netherlands) operating at an accelerating voltage of 100 KV.

Western blot analysis of plasma-derived exosomes

Exosomes were lysed in cell lysis buffer (RIPA buffer; CytoMatin Gene, Iran) supplemented with protease inhibitors (Sigma FAST™, USA) on ice. The concentration of exosomal lysates was determined using BCA Protein Assay Kit (Parsons Biotechnology, Iran). Approximately 50 μg of exosomal lysates were loaded per well. Proteins were separated on a 12% gel (Bio-Rad, UK) and transferred to nitrocellulose membranes (Bio-Rad, UK). To prevent non-specific binding, the membranes were blocked with 2.5% bovine serum albumin (BSA, CytoMatin Gene, Iran) powder diluted in tris-buffered saline-Tween (TBS-T), for 2 hours at room temperature (RT).

The membranes were then incubated with monoclonal anti-CD63 (rabbit IgG, diluted 1:1000; System Biosciences, USA), mouse monoclonal CD81 (TAPA-1; clone 5A6, diluted 1:1000; Bio-Legend, USA) and rabbit polyclonal anti-Histone H3 (clone poly6019, diluted 1:500; Bio-Legend), as negative control overnight at 4˚C. All antibody dilutions were made in TBS-T supplemented with 0.5% BSA. After

incubation with primary antibodies, membranes were washed for 3×10 minutes in TBS-T (used for each wash step). The membranes were incubated with secondary horseradish peroxidase (HRP)-conjugated antibodies for 2 hours at RT. The secondary antibodies were goat anti-rabbit HRP IgG (diluted 1:20,000; System Biosciences, USA) and goat anti-mouse IgG (H+L, diluted 1:3000; Bio-Rad, UK). The membranes were washed 3×10 minutes. Finally, the signals were visualized using the ECL Western blotting kit (CMG, Iran), according to the manufacturer's instructions.

Protein quantification of plasma-derived exosome or exosomal lysates

Five to ten microliters of plasma-derived exosome or exosomal lysate was dispensed into the wells of a 96-well plate. Then, the assay was performed by BCA Protein Assay Kit (Parstous Biotechnology, Iran) according to the manufacturer's protocol. Protein content of the exosome lysates and exosomal total protein concentration were determined using a linear standard curve. A series of BSA was used to develop a standard curve.

Isolation, purification, and expansion of natural killer cells

Blood samples were collected from refractory/relapsed patients, responsive patients and healthy donors. PBMCs were separated on a Ficoll-Hypaque gradient. NK cells were purified by negative selection, using NK cell isolation kit and LS columns (MiltenyiBiotec, Germany). The purity of N cells was confirmed as 85-90% by flow-cytometery (BD Company, USA) using PE-cy5-labeled anti-CD56 and FITCI-labeled anti-CD3 (both from eBioscience, USA). The range of CD3 positive cell contamination in purified NK cells was 10-15%.

To obtain polyclonal NK cell populations, PBMCs were γ-ray irradiated (25 Gy) and they were used as autologous feeder cells for co-culture with NK cells at a ratio of 4:1 feeder-NK cell. NK cells were expanded in Cellgro SCGM serum-free media (CellGenix, USA) supplemented with 5% human AB serum, 10% fetal bovine serum (FBS, Gibco, USA), 50 U/ml penicillin, 50 µg/ml streptomycin, 500 IU/ml recombinant human interleukin-2 (IL-2, MiltenyiBiotec AG, Germany), 10 ng/ml recombinant human interleukin-15 (IL-15, MiltenyiBiotec AG, Germany) at a density of 5×10^5 cells/ml in T-25 flask for 3 weeks.

Treatment of natural killer cells with plasma-derived exosomes

NK cells were seeded in 24-well plates at a density of 4×10^5 cells per well in DMEM/F12 culture medium without FBS/AB serum. NK cell from healthy donors and DLBCL patients were treated with 20 µg plasma-derived exosomes of DLBCL patients (refractory/relapsed or responsive patients) at 37˚C for 20 hours. Control wells contained no exosomes.

RNA isolation and cDNA synthesis

Total RNA was extracted from NK cells using the miRCURY™ Isolation Kit-Cells (Exiqon, Denmark). Then, total RNA was quantified and converted to cDNA using the Universal cDNA Synthesis Kit II (Exiqon, Denmark) according to the following protocol: firstly, total RNA was incubated for 60 minutes at 42˚C. Next, the reaction was followed by heat-inactivation of the reverse transcriptase for 5 minutes at 95˚C. In addition, synthesis of cDNA was done by Thermo Scientific RevertAid First Strand cDNA Synthesis Kit (Fermentas, Thermo Fisher Scientific Inc., USA) according to the following protocol: first, total RNA and oligo $(dT)_{18}$ were incubated for 5 minutes at 65˚C and they were next chilled on ice. Then the mixture of 5x Reaction Buffer, RiboLock RNase inhibitor, 10 mM dNTP mix and ReverAID M-MuLVRT was performed and it was incubated for 5 minutes at 25˚C, followed by incubation for 60 minutes at 42˚C. Ultimately, the reaction was terminated by incubation at 70˚C for 5 minutes.

Quantitative reverse transcription-polymerase chain reaction for *hsa-miR-155-5p* and *hsa-let-7g-5p* as well as *SOCS-1* and *INPP5D:* gene expression assay

We used pre-designed primers (Exiqon, Denmark) for *hsa-let-7g-5p*, *hsa-miR-155-5p* and *SNORD44* (as reference gene). For mRNA quantification, specific primers were designed for *SOCS-1* and *INPP5D* (Pishgaman, Iran), using Allele ID software and BLAST (NCBI online server). Details of the primers are as following:

GAPDH-
F: 5′-CCA GTG GAC TCC ACG ACG TA-3′
R: 5′-ACT AAA ACC TCC CTA GAG CG-3′

SOCS-1-
F: 5′-GTA GGA GGT GCG AGT TCA GG-3′
R: 5′-GAC CCC TTC TCA CCT CCT GA-3′

INPP5D-
F: 5′-AAG CCT GTT GTC GTC CAT TG-3′
R: 5′-AGA CTC TGC CTT CAC CTC AAA-3′

All quantitative reverse transcription -polymerase chain reaction (qRT-PCR) reactions were performed duplicately at a final volume of 10 µl per well, using a 2x Real-Time PCR Master Mix (BioFACT™, Korea) and StepOne Plus™ quantitative real-time PCR detection system (Applied Biosystems, Thermo Fisher Scientific Inc.). The following thermal cycling conditions were applied: polymerase activation/denaturation at 95˚C for 15 minutes, 45 amplification cycles at 95˚C for 20 second, 60˚C for 20 seconds and 72˚C for 30 seconds. Threshold values for the threshold cycle determination (Ct) were generated automatically by the Step One Software v2.3 software. The microRNA and mRNA fold changes were determined compared to the control samples. Relative quantification method was employed, where the ΔΔCt value was obtained by analyzing difference between ΔCt of the sample and ΔCt of the calibrator (no exosomes).

Measurement of interferon-gamma by ELISA

The culture supernatant was collected from NK cell medium

treated with or without plasma-derived exosomes after 72 hours. The culture supernatant was stored in a -80˚C freezer until assessment of the cytokine. Concentrations of IFN-γ in the culture supernatant were measured using the Human IFN-γ ELISA MAX™ Deluxe (Bio-Legend, USA). All procedures were performed according to the manufacturer's instructions.

DLBCL patients' plasma-derived exosomes effects on the rate of natural killer cells expressing CD16, NKG2D and CD69

NK cells were seeded into 96-well plates at a density of 1×10^5 cells per well in DMEM/F12 culture medium without FBS/AB serum. Then, NK cells were treated with or without 20 µg (21) plasma-derived exosomes of refractory/relapsed or responsive patients with DLBCL at 37˚C, 5% CO2 for 24 hours. NK cells were harvested and the percentage of NK cells expressing CD16, NKG2D and CD69 was determined by flow-cytometry, followed by comparing them in DLBCL patients and healthy donors.

The following anti-human monoclonal antibodies were used for flow-cytometry: CD16 monoclonal antibody (B73.1, PE); CD314 (NKG2D) monoclonal antibody (1D11, PE); CD56 (NCAM) monoclonal antibody (CMSSB, PE); CD3 monoclonal antibody (OKT3, FITC) and CD69 monoclonal antibody (FN50, FITC; all purchased from eBioscience™). The cells were also stained with their corresponding isotype-matched control mAbs (Bio-Legend, USA). All samples were analyzed using the BD FACS Calibur system (Becton Dickinson Co., USA). Flowing Software version 2.5.1 (TerhoPerttu, Finland) was used for data acquisition and analysis.

Proliferation assay

Carboxyfluorescein succinimidyl ester (CFSE) was prepared as 5 mg/ml stocks in dimethyl sulfoxide (DMSO) and stored at -20˚C. NK cells isolated from DLBCL patients and healthy donors were washed with PBS and resuspended in PBS (1×10^6 cells/ml). NK cells were labeled with CFSE according to the protocol of CFSE Cell Division Tracker Kit (final concentration of 5 µM, Bio-Legend, USA) and incubated for 20 minutes at RT. After stopping the reaction with BSA in PBS (0.1% w/v), NK cells were washed and cultured in the absence or presence plasma-derived exosome of DLBCL patients (refractory/relapsed or responsive patients). Proliferation was analyzed after three days.

Natural killer cytotoxicity assay

NK cells obtained from healthy donors and DLBCL patients, were co-incubated for 24 hours in the presence or absence of 20 µg exosomes isolating from patients with DLBCL. Treated NK cells (effector cells) were co-cultured with 50,000 CFSE labeled K562 target cells at different effector-to-target (E:T) ratios from 8:1, 4:1, 2:1 and 1:1 in 96-well plates containing 150 µl culture media. Target cells, including K562 cell lines, were labeled with CFSE according to the protocol of CFSE Cell Division Tracker Kit (final concentration of 5 µM, Bio-Legend) to discriminate target cells from effector cells. K562 and NK cells were co-cultured in DMEM/F12 medium supplemented with 500 U/ml IL-2 and 150 ng/ml IL-15 (MiltenyiBiotec AG, Germany) for 4 hours at 37˚C. These cells were stained with 0.05 µg of 7-amino-actinomycin D (7-AAD, Bio-Legend, USA) for 10 minutes in dark. Furthermore, the following control samples were prepared: unstained effector cells, unstained target cells, CFSE-stained target cells, target cells stained with both CFSE and 7-AAD, target cells permeabilized with 5% (v/v) Triton X-100 TM (Sigma, USA) in PBS and stained with 7-AAD. Flow-cytometry data were acquired from a FACS Calibur flow-cytometer (Becton Dickinson Co.) and they were analyzed by Flowing Software version 2.5.1 (TerhoPerttu, Finland). NK cytotoxicity rate was calculated as the percentage of specific lysis using the following formula: (% of target cell lysis in the test-% of spontaneous cell death)/(% of maximum lysis-% of spontaneous cell death). Spontaneous cell death was obtained from target cells in the medium cultured alone. To obtain maximum cell lysis rate, target cells were treated with 5% Triton-X100.

Statistical analysis

Data were summarized by descriptive statistics: mean ± standard error (SE). Statistical analyses were performed using one-way analysis of variance (ANOVA) test for comparison among three groups (healthy donors, responsive or refractory/relapsed patients with DLBCL). In addition, one-way ANOVA test was used to determine statistically significant differences between NK cells treated with exosomes and untreated NK cells. Multiple comparisons of data were conducted using LSD post-hoc test between different treated groups. $P<0.05$ was considered statistically significant. IBM SPSS Statistics for Windows, version 21 (IBM Corp., Armonk, NY, USA) was used for data analysis.

Ethical considerations

This study has been approved by the Bioethical Committee of the Isfahan University of Medical Sciences, Isfahan, Iran (IR.MUI.REC.1394.3.655/2015). The performed experiments comply with the current laws of Iran. All blood samples were taken from the patients after written informed consent and ethical permission was obtained for participation in the study.

Results

Assessment of the plasma-derived exosome quality

The exosomes were identified based on their size, morphology and absence or presence of their specific proteins. Plasma-derived exosomes of the patients with DLBCL were evaluated by TEM (Fig.1B), Zetasizer (Fig.1C) and western blots (Fig.1D). TEM images showed spherical vesicles with morphological properties of the exosome and diameter of 50-150 nm. Moreover, Zetaseizer analysis demonstrated that the exosomes were spherical particles with a z-average diameter size of 90.18 nm.

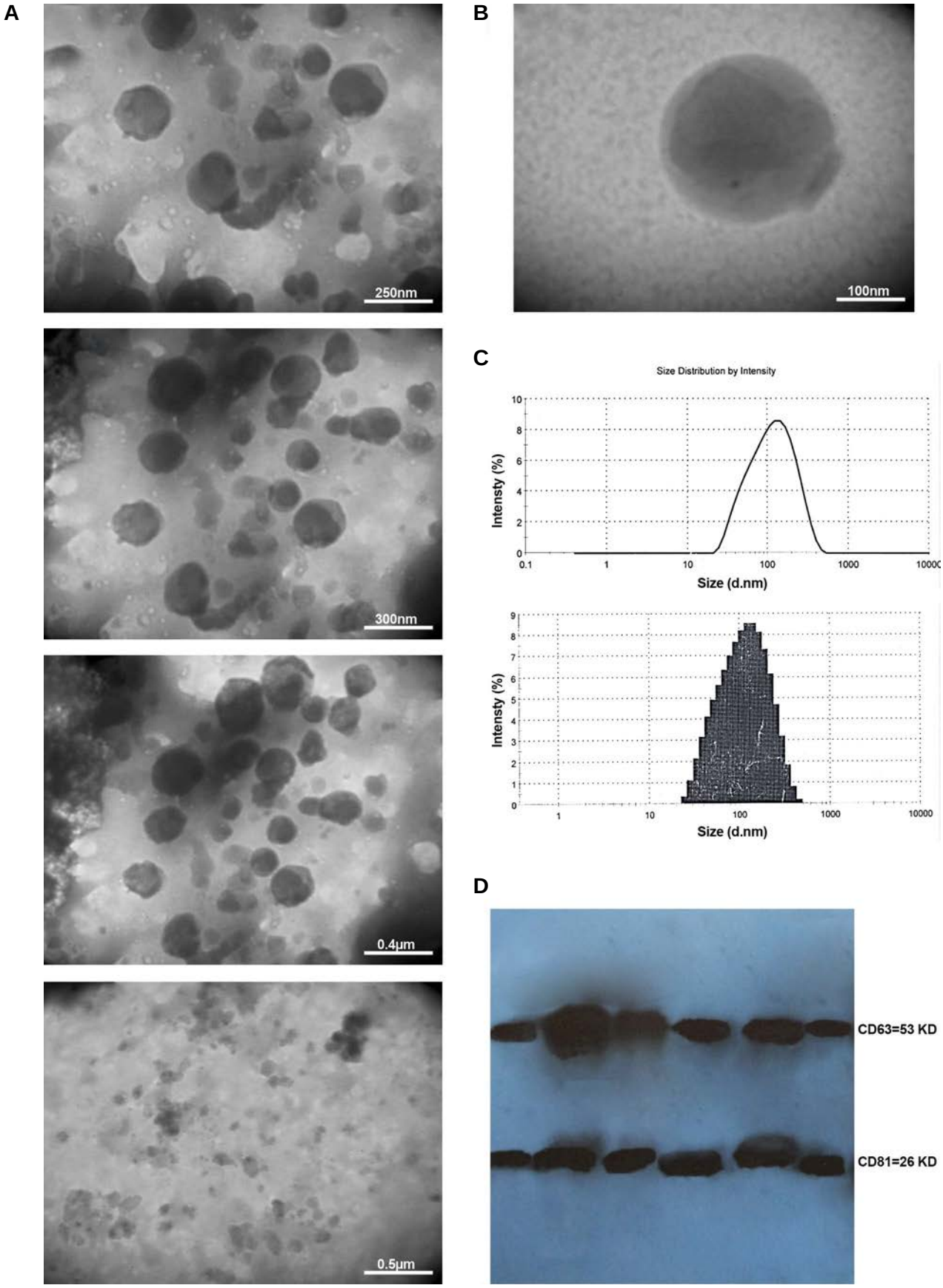

Fig.1: Properties of plasma-derived exosome of DLBCL patients. **A.** Effects of differential centrifugation and ultrafiltration of plasma on isolated exosomes, **B.** The representative TEM image of plasma-derived exosomes (exosomes size: 100 nm), **C.** Size of the all particles in the pellets was determined using a Zetasizer. The z-average particle size was 90.18 nm in diameter, and **D.** The lysed exosomes were separated using polyacrylamide gel electrophoresis and then transferred to the nitrocellulose membrane. The membrane was probed using anti-CD63, anti-CD81 as well as anti-histone H3 and ECL Western blotting systems. DLBCL; Diffuse large B-cell lymphoma and TEM; Transmission electron microscopy.

Exosomes identity was confirmed by Western blot analysis. When the lysed exosomes were probed with anti-CD63 (tetraspanin, 54 KD) and anti-CD81 (tetraspanin, 26 KD), strong bands were detected on the blots. The morphology, size of <150 nm and presence of two CD63 and CD81 proteins, in the absence of Histone H3, strongly suggest that the studied vesicles were exosomes.

Effect of plasma-derived exosomes on the expression level of microRNAs (*hsa-miR-155-5p* and *hsa-let-7g-5p*) and mRNAs (*SOCS-1* and *INPP5D*)

Since *hsa-miR-155-5p* is critical for the homeostasis of NK cells, we investigated whether the expression level of this miRNA is up-regulated in the NK cells treated with plasma-derived exosomes obtaining from patients with DLBCL in comparison with untreated NK cells (14, 22). Therefore, we established a model *in vitro* system comprised of isolated exosomes co-incubated with human NK cells for 20 hours. Following co-incubation with exosomes, total RNA was extracted from NK cells, reverse transcribed and analyzed by qRT-PCR, as described in the "Materials and Methods" section. Changes in the expression levels of selected *hsa-miR-155-5p*, *hsa-let-7g-5p* as well as, and *SOCS-1* and *INPP5D* were simultaneously measured in NK cells, relative to the control groups (no exosomes).

Our results showed a significant increase in the expression levels of *hsa-miR-155-5p* of NK cells treated with plasma-derived exosomes of refractory/relapsed DLBCL patients compared to untreated NK cells in healthy donors, refractory/relapsed DLBCL patients and responsive DLBCL patients (P=0.0001, LSD post-hoc test). Furthermore, a significant increase was observed in expression level of *hsa-miR-155-5p* in NK cells treated with plasma-derived exosomes of responsive DLBCL patients compared to untreated NK cells in refractory/relapsed DLBCL patients (P=0.009, LSD post-hoc test) and healthy donors (P=0.0001, LSD post-hoc test). The expression level of *hsa-miR-155-5p* in refractory/relapsed patients was lower than healthy donors and responsive patients in the presence of plasma-derived exosome of DLBCL patients (P=0.0001, Fig.2A).

We observed a significant decrease in *hsa-let-7g-5p* expression level of NK cells treated with plasma-derived exosomes of refractory/relapsed DLBCL patients compared to untreated NK cells in refractory/relapsed DLBCL patients (P=0.0001, LSD post-hoc test). A significant decrease was observed in the expression level of *hsa-let-7g-5p* in NK cells treated with plasma-derived exosomes of responsive DLBCL patients compared to untreated NK cells in healthy donors (P=0.040), responsive DLBCL patients (P=0.042) and refractory/relapsed DLBCL patients (P=0.0001). In addition, there was a significant increase in the *hsa-let-7g-5p* expression level of NK cells treated with IL-2/IL-15, compared to untreated NK cells in each group (P=0.0001, Fig.2B). The expression level of *hsa-let-7g-5p* for refractory/relapsed patients was lower than healthy donors and responsive patients, in the presence of plasma-derived exosome of DLBCL patients (P=0.0001).

Some studies showed the *SOCS-1* and *INPP5D* are two direct targets of *hsa-miR-155-5p* in many cell types. To determine whether plasma-derived exosomes of responsive or refractory/relapsed DLBCL patients are able to alter expression levels of *SOCS-1* and *INPP5D,* we examined these expression levels in NK cells of healthy donors and DLBCL patients.

Our finding indicated that there was significant decrease in the expression levels of *SOCS-1* in NK cells treated with IL-2/IL-15 and plasma-derived exosomes of responsive DLBCL patients compared to untreated NK cells in healthy donors (P=0.016 and P=0.0001, respectively), responsive DLBCL patients (P=0.015 and P=0.0001, respectively) and refractory/relapsed DLBCL patients (P=0.014 and P=0.0001, respectively). Additionally, a significant decrease in the expression level of *SOCS-1* was observed in NK cells treated with plasma-derived exosomes of refractory/relapsed DLBCL patients compared to untreated NK cells in refractory/relapsed DLBCL patients (P=0.0001) and responsive DLBCL patients (P=0.0001, Fig.2C).

There was a significant increase in *INPP5D* expression level of NK cells treated with plasma-derived exosomes of responsive or refractory/relapsed DLBCL patients compared to untreated NK cells in healthy donors (P=0.039 and P=0.0001, respectively). There was no significant difference in the *INPP5D* expression level of NK cells treated with plasma-derived exosome of DLBCL patients compared to untreated NK cells in refractory/relapsed DLBCL patients and responsive DLBCL patients (Fig.2D).

IFN-γ level in the natural killer cells culture supernatants in the presence of plasma-derived exosomeof DLBCL patients

It was reported that *SOCS-1* and *INPP5D* negatively regulate IFN-γ production in NK cells. The IFN-γ concentration in culture supernatants of NK cells was determined by ELISA in the absence or presence of IL-2/IL-15 and plasma-derived exosomes of refractory/relapsed patients and responsive patients after 72 hours of culture in an FBS-free or AB serum-free media.

Our data showed increased level of *hsa-miR-155-5p* and decreased level of *SOCS-1* in healthy donors and DLBCL patients. A significant increase was observed in the cultured supernatant IFN-γ concentration of NK cells treated with IL-2/IL-15, plasma-derived exosome of responsive patients and plasma-derived exosome of refractory/relapsed patients compared to untreated NK cells in healthy donors (P=0.0001, P=0.01 and P=0.0001, respectively). However, there was no significant difference in the culture supernatant IFN-γ concentration of NK cells treated with IL-2/IL-15 and plasma-derived exosome of *DLBCL* patients compared to the untreated NK cells in responsive patients or refractory/relapsed patients. The data are shown in Figure 3.

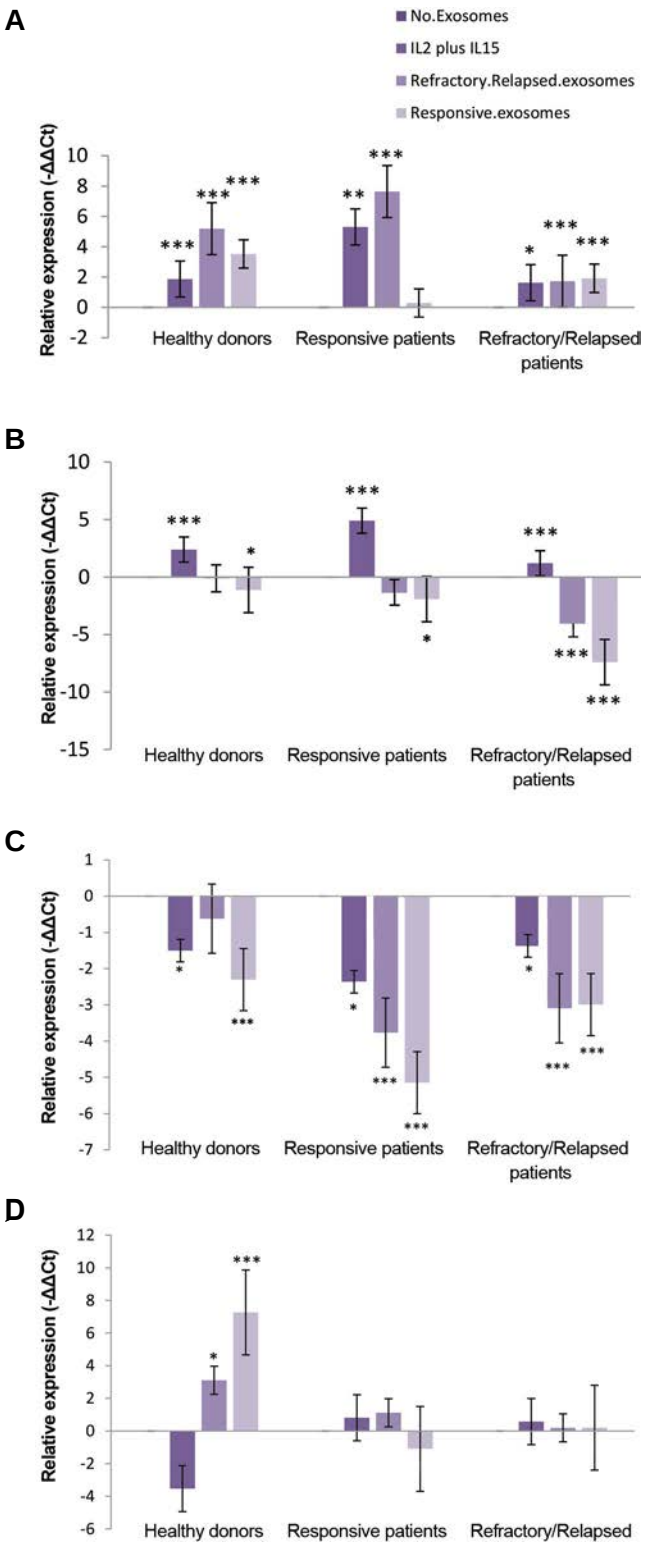

Fig.2: Effect of plasma-derived exosomes on the expression levels of microRNAs and mRNAs. *T*he expression levels of **A.** *hsa-miR-155-5p*, **B.** *hsa-let-7g-5p*, **C.** *SOCS-1* and **D.** *INPP5D* in the NK cells treated with IL-2/IL-15 and plasma-derived exosome of patients with DLBCL compared to the untreated NK cells were determined in healthy donors, responsive DLBCL patients and refractory/relapsed DLBCL patients. NK cells were treated with 20 µg plasma-derived exosome of patients with DLBCL for 20 hours and they were then collected for preparation of total RNA. miRNAs (*hsa-miR-155-5p* and *hsa-let-7g-5p*) and RNA expression (*SOCS-1* and *INPP5D*) were quantified by qRT-PCR. Degree of significance in treated NK cells with exosomes compared to the untreated NK cells was indicated by *P≤ 0.05, **P≤ 0.01 and ***P≤ 0.001 in each group. Each column shows mean of -ΔΔCt ± standard error (SE). NK cells; Natural killer cells, IL; Interleukin, DLBCL; Diffuse large B-cell lymphoma, and qRT-PCR; Quantitative reverse transcription polymerase chain reaction.

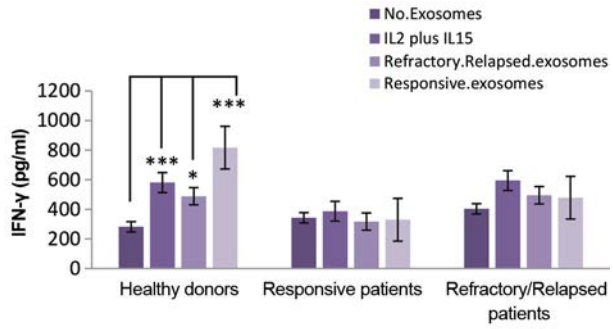

Fig.3: Effect of plasma-derived exosomes of responsive or refractory/relapsed patients on the levels of IFN-γ. The media were harvested and IFN-γ concentration was measured by sandwich ELISA after 72 hours. Statistical relationships were determined in NK cells treated with IL-2/IL-15, and plasma-derived exosomes of responsive or refractory/relapsed patients compared to untreated NK cells. Results were expressed as mean ± SE. *P<0.05, ***P<0.001 showed significant differences. IFN-γ; Interferon gamma, NK; Natural killer cells, and IL; Interleukin.

In addition, IFN-γ concentration in the culture supernatant of NK cells from refractory/relapsed DLBCL patients was lower than the responsive DLBCL patients in the presence of IL-2/IL-15, plasma-derived exosome of responsive patients and refractory/relapsed patients (P=0.002, P=0.001 and P=0.002, respectively).

Effects of plasma-derived exosome of DLBCL patients on the percentage of natural killer cells expressing CD16, CD69 and NKG2D

The percentage of NK cells expressing CD16, CD69 and NKG2D was determined by flow-cytometer in the absence or presence of IL-2/IL-15 and 20 µg of plasma-derived exosome of DLBCL patients in each group (healthy donors and responsive or refractory/relapsed patients with DLBCL) after 24 hours of culture in a FBS-free or AB serum-free media (Fig.4I).

Our findings showed that the percentage of $CD16^+$ NK cells from healthy donors was more than refractory/relapsed DLBCL patients in the absence of exosomes or in the presence of IL-2/IL-15, plasma-derived exosome of responsive DLBCL patients and plasma-derived exosome of responsive DLBCL patients plus IL-2/IL-15 (P=0.0001, P=0.0001, P=0.008 and P=0.001, respectively). Moreover, the results showed that percentage of the $CD16^+$ NK cells from responsive DLBCL patients was more than refractory/relapsed DLBCL patients in the absence of exosomes or presence of IL-2/IL-15 (P=0.0001 and P=0.002, respectively).

In addition, a significant reduction was observed in the percentage of $CD16^+$ NK cells in the presence of plasma-derived exosomes of refractory/relapsed DLBCL patients in responsive DLBCL patients (P=0.02) and healthy donors (P=0.0001). A significant increase was observed in the percentage of $CD16^+$ NK cells in the presence of IL-2/IL-15 in healthy donors (P=0.0001).

The percentage of $CD69^+$ NK cells from healthy donors was more than refractory/relapsed DLBCL patients in the absence of exosomes (P=0.003). The percentage of $CD69^+$ NK cells from

healthy donors was also more than refractory/relapsed DLBCL patients and responsive DLBCL patients in the presence plasma-derived exosome of refractory/relapsed DLBCL patients plus IL-2/IL-15 (P=0.018 and P=0.034, respectively, ANOVA test).

Furthermore, there was a significant increase in the percentage of $CD69^+$ NK cells in the presence IL-2/IL-15 compared to the absence of exosomes in refractory/relapsed DLBCL (P=0.038), responsive DLBCL patients (P=0.0001) and healthy donors (P=0.001). We also observed significantly increased $CD69^+$ NK cell percentage in the presence plasma-derived exosome of refractory/relapsed DLBCL patients plus IL-2/IL-15 in comparison with the absence of exosomes in responsive DLBCL patients and healthy donors (P=0.014 and P=0.005, respectively, LSD Post-Hoc). In addition, there was an increased $CD69^+$ NK cell percentage in the presence plasma-derived exosome of responsive DLBCL patients plus IL-2/IL-15 compared to the absence of exosomes in responsive DLBCL patients and healthy donors (P=0.0001 and P=0.022, respectively, LSD Post-Hoc).

The percentage of $NKG2D^+$ NK cells from healthy donors was more than DLBCL patients in the absence of exosomes or in the presence of IL-2/IL-15, plasma-derived exosome of refractory/relapsed DLBCL patients, plasma-derived exosome of refractory/relapsed DLBCL patients plus IL-2/IL-15 and plasma-derived exosome of responsive DLBCL patients ($P<0.05$, $P<0.01$ and $P<0.001$, ANOVA test). Data is presented in Figure 4II.

There was no significant difference in the percentage of $NKG2D^+$ NK cells in the presence of plasma-derived exosome of DLBCL patients in each group. There was significant increase in percentage of $NKG2D^+$ NK cells in the presence of IL-2/IL-15 in comparison with the absence of exosomes in refractory/relapsed DLBCL patients (P=0.05), responsive DLBCL patients (P=0.0001) and healthy donors (P=0.014). We also observed significant increase in the percentage of $NKG2D^+$ NK cells in the presence of plasma-derived exosome of responsive DLBCL patients plus IL-2/IL-15 in comparison with the absence of exosomes in responsive DLBCL patients (P=0.02) and healthy donors (P=0.003). There was a significant increase in the percentage of $NKG2D^+$ NK cells in the presence of plasma-derived exosome of refractory/relapsed DLBCL patients plus IL-2/IL-15 compared to the absence of exosomes in refractory/relapsed DLBCL patients (P=0.011) and healthy donors (P=0.028).

Effect of plasma-derived exosomes of DLBCL patients on natural killer cell proliferation

We investigated whether plasma-derived exosomes of responsive or refractory/relapsed patients with DLBCL plays role in the proliferation of NK cells (Fig.5). Proliferation rate of NK cells from healthy donors was more than responsive DLBCL patients and refractory/relapsed DLBCL patients in the absence of exosomes or in presence of IL-2/IL-15 as well as plasma-derived exosome of DLBCL patients (P<0.001).

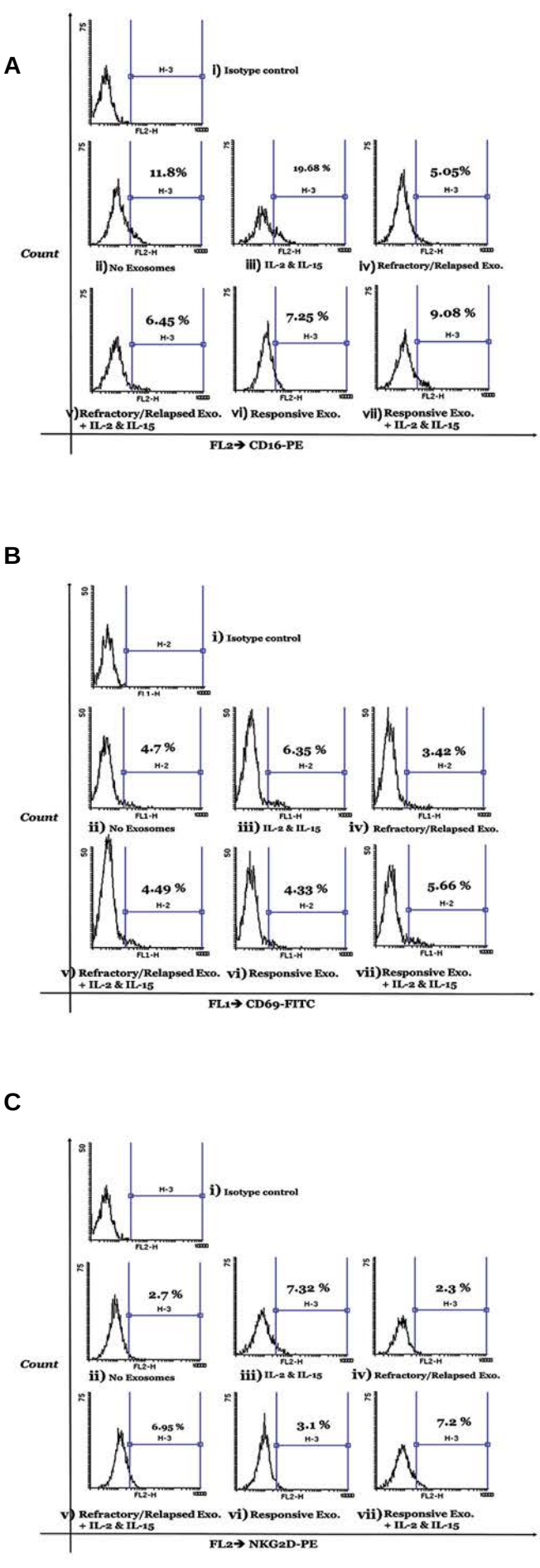

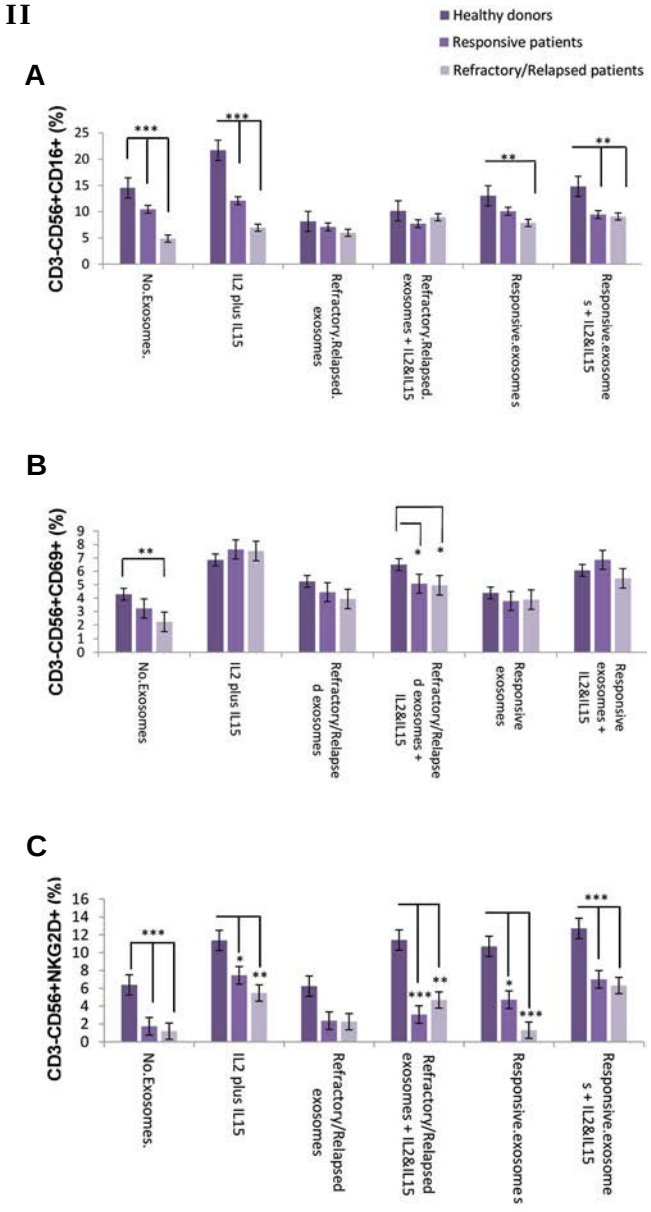

Fig.4: Flow cytometer analysis of NK cell surface markers (CD16, NKG2D, and CD69) in the absence or presence of plasma-derived exosome of DLBCL patients. I. These surface markers were analyzed by gating on the live NK cells ($CD56^{+}CD3^{-}$) of a representative DLBCL patient. **A.** NK cell labeled with PE-anti-human CD16 and PE Mouse IgG1, k Isotype control, **B.** NK cell labeled with FITC-anti-human CD69 and FITCI Mouse IgG1, k Isotype control, **C.** NK cell labeled with PE-anti-human CD314 (NKG2D) and PE Mouse IgG1, k Isotype control, i. Isotype control, ii. Unstimulated NK cell, iii. IL-2/ IL-15, iv. Plasma-derived exosomes of DLBCL refractory/ relapsed patients, v. Plasma-derived exosomes of DLBCL refractory/ relapsed patients plus IL-2/IL-15, vi. Plasma-derived exosome of responsive DLBCL patients and vii. Plasma-derived exosome of responsive DLBCL patients plus IL-2/IL-15. II. Average of the percentage of NK cells expressing **A.** CD16, **B.** CD69 and **C.** NKG2D was determined in each group (responsive DLBCL patients and refractory/relapsed DLBCL). Degree of significance was indicated by *P<0.05, **P<0.01, ***P<0.001. Each bar illustrates the mean ± SE. NK; Natural killer cells and DLBCL; Diffuse large B-cell lymphoma

Furthermore, there is a significant increase in the proliferation of NK cells treated with IL-2/IL-15 in responsive patients (P=0.0001) and refractory/relapsed patients (P=0.007, Fig.5). Additionally, there was a significant decrease in the proliferation of NK cells treated with plasma-derived exosomes of refractory/relapsed patients compared to the untreated NK cells in healthy donors (P=0.0001), responsive patients (P=0.044) and refractory/relapsed patients (P=0.0001). A significant decrease was also determined in the proliferation of NK cells treated with plasma-derived exosome of responsive patients compared to untreated NK cells in healthy donors (P=0.009).

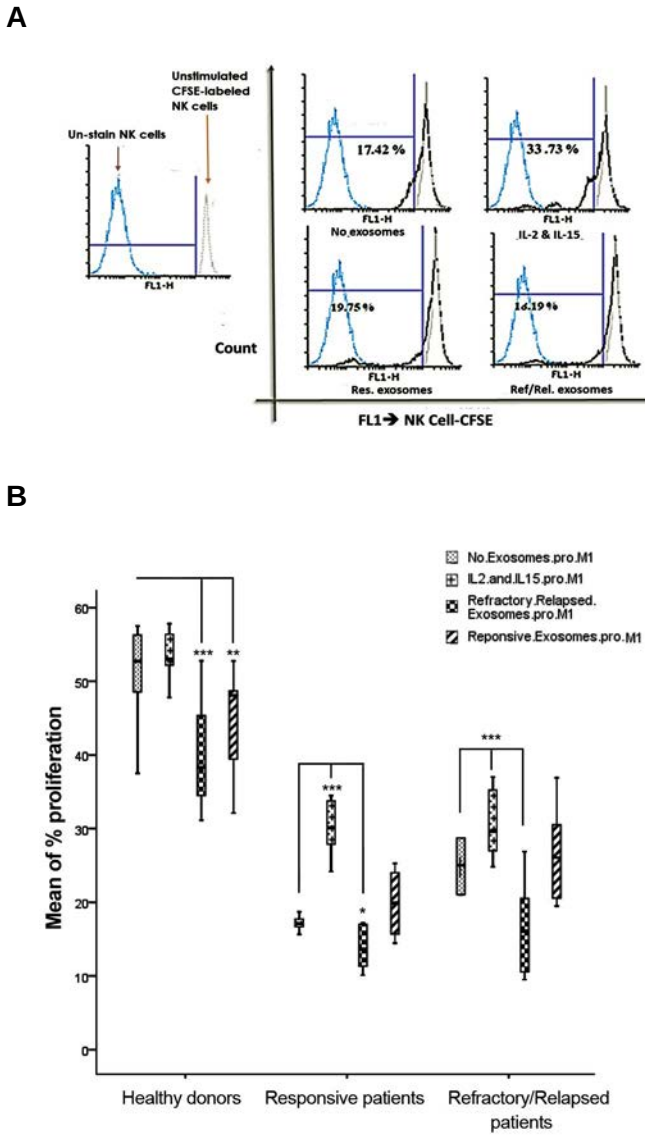

Fig.5: Effect of plasma-derived exosome of DLBCL patients on proliferation of labeled NK cell with CFSE. **A.** CFSE-positive NK cell population of a representative responsive DLBCL patient was cultured in the absence or presence of plasma-derived exosome from DLBCL patients, for three days. The dotted blue line represents unstained NK cells. Gray line with an empty profile in histograms indicates unstimulated CFSE-labeled NK cells and **B.** Degree of significance in the treated NK cells with plasma-derived exosomes of responsive or refractory/relapsed patients with DLBCL compared to the untreated NK cells, is indicated by *P≤0.05, **P≤0.01, and ***P≤0.001 in each group. Each column illustrates the mean SE for proliferation rate of NK cells. DLBCL; Diffuse large B-cell lymphoma and NK; Natural killer cells.

Effect of plasma-derived exosome of DLBCL patients on natural killer cell cytotoxicity

NK cell-mediated cytotoxicity was measured after co-culture of K562 cells with untreated NK cells or NK cells treated with plasma-derived exosome of DLBCL patients

at different effector-to-target (E:T) ratios (8:1, 4:1, 2:1 and 1:1). More than 92% of K562 cells were stained with CFSE and spontaneous lysis was in the range 1.23 -7.94 (Fig.6I). Our data showed that NK cells cytotoxicity (at ratios of 8:1, 4:1 , 2:1 and 1:1) in the absence or presence plasma-derived exosome of DLBCL patients in healthy donors was more than DLBCL patients (P=0.0001, ANOVA test).

There was a significant decrease in NK cell-mediated cytotoxicity treated with plasma-derived exosomes of refractory/relapsed DLBCL patients compared to untreated NK cell in refractory/relapsed DLBCL patients [at ratios of 8:1 (P=0.001), 4:1 (P=0.003), 2:1 (P=0.021) and 1:1 (P=0.001)] and in refractory/relapsed DLBCL patients [at 8:1 ratios (P=0.001)]. In addition, a significant decrease was observed in NK Cell-mediated cytotoxicity treated with plasma-derived exosome of responsive patients with DLBCL compared to untreated NK cell in responsive patients (at 1:1 ratio, P=0.033). The results of cytotoxicity assay are presented in Figure 6II. As well, there was the significant decrease in NK cells-mediated cytotoxicity treated with plasma-derived exosomes of refractory/relapsed DLBCL patients (P=0.03) and plasma-derived exosomes of responsive DLBCL patients (P=0.01) in healthy donors at ratio of 8:1.

I

A

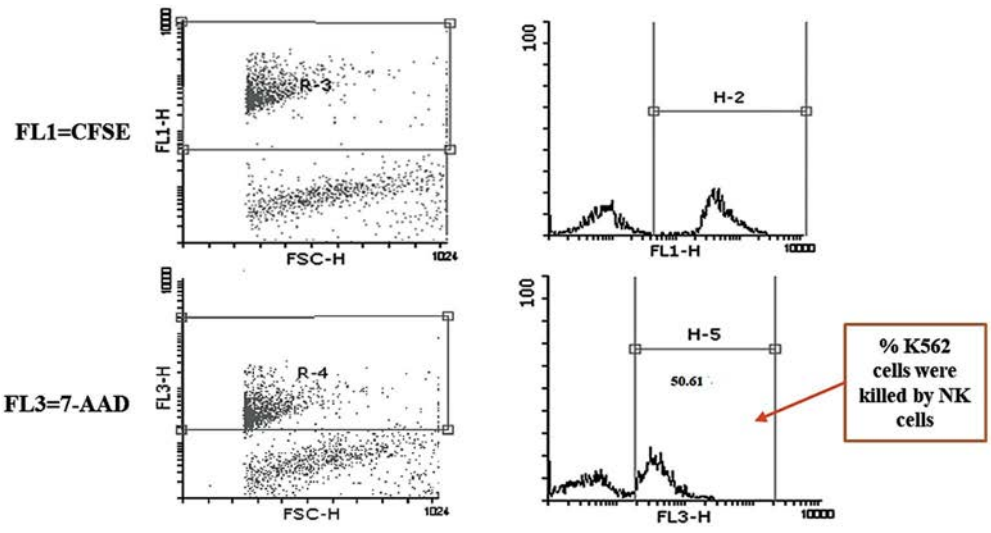

NK cells treated with 20 µg Ref/Rel. exosomes in healthy donor	Ratio	H-2: % CFSE	H-5: % 7-AAD
	2:1	52.38	50.61

B

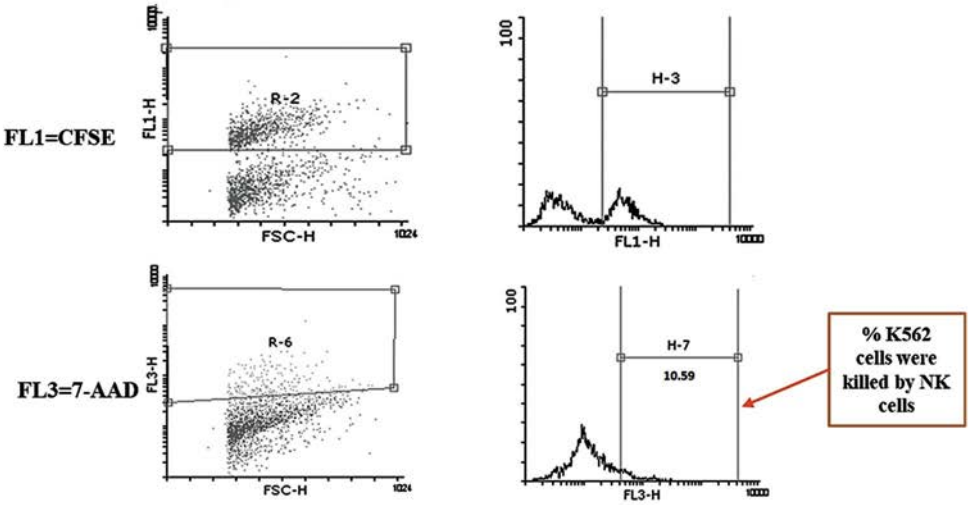

NK cells treated with 20 µg Ref/Rel. exosomes in refractory/ relapsed patients	Ratio	H-2: % CFSE	H-5: % 7-AAD
	2:1	44.41	10.56

II

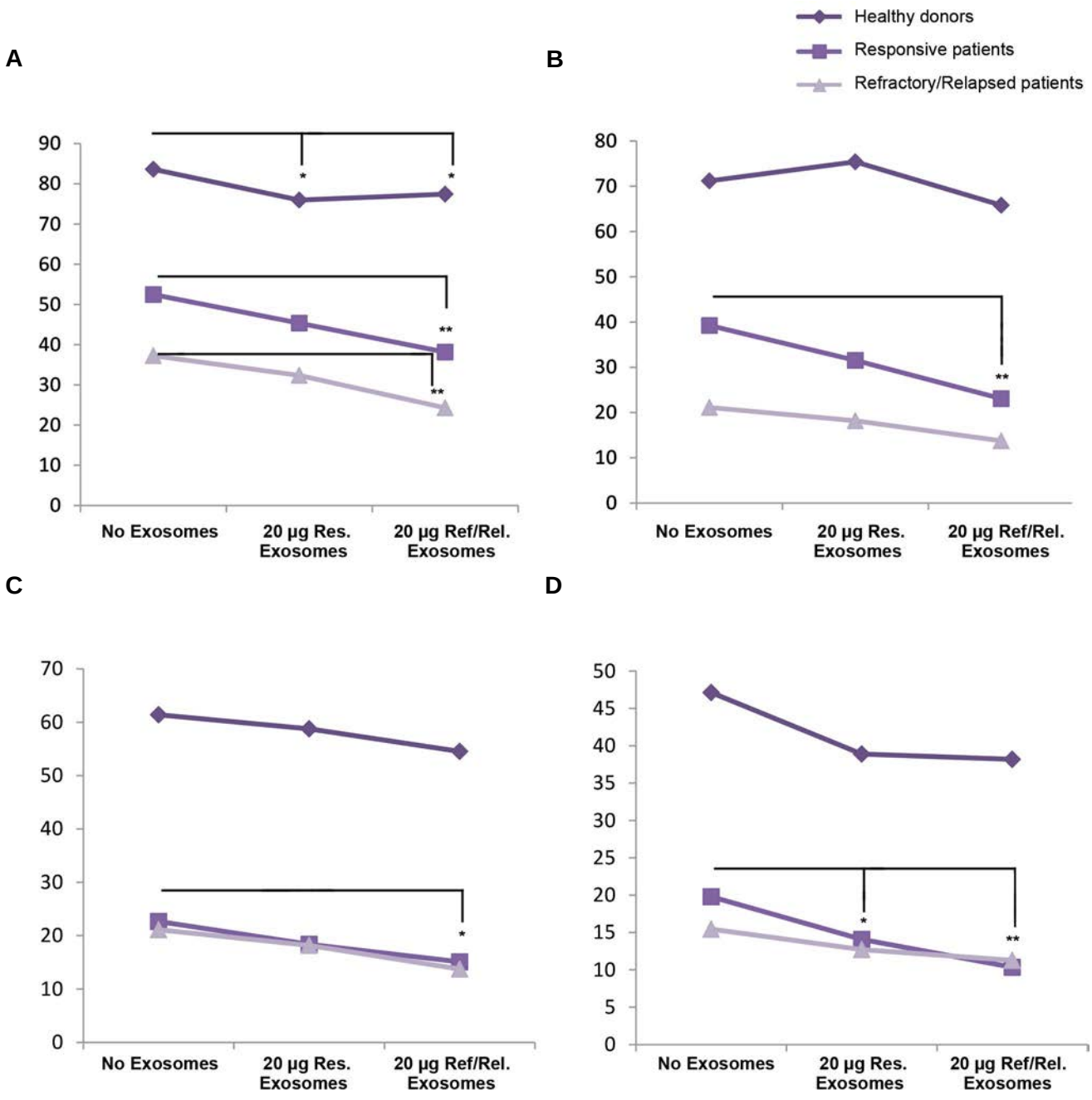

Fig.6: Effect of plasma-derived exosome of DLBCL patients on the NK cell cytotoxicity. I. CFSE-stained K562 cells were co-cultured with NK cells at different E/T ratios. The CFSE-stained K562 cells were first gated by FSC and SSC characteristics. Both dot plots and histograms show that CFSE-stained K562 target cells were killed by NK cells treated with 20 µg plasma-exosomes of refractory/relapsed patients in **A.** Healthy donor and **B.** Responsive patient using E/T ratio of 2:1. The numbers in the panels denote percentage of 7-AAD positive cells. II. Variety of these killing activities were statistically analyzed at different E/T ratios, including **A.** 8:1, **B.** 4:1, **C.** 2:1, and **D.** 1:1 in the absence or presence of plasma-derived exosome of patients with DLBCL in healthy donors, responsive DLBCL patients and refractory/relapsed DLBCL patients. Degree of significance is highlighted by *P≤0.05 and **P≤0.01 in each group. Each point illustrates mean of the NK cell cytotoxicity percentage in each group. DLBCL; Diffuse large B-cell lymphoma and NK; Natural killer cells.

Discussion

Several reports have indicated that tumor-derived exosomes down-regulate signaling in NK cells (23). The exact nature of the signals delivered via exosomes and the mode of action are unknown (22). Studies reveal that regulation of NK cell activation by *hsa-miR-155-5p* is complex and *hsa-miR-155-5p* can function as a dynamic tuner for NK cell activation (24). We considered the possibility that plasma-derived exosome of patients with DLBCL can cause some effects on the *miR-155*-IFN-γ pathway in NK cells as well as proliferation and cytotoxicity of NK cells. The present study provides evidence of some signatures of plasma-derived exosome of patients with DLBCL on NK cell function.

We showed a significant increase in proliferation, *hsa-let-7g-5p* level as well as the percentage of $CD69^{+}$ and $NKG2D^{+}$ NK cells in the presence of IL-2/IL-15. Findings obtained from the current investigation was consistent with previous studies reporting that IL-15 and IL-2 stimulate proliferation and activation of NK

cells (25). In this study, we observed significant decrease in the percentage of $CD69^+$ NK cells, $CD16^+$ NK cells and $NKG2D^+$ NK cells, IFN-γ production, NK cell proliferation and cytotoxicity in the absence or presence of IL-2/IL-15 in refractory/relapsed patients compared to responsive patients and healthy donors. Furthermore, we found that exposure of NK cells from healthy donors in the presence of 20 µg exosomes, isolated from DLBCL patients, increased *hsa-miR-155-5p* and IFN-γ levels and reduced NK cells proliferation. Moreover, the exposure of NK cells from patients with DLBCL in the presence of 20 µg exosomes, isolated from refractory/relapsed DLBCL patients, increased *hsa-miR-155-5p* level and reduced proliferation and cytotoxicity of NK cells.

Our finding showed a significant increase in *hsa-miR-155-5p* level and a significant decrease in *SOCS*-1 level in NK cells treated with 20 µg plasma-derived exosome of DLBCL patients in comparison with the untreated NK cell in healthy donors. Additionally, we observed an increased level of *hsa-miR-155-5p* in association with increased level of IFN-γ, in the presence of plasma-derived exosome of DLBCL patients in healthy donors. These results were consistent with the previous studies. These studies report that *hsa-miR-155-5p* is a positive regulator of IFN-γ production. The cytokine-induced up-regulation of *hsa-miR-155-5p* enhances IFN-γ production by targeting and suppressing *INPP5D* and *SOCS-1* (as the negative regulators), in the activated NK cell through cytokines (IL-12 and IL-18) and CD16 (8, 26).

An increased level of *hsa-miR-155-5p* and a decreased level of *SOCS*-1 were observed in the presence of 20 µg plasma-derived exosome of DLBCL patients, in patients with DLBCL. Nevertheless, no significant difference was observed in the *INPP5D* and IFN-γ expression levels in the presence of 20µg plasma-derived exosomes of responsive or refractory/relapsed patients, in DLBCL patients. Therefore, plasma-derived exosome of DLBCL patients may carry or target other microRNAs (*has-miR-29*, *hsa-miR-155-5p* and *has-miR-15/16*) or other upstream pathways regulating IFN-γ level in NK cells of the DLBCL patients (27).

Although we observed significant increase in *INPP5D* level, a significant increase was determined in IFN-γ level produced by NK cells treated with plasma-derived exosome of DLBCL patients in healthy donors. These findings were contrary to the previous studies. Since mRNA may undergo post-transcriptional modifications, quantification in the both mRNA and protein levels are necessary to understand how the cells work in different condition (28). Therefore, we should evaluate *INPP5D* and *SOCS-1* expressions in the levels of mRNA and protein to find the effect of exosomes isolated from patients on IFN-γ production.

We observed a decreased level of *hsa-let-7g-5p* in NK cells, treated with 20 µg plasma-derived exosome of responsive DLBCL patients in comparison with untreated NK cell in healthy donors and DLBCL patients. These results explain unknown factors, in the exosomes, which could contribute to the reduction of *hsa-let-7g-5p* level. A report showed that decreased level of *hsa-let-7g-5p* associated with a higher risk of tumor relapse in patients with advanced pathological stage of gastric and breast cancers (29). Some studies suggest that low expression levels of *hsa-let-7g-5p* have a longer event free survival time (30). In other word, some evidence demonstrates that *hsa-let-7g-5p* can suppress NF-κB signaling pathways and secretion of pro-inflammatory cytokines, while *hsa-miR-155-5p* up-regulates NF-κB through down-regulation of IKKs and other genes (31-33). Thus, decreased expression level of *hsa-let-7g-5p* and increased expression level of *hsa-miR-155-5p* in the presence of exosome isolated from patients might be associated with up-regulation of NF-κB in NK Cells. It is necessary to investigate roles of *hsa-miR-155-5p* and *hsa-let-7g-5p* in NF-kB pathway, in the absence or presence of exosome isolated from patients, in PBMCs obtained from DLBCL patients.

We investigated NK cells proliferation after three days and a significant decrease was observed in NK cells treated with plasma-derived exosome of refractory/relapsed DLBCL patients compared to untreated NK cells in three groups. Some reports have shown that the exosomes isolated from tumor cell supernatants and patients' sera inhibit proliferation of $CD8^+$ T-cells (21, 34). Clayton et al. (35) indicates that tumor exosomes inhibit IL-2 mediated lymphocyte proliferation (50%) in purified $CD4^+$ T-cell population. However, in the presence of tumor exosomes, NK cell proliferation has only been slightly decreased. They revealed that exosomes-associated transforming growth factor-β1 (TGF-β1) contributed to anti-proliferative effects. This reduction might be due to the presence of TGF-β1 or other anti-proliferation agents in plasma-derived exosomes of refractory/relapsed DLBCL patients. On the other hand, we observed that plasma-derived exosomes of refractory/relapsed DLBCL patients decreased expression levels of SOCS-1 and NK cell proliferation in DLBCL patients. The results of this study are in line with another study in the mouse model. They report that *miR-155-5p* containing exosomes produced by macrophage under stress, suppress proliferation of the fibroblast by down-regulation of SOCS-1 protein expression (36). Thus, a decrease in the expression levels of SOCS-1 might result in a decrease in NK cell proliferation. In addition, an increased level of *hsa-miR-155-5p* and decreased levels of *SOCS-1* and *hsa-let-7g-5p* in the presence of plasma-derived exosome of DLBCL patients might result in an increase of inflammation. However, we did not investigate effect of inflammatory cytokines, such as IL-6 and TNF-β.

A study showed that decreased CD16 expression level in the NK cells of patients with DLBCL can lead to the impairment in rituximab-mediated ADCC (37). We observed significant decreased percentage of $CD16^+$ NK cells in the presence of 20 µg plasma-derived exosome of refractory/relapsed patients in responsive patients and healthy donors. This finding showed that plasma-derived

exosome of refractory/relapsed patients might impair ADCC.

No significant difference was found in the percentage of $CD69^+$ or $NKG2D^+$ NK cells in the presence of plasma-derived exosome of DLBCL patients in each group. Contrarily, some studies demonstrated that NKG2D expression is down-regulated by micro-vesicles or exosomes, associated with TGF-β1 and IL-10 and/or exosomes bearing NKG2D ligands. Down-regulation of NKG2D surface protein causes decreased ability of NK cells to recognize malignant cells (10, 37, 38). In addition, a study has described that exosome of cancer patients mediated higher immune suppression by reducing CD69 expression in activated $CD4^+$ T effector cells after 7 hours (39). These results might be due to the small sample size, using no FBS or AB serum for NK cell culture, incubation time and sample type (responsive DLBCL patients vs. refractory/relapsed patients).

A recent review study explained that tumor-derived exosomes inhibit NK cell activation, cytotoxicity and proliferation. In fact, these exosomes bear TGF-β1 or apoptosis-inducing ligands (Fas ligand and TNF-related apoptosis-inducing ligand). Therefore, they can initiate T cell apoptosis or disrupt IL-2 signaling in NK cells (40). Similarly, we observed a significant decreased NK cell cytotoxicity, in the presence of plasma-derived exosome of DLBCL patients, in DLBCL patients. However, the exposure of NK cells from healthy donors, in presence of 20 μg plasma-derived exosome of DLBCL patients, did not have any effects on NK cell cytotoxicity. Therefore, it was better to evaluate cytotoxicity of NK cells against DLBCL cell lines to understand the main effect of exosomes released from DLBCL cell line on NK cell function. Disruption in the cytotoxic machinery of NK cells might also result from down-regulation of NKG2D expression. However, we did not observe any significant difference in the percentage of $NKG2D^+$ NK cells, in the absence or presence of plasma-derived exosome of DLBCL patients.

Conclusion

To sum up, the importance of NK-cell in removing hematopoietic cancer provides a strong rationale to use NK-cells therapy instead of autologous stem cell transplantation for treatment of refractory/ relapsed patients with DLBCL. Our report indicates decreased percentage of $CD16^+CD69^+NKG2D^+$ NK cells, low IFN-γ levels in the supernatant of NK cell cultures, decreased NK cell proliferation and reduced NK cell cytotoxic activity in DLBCL patients compared to the healthy donors in the absence plasma-derived exosome of DLBCL patients. This could become the foundation of new therapeutic agent developments to target the NK cell activation and NK cell cytotoxicity. Our findings demonstrated decreased proliferation and cytotoxicity of NK cell in the absence or presence of plasma-derived exosome of DLBCL patients. It seems that elimination of plasma-derived exosome of patients using some drugs and also other procedures could be a great way to improve NK-cell functions. Ultimately, use of dendritic cell-derived exosomes and NK cell-derived exosomes might be helpful as cell-free cancer vaccines in the clinical setting.

Acknowledgements

This work was financially supported by Isfahan University of Medical Sciences. The authors thank the personnel of Sayed Al-Shohada Hospital. They also gratefully acknowledge in cooperation of the Isfahan Blood Transfusion Organization for gamma irradiation of peripheral blood mononuclear cells (PBMC). The authors declare that they have no competing interests.

Authors' Contributions

N.Z., S.H.J., N.E., V.M.; Conception, design, administrative, technical and material support. N.Z., S.H.J.; Development of methodology. N.Z., V.M.; Acquisition of data. N.Z., N.E.; Analysis and interpretation of data, writing, review and/or revision of the manuscript. All authors read and approved the final manuscript.

References

1. Dotan E, Aggarwal C, Smith MR. Impact of rituximab (Rituxan) on the treatment of B-cell non-Hodgkin's lymphoma. P T. 2010; 35(3): 148-157.
2. Sehn LH, Gascoyne RD. Diffuse large B-cell lymphoma: optimizing outcome in the context of clinical and biologic heterogeneity. Blood. 2015; 125(1): 22-32.
3. Park KH, Park H, Kim M, Kim Y, Han K, Oh EJ. Evaluation of NK cell function by flowcytometric measurement and impedance based assay using real-time cell electronic sensing system. Biomed Res Int. 2013; 2013: 210726.
4. Danielou-Lazareth A, Henry G, Geromin D, Khaznadar Z, Briere J, Tamouza R, et al. At diagnosis, diffuse large B-cell lymphoma patients show impaired rituximab-mediated NK-cell cytotoxicity. Eur J Immunol. 2013; 43(5): 1383-1388.
5. Cooper MA, Fehniger TA, Caligiuri MA. The biology of human natural killer-cell subsets. Trends Immunol. 2001; 22(11): 633-640.
6. Perussia B. Fc receptors on natural killer cells. Curr Top Microbiol Immunol. 1998; 230: 63-88.
7. Ye J, Guo R, Shi Y, Qi F, Guo C, Yang L. miR-155 regulated inflammation response by the SOCS1-STAT3-PDCD4 axis in atherogenesis. Mediators Inflamm. 2016; 2016: 8060182.
8. Trotta R, Chen L, Ciarlariello D, Josyula S, Mao C, Costinean S, et al. miR-155 regulates IFN-γ production in natural killer cells. Blood. 2012; 119(15): 3478-3485.
9. Liu X, Wang Y, Sun Q, Yan J, Huang J, Zhu S, et al. Identification of microRNA transcriptome involved in human natural killer cell activation. Immunol Lett. 2012; 143(2): 208-217.
10. Ashiru O, Boutet P, Fernández-Messina L, Agüera-González S, Skepper JN, Valés-Gómez M, et al. Natural killer cell cytotoxicity is suppressed by exposure to the human NKG2D ligand MICA*008 that is shed by tumor cells in exosomes. Cancer Res. 2010; 70(2): 481-489.
11. Lugini L, Cecchetti S, Huber V, Luciani F, Macchia G, Spadaro F, et al. Immune surveillance properties of human NK cell-derived exosomes. J Immunol. 2012; 189(6): 2833-2842.
12. Bradshaw G, Sutherland HG, Haupt LM, Griffiths LR. Dysregulated microRNA expression profiles and potential cellular, circulating and polymorphic biomarkers in non-hodgkin lymphoma. Genes (Basel). 2016; 7(12). pii: E130.
13. Zare N, Haghjooy Javanmard S, Mehrzad V, Eskandari N, Kefayat A. Evaluation of exosomal miR-155, let-7g and let-7i levels as a potential noninvasive biomarker among refractory/relapsed patients, responsive patients and patients receiving R-CHOP. Leuk Lymphoma. 2019: 1-13 (ahead of print).
14. Paggetti J, Haderk F, Seiffert M, Janji B, Distler U, Ammerlaan W,

et al. Exosomes released by chronic lymphocytic leukemia cells induce the transition of stromal cells into cancer-associated fibroblasts. Blood. 2015; 126(9): 1106-1117.
15. Barh D, Malhotra R, Ravi B, Sindhurani P. MicroRNA let-7: an emerging next-generation cancer therapeutic. Curr Oncol. 2010; 17(1): 70-80.
16. Guan J , Guo S, Liu M. Let-7 Family miRNAs represent potential broad-spectrum therapeutic molecules for human cancer. J Genet Syndr Gene Ther. 2015; 6(3): 271.
17. Wang X, Cao L, Wang Y, Wang X, Liu N, You Y. Regulation of let-7 and its target oncogenes (Review). Oncol Lett. 2012; 3(5): 955-960.
18. Peng SC, Liao CT, Peng CH, Cheng AJ, Chen SJ, Huang CG, et al. MicroRNAs MiR-218, MiR-125b, and Let-7g predict prognosis in patients with oral cavity squamous cell carcinoma. PLoS One. 2014; 9(7): e102403.
19. Atai NA, Balaj L, van Veen H, Breakefield XO, Jarzyna PA, Van Noorden CJ, et al. Heparin blocks transfer of extracellular vesicles between donor and recipient cells. J Neurooncol. 2013; 115(3): 343-351.
20. Théry C, Amigorena S, Raposo G, Clayton A. Isolation and characterization of exosomes from cell culture supernatants and biological fluids. Curr Protoc Cell Biol. 2006; Chapter 3: Unit 3. 22.
21. Piao YJ, Kim HS, Hwang EH, Woo J, Zhang M, Moon WK. Breast cancer cell-derived exosomes and macrophage polarization are associated with lymph node metastasis. Oncotarget. 2017; 9(7): 7398-7410.
22. Lopez-Santillan M, Larrabeiti-Etxebarria A, Arzuaga-Mendez J, Lopez-Lopez E, Garcia-Orad A, Lopez-Santillan M, et al. Circulating miRNAs as biomarkers in diffuse large B-cell lymphoma: a systematic review. Oncotarget. 2018; 9(32): 22850-22861.
23. Raposo G, Nijman HW, Stoorvogel W, Liejendekker R, Harding C V, Melief CJ, et al. B lymphocytes secrete antigen-presenting vesicles. J Exp Med. 1996; 183(3): 1161-1172.
24. Sullivan RP, Fogel LA, Leong JW, Schneider SE, Wong R, Romee R, et al. MicroRNA-155 tunes both the threshold and extent of NK cell activation via targeting of multiple signaling pathways. J Immunol. 2013; 191(12): 5904-5913.
25. Choi SS, Chhabra VS, Nguyen QH, Ank BJ, Stiehm ER, Roberts RL. Interleukin-15 enhances cytotoxicity, receptor expression, and expansion of neonatal natural killer cells in long-term culture. Clin Diagn Lab Immunol. 2004; 11(5): 879-888.
26. Leung W-H, Tarasenko T, Bolland S. Differential roles for the inositol phosphatase SHIP in the regulation of macrophages and lymphocytes. Immunol Res. 2009; 43(1-3): 243-251.
27. Leong JW, Sullivan RP, Fehniger TA. Natural killer cell regulation by microRNAs in health and disease. J Biomed Biotechnol. 2012; 2012: 632329.
28. Greenbaum D, Colangelo C, Williams K, Gerstein M. Comparing protein abundance and mRNA expression levels on a genomic scale. Genome Biol. 2003; 4(9): 117.
29. Jardin F, Figeac M. MicroRNAs in lymphoma, from diagnosis to targeted therapy. Curr Opin Oncol. 2013; 25(5): 480-486.
30. Ni H, Tong R, Zou L, Song G, Cho WC. MicroRNAs in diffuse large B-cell lymphoma. Oncol Lett. 2016; 11(2): 1271-1280.
31. Wang YS, Hsi E, Cheng HY, Hsu SH, Liao YC, Juo SH. Let-7g suppresses both canonical and non-canonical NF-κB pathways in macrophages leading to anti-atherosclerosis. Oncotarget. 2017; 8(60): 101026-101041.
32. Rom S, Dykstra H, Zuluaga-Ramirez V, Reichenbach NL, Persidsky Y. miR-98 and let-7g* Protect the Blood-Brain Barrier Under Neuroinflammatory Conditions. J Cereb Blood Flow Metab. 2015; 35(12): 1957-1965.
33. Ma X, Becker Buscaglia LE, Barker JR, Li Y. MicroRNAs in NF-kappaB signaling. J Mol Cell Biol. 2011; 3(3): 159-166.
34. Kim JW, Wieckowski E, Taylor DD, Reichert TE, Watkins S, Whiteside TL. Fas ligand-positive membranous vesicles isolated from sera of patients with oral cancer induce apoptosis of activated T lymphocytes. Clin Cancer Res. 2005; 11(3): 1010-1020.
35. Clayton A, Mitchell JP, Court J, Mason MD, Tabi Z. Human tumor-derived exosomes selectively impair lymphocyte responses to interleukin-2. Cancer Res. 2007; 67(15): 7458-7466.
36. Wang C, Zhang C, Liu L, A X, Chen B, Li Y, et al. Macrophage-derived mir-155-containing exosomes suppress fibroblast proliferation and promote fibroblast inflammation during cardiac injury. Mol Ther. 2017; 25(1): 192-204.
37. Szczepanski MJ, Szajnik M, Welsh A, Whiteside TL, Boyiadzis M. Blast-derived microvesicles in sera from patients with acute myeloid leukemia suppress natural killer cell function via membrane-associated transforming growth factor- 1. Haematologica. 2011; 96(9): 1302-1309.
38. Lanier LL. NKG2D receptor and its ligands in host defense. Cancer Immunol Res. 2015; 3(6): 575-582.
39. Muller L, Hong CS, Stolz DB, Watkins SC, Whiteside TL. Isolation of biologically-active exosomes from human plasma. J Immunol Methods. 2014; 411: 55-65.
40. Barros FM, Carneiro F, Machado JC, Melo SA. Exosomes and immune response in cancer: friends or foes? Front Immunol. 2018; 9: 730.

Original Article

DGC/Zeta as A New Strategy to Improve Clinical Outcome in Male Factor Infertility Patients following Intracytoplasmic Sperm Injection: A Randomized, Single-Blind, Clinical Trial

Nazanin Karimi, M.Sc.[1], Homa Mohseni Kouchesfahani, Ph.D.[1]*, Mohammad Hossein Nasr-Esfahani, Ph.D.[2]*, Marziyeh Tavalaee, Ph.D.[2], Abdolhossein Shahverdi, Ph.D.[3, 4], Hamid Choobineh, Ph.D.[5]

1. Department of Animal Biology, Faculty of Biological Sciences, Kharazmi University, Tehran, Iran
2. Department of Reproductive Biotechnology, Reproductive Biomedicine Research Center, Royan Institute for Biotechnology, ACECR, Isfahan, Iran
3. Reproductive Epidemiology Research Center, Royan Institute for Reproductive Biomedicine, ACECR, Tehran, Iran
4. Department of Embryology, Reproductive Biomedicine Research Center, Royan Institute for Reproductive Biomedicine, ACECR, Tehran, Iran
5. School of Allied Medical Science, Tehran University of Medical Sciences, Tehran, Iran

***Corresponding Addresses: P.O. Box: 15815/3587, Department of Animal Biology, Faculty of Biological Sciences, Kharazmi University, Tehran, Iran P.O.Box: 8165131378, Department of Reproductive Biotechnology, Reproductive Biomedicine Research Center, Royan Institute for Biotechnology, ACECR, Isfahan, Iran**
Emails: kouchesfehani@khu.ac.ir, mh.nasr-esfahani@royaninstitute.org

Received: 5/November/2018, Accepted: 2/March/2019

Abstract

Objective: The aim of this blind randomised clinical trial study was to assess the clinical efficiency of combined density gradient centrifugation/Zeta (DGC/Zeta) sperm selection procedure compared to conventional DGC in infertile men candidates for intracytoplasmic sperm injection (ICSI). The literature shows that DGC/Zeta is more effective compared to DGC alone in selection of sperms with normal chromatin and improves the clinical outcome of the ICSI procedure. Therefore, this study re-evaluates the efficiency of DGC/Zeta in improving the clinical outcomes of ICSI in an independent clinical setting.

Materials and Methods: In this randomized, single-blind, clinical trial, a total of 240 couples with male factor infertility and at least one abnormal sperm parameter were informed regarding the study and 220 participated. Based on inclusion and exclusion criteria, 103 and 102 couples were randomly allocated into the DGC/Zeta and DGC groups, respectively. ICSI outcomes were followed and compared between the two groups.

Results: Although there was no significant difference in fertilization rate (P=0.67) between the DGC/Zeta and DGC groups, mean percentage of good embryo quality (P=0.04), good blastocysts quality (P=0.049), expanded blastocysts (P=0.007), chemical pregnancies (P=0.005) and clinical pregnancies (P=0.007) were significantly higher in the DGC/Zeta group compared to DGC. In addition, implantation rate was insignificantly higher in DGC/Zeta compared to DGC (P=0.17).

Conclusion: This is the second independent study showing combined DGC/Zeta procedure improves ICSI outcomes, especially the pregnancy rate, compared to the classical DGC procedure and this is likely related to the improved quality of sperm selected by the DGC/Zeta procedure (Registration number: IRCT20180628040270N1).

Keywords: DGC/Zeta, Embryo Quality, Fertilization, Pregnancy

Cell Journal(Yakhteh), Vol 22, No 1, April-June (Spring) 2020, Pages: 55-59

Citation: **Karimi N, Mohseni Kouchesfahani H, Nasr-Esfahani MH, Tavalaee M, Shahverdi A, Choobineh H. DGC/Zeta as a new strategy to improve clinical outcome in male factor infertility patients following intracytoplasmic sperm injection: a randomized, single-blind, clinical trial. Cell J. 2020; 22(1): 55-59. doi: 10.22074/cellj.2020.6525.**

Introduction

Preparation of a sperm population with high chromatin normality is a basic parameter which is strived for in intracytoplasmic sperm injection (ICSI) procedures. Today, selection of sperm for ICSI is based on sperm morphology and viability (1). The percentage of sperm with strict normal morphology is believed to be correlated with percentage of sperm with normal DNA content, however, this concept has been highly debated (2, 3). There are reports that the percentage of sperm with fragmented DNA but normal morphology increases in subfertile/infertile individuals compared to fertile men (4, 5). In this regrade, previous studies have showed that the percentage of DNA fragmentation in sperm from neat semen of infertile men with normal and abnormal semen parameters are around 30 and, 20-40%, respectively. Sperm with fragmented DNA may fertilize an oocyte, but it has a reduce chance of pre- or post-implantation development (6).

A recent meta-analysis has suggested that assessment of sperm DNA fragmentation is beneficial in predicting male fertility (7). A plethora of studies have also concluded that routine sperm preparation procedures such as swim up, and density gradient centrifugation (DGC) alongside novel sperm preparation procedures based on sperm molecular and cellular characteristics can separate a higher percentage of normal sperm with intact DNA compared to routine sperm preparation procedures, especially in infertile couples with severe male factor infertility (1, 8, 9).

Sperm preparation based on surface electrical charge or Zeta potential has been introduced as one of the novel sperm preparation procedures. This procedure, was initially introduced by Chan et al. (10) who showed Zeta potential is an effective and feasible procedure for selecting of sperm with intact DNA structure. Sperm with a high level of surface negative electrical charge are more mature and several studies have shown that the percentage of sperm with fragmented DNA were significantly lower in sperm selected in this way. Subsequent studies verified that sperm selected based on Zeta potential have a higher chance of having normal intact chromatin (11, 12). Later, this procedure was compared to another novel sperm preparation method based on hyaluronic acid binding and the results showed that although both novel sperm preparation procedures can improve the percentage of sperm with DNA fragmentation, the Zeta method was more efficient (13). In addition, it was shown that combined DGC/Zeta procedures boost the quality of the sperm selected for ICSI and lead to higher clinical pregnancy rates per embryo transfer cycle (14, 15). Considering the need for further clinical studies to evaluate the impact of sperm quality on assisted reproductive technology (ART) outcomes, wider multi-center randomized studies are required to verify the beneficial effects of DGC/Zeta sperm selection. Therefore, the aim of this blind randomised clinical trial was to evaluate the effectiveness of the DGC/Zeta procedure in improving clinical outcomes in infertile men in an independent center.

Material and Methods

Patients

All procedures performed involving human participants were in accordance with the ethical standards of the institutional research committee and with the 1975 Helsinki declaration and its later amendments or comparable standards. We performed a randomized, single-blind, clinical trial study from April 2015 till August 2017 at Rouyesh Infertility and Fertility Center belonging to the Red Crescent (IRCT20180628040270N1), after approval by the Ethical Committee of Tehran Royan Institute [Code No: IR.ACECR.Royan.REC.1396.253].

All participants received a complete explanation of the trial prior to the start of the study. They were especially ensured that their semen samples would not be exposed to chemical agents. Following voluntary completion of the questionnaire, the couples signed informed consent forms. Eligible individuals were assured of confidentiality and anonymity, and that their decision to participate in, or withdraw from the study would not impact their current or future relation with the clinic or their future treatment. In this parallel blind randomized clinical trial, 205 candidate couples for ICSI cycles were randomly assigned to the DGC or DGC/Zeta groups based on a computer generated random table.

Inclusion criteria

Females were between 20 and 40 years old, with no report of endometriosis or polycystic ovaries. Presence of at least 2 to 3 follicles more than18 mm in diameters with suitable endometrium for embryo transfer in their last ultrasound before administration of human chorionic gonadotropin (hCG). Only couples with male factor infertility and at least one abnormal sperm parameter (sperm motility, concentration and morphology) below world health organization (WHO, 2010) criteria were included in this study (16).

Exclusion criteria

Couples whose rate of oocytes with abnormal features (without polar body, germinal vesicle, granularity, refractile bodies, fragmented, or degenerated polar bodies) exceeded 10%, were excluded from the study. Couples that did not meet the above-mentioned ultrasound criteria were also exclude from the study. As were infertile men with varicocele.

Sperm preparation using density gradient centrifugation

A two-layer density gradient system (40 and 80%) was prepared using PureSperm (Nidacon, Göteborg, Sweden). Following semen liquefaction, each semen sample was placed on the gradients and centrifuged at 300 g for 20 minutes. Then, the pellet was collected and re-suspend into 5mlof sperm processing medium supplemented with 10% human serum albumin (HSA, Octalbin, Switzerland). The sperm suspension was then centrifuged at 300 g for 7 minutes. For insemination; the resultant pellet was diluted into 0.3 mL of sperm processing medium containing10% HAS albumin (14).

Density gradient centrifugation/Zeta procedure

For DGC/Zeta procedure, sperm pellets were washed with sperm processing media without HSA, and subsequently diluted in 4 ml sperm processing media without HSA, immediately after DGC. Subsequently, the tube was exposed to a positive charge using a rubber latex tube (14). The tube was then removed from the latex tube and held by the cap for one minute to provide the time needed for the sperm with adequate negative charge to attach to the charged tube. Then the sperm processing media containing unattached sperm was withdrawn from the tube and the tube was washed with sperm processing medium containing HSA in order to detach the attached sperm. Ultimately, the content of each tube was centrifuged and the pellet was diluted in sperm processing media with HSA and used for ICSI. To reduce inter-sample variation, a single trained individual carried out all the procedures for sperm processing. The embryologist who inseminated the sperm was blind to the allocation of the sperm to the two groups; DGC and DGC/Zeta.

Intracytoplasmic sperm injection procedure

Stimulation and ovum pick up procedures were performed base on a single standard protocol for all cases

(17). Around 16-18 hours post-ICSI, the presence of male and female pronuclei was considered as a sign of successful fertilization and the rate of fertilization was calculated as the percentage of injected oocytes that became fertilized. An embryo was selected and considered to be a top quality embryo if there were six to eight blastomeres on day 3 with fragmentation less than 25% and the absence of multi nucleated blastomeres at any stage of early development. The percentage of top quality embryos was defined as the number of top embryos obtained from the total number of cleaved embryos. Procedures of embryo transfer were similar in both groups and were carried out by an embryologist who was not aware of the design of the clinical trial. The embryologist was asked to select the best embryos for transfer and a minimum of one and a maximum of three embryos were transferred. Based on the internal policy of the center, individuals under the age of 35 can receive a maximum of 2 embryos whileindividualsover35 were allowed to request for the transfer of a maximum of 3 embryos if two top quality embryos are not available. Blastocyst quality was assessed on day 5 (18). All embryos were transferred fresh. Chemical and clinical pregnancy were defined as β-hCG levels higher than 10 IU and the presence of a gestational sac, 5 weeks after embryo transfer, respectively.

Statistical analysis

SPSS for Windows Version 18 (SPSS Inc., Chicago, IL, USA) was used for all statistical analyses. Data are presented as means ± SEM for continuous variables. Independent-samples t test was used for comparisons of couples' age and sperm parameters between DGC/Zeta and DGC groups (Table 1). Independent student's t test and Chi-square carried out for statically analyzing was used for comparisons of fertilization, good-quality embryo, pregnancy, implantation, and miscarriage (Table 2). The value of $P<0.05$ was considered statistically significant. This clinical trial study was a continuation of the Nasr-Esfahani group study (15). To detect the effect of DGC/Zeta on clinical outcome in male factor infertility patients following ICSI which is in agreement with the study of Nasr Esfahani et al. (15) with a power of 80%, a sample size of 103 patients per group was necessary, given an anticipated dropout rate of 10%.

Table 1: Comparison of couples age, and sperm parameters between density gradient centrifugation (DGC)/Zeta and DGC groups

Parameters	DGC/Zeta	DGC	P value
Male age (Y)	36.40 ± 3.28	35.87 ± 2.35	0.25^{NS}
Female age (Y)	31.25 ± 0.44	32.04 ± 0.58	0.23^{NS}
Sperm concentration (10^6/ml)	34.44 ± 3.41	35.22 ± 3.20	0.38^{NS}
Total sperm motility (%)	37.74 ± 1.41	38.21 ±1.37	0.90^{NS}
Progressive motility (%)	14.83 ± 1.61	15.01 ± 1.48	0.54^{NS}
Sperm normal morphology (%)	3.20 ± 0.41	4.04 ± 0.65	0.11^{NS}

Data are presented as mean ± SEM and analyzed by independent-samples t test. Asterisk indicate significant difference; *; P<0/05, and NS; Non significant.

Table 2: Comparison of clinical outcomes between density gradient centrifugation (DGC)/Zeta and DGC groups

Parameters	DGC/Zeta n=103	DGC n=102	P value
Number of oocyte retrievals	6.54 ± 0.35	7.12 ± 0.30	0.15^{NS}
Fertilization rate (%)	64.75 ± 1.67	58.88 ± 1.83	0.67^{NS}
Number of embryos transferred	2.40 ± 0.11	2.28 ± 0.10	0.80^{NS}
Good quality of embryo at day 3 (%)	41.89 ± 2.01	30.64 ± 3.51	0.04^{*}
Blastocyst formation rate on day 5 (%)	41.5 ± 1.53	37.84 ± 1.71	0.51^{NS}
Good quality blastocyst (%)	33.69 ± 1.22	23.86 ± 1.51	0.049^{**}
Expand blastocyst (%)	48.2 ± 2.11	39.24 ± 2.75	0.007^{**}
Hatching blastocyst (%)	1.2 ± 0.82	0.4 ± 0.68	0.005^{**}
Clinical pregnancy rate (%)	36/103 (35%)	21/102 (20.68%)	0.007^{**}
Implantation rate (%)	21/103 (20.48%)	12/102 (11.42%)	0.17^{NS}
Miscarriages rate (%)	5/56 (8.92%)	6/31 (19.35%)	0.04^{*}
Chemical pregnancy (%)	44/103 (42.71%)	22/102 (21.56%)	0.005^{**}

Data are presented as mean ± SEM and analyzed by Independent student's t test and Chi-square. Asterisks indicate significant difference; **; P<0/01 , *; P<0/05, and NS; Non significant.

Results

In this randomized clinical trial, a total of 240 infertile couples were recruited and 220 couples agreed to partake in this study. These couples were randomly divided into two groups based on the randomization table generated by a computer into the DGC/Zeta or DGC groups. Of the 220 infertile couples, 7 couples were excluded from the study based on exclusion criteria (3 and 4 couples in the DGC/Zeta and DGC groups, respectively). Of the 213 remaining couples 8 couples decided to leave the study for personal reasons. Finally, of the 205 remaining couples 103 and 102 belonged to DGC/Zeta and DGC groups, respectively. Baseline characteristics of the DGC/Zeta and DGC groups including male age (P=0.25), female age (P=0.23) semen parameters including [sperm concentration (P=0.38), total motility (P=0.9) and normal morphology (P=0.11)] were analyzed and compared between the two groups. These were found to be similar in both groups and no significant differences were observed (Table 1).

The clinical outcomes

The clinical outcomes of a total 205 cycles in two groups were evaluated and compared (Table 2). The mean number of retrieved oocytes and transferred embryos in the two groups were similar without any significant differences. An obvious drift towards a superior fertilization rate was seen in the DGC/Zeta procedure compared to DGC alone (64.75 ± 1.67 vs. 58.88 ± 1.83, P=0.67). Although, there was no statistically significant difference in the mean number of embryos transferred between the two groups (P=0.8), but mean percentage of good embryo quality at day 3 (41.89 ± 2.01 vs. 30.64 ± 3.51, P=0.04), good quality of blastocysts (33.69 ± 1.22 vs. 23.86 ± 1.51, P=0.049), expanded blastocysts (48.2 ± 2.11 vs. 39.24 ± 2.75, P=0.007), and mean of hatching blastocysts (1.2 ± 0.82 vs. 0.4 ± 0.68, P=0.005) were significantly higher in the DGC/Zeta group compared to the DGC group. The percentage of chemical (P=0.005) and clinical (P=0.007) pregnancy rates in the DGC/Zeta group were 42.47 and 35.03, respectively. However these rates were 21.10% and 20.43% respectively in the DGC group. The mean percentage of implantation rate were insignificantly (P=0.17) higher in the DGC/Zeta group (20.80) compared to the DGC group (11.96). While the mean percentage of missed spontaneous abortion/missed miscarriages were significantly (P=0.04) lower in the DGC/Zeta group (8.9) compared to the DGC group (19.01).

Discussion

Numerous methods have been developed to eliminate morphologically normal sperm with damaged DNA from being inseminated during the ICSI procedure, which is a shortcoming of conventional ICSI procedures. Each of these approaches has advantages and disadvantage which have been covered by extensive reviews in this filed (1, 8, 9). The outer surface of the sperm plasma membrane is rich in sialic acids. These sialic acids are responsible for the membrane's negative electrical charge of around −16 to −20 mV called the "Zeta potential" or electrokinetic potential (19, 14). Sperm selection based on Zeta potential is a new strategy in order to acquire functional sperm in a manner that optimizes sperm recovery rates specially of sperm with normal DNA integrity to improve ICSI outcomes (20, 21).

Despite clear evidence showing benefits of selecting sperm based on Zeta potential, low enthusiasm for the implementation of this technique is due to the limited number of clinical trials. Ainsworth et al. (22-24) and Fleming et al. (25) introduced a device based on Zeta potential or electrophoresis and their preliminary studies showed that ICSI outcomes can be improved by this approach. In this regard, the first pregnancy reported using the electrophoresis method in infertile couples with previous repeated failed fertilization, and high sperm DNA fragmentation (22). In addition, Fleming et al. (25) compared clinical outcomes of ICSI or IVF between the electrophoretic method and the DGC procedure, and concluded that the mean fertilization rate, and embryo quality were similar between the two groups. Then, they reported that the electrophoretic method can be harmful for sperm motility. Unlike the electrophoretic method, the Zeta method is simple, low cost, fast, and no chemicals are used during the preparation of the sperm. In this regard, the Nasr-Esfahani et al. (15), by inducing positive charge on the surface of a tube showed that ICSI outcome, especially clinical pregnancy rate can be improved by this technique compared to DGC alone. Based on their experience, we also decided to assess the efficiency of this technique in a sister clinic in different location independently of this group but through their collaboration and with the transfer of experience. Thus, following randomization, a total of 103 and 102 infertile couples were allocated to the DGC/Zeta and DGC groups, respectively and the clinical outcomes were evaluated. In this study, higher rates of good embryo quality, blastocysts, expanded blastocysts, hatching blastocysts, chemical and clinical pregnancy were seen in the DGC/Zeta group. In addition, the results of this study also revealed that the selection of sperm through the DGC/Zeta procedure did not significantly affect the fertilization rate but significantly improves embryo quality. This is consistent with the results of previous studies suggesting that sperm DNA damage does not necessarily preclude sperm from participating in the process of fertilization but can significantly affect the embryo quality especially during maternal-embryonic genomic transition (26). These results are in agreement with a previous randomized trial study by Nasr Esfahani et al. (15) and represented an improvement in clinical outcomes after injection of sperm with DGC/Zeta processing. Major causes of significant difference in clinical consequences between the two procedures, (DGC/Zeta vs. DGC alone), may be due to the ability of DGC/Zeta for selecting mature sperm with lower DNA damage compared to DGC alone. Indeed, a high rate of sperm DNA damage has been associated with reduced clinical outcomes following assisted reproduction, increased time to conception and high rate of abortion (11, 26-29).

Conclusion

The results of this blind clinical trial along with other reports in the literature reveal that selection of sperm based on Zeta is able to recover a population of mature sperm with intact DNA and eliminate sperm with a high degree of DNA fragmentation. Therefore, the improved efficacy should be particularly valuable in ART. Accordingly, we recommend specialists working in field of assisted reproduction to evaluate the capacity of Zeta procedure especially for couples with previous implantation failures. However, use of a device for the selection of sperm based on Zeta potential may even further improve the efficiency of clinical outcomes post ICSI and reduce variations between different studies.

Acknowledgements

The authors express their gratitude to Royan Institute and Kharazmi University for its financial support and the staff of Rouyesh Fertility and Infertility Center belonging to the Red Crescent, for their kind collaboration. The authors declare no conflicts of interest.

Authors' Contributions

M.H.N.-E; Contributed to conception and design, contributed extensively in interpretation of the data and the conclusion, and were responsible for overall supervision. H.M.K.; Supervised the analysis and interpretation of the data. A.H.Sh.; Contributed to the statistical analysis, and interpretation of data. H.Ch.; Contributed to the data collection and interpretation of data. N.K.; Performed the experiment and contributed to the data collection and evaluation. M.T; Participated in study design, were responsible for overall supervision. All authors read and approved the final manuscript.

Reference

1. Rappa KL, Rodriguez HF, Hakkarainen GC, Anchan RM, Mutter GL, Asghar W. Sperm processing for advanced reproductive technologies: Where are we today? Biotechnol Adv. 2016; 34(5): 578-587.
2. Boitrelle F, Guthauser B, Alter L, Bailly M, Bergere M, Wainer R, et al. High-magnification selection of spermatozoa prior to oocyte injection: confirmed and potential indications. Reprod Biomed Online. 2014; 28(1): 6-13.
3. Maettner R, Sterzik K, Isachenko V, Strehler E, Rahimi G, Alabart JL, et al. Quality of human spermatozoa: relationship between high-magnification sperm morphology and DNA integrity .Andrologia. 2014; 46(5): 547-555.
4. Avendaño C, Oehninger S. DNA fragmentation in morphologically normal spermatozoa: how much should we be concerned in the ICSI era? J Androl. 2011; 32(4): 356-363.
5. Avendaño C, Franchi A, Duran H, Oehninger S. DNA fragmentation of normal spermatozoa negatively impacts embryo quality and intracytoplasmic sperm injection outcome. Fertil Steril. 2010; 94(2): 549-557.
6. Esteves SC, Roque M, Bradley CK, Garrido N. Reproductive outcomes of testicular versus ejaculated sperm for intracytoplasmic sperm injection among men with high levels of DNA fragmentation in semen: systematic review and meta-analysis. Fertil Steril. 2017; 108(3): 456-467. e1.
7. Santi D, Spaggiari G, Simoni M. Sperm DNA fragmentation index as a promising predictive tool for male infertility diagnosis and treatment management - meta-analyses. Reprod Biomed Online. 2018; 37(3): 315-326.
8. McDowell S, Kroon B, Ford E, Hook Y, Glujovsky D, Yazdani A. Advanced sperm selection techniques for assisted reproduction. Cochrane Database Syst Rev. 2014; (10): CD010461.
9. Nasr-Esfahani MH, Deemeh MR, Tavalaee M. New era in sperm selection for ICSI. Int J Androl. 2012; 35(4): 475-484.
10. Chan PJ, Jacobson JD, Corselli JU, Patton WC. A simple zeta method for sperm selection based on membrane charge. Fertil Steril. 2006; 85(2): 481-486.
11. Simon L, Ge SQ, Carrell DT. Sperm selection based on electrostatic charge. Methods Mol Biol. 2013; 927: 269-278.
12. Zarei-Kheirabadi M, Shayegan Nia E, Tavalaee M, Deemeh MR, Arabi M, Forouzanfar M, et al. Evaluation of ubiquitin and annexin V in sperm population selected based on density gradient centrifugation and zeta potential (DGC-Zeta). J Assist Reprod Genet. 2012; 29(4): 365-371.
13. Razavi SH, Nasr-Esfahani MH, Deemeh MR, Shayesteh M, Tavalaee M. Evaluation of zeta and HA-binding methods for selection of spermatozoa with normal morphology, protamine content and DNA integrity. Andrologia. 2010; 42(1): 13-19.
14. Kheirollahi-Kouhestani M, Razavi S, Tavalaee M, Deemeh MR, Mardani M, Moshtaghian J, et al. Selection of sperm based on combined density gradient and Zeta method may improve ICSI outcome. Hum Reprod. 2009; 24(10): 2409-2416.
15. Nasr- Esfahani MH, Deemeh MR, Tavalaee M, Sekhavati MH, Gourabi H. zeta sperm selection improves pregnancy rate and alters sex ratio in male factor infertility patients: a double-blind, randomized clinical trial. Int J Fertil Steril. 2016; 10(2): 253-260.
16. World Health Organization. WHO Laboratory Manual for the examination and processing of human semen. 5th ed. Geneva, Switzerland: WHO Press; 2010; 1-271.
17. Verberg M, Macklon N , Nargund G , Frydman R, Devroey P, Broekmans FJ, et al. Mild ovarian stimulation for IVF. Hum Reprod Update. 2009; 15(1): 13-29.
18. Baczkowski T, Kurzawa R, Głabowski W. Methods of embryo scoring in in vitro fertilization. Reprod Biol. 2004; 4(1): 5-22.
19. Schröter S, Osterhoff C, McArdle W, Ivell R. The glycocalyx of the sperm surface. Hum Reprod Update. 1999; 5(4): 302-313.
20. Zahedi A, Tavalaee M, Deemeh MR, Azadi L, Fazilati M, Nasr-Esfahani MH. Zeta potential vs apoptotic marker: which is more suitable for ICSI sperm selection? J Assist Reprod Genet. 2013; 30(9): 1181-1186.
21. Kam TL, Jacobson JD, Patton WC, Corselli JU, Chan PJ. Retention of membrane charge attributes by cryopreserved- thawed sperm and Zeta selection. J Assist Reprod Genet. 2007; 24(9): 429-434.
22. Ainsworth C, Nixon B, Jansen RP, Aitken RJ. First recorded pregnancy and normal birth after ICSI using electrophoretically isolated spermatozoa. Hum Reprod. 2007; 22(1): 197-200.
23. Ainsworth C, Nixon B, Aitken RJ. Development of a novel electrophoretic system for the isolation of human spermatozoa. Hum Reprod. 2005; 20(8): 2261-2270.
24. Ainsworth CJ, Nixon B, Aitken RJ. The electrophoretic separation of spermatozoa: an analysis of genotype, surface carbohydrate composition and potential for capacitation. Int J Androl. 2011; 34(5 Pt 2): e422-e434.
25. Fleming SD, Ilad RS, Griffin AM, Wu Y, Ong KJ, Smith HC, et al. Prospective controlled trial of an electrophoretic method of sperm preparation for assisted reproduction: comparison with density gradient centrifugation. Hum Reprod. 2008; 23(12): 2646-2651.
26. Zheng WW, Song G, Wang QL, Liu SW, Zhu XL, Deng SM, et al. Sperm DNA damage has a negative effect on early embryonic development following in vitro fertilization. Asian J Androl. 2018; 20(1): 75-79.
27. Tavalaee M, Razavi S, Nasr-Esfahani MH. Influence of sperm chromatin anomalies on assisted reproductive technology outcome. Fertil Steril. 2009; 91(4): 1119-1126.
28. Simon L, Zini A, Dyachenko A, Ciampi A, Carrell DT. A systematic review and meta-analysis to determine the effect of sperm DNA damage on in vitro fertilization and intracytoplasmic sperm injection outcome. Asian J Androl. 2017; 19(1): 80-90.
29. Cissen M, Wely MV, Scholten I, Mansell S, Bruin JP, Mol BW, et al. Measuring sperm DNA fragmentation and clinical outcomes of medically assisted reproduction: a systematic review and meta-analysis. PLoS One. 2016; 11(11): e0165125. Androl. 2017; 19(1): 80-90.

Original Article

Comparison of *PLZF* Gene Expression between Pluripotent Stem Cells and Testicular Germ Cells

Hossein Azizi, Ph.D.[1*], Morteza Koruji, Ph.D.[2], Thomas Skutella, Ph.D.[3]

1. Faculty of Biotechnology, Amol University of Special Modern Technologies, Amol, Iran
2. Cellular and Molecular Research Center and Department of Anatomical Sciences, Iran University of Medical Sciences (IUMS), Tehran, Iran
3. Institute for Anatomy and Cell Biology, Medical Faculty, University of Heidelberg, Im Neuenheimer Feld 307, Heidelberg, Germany

Corresponding Address: P.O.Box: 46168-49767, Faculty of Biotechnology, Amol University of Special Modern Technologies, Amol, Iran
Email: h.azizi@ausmt.ac.ir

Received: 9/November/2018, Accepted: 15/January/2019

Abstract

Objective: Spermatogonial stem cells (SSCs), as unipotent stem cells, are responsible for the production of sperm throughout the male's life. Zinc finger and BTB domain containing 16 (*ZBTB16/PLZF*) genes provide various functions in the cell development, signaling pathway, growth regulatory and differentiation. Here, we aimed to investigate expression of the PLZF germ cell gene marker in testis, SSCs, pluripotent embryonic stem cells (ES cells) and ES-like cells of mouse testis.

Materials and Methods: In this experimental study, we examined the expression of the PLZF germ cell marker in the testis section and testicular cell culture of neonate and adult mice by immunohistochemistry (IMH), immunocytochemistry (ICC) and Fluidigm Real-Time polymerase chain reaction (PCR).

Results: IMH data indicated that the PLZF protein was localized in the neonate testis cells of the tubules center as well as the basal compartment of adult testis seminiferous tubules. Counting PLZF IMH-positive cells in the sections of seminiferous tubules of adult and neonate testis revealed significant expression of positive cells in adult testis compared to the neonate ($P<0.05$). Under *in vitro* conditions, isolated SSC colonies were strongly ICC-positive for the PLZF germ cell marker, while ES cells and ES-like cells were negative for PLZF. Fluidigm Real-Time-PCR analysis demonstrated a significant expression of the *PLZF* germ cell gene in the neonate and adult SSCs, compared to ES cells and ES-like cells ($P<0.05$).

Conclusion: These results indicate that PLZF is a specific transcription factor of testicular germ cell proliferation, but it is down-regulated in pluripotent germ cells. This can be supportive for the analysis of germ cells development both *in vitro* and *in vivo*.

Keywords: Embryonic Stem Cells, Germ Cells, *PLZF* Gene, Spermatogonial Stem Cells

Cell Journal(Yakhteh), Vol 22, No 1, April-June (Spring) 2020, Pages: 60-65

Citation: **Azizi H, Koruji M, Skutella T. Comparison of PLZF gene expression between pluripotent stem cells and testicular germ cells. Cell J. 2020; 22(1): 60-65. doi: 10.22074/cellj.2020.6532.**

Introduction

Germ cells are formed and matured during early embryogenesis from primordial germ cells (PGCs) (1). Spermatogonial stem cells (SSCs) are the adult stem cells located in the basal membrane of seminiferous tubules of testis. They receive cytokines from somatic cells including Sertoli cells, blood vessels, Leydig cells and macrophages. SSCs can be isolated by fluorescence-activated cell sorting (FACS), magnetic-activated cell sorting (MACS), matrix selection and morphology-based selection (2-4). SSCs have the potential for conversion into embryonic stem (ES)-like pluripotent stem cells under defined *in vitro* culture conditions (2-5).

Extrinsic secreted growth factors from the SSCs niche and intrinsic gene expression play a crucial role in the maintenance of SSCs (2, 6). Extrinsic factors which are produced and secreted by Sertoli cells include glial cell-derived neurotrophic factor (GDNF) and KIT ligand (KITL) (7). Intrinsic factors include PLZF (8, 9), ETV5 (10), Taf4b (11), Bcl6b (12), Pou5f1, Nrg1, Nanog and Gja1 (13-15) as well as Gfra1 and RET (16). The transcription factor PLZF, as a transcriptional repressor that regulates the epigenetic state of undifferentiated cells, is involved in different cellular functions such as cell proliferation, apoptosis and differentiation during spermatogenesis, neurogenesis and embryonic development (8, 17, 18).

Filipponi et al. (19) demonstrated that PLZF directly represses the transcription of kit, a marker of spermatogonial differentiation. PLZF plays an essential role in the self-renewal and maintenance of the SSC in the testis niche (8). It has been shown that PLZF is co-expressed with Oct4 in undifferentiated spermatogonia. It has also been demonstrated that loss of the encoding *PLZF* gene produces limited numbers of normal spermatozoa and then leading progressively to the lack of respected germline after birth. During embryogenesis, PLZF regulates the stage of gene expressions of limb and axial skeletal patterning (8, 9, 20). During limb development, it has been demonstrated that PLZF has genetic relationship with *Gli3* and *Hox5* genes (21, 22). Previous studies showed that PLZF was expressed in testis and SSCs, therefore recognized as a SSC marker (23-25). In the present research we have extended our study to the expression of PLZF marker in the neonate and adult testis sections, isolated SSCs, ES cells and generated ES-like cells from mouse testicular culture to evaluate if PLZF has the same expression pattern in both testicular germ cells and pluripotent stem cells. The results indicated that PLZF is clearly expressed in germ cells, but not in pluripotent stem cells.

Material and Methods

Digestion and culture of testicular cells

In this experimental study, neonate and adult C57BL/6 mouse strain testis cells were isolated by collagenase IV (0.5 mg/ml), DNase (0.5 mg/ml) and Dispase (0.5 mg/ml, all from Sigma-Aldrich, USA) enzymatic digestion solution solved in Hank's Balanced Salt Solution (HBSS) buffer containing Ca^{2+} and Mg^{2+} (PAA, USA). Digested testicular cells was cultured in SSC condition medium, composed of StemPro-34 medium, 6 mg/ml D+glucose (Sigma-Aldrich, USA), 1% L-glutamine (PAA, USA), 1% N2-supplement (Invitrogen, USA), 0.1% β-mercaptoethanol (Invitrogen, USA), 1% penicillin/streptomycin (Pen/Strep, PAA, USA), 5 µg/ml bovine serum albumin (BSA, Sigma-Aldrich, USA), 1% non-essential amino acids (NEAA, PAA, USA), 30 ng/ml estradiol (Sigma-Aldrich, USA), 60 ng/ml progesterone (Sigma-Aldrich, USA), 20 ng/ml epidermal growth factor (EGF, Sigma-Aldrich, USA), 10 ng/ml fibroblast growth factor (FGF, Sigma-Aldrich, USA), 8 ng/ml GDNF (Sigma-Aldrich, USA), 100 U/ml human leukemia inhibitory factor (LIF, Millipore, USA), 1% Minimum Essential Medium (MEM) vitamins (PAA, USA), 1% ES cell qualified fetal bovine serum (FBS, Gibco, USA), 100 µg/ml ascorbic acid, 30 µg/ml pyruvic acid and 1 µl/ml DL-lactic acid (all from Sigma Aldrich, USA) at 37˚C and 5% CO_2 in air (2).

Culture of the embryonic stem and ES-like cells

ES and ES-like cell lines were originated from our previous study (2). These cells were cultured in medium with KO-DMEM, composed of 1% NEAA solution, 15% FBS, 1% L-glutamine, 0.1% β-mercaptoethanol, LIF at a final concentration of 1000 U/ml and 1% Pen/Strep (2).

Gene expression analyses on the Fluidigm Biomark system

Quantity of the *PLZF* gene expression (Mm01176868_m1) in the neonate SSCs, adult SSCs, ES cells, and ES-like cells were examined by dynamic array chips (Fluidigm). Glyceraldehyde-3-phosphate dehydrogenase (*GAPDH*, Mm99999915_g1) was used as housekeeping gene for normalization. Cultured cells were selected with a micromanipulator, lysed with lysis buffer solution containing 1.3 µl TE buffer, 0.2 µl RT/Taq Superscript III (Invitrogen, USA), 9 µl RT-PreAmp Master Mix, 5.0 µl Cells Direct 2× Reaction Mix (Invitrogen, USA), and 2.5 µl 0.2× assay pool. Using TaqMan real-time PCR on the BioMark Real-Time quantitative PCR (qPCR) system, the amount of RNA-targeted copies was evaluated. Samples were examined in two technical repeats. The Ct values were analyzed by GenEx software from the MultiD analysis (2, 3, 6).

Immunocytochemical staining

SSCs, ES cells and ES-like cells were fixed with 4% paraformaldehyde and then permeabilized with 0.1% Triton/PBS. Cells were blocked with 1% BSA/PBS and followed by incubation with primary antibody PLZF. In the next step, we used overnight incubation fluorochrome species-specific secondary antibody and the labeled cells were nuclear counterstained with 0.2 µg/ml of 4', 6-diamidino-2-phenylindole (DAPI) dye. The labeled positive cells were studied with a confocal microscope Zeiss LSM 700 (Germany), and images were acquired using a Zeiss LSM-TPMT camera (Germany) (2, 26-28).

Tissue processing for immunohistofluorescence staining

Mouse testis tissue was washed with PBS and fixed in 4% paraformaldehyde. Dehydrated tissue was surrounded in Paraplast Plus and cut with a microtome machine at 10 µm thickness. Testis tissue sections were mounted on Superfrost Plus slides and kept at room temperature until used. For processing of immunohistofluorescence staining, samples were washed with xylene followed by gradually replacing with water in ethanol before staining. For the tissue sections, antigen retrieval was performed by heat-induced epitope retrieval at 95˚C for 20 minutes, non-specific binding site of tissue samples was blocked with 10% serum/0.3% Triton in PBS. The experiment of immunofluorescence staining for these samples was continued as explained above (2).

Statistical analysis

The expression of PLZF in the indicated groups was calculated using one-way analysis of variance (ANOVA), continued with the Tukey's post-hoc tests (t Test) and compared with the non-parametric Mann-Whitney's test. The difference among groups was considered statistically significant if $P<0.05$.

Results

We first studied the localization of PLZF in the neonate and adult mouse testis (Fig.1). Immunohistochemical analysis for the cross-section of testis demonstrated that PLZF protein was expressed in the cells located on the basal membrane of adult testis seminiferous tubule, while in the neonate testis, these cells were located in the center of the tubules (Fig.1). Counting PLZF positive cells in the testis sections of the adult and neonate testis revealed significantly higher expression ($P<0.05$) of these cells in the adult compared to neonate (Fig.2). Furthermore, neonate and adult SSCs, ES cells and ES-like cells were cultivated *in vitro*, in the defined medium to investigate *PLZF* expression. Neonate and adult SSCs were isolated after enzyme digestion and generated cells cultivated in the presence of growth factors supporting SSC cultivation (Fig.3). Characterization of the isolated SSCs was conducted as described in our former study (2). Immunocytochemistry (ICC) analysis revealed that SSCs were positive, while pluripotent ES and ES-like cells were negative for the PLZF protein (Figs.3, 4). ES-like cell lines containing promoter-reporter *Oct4-GFP* transgenic mice revealed that these pluripotent cells were positive for Oct-4, but they were negative for PLZF (Fig.4). Similarly, Fluidigm real-time RT-PCR results showed significant *PLZF* gene expression in the neonate and 12-weeks old SSCs, compared to ES cells and ES-like cells ($P<0.05$, Fig.5).

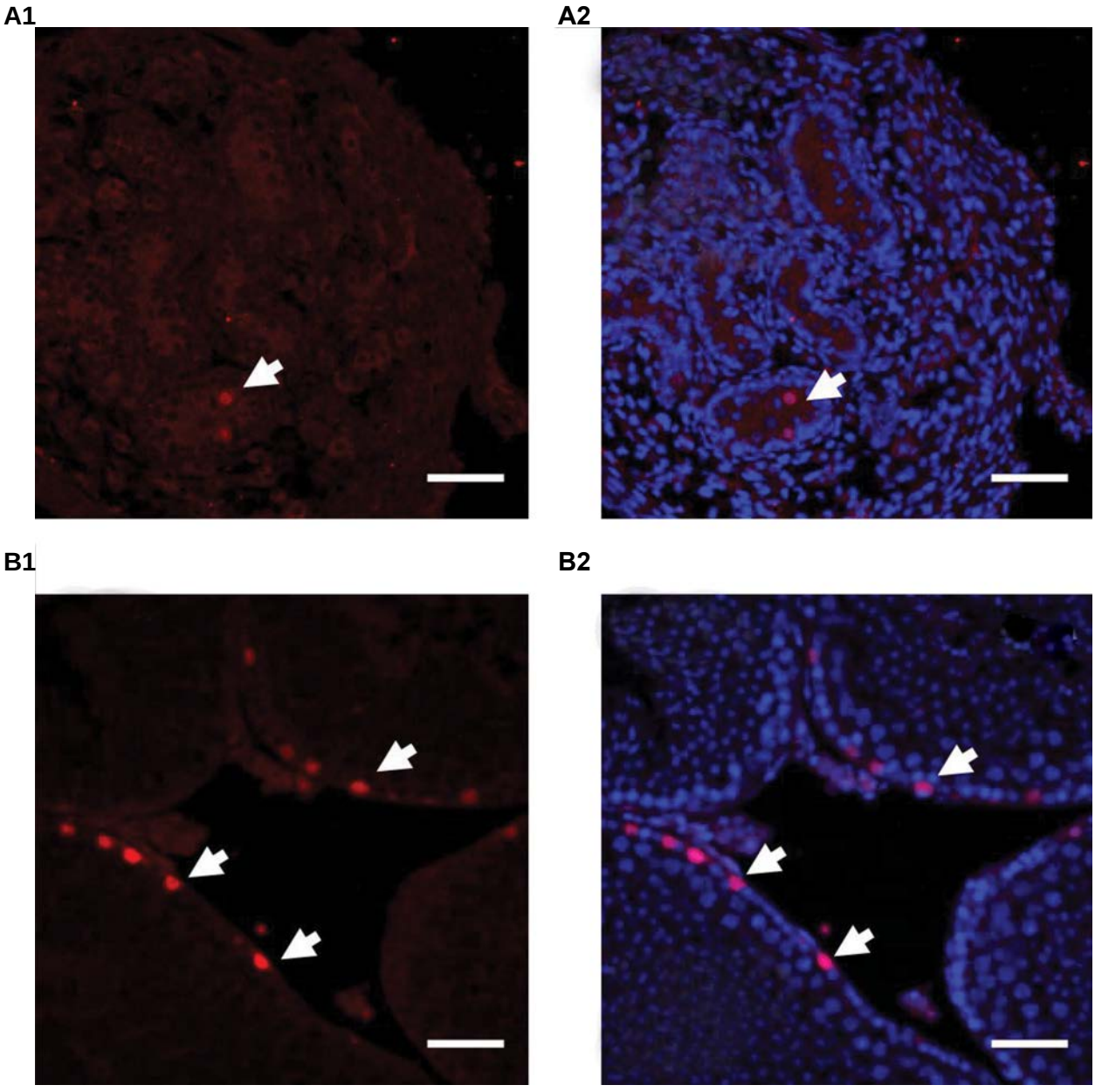

Fig.1: Immunohistochemistry characterization of PLZF in testis section. **A1.** PLZF expression in neonate, **A2.** Representation of the merged images with DAPI, **B1**. PLZF expression in Adult, and **B2.** Representation of the merged images with DAPI. PLZF; Red and DAPI; Blue.

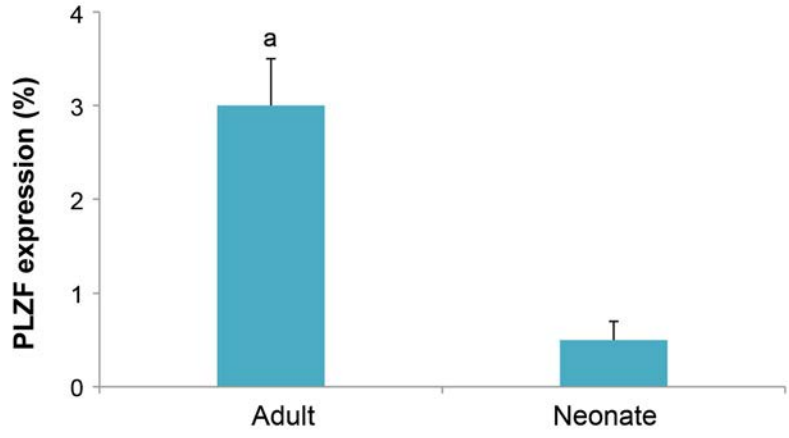

Fig.2: PLZF positive cell counting in testis section. Counting PLZF positive cells in the sections of neonate and adult testes. Number of PLZF positive cells in the adult testis was higher than neonate. a; At least $P<0.05$ versus other groups. Data are presented as mean ± SD.

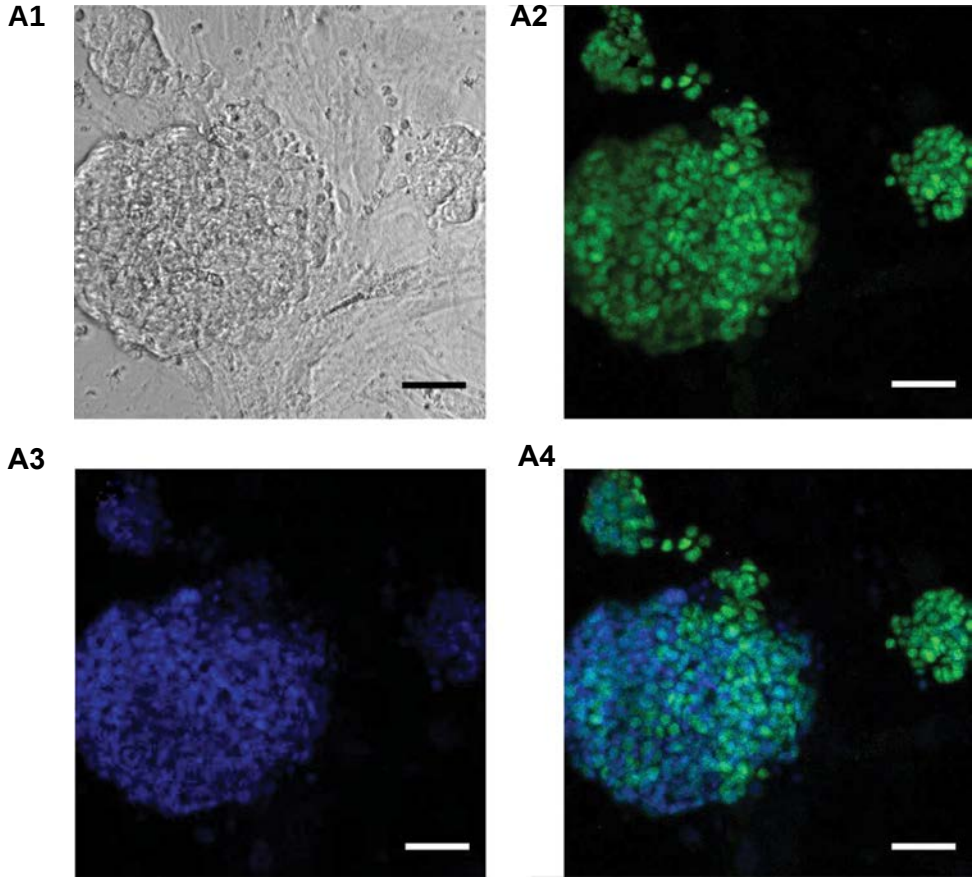

Fig.3: Immunocytochemical characterization of PLZF in spermatogonial stem cells (SSCs). Immunocytochemistry analysis of PLZF expression in the SSC (scale bar: 50 µm). **A1.** Bright field, **A2.** Green fluorescence shows PLZF expression, **A3.** Blue shows DAPI, and **A4.** Representation of the merged images.

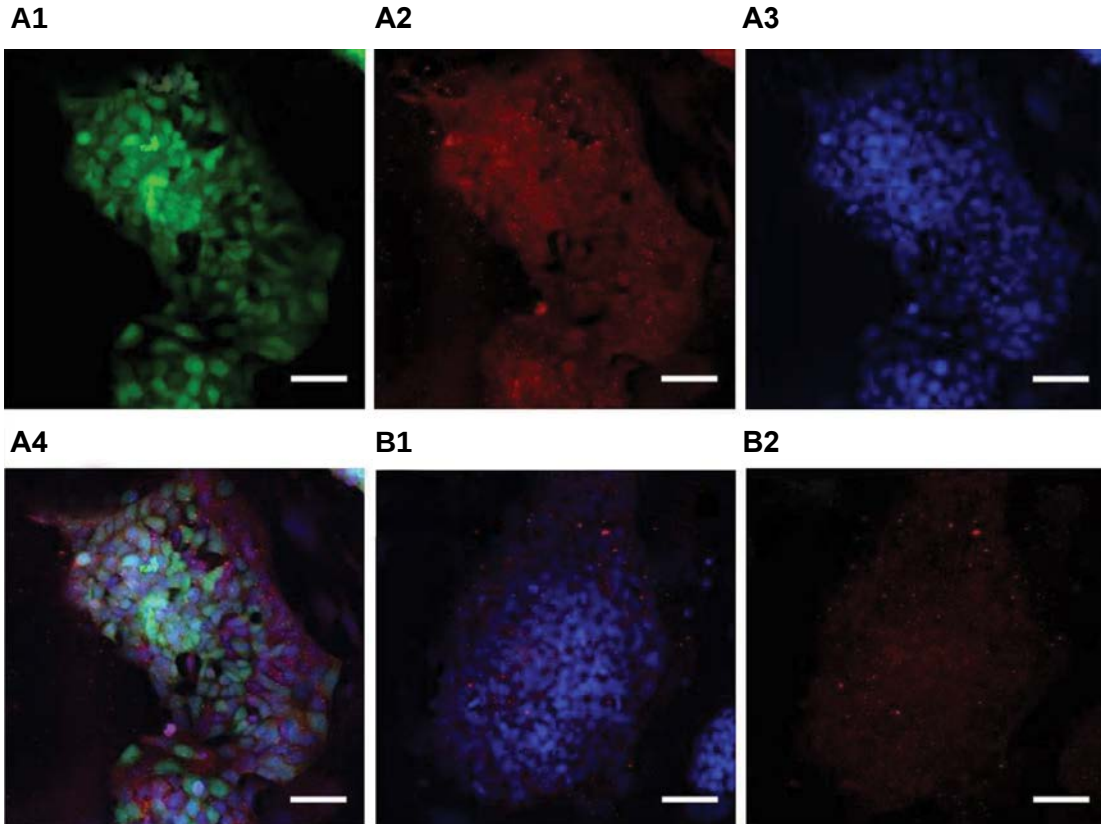

Fig.4: Immunocytochemical characterization of PLZF in the pluripotent cells. Immunocytochemistry analysis showed negative expression of PLZF in the embryonic stem (ES)-like and ES cells (scale bar: 50 µm). **A1.** ES-like, green fluorescence for Oct4, **A2.** ES-like, red fluorescence for PLZF, **A3.** ES-like, blue fluorescence for DAPI, **A4.** ES-like, merged images, **B1.** ES, blue fluorescence for DAPI, and **B2.** ES, red fluorescence fluorescence for PLZF.

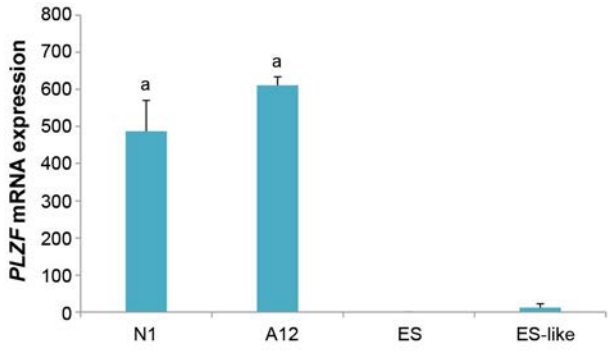

Fig.5: mRNA expression of *PLZF* gene. Fluidigm quantitative polymerase chain reaction (PCR) analysis for *PLZF* expression in the neonate (N1), 12-weeks testis (A12), ES-like and ES cells (a; at least P<0.05 versus other groups). Significant *PLZF* expression levels difference in neonate and adult SSCs compared to ES-like and ES cells. Data are presented as mean ± SD.

Discussion

It has been demonstrated that PLZF transcription factor is a key regulator in SSCs (2). Our histological analysis specified localization of the PLZF positive cells in the center of neonatal testicular cords and basal compartment of the seminiferous tubules of adult testis, co-localized with Oct4 positive cells. PLZF/Oct4 co-localization, in a few single SSCs attached to the basal membrane, implies that these cells are SSCs, but not progenitor cells. The cultured SSCs, which are grown under GDNF stimulation, are also positive for PLZF. Although the number of PLZF positive cells in adult testis was higher than neonate, *PLZF* mRNA expression level in the neonate and adult SSCs was similar. Protein analyses using immunohisto/cytochemistry revealed that PLZF was expressed in SSC, but neither in the differentiating germ cells nor in the ES-like cells directly generated from SSCs. It can be concluded that PLZF is down-regulated during both differentiation (spermatogenesis) and conversion of the unipotent SSCs into pluripotent ES-like cells. Similarly, pluripotent ES cells generated from the inner cell mass were negative for PLZF. This finding was also confirmed by Fluidigm real-time RT-PCR and ICC. These observations imply that PLZF strictly bind to and hold the molecular state of a stem cell SCCs. It is proposed that PLZF is a transcriptional repressor and activator involved in the control of SCC (29).

In undifferentiated spermatogonia, it has been shown that PLZF is co-expressed with Oct4. Mutations in the PLZF gene restrict the numbers of spermatozoa cells (9). Mutations in the PLZF display a progressive defect of SSCs and structure of the seminiferous tubule, while the function of supporting Sertoli cells is normal (20). In type A and B spermatogonia, PLZF was found to be localized in the nucleus of undifferentiated SSCs of zebrafish (30). Further studies in SSCs have indicated that the PLZF mutant shows an increase of c-Kit expression (as a marker required for differentiated SSCs), implying that PLZF maintains pool of the SSCs (19). It has been demonstrated that PLZF suppresses transcription activity of the retinoic acid receptors (31).

Although PLZF expression is positive in undifferentiated cells of stem cell compartment near the basement membrane of adult mouse testis seminiferous tubules but not in spermatocytes, it is unknown whether or not PLZF expression is necessary for initiating differentiation of the SSCs towards spermatocytes. It has been well documented that PLZF plays an important role in the self-renewal and maintenance of gonocytes and undifferentiated spermatogonia (8). PLZF has been demonstrated as a distinguished marker for the isolation of human (23, 32, 33), mouse (24, 34) and sheep SSCs in testicular culture (35).

It is well-known that PLZF can function as both transcription activator and transcription repressor. A direct activated target of PLZF is REDD1. REDD1 mediates PLZF-dependent down-regulation of TORC1 and it is responsible for the maintenance of spermatogonial progenitor cells in culture by mediating effective signaling from GDNF, while it is normally blocked by TORC1 activity. It has been postulated that the effect of REDD1 on TORC1 could also raise the possibility that REDD1 controls cell growth, tumorigenicity and senescence (36).

PLZF activates PTEN/AKT/FOXO3 signaling pathways which can suppress prostate tumorigenesis (37). Deficiency of PLZF expression in prostate cancer is associated with tumor aggressiveness and metastasis (38). Shen et al. (39) showed that PLZF expression inhibited proliferation and metastasis via regulation of the interferon-induced protein with tetratricopeptide repeat 2 and increasing STAT1 protein level.

Conclusion

Our data demonstrated that PLZF is expressed in unipotent $Oct4^{+}/VASA^{-}$ SCCs in the basal compartment of adult testis seminiferous tubules. Our findings indicate that in comparison with unipotent SSCs, PLZF expression is not detectable in pluripotent ES-like cells which are directly derived from SCCs. Furthermore pluripotent ES cells do not express PLZF. Therefore, it could be proposed that PLZF represses and activates target genes which are specifically important for the maintenance of SSC. In the future, it would be interesting to anlyse the mechanism of PLZF down-regulation while SSCs shift to plutipotency and vice versa, during differentiation of pluripotent stem cells towards SSC *in vitro*.

Acknowledgements

This research was granted by the International Scientific Meeting Office, Ministry of Science, Research and Technology of Islamic Republic of Iran and Department of Neuroanatomy, Institute for Anatomy and Cell Biology III, University of Heidelberg, Germany. There is no conflict of interest in this study.

Authors' Contributions

H.A., T.S.; Designed and carried out the experiment. H.A., M.K., T.S.; Provided critical feedback, data analysis

and wrote the manuscript. All authors read and approved the final manuscript.

References

1. Nikolic A, Volarevic V, Armstrong L, Lako M, Stojkovic M. Primordial germ cells: current knowledge and perspectives. Stem Cells Int. 2016; 2016: 1741072.
2. Azizi H, Conrad S, Hinz U, Asgari B, Nanus D, Peterziel H, et al. Derivation of pluripotent cells from mouse SSCs seems to be age dependent. Stem Cells Int. 2016; 2016: 8216312.
3. Conrad S, Azizi H, Hatami M, Kubista M, Bonin M, Hennenlotter J, et al. Expression of Genes related to germ cell lineage and pluripotency in single cells and colonies of human adult germ stem cells. Stem Cells Int. 2016; 2016: 8582526.
4. Conrad S, Azizi H, Hatami M, Kubista M, Bonin M, Hennenlotter J, et al. Differential gene expression profiling of enriched human spermatogonia after short- and long-term culture. Biomed Res Int. 2014; 2014: 138350.
5. Bojnordi MN, Azizi H, Skutella T, Movahedin M, Pourabdolhossein F, Shojaei A, et al. Differentiation of spermatogonia stem cells into functional mature neurons characterized with differential gene expression. Mol Neurobiol. 2017; 54(7): 5676-5682.
6. Conrad S, Azizi H, Skutella T. Single-cell expression profiling and proteomics of primordial germ cells, spermatogonial stem cells, adult germ stem cells, and oocytes. Adv Exp Med Biol. 2018; 1083: 77-87.
7. Naughton CK, Jain S, Strickland AM, Gupta A, Milbrandt J. Glial cell-line derived neurotrophic factor-mediated RET signaling regulates spermatogonial stem cell fate. Biol Reprod. 2006; 74(2): 314-321.
8. Costoya JA, Hobbs RM, Barna M, Cattoretti G, Manova K, Sukhwani M, et al. Essential role of Plzf in maintenance of spermatogonial stem cells. Nat Genet. 2004; 36(6): 653-659.
9. Buaas FW, Kirsh AL, Sharma M, McLean DJ, Morris JL, Griswold MD, et al. Plzf is required in adult male germ cells for stem cell self-renewal. Nat Genet. 2004; 36(6): 647-652.
10. Chen C, Ouyang W, Grigura V, Zhou Q, Carnes K, Lim H, et al. ERM is required for transcriptional control of the spermatogonial stem cell niche. Nature. 2005; 436(7053): 1030-1034.
11. Falender AE, Shimada M, Lo YK, Richards JS. TAF4b, a TBP associated factor, is required for oocyte development and function. Dev Biol. 2005; 288(2): 405-419.
12. Oatley JM, Avarbock MR, Telaranta AI, Fearon DT, Brinster RL. Identifying genes important for spermatogonial stem cell self-renewal and survival. Proc Natl Acad Sci USA. 2006; 103(25): 9524-9529.
13. Hamra FK, Chapman KM, Nguyen D, Garbers DL. Identification of neuregulin as a factor required for formation of aligned spermatogonia. J Biol Chem. 2007; 282(1): 721-730.
14. Yoshida S, Sukeno M, Nakagawa T, Ohbo K, Nagamatsu G, Suda T, et al. The first round of mouse spermatogenesis is a distinctive program that lacks the self-renewing spermatogonia stage. Development. 2006; 133(8): 1495-1505.
15. Brehm R, Zeiler M, Ruttinger C, Herde K, Kibschull M, Winterhager E, et al. A sertoli cell-specific knockout of connexin43 prevents initiation of spermatogenesis. Am J Pathol. 2007; 171(1): 19-31.
16. Jijiwa M, Kawai K, Fukihara J, Nakamura A, Hasegawa M, Suzuki C, et al. GDNF-mediated signaling via RET tyrosine 1062 is essential for maintenance of spermatogonial stem cells. Genes Cells. 2008; 13(4): 365-374.
17. Pearson R, Fleetwood J, Eaton S, Crossley M, Bao S. Kruppel-like transcription factors: a functional family. Int J Biochem Cell Biol. 2008; 40(10): 1996-2001.
18. Liu TM, Lee EH, Lim B, Shyh-Chang N. Concise review: balancing stem cell self-renewal and differentiation with PLZF. Stem Cells. 2016; 34(2): 277-287.
19. Filipponi D, Hobbs RM, Ottolenghi S, Rossi P, Jannini EA, Pandolfi PP, et al. Repression of kit expression by Plzf in germ cells. Mol Cell Biol. 2007; 27(19): 6770-6781.
20. Barna M, Hawe N, Niswander L, Pandolfi PP. Plzf regulates limb and axial skeletal patterning. Nat Genet. 2000; 25(2): 166-172.
21. Barna M, Pandolfi PP, Niswander L. Gli3 and Plzf cooperate in proximal limb patterning at early stages of limb development. Nature. 2005; 436(7048): 277-281.
22. Xu B, Hrycaj SM, McIntyre DC, Baker NC, Takeuchi JK, Jeannotte L, et al. Hox5 interacts with Plzf to restrict Shh expression in the developing forelimb. Proc Natl Acad Sci USA. 2013; 110(48): 19438-19443.
23. Koruji M, Shahverdi A, Janan A, Piryaei A, Lakpour MR, Gilani Sedighi MA. Proliferation of small number of human spermatogonial stem cells obtained from azoospermic patients. J Assist Reprod Genet. 2012; 29(9): 957-967.
24. Shakeri M, Kohram H, Shahverdi A, Shahneh AZ, Tavakolifar F, Pirouz M, et al. Behavior of mouse spermatogonial stem-like cells on an electrospun nanofibrillar matrix. J Assist Reprod Genet. 2013; 30(3): 325-332.
25. Azizollahi S, Aflatoonian R, Sadighi Gilani MA, Behnam B, Tajik N, Asghari-Jafarabadi M, et al. Alteration of spermatogenesis following spermatogonial stem cells transplantation in testicular torsion-detorsion mice. J Assist Reprod Genet. 2016; 33(6): 771-781.
26. Azizi H, Mehrjardi NZ, Shahbazi E, Hemmesi K, Bahmani MK, Baharvand H. Dehydroepiandrosterone stimulates neurogenesis in mouse embryonal carcinoma cell- and human embryonic stem cell-derived neural progenitors and induces dopaminergic neurons. Stem Cells Dev. 2010; 19(6): 809-818.
27. Bojnordi MN, Azizi H, Skutella T, Movahedin M, Pourabdolhossein F, Shojaei A, et al. Differentiation of spermatogonia stem cells into functional mature neurons characterized with differential gene expression. Mol Neurobiol. 2017; 54(7): 5676-5682.
28. Conrad S, Azizi H, Skutella T. Single-Cell expression profiling and proteomics of primordial germ cells, spermatogonial stem cells, adult germ stem cells, and oocytes. Adv Exp Med Biol. 2018; 1083: 77-87.
29. Hobbs RM, Seandel M, Falciatori I, Rafii S, Pandolfi PP. Plzf regulates germline progenitor self-renewal by opposing mTORC1. Cell. 2010; 142(3): 468-479.
30. Ozaki Y, Saito K, Shinya M, Kawasaki T, Sakai N. Evaluation of Sycp3, Plzf and Cyclin B3 expression and suitability as spermatogonia and spermatocyte markers in zebrafish. Gene Expr Patterns. 2011; 11(5-6): 309-315.
31. Martin PJ, Delmotte MH, Formstecher P, Lefebvre P. PLZF is a negative regulator of retinoic acid receptor transcriptional activity. Nucl Recept. 2003; 1(1): 6.
32. Sadri-Ardekani H, Mizrak SC, van Daalen SK, Korver CM, Roepers-Gajadien HL, Koruji M, et al. Propagation of human spermatogonial stem cells in vitro. JAMA. 2009; 302(19): 2127-2134.
33. Gholami K, Pourmand G, Koruji M, Ashouri S, Abbasi M. Organ culture of seminiferous tubules using a modified soft agar culture system. Stem Cell Res Ther. 2018; 9(1): 249.
34. Shabani R, Ashjari M, Ashtari K, Izadyar F, Behnam B, Khoei S, et al. Elimination of mouse tumor cells from neonate spermatogonial cells utilizing cisplatin-entrapped folic acid-conjugated poly(lactic-co-glycolic acid) nanoparticles in vitro. Int J Nanomedicine. 2018; 13: 2943-2954.
35. Qasemi-Panahi B, Movahedin M, Moghaddam G, Tajik P, Koruji M, Ashrafi-Helan J, et al. Isolation and Proliferation of Spermatogonial Cells from Ghezel Sheep. Avicenna J Med Biotechnol. 2018; 10(2): 93-97.
36. Kolesnichenko M, Vogt PK. Understanding PLZF: two transcriptional targets, REDD1 and smooth muscle alpha-actin, define new questions in growth control, senescence, self-renewal and tumor suppression. Cell Cycle. 2011; 10(5): 771-775.
37. Cao J, Zhu S, Zhou W, Li J, Liu C, Xuan H, et al. PLZF mediates the PTEN/AKT/FOXO3a signaling in suppression of prostate tumorigenesis. PLoS One. 2013; 8(12): e77922.
38. Xiao GQ, Unger P, Yang Q, Kinoshita Y, Singh K, McMahon L, et al. Loss of PLZF expression in prostate cancer by immunohistochemistry correlates with tumor aggressiveness and metastasis. PLoS One. 2015; 10(3): e0121318.
39. Shen H, Zhan M, Zhang Y, Huang S, Xu S, Huang X, et al. PLZF inhibits proliferation and metastasis of gallbladder cancer by regulating IFIT2. Cell Death Dis. 2018; 9(2): 71.

Original Article

Regulated Acyl-CoA Synthetase Short-Chain Family Member 2 Accumulation during Spermatogenesis

Afsaneh Goudarzi, Ph.D.[1, 2*], Amir Amiri-Yekta, Ph.D.[3]

1. Department of Clinical Biochemistry, School of Medicine, Shahid Beheshti University of Medical Sciences, Tehran, Iran
2. CNRS UMR 5309; INSERM, U1209; Université Grenoble Alpes; Institute for Advanced Biosciences, 38700 Grenoble, France
3. Department of Genetics, Reproductive Biomedicine Research Center, Royan Institute for Reproductive Biomedicine, ACECR, Tehran, Iran

Corresponding Address: P.O.Box: 1985717443, Department of Clinical Biochemistry, School of Medicine, Shahid Beheshti University of Medical Sciences, Tehran, Iran
Email: Afsaneh.goudarzi@sbmu.ac.ir

Received: 18/August/2018, Accepted: 19/January/2019

Abstract

Objective: Acyl-CoA synthetase short-chain family member 2 (ACSS2) activity provides a major source of acetyl-CoA to drive histone acetylation. This study aimed to unravel the ACSS2 expression during mouse spermatogenesis, where a dynamic and stage-specific genome-wide histone hyperacetylation occurs before histone eviction.

Materials and Methods: In this experimental study, ACSS2 expression levels during spermatogenesis were verified by Immunodetection. Testis paraffin-embedded sections were used for IHC staining with anti-H4 pan ac and anti-ACSS2. Co-detection of ACSS2 and H4K5ac was performed on testis tubular sections by immunofluorescence. Proteins extracts from fractionated male germ cells were subjected to western-blotting and immunoblot was probed with anti-ACSS2 and anti-actin.

Results: The resulting data showed that the commitment of progenitor cells into meiotic divisions leads to a robust accumulation of ACSS2 in the cell nucleus, especially in pachytene spermatocytes (P). However, ACSS2 protein drastically declines during post-meiotic stages, when a genome-wide histone hyperacetylation is known to occur.

Conclusion: The results of this study are in agreement with the idea that the major function of ACSS2 is to recycle acetate generated after histone deacetylation to regenerate acetyl-CoA which is required to maintain the steady state of histone acetylation. Thus, it is suggested that in spermatogenic cells, nuclear activity of ACSS2 maintains the acetate recycling until histone hyperacetylation, but disappears before the acetylation-dependent histone degradation.

Keywords: Acyl-CoA Synthetase Short-Chain Family Member 2, Epigenetics, Histone Modifications, Spermatogenesis

Cell Journal(Yakhteh), Vol 22, No 1, April-June (Spring) 2020, Pages: 66-70

Citation: **Goudarzi A, Amiri-Yekta A. Regulated acyl-coA synthetase short-chain family member 2 accumulation during spermatogenesis. Cell J. 2020; 22(1): 66-70. doi: 10.22074/cellj.2020.6306.**

Introduction

Acetylation of histones is an important controlled process playing a crucial role in the regulation of gene expression (1). Although several families of histone acetyltransferases (HATs) have thus far been identified and they have been extensively studied, the precise source of acetyl-CoA (as the universal donor of acetyl group used by these enzymes) has just recently attracted attention. Acetyl-CoA used by HATs, comes from different sources due to the activity of cytoplasmic/nuclear enzymes, including ATP citrate lyase (ACLY) and ACSS2 (2-5).

Recent investigations have particularly highlighted important role of ACSS2 in general and locus-specific histone acetylation (6). Taking into account the important role of ACSS2 in the control of histone acetylation and tissue-specific gene expression, the question of the expression pattern of its encoding gene is a highly relevant issue. In this regard, spermatogenic cell differentiation is particularly an interesting system, since this differentiation program involves a genome-wide histone hyperacetylation during its late stages, just before the occurrence of a global histone-to-protamine replacement (7). Spermatogenesis is a process generating spermatozoa from progenitor male germ cells, spermatogonia. It involves roughly three different phases including mitotic, meiotic and post-meiotic cells. At the end of mitotic phase, spermatocytes are produced which undergo two meiotic divisions, giving rise to round haploid cells named spermatids. In the post-meiotic phase, these round haploid cells differentiate into elongating/condensing spermatids. This process is accompanied by a genome-wide histone removal and their replacement by small basic proteins, transition proteins (TPs) and protamines, following a series of event coordinated by the histone variant H2A.L.2 (7, 8).

Ultimately, the elongating spermatids (EIS) undertake a real metamorphosis to become mature spermatozoa (9, 10). Despite the importance of this genome-wide exchange of histones by small basic proteins and the

associated chromatin compaction in protecting the male genome, the molecular mechanisms underlying histone disappearance have remained poorly explored (9). Previous works have described a wave of genome-wide histone H4 hyperacetylation that occurs in EIS right before histone removal. Recent works suggest that this acetylation signals the recruitment of BRDT (as a double bromodomain containing testis-specific factor) whose first bromodomain is indispensable for the removal of above-mentioned acetylated histones (7, 11). This unique physiological situation, where a global histone hyperacetylation occurs in spermatogenic cells, prompted us to consider spermatogenesis as an interesting and relevant system to monitor the stage-specific ACSS2 protein accumulation.

Materials and Methods

Chemical and reagents

In this experimental study, the utilized antibodies were as follow: ACSS2 antibody (Cell signaling, USA), anti-Actin (Sigma, Germany) and anti-H4 pan-acetyl (Millipore, Germany). Anti-H4K5ac was kindly provided by Dr. Kimura, Department of Biological Sciences, Tokyo Institute of Technology, Japan.

Protein extraction and Western-Blotting

Total protein content from whole testes and fractionated male germ cells were extracted in 8M urea and they were sonicated using Bioruptor sonication system (Diagenode, Belgium) at 250 J. Protein dosage was assessed using Bradford assay.

Male germ cells fractionation

Male germ cells at different stages of spermatogenesis including pachytene spermatocytes (P), round spermatids (RS) and ElS, were obtained by enrichment on a BSA gradient, as previously described (12).

Immunofluorescence, histology and immunohisto-chemistry

Alcohol-formalin-acetic acid-fixed (AFA-Fixed) testes were embedded in paraffin and immunostaining of ACSS2 and H4 pan-acetylation were followed by using immunohistochemistry (IHC) technique, as previously described (11). ACSS2 and histone acetylation were co-detected using anti-ACSS2 and anti-H4K5ac in prepared mouse seminiferous tubules by immunofluorescence assay, as previously described (13).

Statistical analysis

The expression levels of ACSS2 in male germ cells were normalized, according to Affymetrix or Illumina standardized processes respectively, and statistics were performed using R software and appropriate script packages. Data are expressed as mean ± standard error of mean (SEM), expression levels were compared between the different groups using t tests, and $P<0.01$ were considered to be statistically significant.

Results

Cell type-specific accumulation of ACSS2 during spermatogenesis

To investigate the potential role of ACSS2 in generating essential acetyl-CoA required for the histone H4 hyperacetylation during spermatid elongation, we focused on the expression level of corresponding protein, during the mouse spermatogenesis. To this end, we took advantage of the previously established stage-specific transcriptomic data (14, 15). This analysis showed a marked increase of ACSS2 expression between spermatogonia and spermatocytes, followed by a slight but not significant decrease in post-meiotic RS and condensing spermatids (Fig.1). Next, to determine the precise pattern of ACSS2 expression during spermatogenesis, we used sections of paraffin-embedded testes and IHC. Figure 2 confirms that ACSS2 could be easily detected in spermatocytes. Rather unexpectedly, this analysis also shows that ACSS2 is not detectable in post-meiotic cells, where histone hyperacetylation occurs (Fig.2).

To better monitor ACSS2 accumulation in spermatogenic cells and more specifically consider its intracellular localization, we used a more sensitive immunodetection of ACSS2 by immunofluorescence. In fact, Figure 3A shows that ACSS2 is robustly accumulated in P, while the protein was predominantly detected in the nucleus. The protein was also detected in post-meiotic cells, especially in EIS, but it did not significantly colocalize with the areas bearing hyperacetylated H4. In contrast, ACSS2 was rather present in nuclear regions where the histones had already been removed, since the regions was devoid of H4K5ac signal corresponding to removed histones and ACSS2 is present in this zone (Fig.3A merged image). Finally, in late elongating/condensing spermatids, ACSS2 was almost undetectable.

To make sure that the detection of ACSS2 was specific and that the absence of protein in elongating and condensing spermatids was not due to chromatin compaction and the inability of the antibody to detect the protein in situ, we prepared cells enriched at specific stages of spermatogenesis by fractionating spermatogenic cells and performed Western blots, to detect ACSS2 in these fractionated cells.

The results shown in Figure 3B confirm that ACSS2 is decreased in post-meiotic cells compared to spermatocytes. This also indicates that elongating/condensing spermatids contain only residual amounts of ACSS2.

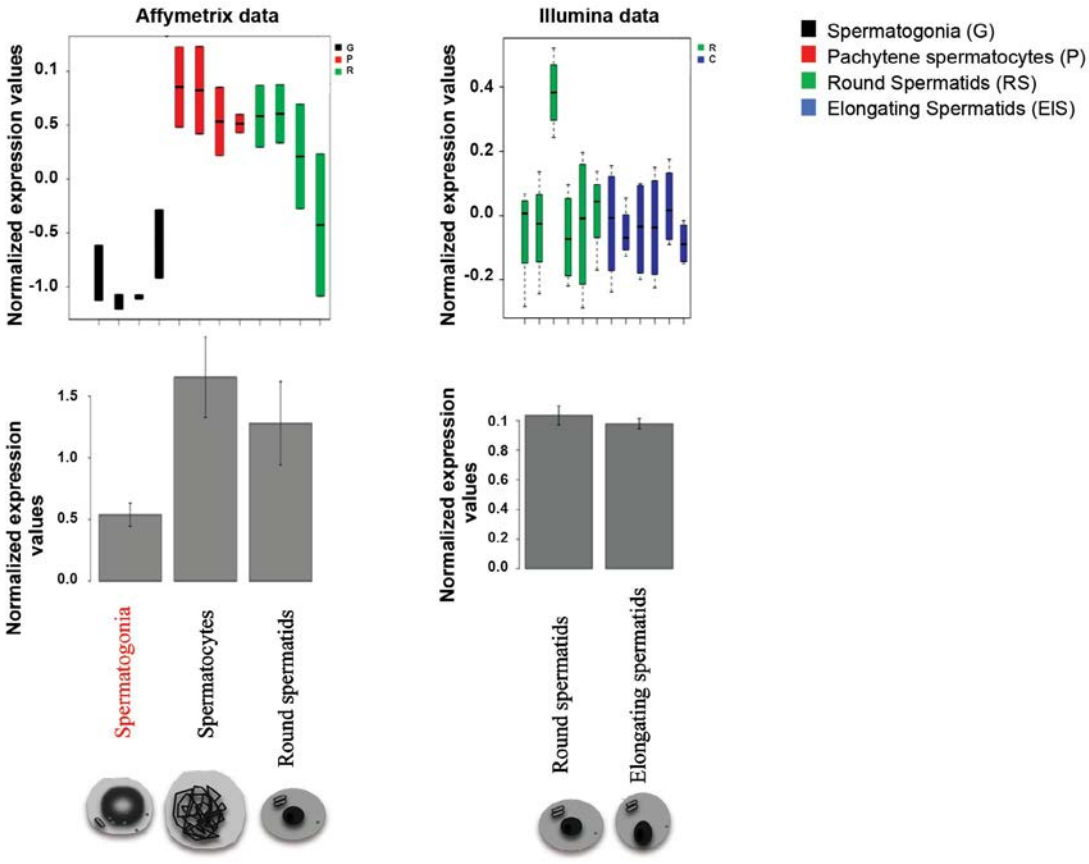

Fig.1: Stage-specific Acyl-CoA synthetase short-chain family member 2 (ACSS2) expression during spermatogenesis. Diagrams show the expression levels of ACSS2 in spermatogonia, spermatocytes, round spermatids and elongating/condensing spermatids. The expression data were obtained from microarray data, available on GEO on the Affymetrix platform GPL1261 (GSE4193, GSE21749, left panel) or the Illumina platform GPL6887 (GSE55767, right panel) (15). A significant increase in the expression level of ACSS2 was observed in meiotic cells (spermatocytes), compared to spermatogonia ($P<0.01$). Box plots are represented using the default parameters of the function "box plot" in R (black line corresponds to median value and whiskers=1.5 * interquartile range). The histograms represent mean values + standard error of mean (SEM).

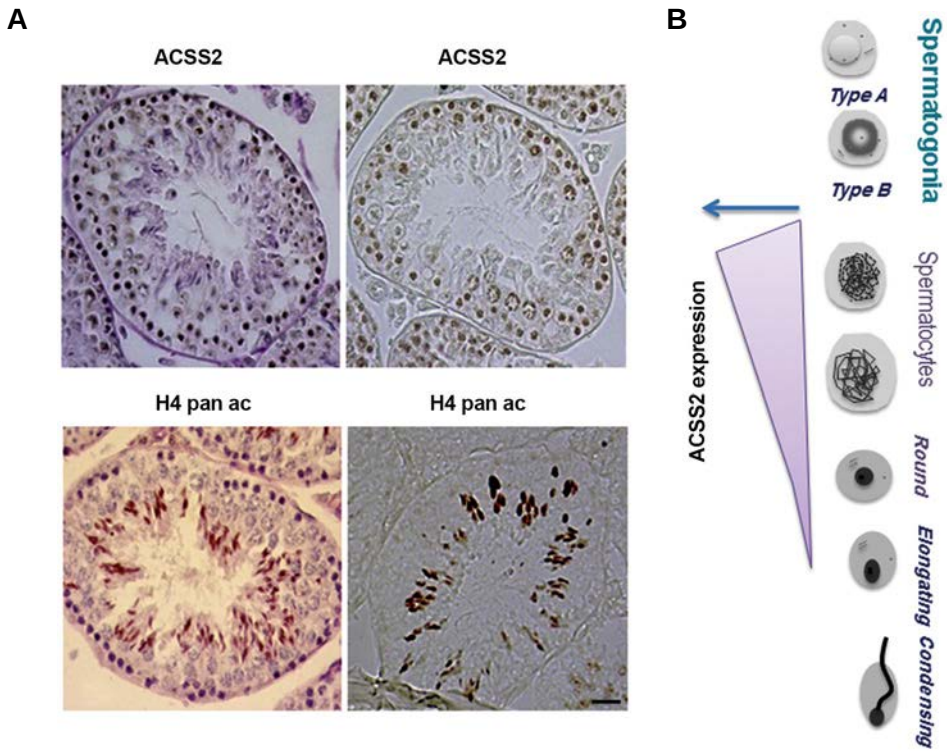

Fig.2: Acyl-CoA synthetase short-chain family member 2 (ACSS2) expression in the mouse testis. **A.** Immunohistochemistry (IHC) assay was performed on testis paraffin-embedded sections using anti-ACSS2 and H4 pan-acetylated antibodies. The two upper IHC images on the left side represent the ACSS2 signal in sections with and without counter-staining. The two lower IHC images on the left side represent H4 pan-acetylated signal in sections with and without counter-staining (scale bar: 20 µm) and **B.** The right panel shows ACSS2 expression along spermatogenesis.

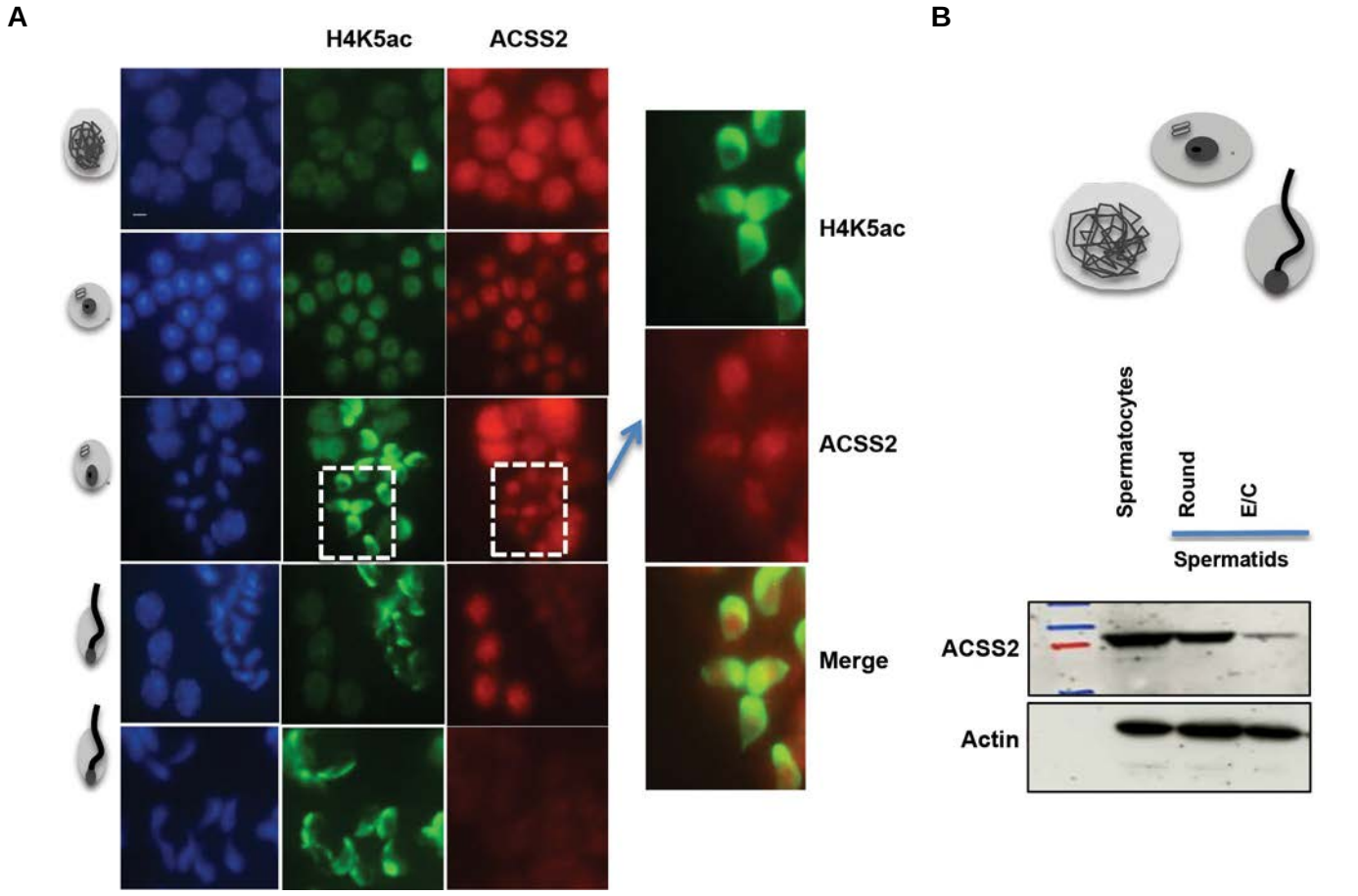

Fig.3: Acyl-CoA synthetase short-chain family member 2 (ACSS2) starts to disappear along with histone removal in post-meiotic cells. **A.** Immunofluorescent co-detection of H4K5ac (in green) and ACSS2 (in red) in mouse male germ cells. DAPI staining was used to visualize cell nuclei (scale bar: 5 µm) and **B.** Extracted total proteins from fractionated mouse male germ cells were used to detect ACSS2 in spermatocytes, round spermatids and elongating/condensing spermatids fractions using Western-blot.

Discussion

ACSS2 seems to be a major provider of acetyl-CoA for histone acetylation (16). This enzyme could directly use acetate from extracellular or intracellular sources to generate acetyl-CoA (17). One of the important missions of this enzyme is to recycle acetate released after the action of HDACs in the nucleus to feed HATs and maintain the histone acetylation turnover (18). This detailed analysis of ACSS2 expression in parallel with histone acetylation during spermatogenesis actually supports the idea that ACSS2 is, in fact, an enzyme with a major function in acetate recycling to maintain an appropriate amount of acetyl-CoA for histone acetylation. Indeed, it is now known that in elongating/condensing spermatids, the hyperacetylated histones are removed and degraded (7). Hence, under this specific circumstance, there is no more histone to acetylate and therefore no need to recycle acetate to regenerate acetyl-CoA. This situation could explain why ACSS2 is not maintained in the post-meiotic cells, at the stages they undergo histone-to-protamine replacement. Using these observations, we can propose different functions for the two major enzymes generating acetyl-CoA in the cytoplasm and nucleus. These enzymes are ACLY and ACSS2. ACLY uses CoA and citrate to generate acetyl-CoA and oxaloacetate. Although ACLY is capable of efficiently producing acetyl-CoA, it does not play role in recycling the acetate which is released after histone deacetylation. The disappearance of ACSS2 in elongating/condensing spermatids at the time of histone removal supports the idea that acetate recycling is precisely the mission of ACSS2.

Conclusion

ACSS2 should be a major actor in maintaining the steady-state of chromatin acetylation, allowing to establish an equilibrium between the action of deacetylases and acetyl-transferases. In elongating/condensing spermatids, hyperacetylated histones are targeted for degradation and hence there is no need to keep active the acetate recycling. This is certainly why ACSS2 disappears in elongating/condensing spermatids at the time of histone removal.

Acknowledgements

We gratefully acknowledge Saadi Khochbin and Sophie Rousseaux for their support and input, reading the manuscript and providing reagents. This work has been funded with a grant from a Marie Curie Initial Training Network (FP7-PEOPLE-2011-ITN, PITNGA-289880) and by CNRS/INSERM institutional funding. AG's

research is supported by Iran National Science Foundation-INSF grant (96009115). We are grateful to Ekaterina Bourouva-Flin, Thierry Buchou, Sophie Barral, Alexandra Vargas, Tao Wang and Florent Chuffart from S. K. laboratory and Dr. Salami for their support and help. The authors declare no conflict of interest.

Authors' Contributions

A.G.; Designed and carried out all the experiments, and wrote the manuscript. A.G., A.A.-Y.; Contributed in the interpretation of data, manuscript finalization and conclusion. All authors read and approved the final manuscript.

References

1. Shahbazian MD, Grunstein M. Functions of site-specific histone acetylation and deacetylation. Annu Rev Biochem. 2007; 76: 75-100.
2. Pietrocola F, Galluzzi L, Bravo-San Pedro JM, Madeo F, Kroemer G. Acetyl coenzyme A: a central metabolite and second messenger. Cell Metab. 2015; 21(6): 805-821.
3. Pinkosky SL, Groot PHE, Lalwani ND, Steinberg GR. Targeting ATP-Citrate Lyase in Hyperlipidemia and Metabolic Disorders. Trends Mol Med. 2017; 23(11): 1047-1063.
4. Lee JV, Berry CT, Kim K, Sen P, Kim T, Carrer A, et al. Acetyl-CoA promotes glioblastoma cell adhesion and migration through Ca(2+)-NFAT signaling. Genes Dev. 2018; 32(7-8): 497-511.
5. Martin-Martin N, Carracedo A, Torrano V. Metabolism and transcription in cancer: merging two classic tales. Front Cell Dev Biol. 2018; 5: 119.
6. Li X, Qian X, Lu Z. Local histone acetylation by ACSS2 promotes gene transcription for lysosomal biogenesis and autophagy. Autophagy. 2017; 13(10): 1790-1791.
7. Goudarzi A, Shiota H, Rousseaux S, Khochbin S. Genome-scale acetylation-dependent histone eviction during spermatogenesis. J Mol Biol. 2014; 426(20): 3342-3349.
8. Barral S, Morozumi Y, Tanaka H, Montellier E, Govin J, de Dieuleveult M, et al. Histone variant H2A.L.2 guides transition protein-dependent protamine assembly in male germ cells. Mol Cell. 2017; 66(1): 89-101.
9. Gaucher J, Reynoird N, Montellier E, Boussouar F, Rousseaux S, Khochbin S. From meiosis to postmeiotic events: the secrets of histone disappearance. FEBS J. 2010; 277(3): 599-604.
10. Rathke C, Baarends WM, Awe S, Renkawitz-Pohl R. Chromatin dynamics during spermiogenesis. Biochim Biophys Acta. 2014; 1839(3): 155-168.
11. Gaucher J, Boussouar F, Montellier E, Curtet S, Buchou T, Bertrand S, et al. Bromodomain-dependent stage-specific male genome programming by Brdt. EMBO J. 2012; 31(19): 3809-3820.
12. Buchou T, Tan M, Barral S, Vitte AL, Rousseaux S, Arechaga J, et al. Purification and analysis of male germ cells from adult mouse testis. Methods Mol Biol. 2017; 1510: 159-168.
13. Govin J, Escoffier E, Rousseaux S, Kuhn L, Ferro M, Thevenon J, et al. Pericentric heterochromatin reprogramming by new histone variants during mouse spermiogenesis. J Cell Biol. 2007; 176(3): 283-294.
14. Namekawa SH, Park PJ, Zhang LF, Shima JE, McCarrey JR, Griswold MD, et al. Postmeiotic sex chromatin in the male germline of mice. Current biology : CB. 2006 Apr 4;16(7):660-7.
15. Boussouar F, Goudarzi A, Buchou T, Shiota H, Barral S, Debernardi A, et al. A specific CBP/p300-dependent gene expression programme drives the metabolic remodelling in late stages of spermatogenesis. Andrology. 2014 May;2(3):351-9.
16. van der Knaap JA, Verrijzer CP. Undercover: gene control by metabolites and metabolic enzymes. Genes & development. 2016 Nov 1;30(21):2345-69.
17. Sivanand S, Rhoades S, Jiang Q, Lee JV, Benci J, Zhang J, et al. Nuclear acetyl-CoA production by ACLY promotes homologous recombination. Mol Cell. 2017; 67(2): 252-265. e6.
18. Bulusu V, Tumanov S, Michalopoulou E, van den Broek NJ, MacKay G, Nixon C, et al. Acetate recapturing by nuclear acetyl-CoA synthetase 2 prevents loss of histone acetylation during oxygen and serum limitation. Cell Rep. 2017; 18(3): 647-658.

Original Article

met1 DNA Methyltransferase Controls *TERT* Gene Expression: A New Insight to The Role of Telomerase in Development

Maryam Zangi, Ph.D.[1], Mohammad Bagher Bagherieh Najjar, Ph.D.[1], Masoud Golalipour, Ph.D.[2]*, Mahnaz Aghdasi, Ph.D.[1]

1. Department of Biology, Faculty of Science, Golestan University, Gorgan, Iran
2. Cellular and Molecular Research Center, Golestan University of Medical Sciences, Gorgan, Iran

Corresponding Address: P.O. Box: 4934174515, Cellular and Molecular Research Center, Golestan University of Medical Sciences, Gorgan, Iran
Email: gapmasood@goums.ac.ir

Received: 14/August/2018, Accepted: 25/December/2018

Abstract

Objective: DNA methylation systems are essential for proper embryo development. Methylation defects lead to developmental abnormalities. Furthermore, changes in telomerase gene expression can affect stability of chromosomes and produces abnormal growth. Therefore, defects in both methylation and telomerase gene expression can lead to developmental abnormalities. We hypothesized that mutation in the methylation systems may induce developmental abnormalities through changing telomerase gene expression.

Materials and Methods: In this experimental study, we used *Arabidopsis thaliana* (At) as a developmental model. DNA was extracted from seedlings leaves. The grown plants were screened using polymerase chain reaction (PCR) reactions. Total RNA was isolated from the mature leaves, stems and flowers of wild type and *met1* mutants. For gene expression analysis, cDNA was synthesized and then quantitative reverse transcription PCR (qRT-PCR) was performed.

Results: Telomerase gene expression level in homozygous *met1* mutant plants showed ~14 fold increase compared to normal plants. Furthermore, *TERT* expression in *met1* heterozygous was~ 2 fold higher than the wild type plants.

Conclusion: Our results suggested that *TERT* is a methyltransferase-regulated gene which may be involved in developmental abnormities causing by mutation in *met1* methyltransferase system.

Keywords: Developmental Abnormalities, *met1*, Telomerase

Cell Journal(Yakhteh), Vol 22, No 1, April-June (Spring) 2020, Pages: 71-74

Citation: Zangi M, Bagherieh Najjar MB, Golalipour M, Aghdasi M. met1 DNA methyltransferase controls TERT gene expression: a new insight to the role of telomerase in development. Cell J. 2020; 22(1): 71-74. doi: 10.22074/cellj.2020.6290.

Introduction

Cytosine methylation is an important epigenetic feature which can be preserved after each round of DNA replication (1). Methylation of cytosine is found in CG, CNG ("N" any nucleotide) and CHH (any asymmetric site, H= A, C or T) sequences (2). Methylation at CG sites in mammals is maintained by DNA methyltransferase *Dnmt1* (3). Mouse *Dnmt1* and *Arabidopsis met1* are orthologues of human *DNMT1*.

Both MET1 and DNMT1 possess large N termini containing bromo-adjacent homology (BAH) domains (4-8). *Dnmt1* mutant mice die nine days after development start. However, *met1 Arabidopsis* mutants with several developmental abnormalities, like reduced apical dominance, altered leaf shape (curled leaves) and altered flowering time, are alive making *Arabidopsis* a suitable model for research on methylation system defects (9, 10). met1 is responsible for 80-90% of methylation on *Arabidopsis* genome (11). The number of *met1* homozygous mutant individuals from heterozygous parents is only 2% of Mendel's prediction (12). Few genes, such as *fwa* and *superman*, were found in the *met1* mutant plants to be misregulated, while they are responsible for some developmental phenotypes (13, 14). On the other hand, in mouse embryonic cells, methylation system defects lead to telomere elongation change. Defect in telomerase gene expression was also reported to cause developmental abnormalities (15). Telomere has a crucial role in chromosome stability and replication. Therefore, changes in telomerase gene expression can influence growth and development (16). Telomerase gene in plants is developmentally regulated, similar to the regulation mechanism in humans (17, 18). Expression analysis revealed that *TERT* overexpression modulate expression of some genes needed to increase longevity (19).

Methylation defects and telomerase down-regulation both lead to developmental abnormalities. Therefore, we hypothesized that mutation in methylation system induces developmental abnormalities through changing telomerase expression.

Material and Methods

Plant material and growth condition

All *met1* heterozygous seeds in this study were kindly provided by Prof. Poszkowski laboratory, University of Geneva, Switzerland. *Arabidopsis met1*$^{+/-}$ heterozygous seeds were grown in the mixture of forest soil and moss with 1:1 ratio, or mixture of forest soil, vermiculite and perlite with 4:3:2 ratios. They were grown at growth chambers at 23˚C using a 16 hours light/8 hours dark photoperiod. After growing seedlings, BASTA was

sprayed on 7-10 days old seedlings and the sensitive plants were removed. Then, seedlings with serrated leaf margins were sampled for genotyping.

DNA and RNA extraction

DNA was extracted from leaves of seedlings, using Dellaporta et al. (20) method. After grinding in liquid nitrogen, 500 µl buffer [Tris-Hcl: 1 M, pH=9.0, LiCl: 2 M, Ethylenediaminetetraacetic acid (EDTA): 0.5 M, 10% w/v sodium dodecyl sulfate (SDS)] was added to them. After five minutes spinning at high speed, 350 µl of supernatant was transferred into a microtube containing 350 µl isopropanol and spun 10 minutes at high speed. The liquid was poured off and the pellet was dried. After that 100-200 µl ddH_2O was added and shacked at room temperature for 30 minutes. Total RNA was extracted from mature wild type, *met1* heterozygous and homozygous mutant plants according to Dellaporta et al. (20) method. Briefly, 0.1-0.5 g of fresh tissue was grinded in liquid nitrogen and transferred into a microtube containing 750 µl of extraction buffer (Tris-Hcl: 100 mM, pH=8.5, NaCl: 100 mM, EDTA: 20 mM, 1% Sarkosyl) and 750 µl of phenol/chloroform. Then the standard protocol of phenol/chloroform extraction was followed and finally the pellet of RNA was dissolved in 20-100 µl of ddH_2O.

Genotyping

The collection was screened using the specific primers. Primers for *met1* wild type were:

5′-GCCTGGTCAAGTGGACTTCATC-3′ and
5′-CCATTCTTCACAGAGCATGCC-3′, while they were 5′-GATTGTGTCTCTACTACAGAGGC-3′ and
5′-TGGACGTGAATGTAGACACGTCG-3′ for the mutant allele.

Polymerase chain reaction (PCR) reactions were performed in the volumes of 25 µl containing 10 ng DNA, 1X PCR buffer, 1.5 mM $MgCl_2$, 0.2 mM dNTP, 0.4 µM each of primers forward and reverse and 0.625 U of DNA polymerase (Takara Shuzo Co., Japan). PCR program was performed as following: 94˚C for 5 minutes, then 30 cycles of respectively 94˚C for 30 seconds, 56˚C for 30 seconds and 72˚C for 30 seconds followed by 72˚C for 10 minutes to complete DNA expansion. PCR products were visualized on 1% agarose gel.

Gene expression analysis

cDNA was synthesized using REVERTAID (Thermoscientific RevertAid cDNA synthesis Kit, USA) according to manufacturer instructions. Then, reverse transcription (RT)-PCR reactions were carried out using TaKaRa kit (TaKaRa, Japan) in 20 µl volume, according to manufacturer's protocol. *actin* was used as an internal control in PCR reaction. Primers were:

5′-TGTGGATCTCCAAGGCCGAGTA-3′and
5′-CCCCAGCTTTTTAAGCCTTTGATC-3′ for *actin* and
5′-CCTGTTTAGCCTGCTTTACA-3′ and
5′-GCAGAGAAAGGTCAATTTCA-3′ for *TERT*.

Quantitative RT-PCR (qRT-PCR) amplifications were carried out in the final volumes of 20 µl containing 10 ng cDNA, 0.4 µM of each primer and SYBR Green PCR Master Mix in iQ5 real thermocycler (Bio-Rad, USA). PCR condition was consisted of 94˚C for 3 minutes, 50 cycles of 94˚C for 10 seconds, 52˚C for 10 seconds, 72˚C for 10 seconds followed by 72˚C for 10 minutes.

CpG island analysis

Selection of the *met1* gene was based on a bioinformatics survey. Thus, the -1000 to +100 region of *AtTERT* gene's promoter was investigated using CpGPlot, CpGIF, PlantPan software for analysis of the methylation islands. The CpG islands found in the CpGPlot and CpGIF software were almost in line with each other. The CpNpG islands were not found in PlantPan software. Therefore, the met1 methyltransferase system, methylating CpG islands, was selected.

Statistical analysis

All experiments were repeated three times. Gene expression levels were analyzed using normalized calibrator method (21). Graphpad Prism version 6 (Graphpad Software, USA) was used for data analysis. A P value less than 0.05 was considered statistically significant.

Results

Wild type and mutant plants

After DNA extraction, genotyping was carried out. As expected amplified fragments size for wild type and mutant strains were 600 bp and 392 bp respectively. So, heterozygous and homozygous mutant plants were selected. Normal *met1* homozygous and heterozygous mutant plants are shown in Figure 1A.

TERT transcript level in the *met1* mutant plants

After RNA extraction, reverse transcription reaction was carried out. As we expected, gel electrophoresis showed respectively 97 bp and 132 bp bands regarding the *actin* and *TERT* genes (Fig.1B).

For evaluating *AtTERT* gene, *actin* gene was used as a reference gene in this study. Cycle threshold (C_T) value of reference gene was identical in wild type and mutant plants, indicating the equal expression of *actin* gene in the wild type and mutant plants. For *TERT* specific gene, different plants had different C_T values, indicating different gene expression in wild types, heterozygous and homozygous mutant plants.

Telomerase gene expression levels in homozygous *met1* mutant plants showed 14.123 fold increase compared to the normal plants. Furthermore, *TERT* expression in heterozygous *met1* mutant plants was 2.009 fold higher than wild type plants (Fig.2).

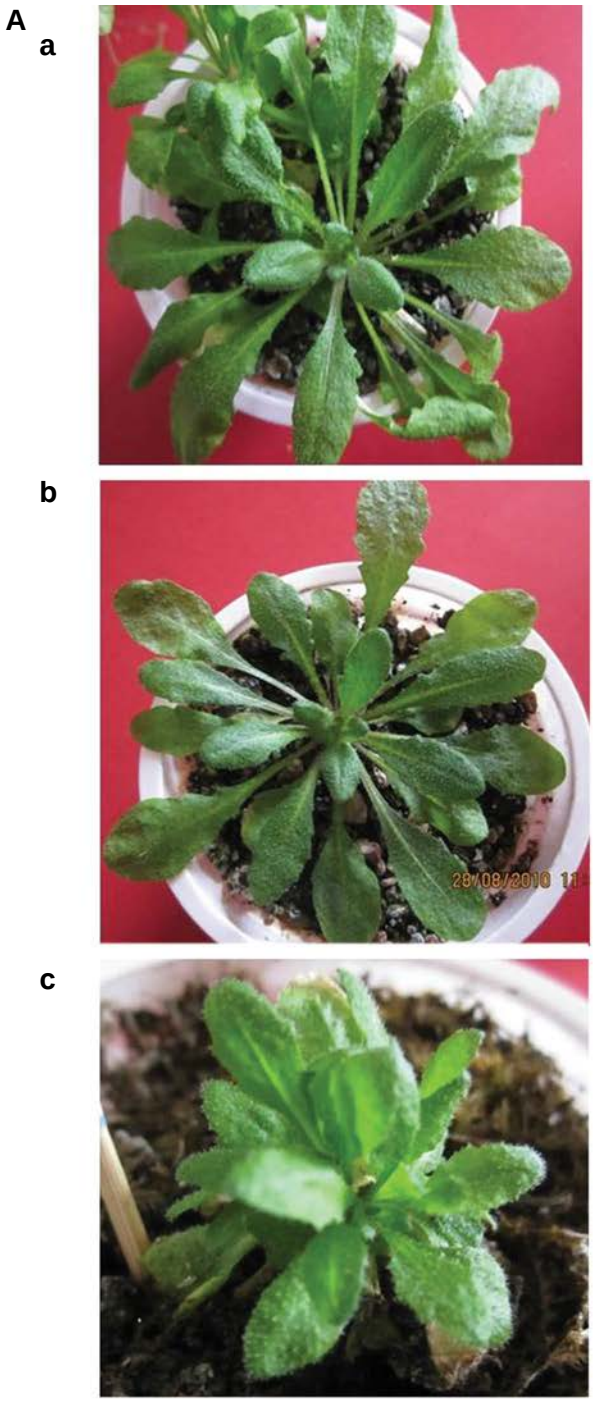

Fig.1: Morphology of wild-type, *met1* homozygotes and heterozygotes. **A.** Wild type plant (a), heterozygous *met1*$^{+/-}$ mutant plant (b), and homozygous*met1*$^{-/-}$ mutant plant (c). All of these plants are 60 days old seedlings and **B.** Reverse transcription polymerase chain reaction (RT-PCR) experiments of *TERT* transcript and *ACTIN* as an internal control (lower panel). The size of bands of *TERT* and *ACTIN* transcripts is 132 bp and 97 bp respectively.

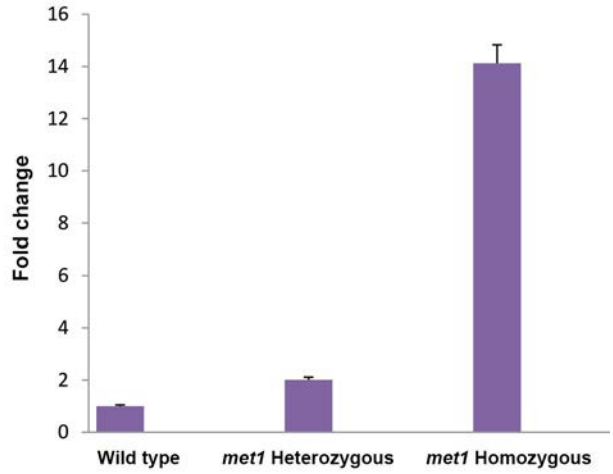

Fig.2: Telomerase gene expression patterns in the control, *met1* heterozygous and homozygous mutant plants.

Discussion

DNA methylation is a major epigenetic mechanism and a key factor affecting normal development in animals and plants (22). Null mutations in the mouse *Dnmt1* or *Dnmt3a/b* genes lead to embryonic abortion but in *met1* mutant *Arabidopsis* plants are alive (23, 24). Therefore, *Arabidopsis* is an excellent genetic model for investigation of methylation defects. In the present study, we evaluated the effects of mutation of met1 DNA methyltransferase on telomerase gene expression.

Telomerase promoter contains methylation islands within the region of -1000 and +100. Promoter hypermethylation mainly occurs in CpG sites and depends on met1 and drm2 methyltransferases (25). Therefore, the telomerase gene may be controlled by met1 system.

Expression of TERT was increased ~14 fold in homozygous and ~2 fold in heterozygous met1 mutated plants. It seems that mutation in met1 methyltransferase systems decreases methylation of the promoter CpG islands of telomerase gene and increases the telomerase gene expression. Overexpression of telomerase leads to telomere lengthening. Long telomeres have detrimental effects on cells and special proteins, such as TZAP, triggered telomere trimming to a balanced level (26). The telomeric repeat sequences are bound to telomere-binding proteins; therefore, long telomere repeats would presumably recruit more of these proteins. Many telomere-binding proteins have non-relevant (non-telomeric) functions (27, 28). The increased telomere length leads to sequestration of telomere-binding proteins and inhibits their binding to non-telomeric sites. Indeed, long telomeres reduce growth and life span (29). Therefore, overexpression of telomerase in met1 mutated plants may be related to the limited growth and developmental abnormalities in Arabidopsis.

Further research is needed to show how homozygous mutant plants survive and grow, despite the severe developmental abnormalities. It is possible that other methylation systems compensate the effects

of *met1* mutation and improves the phenotype. Hypermethylation, caused by *met1* mutation, inhibits the DNA demethylation pathway and activates the *de novo* methylation (12, 30, 31).

Conclusion

Our results suggest that *TERT* is a methyltransferase-regulated gene which may be involved in developmental abnormities caused by mutation in met1 methyltransferase system.

Acknowledgements

This work was funded by a grant from Golestan University (Golestan, Iran). The authors express the gratitude to Dr. Jerzy Paszkowski (Department of Plant Biology, University of Geneva; Geneva, Switzerland) and Dr. Frederic Berger (Gregor Mendel Institute of Molecular Plant Biology; Vienna, Austria) for providing *met1* heterozygous mutant seeds and for comments on the manuscript. There are no conflicts of interest to declare.

Authors' Contributions

M.G., M.B.N.; Initiated the research program and supervised this work. M.B.N.; Conceived and designed the analysis. M.G.; Contributed data or analysis tools. M.Z.; Collected the data, performed the experiments and wrote the manuscript. M.A.; Analyzed the data, discussed the results and commented on the manuscript. All authors have reviewed and approved the final manuscript.

References

1. Jeltsch A, Jurkowska RZ. New concepts in DNA methylation. Trends Biochem Sci. 2014; 39(7): 310-318.
2. Sudan J, Raina M, Singh R. Plant epigenetic mechanisms: role in abiotic stress and their generational heritability. 3 Biotech. 2018; 8(3): 172.
3. Song J, Teplova M, Ishibe-Murakami S, Patel DJ. Structure-based mechanistic insights into DNMT1-mediated maintenance DNA methylation. Science. 2012;709-712 :(6069)335 .
4. Bartee L, Malagnac F, Bender J. Arabidopsis cmt3 chromomethylase mutations block non-CG methylation and silencing of an endogenous gene. Genes Dev. 2001; 15(14): 1753-1758.
5. Lindroth AM, Cao X, Jackson JP, Zilberman D, McCallum CM, Henikoff S, et al. Requirement of CHROMOMETHYLASE3 for maintenance of CpXpG methylation. Science. 2001; 292(5524): 2077-2080.
6. Cao X, Aufsatz W, Zilberman D, Mette MF, Huang MS, Matzke M, et al. Role of the DRM and CMT3 methyltransferases in RNA-directed DNA methylation. Curr Biol. 2003; 13(24): 2212-2217.
7. Kankel MW, Ramsey DE, Stokes TL, Flowers SK, Haag JR, Jeddeloh JA, et al. Arabidopsis MET1 cytosine methyltransferase mutants. Genetics. 2003; 163(3): 1109-1122.
8. Zhang H, Zhu JK. Active DNA demethylation in plants and animals. Cold Spring Harb Symp Quant Biol. 2012; 77: 161-173.
9. Finnegan EJ, Peacock WJ, Dennis ES. Reduced DNA methylation in Arabidopsis thaliana results in abnormal plant development. Proc Natl Acad Sci USA. 1996; 93(16): 8449-8454.
10. Ronemus MJ, Galbiati M, Ticknor C, Chen J, Dellaporta SL. Demethylation-induced developmental pleiotropy in Arabidopsis. Science. 1996; 273(5275): 654-657.
11. Jullien PE, Berger F. DNA methylation reprogramming during plant sexual reproduction. Trends Genet. 2010; 26(9): 394-399.
12. Mathieu O, Reinders J, Caikovski M, Smathajitt C, Paszkowski J. Transgenerational Stability of the arabidopsis epigenome is coordinated by CG methylation. Cell. 2007; 130(5): 851-862.
13. Soppe WJ, Jacobsen SE, Alonso-Blanco C, Jackson JP, Kakutani T, Koornneef M, et al. The late flowering phenotype of fwa mutants is caused by gain-of-function epigenetic alleles of a homeodomain gene. Mol Cell. 2000; 6(4): 791-802.
14. Reinders J, Delucinge Vivier C, Theiler G, Chollet D, Descombes P, Paszkowski J. Genome-wide, high-resolution DNA methylation profiling using bisulfite-mediated cytosine conversion. Genome Res. 2008; 18(3): 469-476.
15. Xie X, Shippen DE. DDM1 guards against telomere truncation in Arabidopsis. Plant Cell Rep. 2018; 37(3): 501-513.
16. Kupiec M. Biology of telomeres: lessons from budding yeast. FEMS Microbiol Rev. 2014; 38(2): 144-171.
17. Riha K, Fajkus J, Siroky J, Vyskot B. Developmental control of telomere lengths and telomerase activity in plants. Plant Cell. 1998; 10(10): 1691-1698.
18. Nelson ADL, Beilstein MA, Shippen DE. Plant Telomeres and telomerase. In: Molecular biology. New York: Springer; 2014: 25-49.
19. Armstrong L, Saretzki G, Peters H, Wappler I, Evans J, Hole N, et al. Overexpression of telomerase confers growth advantage, stress resistance, and enhanced differentiation of ESCs toward the hematopoietic lineage. Stem Cells. 2005; 23(4): 516-529.
20. Dellaporta SL, Wood J, Hicks JB. A plant DNA minipreparation: version II. Plant molecular biology reporter. 1983; 19-21.
21. Golalipour M, Mahjoubi F, Sanati MH, Alimoghaddam K. Gene dosage is not responsible for the upregulation of MRP1 gene expression in adult leukemia patients. Arch Med Res. 2007; 38(3): 297-304.
22. Ideraabdullah FY, Zeisel SH. Dietary modulation of the epigenome. Physiol Rev. 2018; 98(2): 667-695.
23. Chan SW, Henderson IR, Jacobsen SE. Gardening the genome: DNA methylation in Arabidopsis thaliana. Nat Rev Genet. 2005; 6(5): 351-360.
24. Goll MG, Bestor TH. Eukaryotic cytosine methyltransferases. Annu Rev Biochem. 2005; 74: 481-514.
25. Berdasco M, Alcázar R, García-Ortiz MV, Ballestar E, Fernández AF, Roldán-Arjona T, et al. Promoter DNA hypermethylation and gene repression in undifferentiated Arabidopsis cells. PLoS One. 2008; 3(10): e3306.
26. Li JSZ, Fusté JM, Simavorian T, Bartocci C, Tsai J, Karlseder J, et al. TZAP: a telomere-associated protein involved in telomere length control. Science. 2017; 355(6325): 638-641.
27. Shore D, Nasmyth K. Purification and cloning of a DNA binding protein from yeast that binds to both silencer and activator elements. Cell. 1987; 51(5): 721-732.
28. Guarente L. Sir2 links chromatin silencing, metabolism, and aging. Genes Dev. 2000; 14(9): 1021-1026.
29. Austriaco NR Jr, Guarente LP. Changes of telomere length cause reciprocal changes in the lifespan of mother cells in Saccharomyces cerevisiae. Proc Natl Acad Sci USA. 1997; 94(18): 9768-9772.
30. Lister R, O'Malley RC, Tonti-Filippini J, Gregory BD, Berry CC, Millar AH, et al. Highly integrated single-base resolution maps of the epigenome in arabidopsis. Cell. 2008; 133(3): 523-536.
31. Cokus SJ, Feng S, Zhang X, Chen Z, Merriman B, Haudenschild CD, et al. Shotgun bisulphite sequencing of the Arabidopsis genome reveals DNA methylation patterning. Nature. 2008; 452(7184): 215-219.

Original Article

Long-Term Follow-up of Autologous Fibroblast Transplantation for Facial Contour Deformities, A Non-Randomized Phase IIa Clinical Trial

Amir Bajouri, M.D.[1#], Zahra Orouji, M.D.[1#], Ehsan Taghiabadi, M.Sc.[1#], Abdoreza Nazari, M.Sc.[1], Atefeh Shahbazi, M.Sc.[1], Nasrin Fallah, M.Sc.[1], Parvaneh Mohammadi, Ph.D.[1], Mohammad Rezvani, M.D.[1], Zahra Jouyandeh, M.D.[1], Fatemeh Vaezirad, B.Sc.[1], Zahra Khalajasadi, B.Sc.[1], Mahshid Ghasemi, M.D.[1], Aslan Fanni, M.Sc.[1], Sara Haji Hosseinali, M.Sc.[1], Ahad Alizadeh, M.Sc.[2], Hossein Baharvand, Ph.D.[1], Saeed Shafieyan, M.D.[1*], Nasser Aghdami, M.D., Ph.D.[1*]

1. Department of Regenerative Medicine, Cell Science Research Center, Royan Institute for Stem Cell Biology and Technology, ACECR, Tehran, Iran
2. Metabolic Diseases Research Center, Qazvin University of Medical Sciences, Qazvin, Iran

 # The first three authors equally contributed to this work.

Corresponding Address: P.O.Box: 16635-148, Department of Regenerative Medicine, Cell Science Research Center, Royan Institute for Stem Cell Biology and Technology, ACECR, Tehran, Iran
Emails: sshafiiyan@yahoo.com, nasser.aghdami@royaninstitute.org

Received: 1/September/2018, Accepted: 13/May/2019

Abstract

Objective: Recently, the promising potential of fibroblast transplantation has become a novel modality for skin rejuvenation. We investigated the long-term safety and efficacy of autologous fibroblast transplantation for participants with mild to severe facial contour deformities.

Materials and Methods: In this open-label, single-arm phase IIa clinical trial, a total of 57 participants with wrinkles (n=37, 132 treatment sites) or acne scars (n=20, 36 treatment sites) who had an evaluator's assessment score of at least 2 out 7 (based on a standard photo-guide scoring) received 3 injections of autologous cultured fibroblasts administered at 4-6 week intervals. Efficacy evaluations were performed at 2, 6, 12, and 24 months after the final injection based on evaluator and patient's assessment scores.

Results: Our study showed a mean improvement of 2 scores in the wrinkle and acne scar treatment sites. At sixth months after transplantation, 90.1% of the wrinkle sites and 86.1% of the acne scar sites showed at least a one grade improvement on evaluator assessments. We also observed at least a 2-grade improvement in 56.1% of the wrinkle sites and 63.9% of the acne scar sites. A total of 70.5% of wrinkle sites and 72.2% of acne scar sites were scored as good or excellent on patient assessments. The efficacy outcomes remained stable up to 24-month. We did not observe any serious adverse events during the study.

Conclusion: These results have shown that autologous fibroblast transplantation could be a promising remodeling modality with long-term corrective ability and minimal adverse events (Registration Number: NCT01115634).

Keywords: Cell Therapy, Skin Rejuvenation, Wrinkle

Cell Journal(Yakhteh), Vol 22, No 1, April-June (Spring) 2020, Pages: 75-84

Citation: **Bajouri A, Orouji Z, Taghiabadi E, Nazari A, Shahbazi A, Fallah N, Mohammadi P, Rezvani M, Jouyandeh Z, Vaezirad F, Khalajasadi Z, Ghasemi M, Fanni A, Haji Hosseinali S, Alizadeh A, Baharvand H, Shafieyan S, Aghdami N. Long-term follow-up of autologous fibroblast transplantation for facial contour deformities, a non-randomized phase IIa clinical trial. Cell J. 2020; 22(1): 75-84. doi: 10.22074/cellj.2020.6340.**

Introduction

Fibroblasts are the predominant cells of connective tissue that synthetize and organize collagen and other extracellular matrix (ECM) proteins. Furthermore, Fibroblasts secrete soluble cytokines and growth factors such as transforming growth factor-beta (TGF-β), keratinocyte growth factor (KGF), vascular endothelial growth factor (VEGF), and insulin-like growth factor (IGF) to maintain the structural integrity of the skin (1-3).

Skin aging is a complex, multifactorial process defined by progressive loss in skin integrity and function (4). The size, amount, and potency of fibroblasts chronologically decline due to natural cellular and molecular events such as reductions in TGF-β, micro-environment alterations, and Notch signaling disruption (5-8). Aged-fibroblasts secrete higher levels of matrix metalloproteinase that degrade collagen fibrils (9). Since a reciprocal mechanical force between fibroblasts and collagen fibrils is necessary for continuous collagen synthesis, degraded collagen fragments cause a breakdown in the tissue cycle (3, 10, 11).

On the other hand, destruction of fibroblasts and consequent collagen loss seen in acne scars result from a healing defect after local and systemic inflammation. This defect leads to destruction of the dermal structures with subsequent fibrosis (12, 13). Acne scars occur in 95% of acne participants even during standard treatments, in

which 30% progress to significant, permanent scarring with psychosocial complications (14, 15).

In recent years, the promising potential of autologous fibroblast transplantation has become a novel therapeutic modality for replacement of damaged fibroblasts. In this method, the patient's retro-auricular area, which has the least damage by UV irradiation, underwent small biopsies to produce the autologous fibroblast cell line through culturing process (16, 17).

The first autologous fibroblast transplantation was performed in 1995, after which additional studies reported the potentiality of a minimally invasive and autologous rejuvenation method with less complications (16-20). It is presumed that transplanted fibroblasts could stimulate the resident fibroblasts and repair the collagen synthesis system (2, 18, 19, 21).

Previously, we performed a clinical trial of autologous fibroblast transplantation in 20 participants with wrinkles and acne scars. The results showed its safety and feasibility (unpublished data). In the current study, we aimed to evaluate the long-term safety and efficacy of autologous fibroblast transplantation for participants with mild to severe facial contour deformities.

Materials and Methods

Study design

In this open-label, single-arm, and single center clinical trial, we assessed the efficacy and safety of autologous fibroblast transplantation in wrinkle and acne scar. We estimated the sample size using package long power according to "Sample Size Calculations for Longitudinal Data" by R software (22). In this study**,** a sample size of 57 participants achieves 80% minimum power to detect a difference using a two-sided binomial test**.** The powers of other primary hypothesis tests were more than 80%.

We obtained three punch biopsies from the retro-auricular area in each eligible patient and transferred the biopsy specimens to the Royan Clean Room in order to isolate and cultivate the dermal fibroblasts. After 4 to 5 weeks, cultured fibroblasts were transferred to the clinic and injected into the facial contours of participants over three sessions at 4-6 week intervals. At each treatment session, we injected 0.1 ml of the cell suspension (containing $0.5\text{-}1.5\times10^6$ cells) into each cm/cm^2 of the facial contours. Two independent dermatologists evaluated and recorded the treatment outcome as well as adverse events at 2, 6, 12, and 24 months after the third injection. Participants were also asked to assess their response to treatment at each follow up visit. Furthermore, 5 years after the treatment, we asked the participants by phone to rate the efficacy and durability of the treatment outcome**.**

The Institutional Review Board and Ethical Committee of Royan Institute (Tehran, Iran) approved this study. The study was registered at clinicaltrials.gov as NCT01115634.

Patient selection

Among 76 participants who referred to the Dermatology Clinic of the Royan Institute with wrinkles (49 participants) and acne scars (27 participants) from 2011 to 2018, we recruited 62 participants to the study based on eligibility criteria. We completely explained the treatment process to the participants who met the eligibility criteria**.** The enrolled participants signed the informed consent before participation to the study**.**

Wrinkle group

We evaluated the participants' wrinkles based on a 0-7 standard photo guide scoring (20) and included those with wrinkle score of 2-7 (considered as mild to severe). Other eligibility criteria for this group included: 35-65 years of age; wrinkles on the forehead, periorbital, glabella and/or nasolabial fold (NLF); and total treatment site length of 10-50 cm.

We did not include participants with history of laser treatment, immune-suppressive therapy, retinoid derivatives, botulinum toxin or temporary fillers within 6 months before recruitment to the study; history of organ transplantation or blood transfusion; any known cancer; known chronic disease; genetic fibroblast or collagen production disorder; permanent or semi-permanent fillers; allergy to animal collagen or its products; sensitivity to local anesthesia; facial plastic surgery or mesotherapy; hepatitis B, hepatitis C or human immunodeficiency viruses (HIV); and pregnant or lactating.

Acne scar group

We evaluated the participants' acne scars based on a 0-7 standard photo guide scoring (20) and included those with acne scar score of 2-7 (considered as mild to severe). Other inclusion criteria included: 18-65 years of age; acne scars on the cheek, forehead and/or temporal areas; and total treatment site surface area of 10-50 cm^2. Exclusion criteria were the same as the wrinkle group.

Efficacy profile

Efficacy outcomes were based on comparisons of the baseline and follow-up evaluator and participants' assessment scores. The evaluators and participants rated each wrinkle or acne scar treatment site at the first visit and during follow-up visits, independent of previous scores. We photographed the treatment sites during pre- and post-treatment visits. Two independent, trained dermatologists performed the assessments based on the standard photo guide scoring. We recorded the assessment scores according to the following endpoints: "Responders" were defined as number of treatment sites that had at least a 2 grade improvement compared to the baseline score according to the evaluators' assessments. Furthermore, we defined the severity of facial contours as mild (grades 2 and 3), moderate (grades 4 and 5), or severe (grades 6 and 7) and then measured the "Responders" of each group in wrinkle and acne scar sites. Participants scored their treatment sites as: -2 (much worse), -1 (worse), 0 (no

difference), +1 (better or good), and +2 (much better or excellent) during follow-up visits compared to baseline. We considered the 6-month follow-up evaluations as primary endpoint based on evaluators assessment scores.

Adverse events

We prepared a list of probable adverse events before transplantation based on 2010 Common Terminology Criteria for Adverse Events [CTCAE; (23)]. These criteria included local events such as bruising, redness, allergic reaction, pruritus, hemorrhage, nodules and tumors, or systemic events such as infections or allergic reactions. We separately recorded adverse events as well as their duration, severity, and treatment plan of action during the intervention and follow-up visits

Sampling and injection technique

The left retro-auricular area was cleaned with isopropyl alcohol, followed by administration of 2% xylocaine as a local anesthetic. Then, we obtained 3 full-thickness 4-mm punch skin biopsies and transferred the specimens to the Royan Clean Room. We sutured the biopsy sites and then covered them with a sterile dressing.

After isolation and cultivation, the vials that contained cultured fibroblasts were transferred to the clinic. We gently suspended the vial contents and drew it into 1 ml syringes. Before injection, we performed regional blocks via injections of anesthetic agent. The treatment sites were cleaned by an antiseptic solution. Then, the dermatologist injected 0.1 ml of the cell suspension into the superficial and middle layers of dermis of each cm of the wrinkle sites or cm^2 of the acne scar sites applying a 30-gauge needle. Blanching and wheal formation of the injection site were considered as correct injection of the solution. We did not perform any manipulation on the recipient sites after injection. Participants were avoided the use of chemical soaps or materials to the face for 72 hours after injections. We allowed a short period of indirect application of ice on the treatment sites in the case of long lasting reaction, redness or pain.

Cell preparation

The specimens were transferred in 5 ml transporting medium that included Hanks' balanced salt solution (HBSS, Gibco, Germany) and 1% penicillin/streptomycin (pen/strep, Gibco, Germany) to the clean room. Then, we soaked the skin specimen in 70% ethanol for 30 seconds to reduce contamination, washed with HBSS/pen/strep twice and cut into 2×2 mm pieces using a surgical scalpel blade. We incubated the skin pieces with 1.2 U/ml dispase II solution (Gibco, Germany) for 15-18 hours at 4˚C and then 0.1% collagenase type I (Sigma, Germany) for 4 hours at 37˚C. We used a Pasteur pipette to pipette the dermis layer in order to release the cells from this layer. The isolated cells were cultured in advanced Dulbecco's Modified Eagle Medium: Nutrient Mixture F-12 (DMEM/F12, Gibco, Germany) with 10% fetal bovine serum (FBS, PAA, Austria), 2 mM L-glutamine (Gibco, Germany), and 1% pen/strep. Subsequently, we incubated the cells at 37˚C in 5% CO_2. We changed the cultured medium every three days. After 4-5 weeks, we collected passage-3 cultured cells, which consisted of 95 ± 17×10^6 cells for the wrinkle group and 104 ± 15×10^6 cells for the acne scar group. Next, we divided the cells into three equal parts. We injected the first fresh part of the cells into the treatment sites. The two remaining aliquots were frozen for the later injections. The freezing medium contains 40% DMEM/F12 (Gibco, Germany) 50% (v/v) FBS and 10% (v/v) dimethyl sulfoxide (DMSO). The amount of the injection volume was calculated as: "0.1 × total length or surface of treatment sites", in which each ml of injection solution contained 5-15×10^6 cells. Before transplantation, we assessed the cells for any microbial contamination according to sterility, mycoplasma, and endotoxin tests.

Immunofluorescence staining

We fixed the cultured fibroblasts with 4% freshly buffered paraformaldehyde, washed with phosphate buffered saline without Ca^{2+} and Mg^{2+} (PBS^-), and incubated with 10% goat serum, followed by incubation with primary antibody mouse anti-vimentin (Millipore, MAB1687, 1:100) and anti-collagen type 1 (Abcam, ab90395, 1:50). Then, we washed the cells with PBS^- and incubated with Donkey anti mouse Alexa 546 (Invitrogen, USA), and anti-mouse IgG (Sigma, USA) for 60 minutes at room temperature. Nuclei were counter-stained with 5 µg/ml of 4', 6-diamidino-2-phenylindole (DAPI) and analyzed by fluorescent microscopy (Nikon, Japan).

Karyotyping

After the cells reached 70% confluence, we added KaryoMAX® Colcemid™ Solution in PBS-10 µg/ml (Gibco, USA) to each flask to a final dilution of 25 µl/ml, which was then incubated at 37˚C for 45 minutes. We monitored the changes in cell morphology with an inverted microscope until the fibroblasts detached. For hypotonic treatment, we slowly and carefully added 13 ml of 0.056% KCl (Merck, Germany) with distilled water, followed by incubation at 37˚C for 11 minutes, and fixed with methanol: acetic acid (3:1) solution. In order to obtain G-bands, we aged the slides at 60˚C overnight. We carried out the staining procedure using Giemsa solution 1:10 (Gibco, USA). Whenever possible, we analysed 15 metaphases. Before printing out each karyotype and counting each chromosome by writing a number on each sister chromatid pair, we observed the slides under a light microscope at ×10 and ×100 magnifications.

Statistical analysis

We evaluated the normal distribution of the variables by the Kolmogorov-Smirnov test. We analyzed the normal continuous and non-normal variables with the paired t, Mann-Whitney U, and Kruskal-Wallis tests. We utilized the Spearman and Pearson correlation coefficients to analyze the correlation between variables. We performed the repeated measurement model for groups with related dependent variables that represented different measurements of the same attribute. Values have been expressed as mean ± SD. The

level of statistical significance was set at 0.05. We performed the statistical analysis using SPSS version 20 software (SPSS Inc., Chicago, IL, USA).

Results

Participants

Wrinkle group

A total of 49 subjects with contour deformities reffered to the clinic. Table 1 shows the subjects' baseline characteristics. Eight participants were excluded from the study because of the eligibility criteria or refusal to participate. The remaining 41 participants received autologous cultured fibroblasts. During the follow-up period, 4 participants could not attend the 2- and 6-month follow-up visits and were considered lost to follow-up. Therefore, we analyzed data of 37 participants who had at least 2- and 6-month follow-up visits. We followed 20 participants for 12 months, and 13 participants for 24 months after treatment (Fig.1, Table 1).

Participants had a mean age of 47 ± 7 years. There were 33 (89.1%) females. Among 132 treatment sites, there were 43 mild, 43 moderate, and 46 severe wrinkles. The average length of the treatment sites was 40 ± 7 cm (range: 11-47 cm). We transplanted an average of 95 ± 17×10^6 cells during 3 sessions. The mean number of transplanted cells into each treatment site was $0.8 \pm 0.3\times10^6$ cells/cm.

Acne scar group

There were 27 subjects who referred to the clinic from which 6 participants either did not meet the inclusion criteria or declined to participate. A total of 21 participants received the study treatment. One participant was lost to follow-up. We analyzed the data from 20 participants who had at least 2 and 6 months of follow-up. There were 11 participants seen at the 12-month follow-up and we followed 4 participants until 24 months after treatment (Fig.1, Table 1).

Participants had a mean age of 32 ± 9 years. There were 15 (75%) female participants. Among 36 acne scar sites, there were 5 mild, 16 moderate, and 15 severe acne scars. We transplanted an average of 104 ± 15×10^6 cells into the treatment sites. The sites had an average surface area of 31 ± 6 cm^2 (20-44 cm^2). The mean number of transplanted cells into each treatment site was $1.1 \pm 0.3\times10^6$ cells/cm^2.

Efficacy outcomes

Wrinkle group

The median baseline grade in wrinkle sites was 5 that decreased to 3 at 6 months after treatment, based on evaluator's assessments. Moreover, we observed that at 12 and 24 months following transplantation, this score decreased to 2. At 2-month follow-up, average response rates of the treatment sites in comparison with baseline grades were: glabella 1.7 ± 1.3, periorbital 1.5 ± 1.1, NLF 1.4 ± 0.9, and forehead 1.5 ± 1 ($P<0.001$). At 6 months after transplantation, the response rates were: glabella 2 ± 1.5, periorbital 2 ± 1.3, NLF 2 ± 1.2, and forehead 1.7 ± 1.1 ($P<0.001$). The mean response rates for all 132 wrinkle sites at the 2- and 6- month follow-up visits were 1.5 ± 1.1 and 2 ± 1.2, respectively.

We observed that at 6 months following transplantation, the responder sites included: 18 (51.4%) for the glabella, 21 (60%) for the periorbital, 18 (64.3%) for the NLF, and 18 (52.9%) for the forehead. Among 132 wrinkle sites, 75 (56.8%) sites were responders. Our assessments 6 months after transplantation showed that 120 (90.1%) sites of the 132 wrinkle sites improved at least one grade.

Participants did not rate any of the treatment sites as -2 (much worse) or -1 (worse) after 2 and 6 months of follow-up. Self-assessment scores of +1 (good) or +2 (excellent) were reported at the 2- and 6- month follow-up visits as follows: 68.5% and 77.1% (glabella), 67.6% and 71.4% (periorbital), 67.8% and 71.4% (NLF), 52.9% and 61.8% (forehead), and 63.6% and 70.5% for all of the 132 wrinkle treatment sites. Table 2 and Figure 2 show the efficacy outcomes. Furthermore, participants met the 12- and 24-month follow-up visits showed sustained efficacy based on evaluator and self-assessment scores (Figs. 2, 3). At 5-year follow up, 22 participants were accessible through telephone contact. The participants scored the treatment sites as +1 (good) or +2 (excellent) in 64.3% of glabella, 75% of periorbital, 83.3% of NLF, 42.8% of forehead, and 65.2% of the total 69 wrinkle treatment sites.

Table 1: Baseline characteristics of the subjects

Characteristics	Wrinkle group n=37	Acne scar group n=20
Age (Y) (range)	47 ± 7 (35-62)	32 ± 9 (18-45)
Female	33 (89.1)	15 (75)
Sun protection	30 (81.1)	8 (40)
Smoking	8 (21.6)	1 (5)
Previous intervention		
Laser	10 (27)	12 (60)
Botulinum toxin	19 (51.3)	-
Filler injection	7 (18.9)	0
Microderm	0	10 (50)
No intervention	12 (32.4)	4 (20)
Treatment sites*		
Glabella	35 (4.1 ± 1.8, 4)	-
Periorbital	35 (4.9 ± 1.9, 5)	-
NLF	28 (5.2 ± 1.4, 5)	-
Forehead	34 (4.4 ± 1.8, 4)	9 (4.3 ± 1.1, 5)
Temporal	-	7 (5.0 ± 1.6, 5)
Cheek	-	20 (5.7 ± 1.1, 6)
Total sites	132 (4.6 ± 1.7, 5)	36 (5.2 ± 1.2, 5)

Data are presented mean ± SD or n (%). *; n (baseline grade; mean ± SD, median) and NLF; Nasolabial fold.

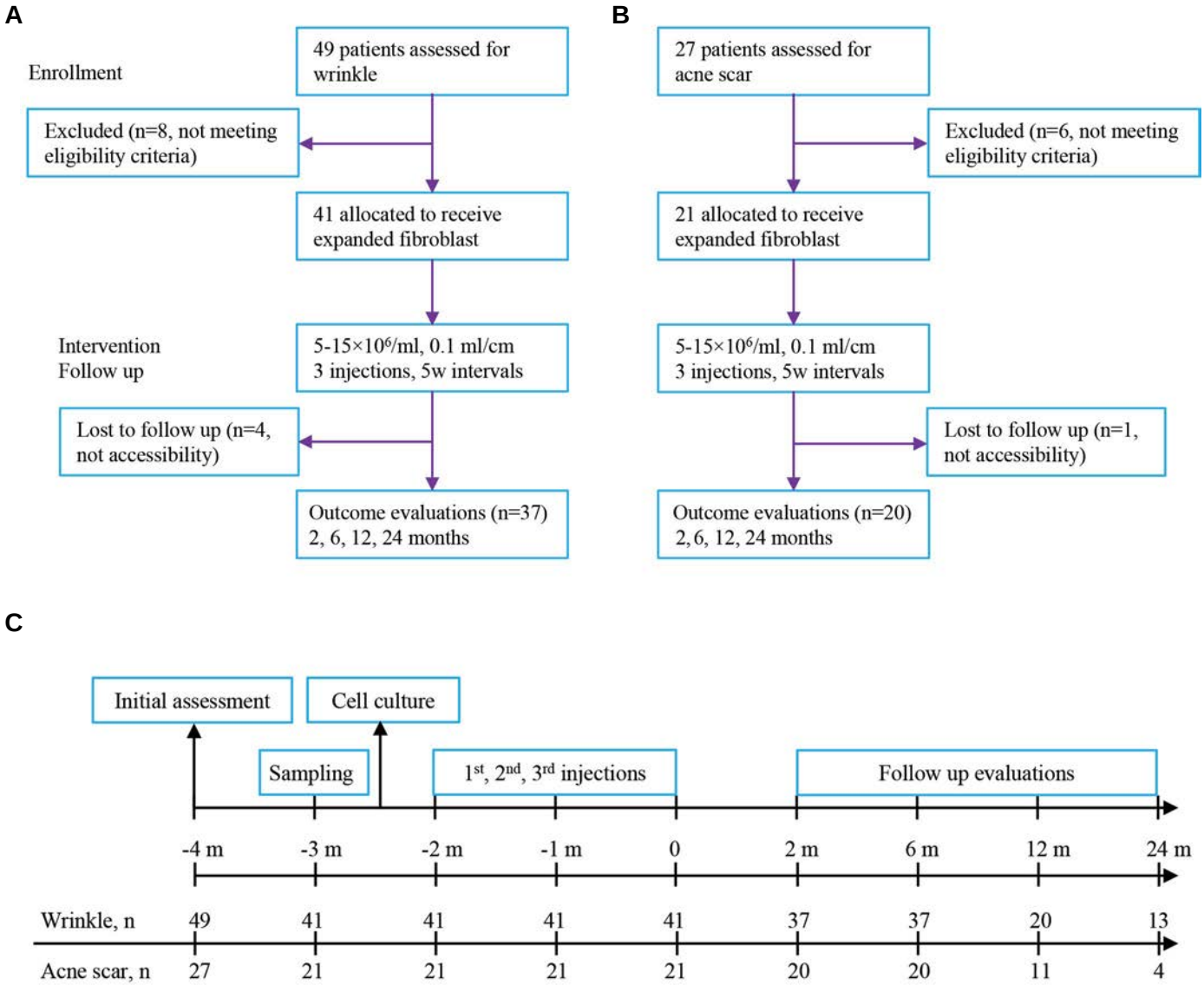

Fig.1: Study design and timeline. **A.** Study design for wrinkle participants, **B.** Study design for acne scar participants, and **C.** Study events and timeline. Eligible participants underwent three autologous cultured fibroblast injections. Efficacy data are based on comparisons of the baseline and follow-up evaluator and patient's assessment scores.

Table 2: Six-month follow-up evaluation of subjects

Assessment	Wrinkle group n=37					Acne scar group n=20			
	Glabella n=35	Periorbital n=35	NLF n=28	Forehead n=34	Total site n=132	Forehead n=9	Temporal n=7	Cheek n=20	Total sites n=36
Evaluator's assessment score, median (range)	2 (0-6)	2 (1-6)	3 (1-6)	3 (1-6)	3 (0-6)	3 (2-5)	2 (1-7)	3 (1-7)	3 (1-7)
Responders[a] (%)	18 (51.4)	21 (60)	18 (64.3)	18 (52.9)	75 (56.8)	4 (44.4)	4 (57.1)	15 (75)	23 (63.9)
≥1 grade improvement (%)	32 (91.4)	32 (91.4)	25 (89.3)	31 (91.2)	120 (90.1)	7 (77.8)	6 (85.7)	18 (90)	31 (86.1)
Self-assessment score of +1 or +2 (%)[b]	27 (77.1)	25 (71.4)	20 (71.4)	21 (61.8)	93 (70.5)	5 (55.5)	6 (85.7)	15 (75)	26 (72.2)

[a]; At least 2-grade improvement by evaluator's assessment, [b]; Impression of good or excellent by self-assessment, and NLF; Nasolabial fold.

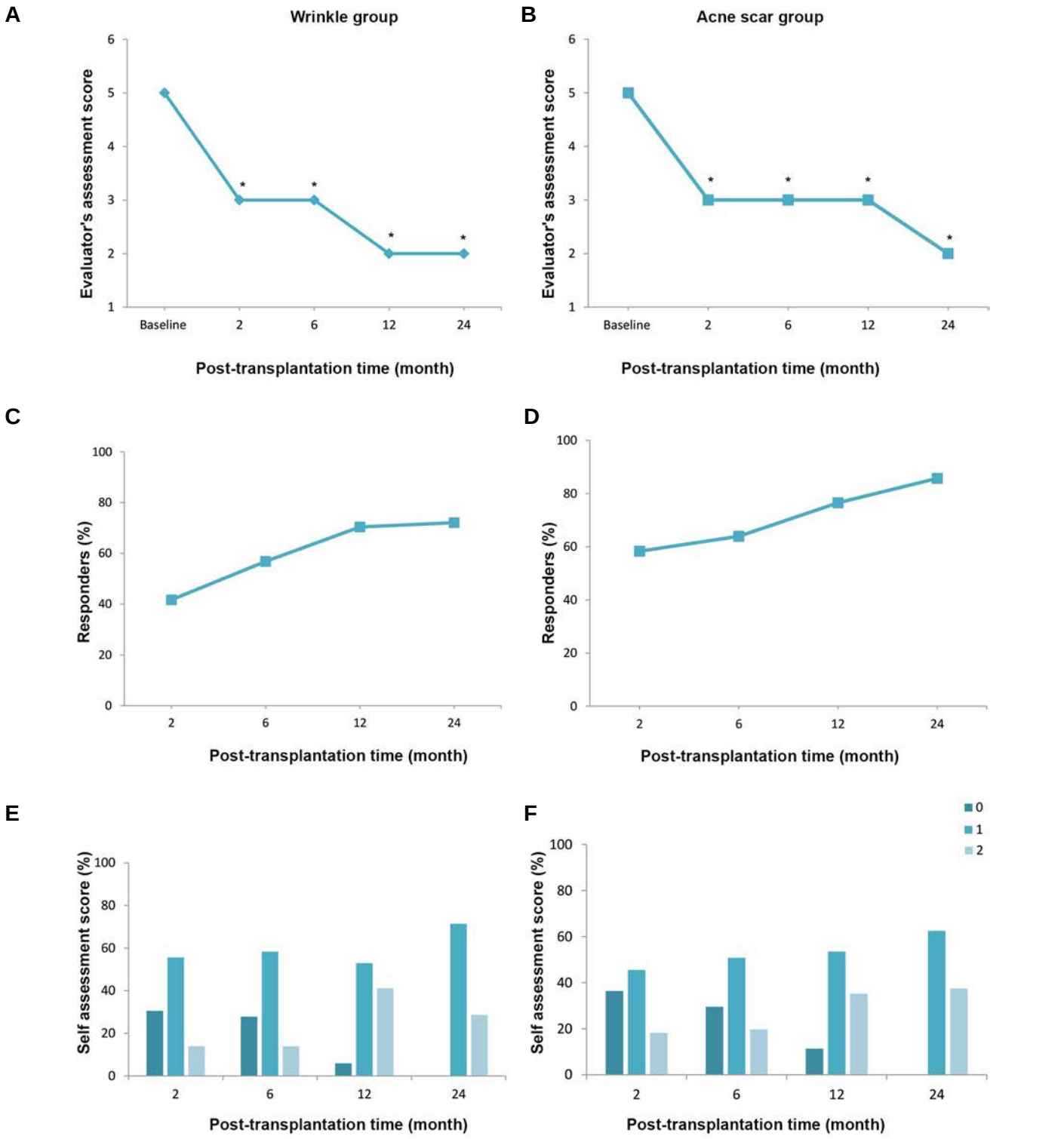

Fig.2: Efficacy outcomes. **A.** Evaluator's assessment score of the total sites in participants with wrinkles. Numbers are median, **B.** Evaluator's assessment score of the total sites in participants with acne scars. Numbers are median, **C.** The percentages of participants with wrinkles with a 2-point improvement based on the evaluator assessment, **D.** The percentages of participants with acne scars with a 2-point improvement based on the evaluator assessment, **E.** Participants' self-assessment scores of the total sites in participants with wrinkles, and **F.** Participants' self-assessment scores of the total sites in participants with acne scars. *; P<0.05. 0; No difference, 1; Better or good, and 2; Much better or excellent.

We observed that at 6 months following transplantation, the responder sites of the participants who were less and more than 45 years old were: glabella (28.5 and 66.6%), periorbital (42.8 and 71.4%), NLF (33.3 and 78.9%), and forehead (38.4 and 61.9%), respectively. Additionally, 2 grade improvements were seen in 60.5 and 86.9% of moderate and severe versus 20.9% of mild wrinkle sites (P<0.05).

Participants which had a history of botulinum toxin in forehead and glabella sites showed non-significant better results after fibroblast transplantation compared to the participants without history of botulinum toxin injection (P=0.16 and P=0.19). Also, participants which had a history of laser therapy on NLF sites showed a mean response rate of 2.5 ± 1.1 versus 1.7 ± 1.2 in participants without history

of laser therapy (P=0.12). Participants used to smoke did not show significant difference on response rates compared to non-smoker participants (P=0.98).

Fig.3: Participants underwent autologous cultured fibroblast transplantation before and after treatment.

Acne scar group

The median baseline grade in acne scar sites was 5 that decreased to 3 at 6 months after treatment, based on evaluator's assessments. Moreover, we observed that at 24 month following transplantation, this score decreased to 2. Average response rates of treatment sites in comparison with baseline grades at the 2-month follow-up were: 2.1 ± 1.1 (cheek), 1.9 ± 1.3 (temporal), 1.1 ± 0.9 (forehead), and 1.8 ± 1.3 for all 36 acne scar sites (P<0.001). The 6-month response rates were: 2.2 ± 1.2 (cheek), 2 ± 1.4 (temporal), 1.4 ± 1.1 (forehead), and 2 ± 1.2 for all 36 acne scar sites (P<0.001, Figs.2, 3).

The evaluators noted that 15 (75%) sites in the cheek, 4 (57.1%) in the temporal area, 4 (44.4%) from the forehead, and 23 (63.9%) out of the total 36 acne scar sites were responders at 6 months follow-up. However, 31 (86.1%) of all acne scar sites had at least a one grade improvement.

Participants scored +1 or +2 (good or excellent) for the following sites at the 2- and 6- month follow-up visits: forehead (55.5 and 55.5%), cheek (75 and 75%), and temporal (71.4 and 85.7%). At 2- and 6- month after final transplantation, a total of 69.4 and 72.2% of all 36 acne scar sites scored +1 or +2, respectively (Fig.2). As seen in Table 2, participants did not rate any of the treatment sites as -2 (much worse) or -1 (worse). Furthermore, participants met the 12- and 24- month follow-up visits showed sustained efficacy based on evaluator and self-assessment scores (Figs.2, 3). At 5-year follow up, 10 participants were accessible and 30% of the participants declared the durability of the treatment on the acne scar sites.

At 6 month following transplantation, 2 grade improvements were seen in 68.7 and 73.3% of moderate and severe versus 20% of mild wrinkle sites (P<0.05). Additionally, participants which had a history of laser therapy or microderm abrasion on cheek site showed a similar response rate compared to the participants without such history (P=1).

Adverse events

All participants experienced temporary, mild burning during and 1-2 hours after transplantation. A total of 3 participants with acne scars and 8 with wrinkles complained of mild to moderate adverse events that included bruising and redness. Of these, 9 reported that the adverse events spontaneously resolved after 24-48 hours. However, bruising in 2 scar participants lasted for 4-5 days which resolved following the application of ice and oral NSAID administration. We observed no major or systemic adverse events during the 24 months of follow-up evaluations.

Cell characteristics

After 4-5 weeks, we collected passage-3 fibroblasts. The fibroblasts showed a spindle-shaped morphology in the culture (Fig.4A). Our data indicated that cell viability at the first transplantation was 97.8 ± 3.5%, whereas the second injection had cell viability of 92.8 ± 12.2% and 93.3 ± 10.1% for the third injection. Immunostaining of cultured fibroblasts showed high-level expressions of vimentin and collagen type 1 (Fig.4B, C). We assessed karyotypes of passage-3 fibroblasts for genomic stability. There were normal 45XX and 45XY karyotypes in all participants with no evidence of any abnormality (Fig.4D).

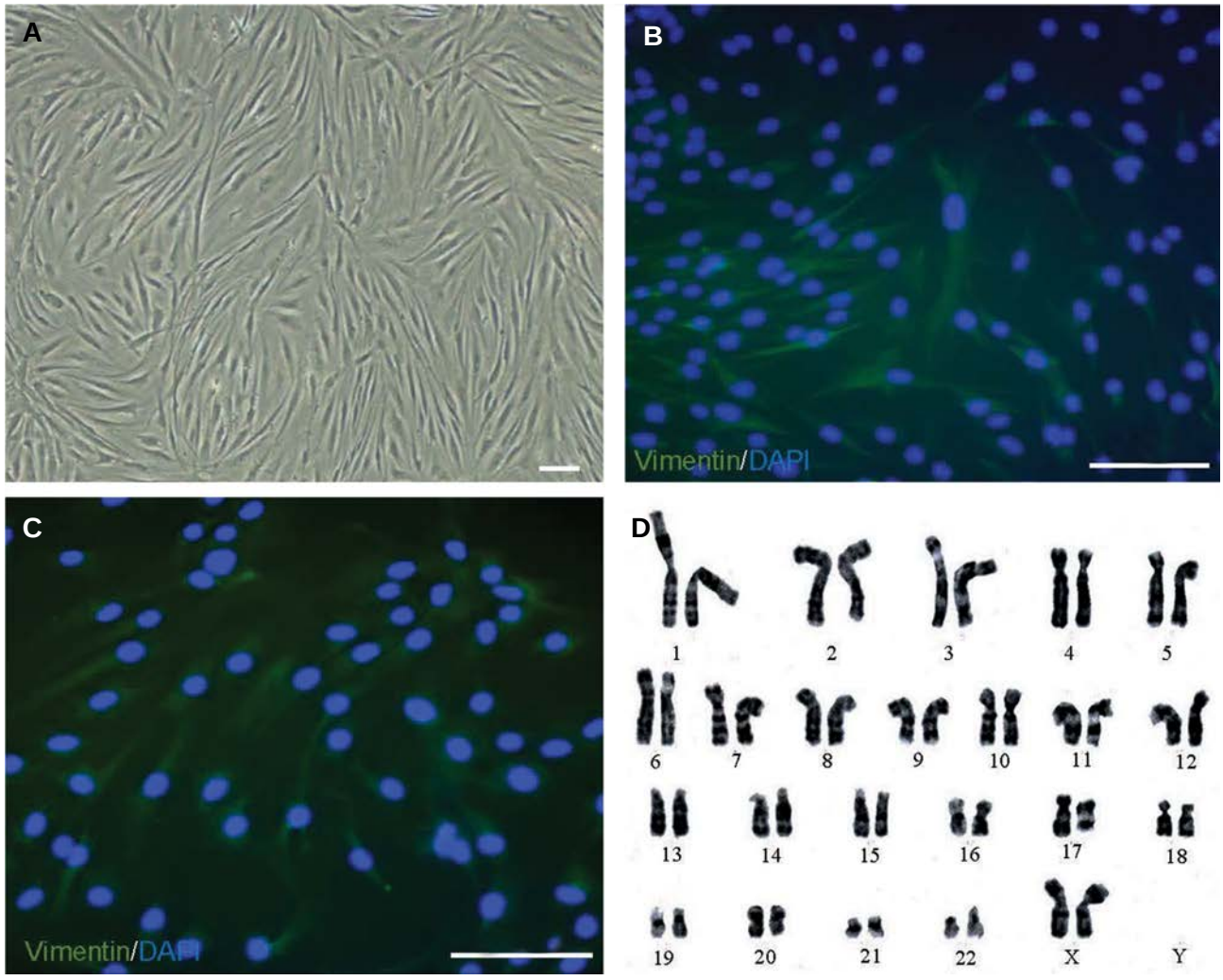

Fig.4: Characteristics of cultured fibroblasts. **A.** Phase-contrast microscopy of fibroblasts shows spindle and elongated cells after cultivation (scale bar: 50 µm). Representative fluorescent staining shows: **B.** Vimentin (scale bar: 100 µm), **C.** Collagen type I expression in cultured fibroblast cells (scale bar: 100 µm). Nuclear stained by DAPI (blue), and **D.** Karyogram of cultured fibroblasts indicates no abnormality in third passage.

Discussion

During the past two decades, many biodegradable and non-biodegradable dermal filler substances such as collagen, hyaluronic acid, and fat grafting have been introduced for reducing facial contour deformities. However, these approaches do not result in durable effects, and are associated with short- and long-term adverse events such as local or systemic infections, injection site abscesses, hypersensivity, nodules, tissue necrosis, and immune reactions. Recently, injection of permanent synthetic fillers for soft tissue augmentation has become common. However, a growing amount of literature has described complications following injection of permanent filling agents such as indurations, infections and inflammations, abscesses, and delayed granulomas (9, 24).

Recent efforts led to the introduction of autologous fibroblast transplantation as a natural corrective approach with fewer adverse events and longer efficacy. The studies have reported a mean improvement of 2 scores based on clinical scorings and responder rates of 30-82.2% (16, 17, 19, 20). Investigations on safety and efficacy of this modality has led to FDA approval of autologous fibroblast applications for nasolabial wrinkles (25). Our study also showed a mean improvement of 2 scores in the wrinkle and acne scar treatment sites at the 6-month follow up, which remained stable for a mean time of 24 months. Our results have revealed that responder rates of 56.8% for the wrinkle group and 63.9% for the acne scar group. The higher efficacy rate in the acne scar group agreed with similar studies and demonstrated that participants with acne scars experienced greater benefits from fibroblast transplantation (16). This could be attributed to subcision-like effect of the injection procedure, which is a common treatment for acne scars.

In the present study, 70.5% of participants with wrinkles and 83.3% of participants with acne scars expressed satisfaction with the clinical results at the 6-month follow up. There was an upward trend observed in the scores reported by participants during the follow up visits, so that all participants assessed the effect of fibroblast transplantation as 'good' or 'excellent' at the 24-month follow up. This prolonged efficacy might be

attributed to previous observation of live and bioactive fibroblasts in the recipient area up to 12 months after transplantation (17, 26). However, participants with acne scar reported a decrease in the self-assessment score from 72.2% at 1-year to 30% at 5-year post transplantation, and participants with wrinkle declared a milder decrease in the primary achieved outcome, from 70.5% at 1-year to 65.2% at 5-year post transplantation.

It is presumed that the efficacy rate of fibroblast transplantation may be affected by several variables, which include treatment location, treatment site severity, patient's age, and treatment protocol. Here, we have observed a lower response rate in the forehead area of both wrinkle and acne scar groups. A higher response rate was seen in the cheek area of participants with acne scars, whereas we did not detect any remarkable higher response rates in the different wrinkle treatment sites. However, West and Alster (27) previously reported a higher efficacy of fibroblast transplantation in NLFs compared to lip and glabella wrinkles. In this study, we observed that moderate to severe treatment sites showed higher efficacy rate compared to the mild sites. We did not observe any significant correlation between age and final outcome, however, participants aged more than 45 years old showed more responder sites compared to the younger participants. Previously, two studies showed similar culture characteristics between aged and young fibroblasts (17, 28). However, two studies previously demonstrated lower responses in fibroblast transplantation for older participants (18, 29).

Regards to the treatment dosage, we injected 0.5-1.5×10^6 fibroblasts per cm or cm^2 of the treatment sites in each session depends on the sites' length or area. Previously, Weiss et al. (20) injected 2×10^6 fibroblasts per cm or cm^2 of wrinkles or acne scars in each session. Later, the study that evaluated the efficacy of autologous fibroblasts for wrinkles, amounts of 1-2×10^6 cells/ cm were administered to the treatment sites (19). However, Zorin et al. (17) who evaluated the effects of fibroblast therapy in wrinkle, administered 0.7×10^6 of cells per cm of treatment sites. Dose finding studies would be necessary to define the optimum cell dose in fibroblast transplantation for contour deformities.

Previous studies indicated that cultured fibroblasts from passages 5, 10, or higher maintain their genomic stability with no mutations or translocations in the cultivation process. However, greater proliferation capacity and higher secretion bioactivity were observed in fibroblasts of passages 3 or 4 (30, 31). Therefore, we injected passage-3 fibroblasts and evaluated the cells according to biosynthetic activity and karyotype normality before transplantation. In our study, we did not observe any serious adverse events over 24 months of follow up, with the exception of temporary, mild reactions that resolved within a few days after transplantation.

Some limitations to the study presented here need to be declared. First, there is no control group in our trial. Second, our results are based on semi-objective assessments.

Conclusion

Our study demonstrated that autologous fibroblast transplantation could be a promising remodeling modality, especially for moderate to severe facial contour deformities in terms of long-term corrective ability with no adverse effects. These results are encouraging to conduct large randomized clinical trials to optimize the treatment protocol.

Acknowledgements

We are grateful to members of the Department of Regenerative Medicine for expertise and feedback. We would especially like to thank the participants and their families for participating in this study. This project was supported in part by a grant from Royan Institute with gran number 90000403. The authors have no potential conflict of interest to report.

Authors' Contributions

N.A., S.Sh.; Conceived, designed the original protocol, and supervised the study. All authors were involved in amending the protocol. S.Sh., A.B., Z.O., M.R.; Conducted the study. E.T., A.N., A.Sh., N.F., P.M., F.V., Z.Kh.; Performed the cell isolation, cultivation, and characterization. A.F.: Performed the Karyotyping. A.B., Z.O., S.Sh., M.R., Z.J.; Were involved in patient recruitment and follow-up visits. Data entry was performed by M.Gh., Z.J. A.A.; Cleaned and analyzed the data. N.A., S.Sh., H.B., A.B.: Were involved in interpretation of the study results. A.B.; Wrote the first draft of the manuscript. A.F., S.H.H.; Performed the karyotyping. All authors read and approved the final manuscript.

References

1. Newton VL, Mcconnell JC, Hibbert SA, Graham HK, Watson RE. Skin aging: molecular pathology, dermal remodelling and the imaging revolution. G Ital Dermatol Venereol. 2015; 150(6): 665-674.
2. Driskell RR, Watt FM. Understanding fibroblast heterogeneity in the skin. Trends Cell Biol. 2015; 25(2): 92-99.
3. Fisher GJ, Shao Y, He T, Qin Z, Perry D, Voorhees JJ, et al. Reduction of fibroblast size/mechanical force down-regulates TGF-β type II receptor: implications for human skin aging. Aging Cell. 2016; 15(1): 67-76.
4. Kammeyer A, Luiten RM. Oxidation events and skin aging. Ageing Res Rev. 2015; 21: 16-29.
5. Bissell MJ, Kenny PA, Radisky DC. Microenvironmental regulators of tissue structure and function also regulate tumor induction and progression: the role of extracellular matrix and its degrading enzymes. Cold Spring Harb Symp Quant Biol. 2005; 70: 343-356.
6. Quan T, He T, Shao Y, Lin L, Kang S, Voorhees JJ, et al. Elevated cysteine-rich 61 mediates aberrant collagen homeostasis in chronologically aged and photoaged human skin. Am J Pathol. 2006; 169(2): 482-490.
7. Fisher GJ, Varani J, Voorhees JJ. Looking older: fibroblast collapse and therapeutic implications. Arch Dermatol. 2008; 144(5): 666-672.
8. Hu B, Castillo E, Harewood L, Ostano P, Reymond A, Dummer R, et al. Multifocal epithelial tumors and field cancerization from loss of mesenchymal CSL signaling. Cell. 2012; 149(6): 1207-1220.
9. De Boulle K, Heydenrych I. Patient factors influencing dermal filler

complications: prevention, assessment, and treatment. Clin Cosmet Investig Dermatol. 2015; 8: 205-214.
10. Fligiel SE, Varani J, Datta SC, Kang S, Fisher GJ, Voorhees JJ. Collagen degradation in aged/photodamaged skin in vivo and after exposure to matrix metalloproteinase-1 in vitro. J Invest Dermatol. 2003; 120(5): 842-848.
11. Varani J, Dame MK, Rittie L, Fligiel SE, Kang S, Fisher GJ, et al. Decreased collagen production in chronologically aged skin: roles of age-dependent alteration in fibroblast function and defective mechanical stimulation. Am J Pathol. 2006; 168(6): 1861-1868.
12. Levy LL, Zeichner JA. Management of acne scarring, part II: a comparative review of non-laser-based, minimally invasive approaches. Am J Clin Dermatol. 2012; 13(5): 331-340.
13. Gozali MV, Zhou B. Effective treatments of atrophic acne scars. J Clin Aesthet Dermatol. 2015; 8(5): 33-40.
14. Halvorsen JA, Stern RS, Dalgard F, Thoresen M, Bjertness E, Lien L. Suicidal ideation, mental health problems, and social impairment are increased in adolescents with acne: a population-based study. J Invest Dermatol. 2011; 131(2): 363-370.
15. Layton AM, Henderson CA, Cunliffe WJ. A clinical evaluation of acne scarring and its incidence. Clin Exp Dermatol. 1994; 19(4): 303-308.
16. Munavalli GS, Smith S, Maslowski JM, Weiss RA. Successful treatment of depressed, distensible acne scars using autologous fibroblasts: a multi-site, prospective, double blind, placebo-controlled clinical trial. Dermatol Surg. 2013; 39(8): 1226-1236.
17. Zorin V, Zorina A, Cherkasov V, Deev R, Kopnin P, Isaev A. Clinical-instrumental and morphological evaluation of the effect of autologous dermal fibroblasts administration. J Tissue Eng Regen Med. 2017; 11(3): 778-786.
18. Boss WK Jr, Usal H, Fodor PB, Chernoff G. Autologous cultured fibroblasts: a protein repair system. Ann Plast Surg. 2000; 44(5): 536-542.
19. Smith SR, Munavalli G, Weiss R, Maslowski JM, Hennegan KP, Novak JM. A multicenter, double-blind, placebo-controlled trial of autologous fibroblast therapy for the treatment of nasolabial fold wrinkles. Dermatol Surg. 2012; 38(7 Pt 2): 1234-1243.
20. Weiss RA, Weiss MA, Beasley KL, Munavalli G. Autologous Cultured fibroblast injection for facial contour deformities: a prospective, placebo-controlled, phase iii clinical trial. Dermatol Surg. 2007; 33(3): 263-268.
21. Erdag G, Sheridan RL. Fibroblasts improve performance of cultured composite skin substitutes on athymic mice. Burns. 2004; 30(4): 322-328.
22. Liu G, Liang K-Y. Sample size calculations for studies with correlated observations. Biometrics. 1997; 53(3): 937-947.
23. National Cancer Institute, National Institutes of Health, US Department of Health and Human Services. Common Terminology Criteria for Adverse Events (CTCAE), Version 4.0. NIH publication 09-7473; 2010.
24. Funt D, Pavicic T. Dermal fillers in aesthetics: an overview of adverse events and treatment approaches. Clin Cosmet Investig Dermatol. 2013; 6: 295-316.
25. Schmidt C. FDA approves first cell therapy for wrinkle-free visage. Nat Biotechnol. 2011; 29(8): 674-675.
26. Zhao Y, Wang J, Yan X, Li D, Xu J. Preliminary survival studies on autologous cultured skin fibroblasts transplantation by injection. Cell Transplant. 2008; 17(7): 775-783.
27. West TB, Alster TS. Autologous human collagen and dermal fibroblasts for soft tissue augmentation. Dermatol Surg. 1998; 24(5): 510-512.
28. Bayreuther K, Francz PI, Rodemann HP. Fibroblasts in normal and pathological terminal differentiation, aging, apoptosis and transformation. Arch Gerontol Geriatr. 1992; 15 Suppl 1: 47-74.
29. Watson D, Keller GS, Lacombe V, Fodor PB, Rawnsley J, Lask GP. Autologous fibroblasts for treatment of facial rhytids and dermal depressions: a pilot study. Arch Facial Plast Surg. 1999; 1(3): 165-170.
30. Keller G, Sebastian J, Lacombe U, Toft K, Lask G, Revazova E. Safety of injectable autologous human fibroblasts. Bull Exp Biol Med. 2000; 130(2): 786-789.
31. Hayflick L, Moorhead PS. The serial cultivation of human diploid cell strains. Exp Cell Res. 1961; 25: 585-621.

Original Article

Internal Transcribed Spacer rDNA and *TEF-1α* Gene Sequencing of Pathogenic Dermatophyte Species and Differentiation of Closely Related Species Using PCR-RFLP of The Topoisomerase II

Zahra Salehi, Ph.D.[1], Masoomeh Shams-Ghahfarokhi, Ph.D.[1]*, Mehdi Razzaghi-Abyaneh, Ph.D.[2]

1. Department of Mycology, Faculty of Medical Sciences, Tarbiat Modares University, Tehran, Iran
2. Department of Mycology, Pasteur Institute of Iran, Tehran, Iran

Corresponding Address: P.O.Box: 14115-331, Department of Mycology, Faculty of Medical Sciences, Tarbiat Modares University, Tehran, Iran
Email: shamsm@modares.ac.ir

Received: 11/September/2018, Accepted: 26/December/2018

Abstract

Objective: Precise identification of dermatophyte species significantly improves treatment and controls measures of dermatophytosis in human and animals. This study was designed to evaluate molecular tools effectiveness of the gene sequencing and DNA-based fragment polymorphism analysis for accurate identification and differentiation of closely-related dermatophyte species isolated from clinical cases of dermatophytosis and their antifungal susceptibility to the current antifungal agents.

Materials and Methods: In this experimental study, a total of 95 skin samples were inoculated into mycobiotic agar for two weeks at 28°C. Morphological characteristics of the isolated dermatophytes were evaluated. DNA was extracted from the fungal culture for amplification of topoisomerase II gene fragments and polymerase chain reaction (PCR) products were digested by Hinf I enzyme. Internal transcribed spacer (ITS) rDNA and *TEF-1α* regions of the all isolates were amplified using the primers of ITS1/4 and EF-DermF/EF-DermR, respectively.

Results: Based on the morphological criteria, 24, 24, 24 and 23 isolates were identified as *T. rubrum, T. interdigitale, T. tonsurans and E. floccosum,* respectively. PCR-restriction fragment length polymorphism (RFLP) results provided identification pattern of the isolates for *T. rubrum* (19 isolates), *T. tonsurans* (28 isolates), *T. interdigitale* (26 isolates) and *E. floccosum* (22 isolates). Concatenated dataset results were similar in PCR-RFLP, except six *T. interdigitale* isolates belonging to *T. mentagrophytes*.

Conclusion: Our results clearly indicated that conventional morphology and PCR-RFLP were not able to precisely identify all dermatophyte species and differentiation of closely related species like *T. interdigitale and T. mentagrophytes*, while ITS rDNA and *TEF-1α* gene sequence analyses provided accurate identification of all isolates at the genus and species level.

Keywords: Dermatophytes, Gene Sequencing, Polymerase Chain Reaction-Restriction Fragment Length Polymorphism, Topoisomerase II

Cell Journal(Yakhteh), Vol 22, No 1, April-June (Spring) 2020, Pages: 85-91

Citation: Salehi Z, Shams-Ghahfarokhi M, Razzaghi-Abyaneh M. Internal transcribed spacer rDNA and TEF-1α gene sequencing of pathogenic dermatophyte species and differentiation of closely related species using PCR-RFLP of the topoisomerase II. Cell J. 2020; 22(1): 85-91. doi: 10.22074/cellj.2020.6372.

Introduction

Dermatophytosis is a superficial fungal infection caused by dermatophytes, affecting nearly 20% of the population worldwide, as a public health problem (1, 2). Previous studies revealed a significant increase in dermatophyte infections (3, 4). Over 40 species of dermatophytes were assigned to three genera, including *Trichophyton*, *Epidermophyton* and *Microsporum* (2, 5). All three groups can infect humans via direct or indirect contact (5). Ordinarily, dermatophyte species like *T. interdigitale*, *T. rubrum*, *T. tonsurans* and *E. floccosum* are major etiologic agents of dermatophytosis in Iran (6-9). Communicating epidemiological statistics of these dermatophytes is greatly impeded, since taxonomic schemes are constantly changing. For example, it has recently been revealed that the previous *T. mentagrophytes* complex is composed of four new species: i. Zoophilic *T. Mentagrophytes* sensustricto, ii. Zoophilic *T. erinacei*, iii. *Trichophyton* anamorph of *A. benhamiae* (zoophilic), and iv. Zoophilic and anthropophilic strains of *T. interdigitale* (10, 11). Based on the latest classification, anthropophilic *T. mentagrophytes* should now be relabelled as *T. interdigitale* (12, 13). Regarding morphological similarity among the dermatophytes spp., epidemiology variation of dermatophytes and emerging new pathogens, it is necessary to identify isolates at the species level (3, 7, 8).

Dermatophytosis is routinely identified by direct examination and culture (14). The phenotypic features depend on many variables such as the slow growth rate, temperature variation, prior therapy and production of spores (2, 7, 15). In addition, the clinical signs of dermatophytosis are often atypical in immunocompromised hosts (7). Moreover, routine procedures are either slow or nonspecific (6, 15, 16), and requires training of personnel and supervisory expertise (17, 18). Furthermore, phenotypic methods fail to closely discriminate the related species. Developing molecular methods provided more accurate and rapid results for differentiating species of dermatophytes. Polymerase chain reaction (PCR) and DNA fragments sequencing of the internal transcribed spacer (ITS) regions, 18S rDNA, translation elongation factor1-α (TEF-1α), restriction fragment length polymorphism analysis (RFLP), nested

PCR, repetitive sequence PCR (rep-PCR), arbitrarily primed-PCR (AP-PCR) and real-time PCR are some examples of these methods (15, 17, 19-25). At present, sequence of the ITS region is considered as the gold standard for dermatophyte analyses (14, 26). *TEF-1α* gene was considered as an alternative to rDNA showing high level of variation rate among the species (25). The results obtained by previous studies suggest that PCR-RFLP assay is more efficient and convenient for fungal diagnosis. PCR-RFLP studies targeting the ITS rDNA have shown that it is a reliable method for identification of dermatophytes at the species level (27-29). It has been reported that DNA topoisomerase II gene is useful as a target for the study of different fungal species (26). Despite various studies about the significance of species identification in dermatophytes, to the best of our knowledge, limited data has been published on the precise differentiation of dermatophytes spp. by combination of the ITS and *TEF-1α* sequences and topoisomerase II PCR-RFLP approach. The present study was evaluated the effectiveness of gene sequencing and DNA-based fragment polymorphism analysis molecular tools for accurate identification and differentiation of closely-related dermatophyte species isolated from clinical cases of dermatophytosis and their antifungal sensitivity to the current antifungal agents.

Materials and Methods

Specimens and conventional assays

In this experimental study, a total of 95 hair and skin samples, from patients suspected to dermatophytosis, were received for routine examination at Department of Mycology of Pasteur Institute (Iran). This study was approved by Ethical Committee of Pasteur Institute of Iran (Code No. IR.PII.REC.1397.021). Patients were informed of the procedure. Direct microscopy examination of the samples was performed using 10% potassium hydroxide and the samples were cultured on mycobiotic agar (Merck, Germany) plates to facilitate growth of the dermatophytes. The plates were incubated at 30˚C for 4 weeks. All fungal isolates were identified by analysis of the morphological characteristics (typical macro/microscopic characters of the colonies, and additional tests like hair perforation or urease tests). The dermatophyte strains including *T. tonsurans*, *T. interdigitale*, *E. floccosum* and *T. rubrum* were identified by morphological characterization. In addition, standard strains of *T. rubrum* (PFCC 51431), *T. mentagrophytes* (PTCC 5054), *T. tonsurans* (CBS 130924) and *E. floccosum* (CBS 767.73) were included in the study. The dermatophyte strains were then cultured and identified by analysis of the molecular methods. To validate standard strains at species level based on the latest classification, all strains were sequenced.

Molecular identification and differentiation of dermatophyte species

DNA extraction

All clinical and standard strains were cultured on mycobiotic agar (Merck, Germany) and incubated at 28˚C for two weeks. A fungal colony was cut from the agar plate with a scalpel, transferred to a mortar and grounded in liquid nitrogen. Then, using the phenol-chloroform-isoamyl alcohol chemicals, DNA was extracted according to Makimura et al. (26).

PCR-RFLP assay targeting the topoisomerase II

The PCR was performed using a Taq DNA Polymerase Master Mix, with topoisomerase II primer (dPsD2)

dDPF2:
5′-GTYTGGAAYAAYGGYCGYGGTATTCC-3′ and

dDPR2:
5′-AAVCCGCGGAACCAKGGCTTCATKGG-3′.

PCR program was performed by the following cycle conditions: an initial denaturation at 95˚C for 5 minutes, followed by 30 cycles of 95˚C for 30 seconds, 63˚C for 15 seconds, and 72˚C for 120 seconds, followed by a final extension at 72˚C for 5 minutes (19). The PCR products with ~2380 bp length were purified using a Min Elute PCR Purification kit (Qiagen, USA).

Restriction fragment length polymorphism analysis of the amplified topoisomerase II

Digestion of all reactions were performed in 15 µl mixture volume containing 2 µl of 10× buffer (Fermentas, USA), 2 µl of each enzyme, 10 µl purified PCR products and sufficient amount of ultrapure water to approach final volume. Digestion was performed using Hinf I reaction enzyme (Fermentas, USA) at 37˚C for 8-10 hours (18). PCR amplicons and restriction enzyme digestion products were loaded in 2.5% (w/v) agarose gels in the presence of a GelRed stain (Biotium Inc., USA) (0.5 µg/ml), while a 100 bp DNA molecular size marker (Fermentas, USA) was used, and the sample were run at 90 V/Cm for 90 minutes.

Internal transcribed spacer and TEF-1α region amplifications by PCR

For each sample, the *TEF-1α* and ITS regions were amplified using the specific primers

EF-Derm
F: 5′-CACATTAACTTGGTCGTTATCG-3′ and
R: 5′-CATCCTTGGAGATACCAGC-3′, as well as
ITS1: 5′- TCCGTAGGTGAACCTGCGG-3′ and
ITS4: 5′-TCCTCCGCTTATTGATATGC-3′.

The reaction PCRs were consisted of initially denaturation at 95˚C for 5 minutes, followed by 30 cycles of 94˚C for 30 seconds, 58˚C for 30 seconds and 72˚C or 45 seconds, followed by a final extension step at 72˚C for 5 minutes (25, 30).

Sequencing

Purified PCR product was sequenced using the ABI PRISM BigDye Terminator Cycle Sequencing Ready Reaction Kit (Applied Biosystems, USA).

Phylogenetic analysis

The best-fit model of molecular evolution was estimated in jModelTest 2.1.10 (31). Sequences of the two loci of each

isolate were combined for phylogenetic analyses with PAUP version 4.0b109 (32). The program MrBayes version 3.2 (33), run on the CIPRES Science Gateway (34). Two simultaneous analyses with eight Metropolis-coupled Markov chain Monte Carlo (MCMC) chains with incremental heating of 0.2 were run for 20 million generations, sampled every 1000 generations. We verified the convergence of parameter estimates and the effective sample sizes were > 200bp for all parameters using Tracer version 1.6 (35).

Antifungal drug susceptibility testing

Terbinafine, griseofulvin and ketoconazole (Sigma-Aldrich, USA) were prepared in dimethyl sulfoxide (DMSO). Final concentration of drugs, fungal spore suspensions, were prepared in the standard RPMI 1640 medium (Sigma-Aldrich, USA) buffered to pH=7.0 with 0.165 mol/l 3-(N-morpholino) propanesulfonic acid (MOPS) with L-glutamine (Sigma-Aldrich, USA), with no bicarbonate, in 96-well round bottom microplates according to CLSI M38-A2 broth microdilution protocol (36). All tests were performed in triplicate. The inoculated microplates were incubated at 35˚C and visually assessed for fungal growth after four days incubation. The minimum inhibitory concentration (MIC) was defined as the point at which the growth of dermatophyte was inhibited by 80% for three antifungals, in comparison with the control. *T. rubrum* (PTCC 5143) and *C. parapsilosis* (ATCC 22019) were used as quality controls. MIC range, as geometric mean, was provided for all of the tested isolates.

Results

Identification of dermatophyte species using conventional assays

Morphological identification of isolated dermatophytes by using a combination of macroscopic (colony morphology, texture and color) and microscopic (hyphae structure, shape of macroconidia and microconidia) features showed that all the isolates were distributed in four species including *T. rubrum* (n=24), *T. tonsurans* (n=24), *T. interdigitale* (n=24) and *E. floccosum* (n=23).

Identification of the dermatophyte species by PCR-RFLP

The genomic DNAs were amplified with dPsD2 and generated a 2380 bp band. Amplification profile of the products were also identified for all 99 strains. The sizes were expected from the region amplified by dPsD2 and the restriction enzyme digestion with Hinf I (Table 1) was obtained from the website NEB cutter (http://tools.neb.com/NEBcutter). The PCR products were digested with Hinf I. The banding patterns obtained by the PCR-RFLP are shown in Figure 1. After amplification of genomic DNAs using dPsD2, the expected size was generated for all isolates. Differences between the fragments with less than 20 bp differences was not showed; therefore, there was overlap in the bands 70 bp and 67 bp in *T. tonsurans* as well as two distinctive bands (255 bp and 260 bp) and (178 bp and 186bp) in *E. floccosum*. All specimens were identified at the species level by the unique banding pattern specified to each species. All of the banding patterns for each species were coincided with its standard strains. PCR-RFLP results provided identification pattern of the isolates as *T. rubrum* (n=19), *T. tonsurans* (n=28), *T. interdigitale* (n=26) and *E. floccosum* (n=22).

Table 1: The expected sizes of DNA fragments generated by enzymatic digestion of *Hinf I*

Dermatophyte species (no.)	DNA fragment (bp)
T. interdigitale (27)	1209, 482, 233, 166, 137, 95, 58
T. rubrum (20)	1267, 482, 370, 262
T. tonsurans (29)	1209, 482, 233, 166, 95, 70, 67, 58
E. floccosum (23)	954, 482, 260, 255, 186, 178, 58

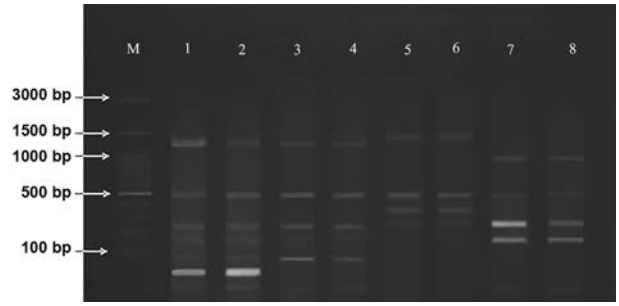

Fig.1: Polymerase chain reaction-restriction fragment length polymorphism (PCR-RFLP) electrophoretic patterns of dermatophytes species by amplification of topoisomerase II gene and digestion of the Hinf I enzyme. Lane M; 100 bp DNA ladder, Lane 1; *T. tonsurans*, Lane 2; *T. tonsurans* (CBS 130924), Lane 3; *T. interdigitale*, Lane 4; *T. mentagrophytes*, Lane 5; *T. rubrum*, Lane 6; *T. rubrum* (PFCC 51431), Lane 7; *E. floccosum,* and Lane 8; *E. floccosum* (CBS 767.73).

Identification of dermatophyte species by PCR sequencing

In the present study, all dermatophytes spp. (clinical and standard strains) were identified based on ITS sequencing. ITS and *TEF-1α* sequences of the isolates were aligned using ClustalW as implemented in MEGA7.0.21 software and edited manually to improve the alignment accuracy. The query sequences were paired with those in the GenBank database, using the Blastn analysis. On the basis of sequencing results, the dermatophyte isolates included *T. rubrum* (n=20), *T. tonsurans* (n=29), *T. interdigitale* (n=21), *T. mentagrophytes* (n=6) and *E. floccosum* (n=23). The ITS/*TEF-1α* sequence interpretations revealed that six isolates were identified as *T. interdigitale*, in contrary of PCR-RFLP results that showed *T. interdigitale* and *T. mentagrophytes* is categorized in same species.

A consensus tree belonging to the ITS and *TEF-1α* fragment was constructed for all species discussed in this study (Fig.2). Four clades were distinguishable. Furthermore, *T. mentagrophytes* and *T. interdigitale* were placed in the distinctive clusters. The dendrogram describes the relationships between all of the studied isolates. Isolates belonging to any species were clustered with a high support (more than 60%) in separate clades.

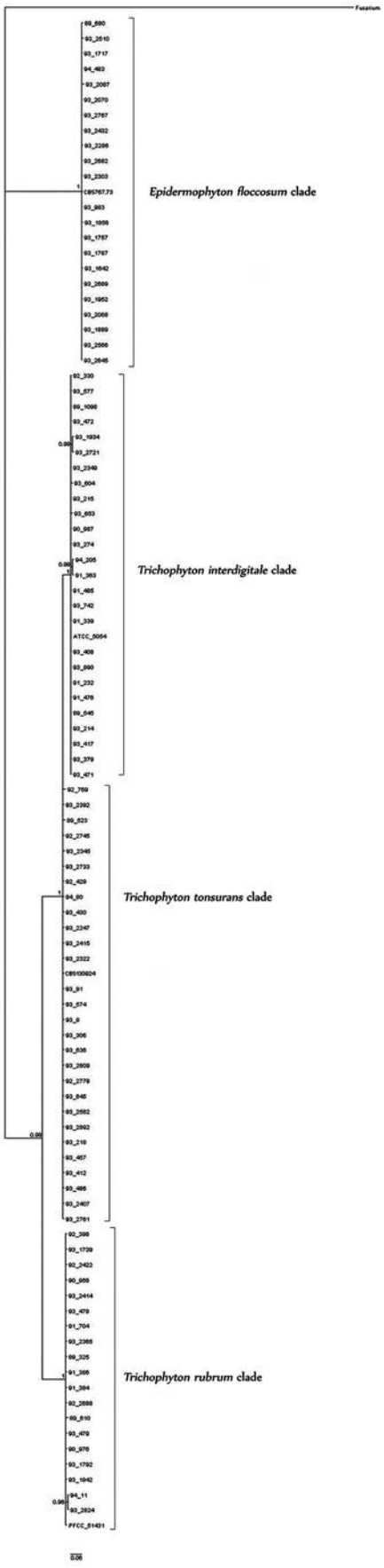

Fig.2: Bayesian tree based on the combined dataset. Phylogenetic analysis of the combined dataset with TIM2+G model of the 95 clinical isolates, four standard strains and *Fusarium*, as the out-group. Posterior probabilities more than 60% are given for the appropriate clades.

Molecular versus conventional method of species identification

Table 2 shows the results of conventional method of species identification and PCR-RFLP. The results of identification of dermatophyte spp. using PCR-RFLP were confirmed by sequencing of the ITS and *TEF-1α* regions. PCR-RFLP showed an increase in the identification rate compared to the conventional method. Analysis dataset of ITS and *TEF-1α* indicated that six isolates belonged to *T. mentagrophytes* and 21 isolates belonged *T. interdigitale*, while topoisomerase II PCR-RFLP failed to discriminate them. Interestingly, a complete overlap was observed between both methods in the case of remaining isolates.

Sensitivity of the molecular method was more than sensitivity of the conventional method. The results indicated that 86.4% of dermatophyte spp. identified by the conventional method was also confirmed by the molecular method. The specificity and sensitivity of sequencing method were found to be approximately 100%. Utilizing molecular method demonstrated that six out of the 24 isolates, identified as *T. rubrum* by conventional method, belonged to another genus and species including, *T. interdigitale* (n=4), *E. floccosum* (n=1) and *T. tonsurans* (n=1), using molecular method. Among the 24 strains identified as *T. interdigitale* by morphological examination, four strains had also been recognized as *T. tonsurans* (n=2), *E. floccosum* (n=1), and *T. rubrum* (n=1) by molecular methods. Three of 23 isolates which were identified as *E. floccosum*, by morphological examination were re-identified and confirmed as *T. interdigitale* (n=2) and *T. tonsurans* (n=1) by molecular characteristics.

Antifungal drug sensitivity of dermatophyte isolates

The MIC range and geometric mean were obtained for the all dermatophyte species (Table 3). A significant sensitivity to terbinafine was reported in *T. tonsurans*. The most sensitive and resistant species to griseofulvin were *T. interdigitale* and *E. floccosum*, respectively. Terbinafine and griseofulvin had the lowest and the highest geometric mean MICs, which were respectively 0.01 and 1.64 μg/ml for *T. interdigitale* and *E. floccosum*. Terbinafine was the most effective antifungal drug against all dermatophyte species.

Table 2: Identification of dermatophytes based on morphological and molecular methods

Dermatophytes spp.	**Morphological identification**			
	T. interdigitale	***T. rubrum***	***T. tonsurans***	***E. floccosum***
T. interdigitale (n=26)	20	4	-	2
T. rubrum (n=19)	1	18	-	-
T. tonsurans (n=28)	2	1	24	1
E. floccosum (n=22)	1	1	-	20
Total	24	24	24	23

Table 3: *In vitro* antifungal susceptibility of dermatophytes against three antifungal agents

Dermatophyte species	Antifungal drug	MIC Range	G mean
T. interdigitale (n=27)	Terbinafine	0.003-0.125	0.01
	Griseofulvin	0.03-64	0.41
	Ketoconazole	0.03-4	0.32
T. rubrum (n=20)	Terbinafine	0.003->32	0.04
	Griseofulvin	0.06-64	0.66
	Ketoconazole	0.06-8	0.28
T. tonsurans (n=29)	Terbinafine	0.003->32	0.01
	Griseofulvin	0.03-64	0.46
	Ketoconazole	0.03-2	0.16
E. floccosum (n=23)	Terbinafine	0.003-1	0.02
	Griseofulvin	0.03-64	1.64
	Ketoconazole	0.03-2	0.11

MIC; Minimum inhibitory concentration (µg/ml) and G mean; Geometric mean MIC.

Discussion

As earlier mentioned, there was high similarity within dermatophytes species. In the present study, the obtained results using DNA sequencing method,to identify common dermatophyte spp., had 100% accuracy. In this study, about 20% of the dermatophyte spp. identified by the conventional method was not correct and molecular analysis showed in fact that 16.6% (n=4 out of the 24) strains identified as *T. rubrum* by morphological examination were *T. interdigitale*. Due to the similarity in the morphological characters of *T.mentagrophytes*, *T. rubrum* and *T. interdigitale*, their differentiation was remained challenge (37, 38).

Interestingly, all 24 isolates, identified as *T. tonsurans* by morphological examination, were confirmed by molecular method. This highlighted the rare production of macroconidia by *T. tonsurans* leading to right identification at the phenotypic level. On the other hand, the *T. tonsurans* isolates with macroconidia were misidentified with *T. rubrum* and *T. interdigitale*. The topoisomerase-RFLP not only differentiated *T. rubrum* from *T. interdigitale*, but also it was a useful method for the differentiation of *T. interdigitale* from *T. tonsurans* by forming the unique bonding pattern for each species. The result was similar to what was reported by Kamiya et al. (7), showing that six dermatophyte spp. were specifically identified by the topoisomerase-RFLP. It should also be noted that similar to the study of Kanbe et al. (27), dermatophyte spp. were amplified by primer dPsD2. This was used for the common species identification of *Trichophyton, Microsporum* and *Epidermophyton*. The study conducted by Mochizuki et al. (29) demonstrated that ITS-RFLP of dermatophyte spp. was a reliable method for rapid identification of this fungus. Besides that, *TEF-1α* gene was considered as an alternative to rDNA that shows a high level of variation rate among the species. Findings obtained by Mirhendi et al. (25) are in accordance with our results. Result of the present study indicated that ITS/*TEF-1α* combination is a valuable approach to omit possible misidentification among the closely related species.

To correctly identify dermatophytes based on morphological characteristics, 2-4 weeks are required, while application of the molecular method showed that DNA derived from a fresh colony -cultured for five days- is suitable for identification these fungi. It was shown that some closely related species like *T. equinum* and *T. tonsurans* as well as *M. canis* and *M. ferrugineum*, showing no pattern difference in the ITS-RFLP (37), should be investigated using topoisomerase-RFLP. Although the topoisomerase-RFLP was rapid, stable and reproducible for the common dermatophytes spp., it is not a convenient tool for distinguishing between *T. interdigitale* and *T. mentagrophytes*.

Conclusion

Precise identification of dermatophyte species significantly improves treatment and control of

dermatophytosis in human and animals. Our results clearly indicated that conventional morphology and PCR-RFLP are not able to precisely identify all dermatophyte species and differentiate the closely related species like *T. interdigitale* and *T. mentagrophytes*, while ITS rDNA and *TEF-1α* gene sequence analyses provided an accurate identification for the all isolates at the genus and species level. Thus, concurrent sequence analysis of these genomic regions is very useful to confirm identity of dermatophyte species identified by routine morphology. It also enables clinicians for recommending effective treatment and control strategies to overcome various clinical types of dermatophytosis, especially chronic infection, which are antifungal drug resistance and quite difficult to treat.

Acknowledgements

This work was financially supported by the Research Deputy of Tarbiat Modares University (Tehran, Iran) and Iran National Science Foundation (INSF, grant number 94003277). The authors have no conflict of interest in this study.

Authors' Contributions

Z.S.; Performed the experiments in molecular section and drafted the manuscript. M.S.-G.; Supervised the study, participated in the study design and approved the final draft. M.R.-A.; Isolated the dermatophytes from clinical specimens, identified them by morphological methods and participated in writing of the manuscript. All authors read and approved the final manuscript.

References

1. Vahidnia A, BekersW, Bliekendaal H, Spaargaren J. High throughput multiplex-PCR for direct detection and diagnosis of dermatophyte species, Candida albicans and Candida parapsilosis in clinical specimen. J Microbiol Methods. 2015; 113: 38-40.
2. Zarrina M, Salehi Z, Zarei Mahmoudabadi A. Identification of dermatophytes by arbitrarily primed PCR. Asian Biomed. 2015; 9(3): 291-298.
3. Bontems O, Hauser P, Monod M. Evaluation of a polymerase chain reaction-restriction fragment length polymorphism assay for dermatophyte and nondermatophyte identification in onychomycosis. Br J Dermatol. 2009; 161(4): 791-796.
4. Didehdar M, Shokohi T, Khansarinejad B, Ali Asghar Sefidgar S, Abastabar M, Haghani I, et al. Characterization of clinically important dermatophytes in North of Iran using PCR-RFLP on ITS region. J Mycol Med. 2016; 26(4): 345-350.
5. Segal E, Frenkel M. Dermatophyte infections in environmental contexts. Res Microbiol. 2015; 166(7): 564-569.
6. Elavarashi E, Kindo AJ, Kalyani J. Optimization of PCR-RFLP directly from the skin and nails in cases of dermatophytosis, targeting the its and the 18s ribosomal dna regions. J Clin Diagn Res. 2013; 7(4): 646-651.
7. Kamiya A, Kikuchi A, Tomita Y, Kanbeb T. PCR and PCR-RFLP techniques targeting the DNA topoisomerase II gene for rapid clinical diagnosis of the etiologic agent of dermatophytosis. J Dermatol Sci. 2004; 34(1): 35-48.
8. Mirzahoseini H, Omidinia E, Shams-Ghahfarokhi M, Sadeghi G, Razzaghi-Abyaneh M. Application of PCR-RFLP to rapid identification of the main pathogenic dermatophytes from clinical specimens. IIJPH. 2009; 38(1): 18-24.
9. Zamani S, Sadeghi G, Yazdinia F, Moosa H, Pazooki A, Ghafarinia Z, et al. Epidemiological trends of dermatophytosis in Tehran, Iran: A five-year retrospective study. J Mycol Med. 2016; 26(4): 351-358.
10. Dolenc-Voljč M. Dermatophyte infections in human being: the current trends and future prospects. In; Razzaghi-Abyaneh M, Shams-Ghahfarokhi M, Rai M, editors. Medical mycology current trends and future prospects. 1st ed. New York: CRC Press; 2015; 3-27.
11. Nenoffl P, Herrmann J, Graser Y. Trichophyton mentagrophytes sive interdigitale? Adermatophytein the course of time. J Dtsch Dermatol Ges. 2007; 5(3): 198-202.
12. de Hoog GS, Dukik K, Monod M, Packeu A, Stubbe D, Hendrickx M, et al. Toward a novel multilocus phylogenetic taxonomy for the dermatophytes. Mycopathologia. 2017; 182(1-2): 5-31.
13. Graser Y, Scott J, Summerbell R. The new species concept in dermatophytes-a polyphasic approach. Mycopathologia. 2008; 166(5-6): 239-256.
14. Bagyalakshmi R, Senthilvelan B, Therese K, Murugusundram S, Madhavan HN. Application of polymerase chain reaction (PCR) and pcr based restriction fragment length polymorphism for detection and identification of dermatophytes from dermatological specimens. Indian J Dermatol. 2008; 53(1): 15-20.
15. Dhib I, Fathallah A, Yaacoub A, Hadj Slama F, Said M, Zemni R. Multiplex PCR assay for the detection of common dermatophyte nail infections. Mycoses. 2014; 57(1): 19-26.
16. Sadeghi G, Abouei M, Alirezaee M, Tolouei R, Shams-Ghahfarokhi M, Mostafavi E, et al. A 4-year survey of dermatomycoses in Tehran from 2006 to 2009. J Med Mycol. 2011; 21(4): 260-265.
17. Neji S, Makni F, Sellami H, Cheikhrouhou F, Sellami A, Ayadi A. Molecular identification of dermatophytes isolated in Sfax-Tunisia. J Mycol Med. 2010; 20(2): 85-90.
18. Klich MA. Identification of clinically relevant aspergilli. Med Mycol. 2006; 44(Supplement_1): S127-S131.
19. Gaudio PA, Gopinathan U, Sangwan V, Hughes TE. Polymerase chain reaction based detection of fungi in infected corneas. Br J Ophthalmol. 2002; 86(7): 755-760.
20. Jaeger EEM, Carroll NM, Choudhury S, Dunlop AAS, Towler HMA, Matheson MM, et al. Rapid detection and identifi cation of Candida, Aspergillus and Fusarium species in ocular specimens using nested PCR. J Clin Microbiol. 2000; 38(8): 2902-2908.
21. Arabatzis M, Bruijnesteijn van Coppenraet LE, Kuijper EJ, de Hoog GS, Lavrijsen AP, Templeton K, et al. Diagnosis of common dermatophyte infections by a novel multiplex real-time polymerase chain reaction detection/identification scheme. Br J Dermatol. 2007; 157(4): 681-689.
22. Kong F, Tong Z, Chen X, Sorrell T, Wang B, Wu Q, et al. Rapid identification and differentiation of Trichophyton species, based on sequence polymorphisms of the ribosomal internal transcribed spacer regions, by rolling-circle amplification. J Clin Microbiol. 2008; 46(4): 1192-1199.
23. Diguta CF, Vincent B, Guilloux-Benatier M, Alexandre H, Rousseaux S. PCR ITS-RFLP: a useful method for identifying filamentous fungi isolates on grapes. Food Microbiol. 2011; 28(6): 1145-1154.
24. Kanbe T, Suzuki Y, Kamiya A, Mochizuki T, Fujihiro M, Kikuchi A. PCR-based identification of common dermatophyte species using primer sets specific for the DNA topoisomerase II genes. J Dermatol Sci. 2003; 32(2): 151-161.
25. Mirhendi H, Makimura K, de Hoog GS, Rezaei-Matehkolaei A, Najafzadeh MJ, Umeda Y, et al. Translation elongation factor 1-α gene as a potential taxonomic and identification marker in dermatophytes. Med Mycol. 2014; 53(3): 215-224.
26. Makimura K, Tamura Y, Mochizuki T, Hasegawa A, Tajiri Y, Hanazawa R, et al. Phylogenetic classification and species identification of dermatophyte strains based on DNA sequences of nuclear ribosomal internal transcribed spacer 1 regions. J Clin Microbiol. 1999; 37(4): 920-928.
27. Kanbe T, Suzuki Y, Kamiya A, Mochizuki T, Kawasaki M, Fujihiro M, et al. Species-identification of dermatophytes Trichophyton, Microsporum and Epidermophyton by PCR and PCR-RFLP targeting of the DNA topoisomerase II gene. J Dermatol Sci. 2003; 33(1): 41-54.
28. Jackson CJ, Barton RC, Evans EG. Species identification and strain differentiation of dermatophyte fungi by analysis of ribosomal-DNA intergenic spacer regions. J Clin Microbiol. 1999; 37(4): 931-936.
29. Mochizuki T, Tanabe H, Kawasaki M, Ishizaki H, Jackson CJ. Rapid identification of *Trichophyton tonsurans* by PCR-RFLP analysis of ribosomal DNA regions. J Dermatol Sci. 2003; 32(1): 25-32.
30. Mohammadi A, Shams-Ghahfarokhi M, Nazarian-Firouzabadi F, Kachuei R, Gholami-Shabani M, Razzaghi-Abyaneh M. Giberella

fujikuroi species complex isolated from maize and wheat in Iran: distribution, molecular identification and fumonisin B1 in vitro biosynthesis. J Sci Food Agric. 2016; 96(4): 1333-1340.
31. Darriba D, Taboada GL, Doallo R, Posada D. jModelTest 2: more models, new heuristics and parallel computing. Nat Methods. 2012; 9(3): 772.
32. Swofford DL. Phylogenetic Analysis Using Parsimony and other methods. Version 4.0 beta. Sunderland, Massachusetts, USA: Sinauer Associates; 2002.
33. Ronquist F, Teslenko M, van der Mark P, Ayres DL, Darling A, Höhna S, et al. MrBayes 3.2: efficient bayesian phylogenetic inference and model choice across a large model space. Syst Biol. 2012; *61(3):* 539-542.
34. Miller MA, Pfeiffer W, Schwartz T. Creating the CIPRES science gateway for inference of large phylogenetic trees. 2010 Gateway Computing Environments Workshop (GCE).
35. Drummond AJ, Rambaut A.BEAST: Bayesian evolutionary analysis by sampling trees. BMC Evol Biol. 2007; 7: 214.
36. Rex JH, Alexander BD, Andes D, Arthington-skaggs B, Brown SD, Chaturveli V, et al. Reference method for broth dilution antifungal susceptibility testing of filamentous fungi; approved standard. CLSI document M38- A2. 2nd ed. Wayne: Clinical and Laboratory Standards Institute; 2008.
37. Rezaei-Matehkolaei A, Makimura K, Shidfar M, Zaini F, Eshraghian M, Jalalizand N, et al. Use of single-enzyme PCR-restriction digestion barcode targeting the internal transcribed spacers (ITS rDNA) to identify dermatophyte species. Iran J Public Health. 2012; 41(3): 82-94.
38. Ahmadi B, Mirhendi H, Shidfar MR, Nouripour-Sisakht S, Jalalizand N, Geramishoar M, et al. A comparative study on morphological versus molecular identification of dermatophyte isolates. J Mycol Med. 2015; 25(1): 29-35.

Original Article

Comparison of The Expression of miR-326 between Interferon beta Responders and Non-Responders in Relapsing-Remitting Multiple Sclerosis

Mahtab Fattahi, M.Sc.[1], Nahid Eskandari, M.D., Ph.D.[2, 3*], Fattah Sotoodehnejadnematalahi, Ph.D.[1], Vahid Shaygannejad, M.D.[4], Mohammad Kazemi, Ph.D.[5]

1. Department of Biology, Science and Research Branch, Islamic Azad University, Tehran, Iran
2. Department of Immunology, School of Medicine, Isfahan University of Medical Sciences, Isfahan, Iran
3. Applied Physiology Research Centre, Isfahan Cardiovascular Research Institute, Isfahan University of Medical Sciences, Isfahan, Iran
4. Department of Neurology, Isfahan Neurosciences Research Center, Isfahan University of Medical Sciences, Isfahan, Iran
5. Department of Genetic and Molecular Biology, School of Medicine, Isfahan University of Medical Sciences, Isfahan, Iran

Corresponding Address: P.O.Box: 8174673461, Department of Immunology, School of Medicine, Isfahan University of Medical Sciences, Isfahan, Iran
Email: neskandari@med.mui.ac.ir

Received: 23/October/2018, Accepted: 27/January/2019

Abstract

Objective: Multiple sclerosis (MS) is an inflammatory disease resulting in demyelination of the central nervous system (CNS). T helper 17 (Th17) subset protects the human body against pathogens and induces neuroinflammation, which leads to neurodegeneration. MicroRNAs (miRNAs) are a specific class of small (~22 nt) non-coding RNAs that act as post-transcriptional regulators. The expression of the miR-326 is highly associated with the pathogenesis of MS disease in patients through the promotion of Th17 development. Recently, studies showed that disease-modifying therapies (DMTs) could balance the dysregulation of miRNAs in the immune cells of patients with relapsing-remitting MS (RRMS). Interferon-beta (IFN-β) has emerged as one of the most common drugs for the treatment of RR-MS patients. The purpose of this study was to evaluate the expression of the miR-326 in RRMS patients who were responders and non-responders to IFN-β treatment.

Materials and Methods: In this cross-sectional study, a total of 70 patients (35 responders and 35 non-responders) were enrolled. We analyzed the expression of the miR-326 in peripheral blood mononuclear cells (PBMCs) of RRMS patients at least one year after the initiation of IFN-β therapy. Real-time polymerase chain reaction (RT-PCR) was applied to measure the expression of the miR-326.

Results: The results showed no substantial change in the expression of the miR-326 between responders and non-responders concerning the treatment with IFN-β. Although the expression of the miR-326 was slightly reduced in IFN-β-responders compared with IFN-β-non-responders; however, the reduction of the miR-326 was not statistically significant.

Conclusion: Overall, since IFN-β doesn't normalize abnormal expression of miR-326, this might suggest that IFN-β affects Th17 development through epigenetic mechanisms other than miR-326 regulation.

Keywords: Interferon-Beta, Lymphocyte, MicroRNA, Multiple Sclerosis

Cell Journal(Yakhteh), Vol 22, No 1, April-June (Spring) 2020, Pages: 92-95

Citation: **Fattahi M, Eskandari N, Sotoodehnejadnematalahi F, Shaygannejad V, Kazemi M. Comparison of the expression of miR-326 between interferon beta responders and non-responders in relapsing-remitting multiple sclerosis. Cell J. 2020; 22(1): 92-95. doi: 10.22074/cellj.2020.6486.**

Introduction

Multiple sclerosis (MS) is an inflammatory disease that leads to demyelination of the central nervous system (CNS). As the incidence of MS disease is rapidly increasing in recent decades, there is a serious need for the treatment, as well as the monitoring of the disease progression and evaluation of patients' response to various therapies.

Recent investigations have shown that transplantation of human embryonic stem cell (hESC) is one of the promising therapeutic strategies in the field of cell-based treatment in MS (1, 2). Studies indicate hESCs play an essential role in the remyelination process and have the preventing roles in demyelination of neural cells (3).

Additionally, numerous biomarkers have been so far proposed such as transcription factors, cytokines, and microRNAs (miRNAs) for the monitoring of the disease progression, as well as the evaluation of drug efficacy in MS (4, 5). Although the etiology of MS disease is still opaque, it has been shown that proinflammatory Th1- and Th17-producing $CD4^+$ T cells contribute to the pathogenesis of MS (6). Th17 subset protects the human body against pathogens and induces neuroinflammation, which leads to neurodegeneration (7, 8).

MicroRNAs are a class of non-coding RNAs with a length of 22 nucleotides that act as post-transcriptional regulators. It has been implicated that miRNAs are involved in the proper function of the immune system and have a vital role in T cell differentiation. Also, the aberrant expression of miRNAs is associated with pathological conditions, such as autoimmune diseases (9).

Some studies revealed that disease-modifying therapies (DMTs) could balance the dysregulation of miRNAs in the cells of the immune system in relapsing-remitting MS

(RRMS) patients (10, 11). Studies have demonstrated that most of the miRNAs upregulated/downregulated during the disease course mediate the differentiation of Th17 cells. The expression of the miR-326 is linked to the pathogenesis of MS disease through the promotion of Th17 development (12).

To date, myriad studies have conducted on the alteration of miRNAs in response to disease-modifying treatments, indicating the importance of these types of RNAs in the monitoring of various disorders. Accordingly, some studies have focused on the changes in the profile expression of miRNAs in MS disease, and they showed that these molecules are altered during the course of disease and treatment (13). Several miRNAs, including miR-155 and miR-326, have been shown to act as regulators of the immune cell response. Thus, evaluating the expression of the miR-326 could be used as a biomarker for the assessment of the immune cell function in MS patients. Interferon-beta (IFN-β) was the first disease-modifying drug used for the treatment of MS with long-lasting effect and well-tolerability (14).

Hence, in this study, we examined whether the treatment of RRMS patients with recombinant IFN-β influences the expression of the miR-326 in PBMCs of patients (15). To show whether RRMS patients are responder/non-responder to IFN-β therapy, the relapse rate and disability progression of patients during the disease course were assessed (16). Therefore, the present study aimed to evaluate the expression of the miR-326 in IFN-β responder and IFN-β-non-responder MS patients.

Material and Methods

Patients

A cross-sectional study was conducted to determine the level of the miR-326 expression in PBMCs of 70 RRMS patients from Isfahan city. The study enrolled 70 RRMS patients who were diagnosed as IFN-β-responders (n=35) and IFN-β-non-responders (n=35). The diagnosis of MS patients was made based on the McDonald' criteria (17). All of RRMS patients were treated with IFN-β for at least one year. Patients were classified based on the modified Rio score (MRS) (18). The modified Rio score is a simplified version of the Rio score, excluding the expanded disability status scale (EDSS) progression and modified items of the relapse rates and MRI activity. These scores are estimated after one year of IFN-β therapy with the aim of characterizing MS patients that will have ongoing disease activity and become suboptimal responders in the following two years (19). MS patients are categorized as IFN-β responders when the score of EDSS remains unchanged, and patients have no relapse during the follow-up period. Accordingly, non-responders are defined as RRMS patients whose EDSS is increased at least one point, and they experience at least one relapse during the follow-up period (Table 1) (20). The study was approved by the local Ethics Committee of Isfahan University of Medical Sciences (code. no. 296075), and all patients were given informed consents. Informed consent was obtained from all individual participated in our study.

Table 1: Demographic and clinical characteristics of RRMS patients

Demographic data	Responders	Non-responders
Mean age (Y)	33.72 ± 8.19	35.44 ± 8.06
Sex		
Female	n=30	n=29
Male	n=5	n=6
EDSS score	0-5	0-5

RRMS; Relapsing-remitting multiple sclerosis and EDSS; Expanded disability status scale.

Peripheral blood mononuclear cells isolation

PBMCs were isolated from fresh heparinized venous blood by centrifugation over Ficoll-Hypaque. The isolated PBMCs were washed twice with phosphate-buffered saline (PBS, Sigma, Germany) at 1800 rpm for 10 minutes. The supernatant was removed, and the pellet was re-suspended into 2 ml of PBS. Trypan blue (Sigma, Germany) was used to determine the cell viability in the cell suspension. Then, PBMCs were rinsed with PBS at 800 g for 10 minutes. After removal of the supernatant, the cells were stored at -80˚C until RNA isolation.

RNA extraction and cDNA synthesis

Total RNA including microRNAs was extracted from PBMCs of RRMS patients using the RiboEx Kit (GeneAll, Korea) following the manufacturer's instructions. The quantity and integrity of the isolated RNA were confirmed using a Nanodrop and agarose gel electrophoresis. For the analysis of the miR-326 expression, 2 µl of RNA (5 ng/µl) was reverse transcribed into complementary DNA (cDNA) using miRCURY™ LNA™ miRNA RT Kit following the manufacturer's (Exiqon, Denmark).

Real-time polymerase chain reaction

The analysis of the microRNA expression was performed using RealQ Plus Master Mix Green (Ampliqon, Denmark) and specific microRNA LNA™ PCR primer set (Exiqon, Denmark) on an ABI 7500 system. The fold change expression of microRNA was calculated using the $2^{-\Delta\Delta ct}$ method and expressed relative to the RNU48 expression level. Real-time polymerase chain reaction (PCR) was performed using a microRNA LNA™ PCR primer set (forward primer: CCTCTGGGCCCTTCCTCCAG) and the RealQplus 2xMasterMixGreenHigh ROX Kit containing the miScript Universal Primer (reverse primer).

Statistical analysis

The analysis of the miR-326 expression was carried

out by the SPSS software version 22 (SPSS, Chicago, IL). The difference of the miR-326 expression between responders and non-responder MS patients to IFN-β therapy was analyzed by Student t test, and the $P<0.05$ was statistically considered significant.

Results

As confirmed in previous studies the levels of miRNAs would be altered in MS patients considering whether they response to IFN-β therapy (10, 11).

The expression of the miR-326 in responders and non-responders RRMS patients

To evaluate the miR-326 expression in response to IFN-β therapy, the expression of the miR-326 at least one year after IFN-β treatment was assessed. Furthermore, the expression of the miR-326 was compared between the responder and non-responder group. The real-time PCR analysis showed that the level of the miR-326 was lower in the responder group in comparison with the non-responder group; however, such a difference was not statistically significant ($P= 0.7$, $P>0.05$, Fig.1).

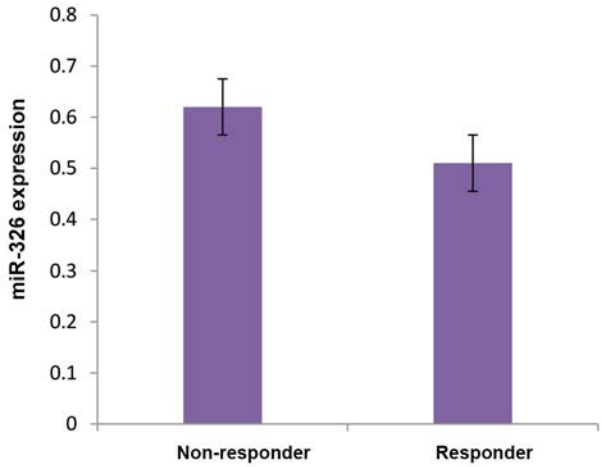

Fig.1: The RT-PCR analysis of miR-326 expression. The expression of the miR-326 was assessed in PBMCs of the responder and non-responder groups to IFN-β. The results are presented as the ratio of miRNA to RNU48. The miR-326 was down-regulated in response to the treatment with IFN-β. Although the expression of the miR-326 was higher in non-responder RRMS patients in comparison with responder RRMS patients, the difference is not statistically significant. Data are presented as mean ± SD. RT-PCR; Real time polymerase chain reaction, PBMCs; Peripheral blood mononuclear cells, IFN-β; Interferon-beta, and RRMS; Relapsing-remitting multiple sclerosis.

Discussion

Several lines of evidence support that autoreactive T cells including Th1 and Th17 cells may mediate autoimmunity in the CNS, leading to axonal degeneration and demyelination (21-24). The aberrant expression of miRNAs is associated with pathological conditions, including autoimmune diseases. Studies have shown that some miRNAs are dysregulated in brain lesions and the blood samples of MS patients. The miR-326 has recently been identified as a crucial regulator of Th17 differentiation and found to promote CNS inflammation in EAE, known as a murine model of MS disease (12).

Moreover, dysregulation of the miR-326 has been reported in patients with MS that is associated with several pathological processes. Emerging evidence has demonstrated that various microRNAs are dysregulated in several types of immune cells in RR-MS and could be fine-tuned by DMTs. The degree of drug responsiveness to IFN-β therapy varies among MS patients as some of them do not respond to therapy. However, there is no consensus on the methods to validate the degree of drug responsiveness in MS patients. Our objective was to evaluate an immunologically relevant miRNAs to classify RRMS patients as responders and non-responders. We focused on the profile expression of the miR-326 since it has been implicated in pro-inflammatory processes in MS pathology. IFNβ therapy may regulate the expression of miRNAs and have benefits for MS patients; however, some patients do not respond to therapy (25-28).

Factors contributing to the treatment failure in some patients are not fully understood. Lack of drug responsiveness in MS patients may stem from genetic, pharmacological, and pathological factors (29). The miR-326 is epigenetically dysregulated in PBMCs and CD4+ T cells of RRMS patients (12). In the current study, we searched whether IFN-β therapy affects the expression level of the miR-326 which has been previously implicated in the Th17-differentiation pathway. According to our findings, there was no significant difference considering the expression of the miR-326 between the responder and non-responder groups. Waschbisch et al. (10) consistently showed that the expression of the miR-326 did not significantly change between the untreated and IFN-β-treated MS patients during at least three months. Likewise, Hecker et al. (11) demonstrated that IFN-β therapy for at least one year did not normalize the aberrant expression of some miRNAs such as miR-326 which is differentially expressed in MS.

Conclusion

Overall, the identification of miRNAs in the blood samples of responder and non-responder MS patients to IFN-β therapy may provide useful biomarkers for the monitoring of the drug responsiveness and disease progression. Besides, the determination of the genetic profile of patients (pharmacogenetics) who are either responders or non-responders would shed light on our understanding about the role of genetics in drug responsiveness in MS patients.

Acknowledgements

The authors wish to thank the authorities in the research council of the Isfahan University of Medical Sciences and the Islamic Azad University of Tehran. Also they would like to thank Nahid Rezaei (Ph.D. student) for her assistance. This study received no specific grant from any funding agency in public, commercial, or not-forprofit

sectors. The authors declare that they have no conflict of interests concerning this study.

Authors' Contributions

N.E., M.F., F.S.; Parcipitated in study design and also contributed to all experimental procedures. V.S.; Visited, diagnosed and preparing for sampling of the MS patients. N.E., M.F., F.S., M.K.; Contributed to the data and statistical analysis, and interpretation of the data. M.F., N.E.; Drafted the manuscript. All authors performed the edition of the manuscript and approved the final version for the submission.

References

1. Shroff G. A review on stem cell therapy for multiple sclerosis: special focus on human embryonic stem cells. Stem Cells Cloning. 2018; 11: 1-11.
2. Cuascut FX, Hutton GJ. Stem cell-based therapies for multiple sclerosis: current perspectives. Biomedicines. 2019; 7(2). pii: E26.
3. Nazm Bojnordi M, Ghasemi HH, Akbari E. Remyelination after lysophosphatidyl choline-induced demyelination is stimulated by bone marrow stromal cell-derived oligoprogenitor cell transplantation. Cells Tissues Organs. 2015; 200(5): 300-306.
4. Castro G, Liu X, Ngo K, De Leon-Tabaldo A, Zhao S, Luna-Roman R, et al. RORγt and RORα signature genes in human Th17 cells. PLoS One. 2017; 12(8): e0181868.
5. Wei B, Pei G. microRNAs: critical regulators in Th17 cells and players in diseases. Cell Mol Immunol. 2010; 7(3): 175-181.
6. El-behi M, Rostami A, Ciric B. Current views on the roles of Th1 and Th17 cells in experimental autoimmune encephalomyelitis. J Neuroimmune Pharmacol. 2010; 5(2): 189-197.
7. Miossec P, Korn T, Kuchroo VK. Interleukin-17 and type 17 helper T cells. N Engl J Med. 2009; 361(9): 888-898.
8. Iwakura Y, Ishigame H. The IL-23/IL-17 axis in inflammation. J Clin Invest. 2006; 116(5): 1218-1222.
9. Thamilarasan M, Koczan D, Hecker M, Paap B, Zettl UK. MicroRNAs in multiple sclerosis and experimental autoimmune encephalomyelitis. Autoimmun Rev. 2012; 11(3): 174-179.
10. Waschbisch A, Atiya M, Linker RA, Potapov S, Schwab S, Derfuss T. Glatiramer acetate treatment normalizes deregulated microRNA expression in relapsing remitting multiple sclerosis. PLoS One. 2011; 6(9): e24604.
11. Hecker M, Thamilarasan M, Koczan D, Schröder I, Flechtner K, Freiesleben S, et al. MicroRNA expression changes during interferon-beta treatment in the peripheral blood of multiple sclerosis patients. Int J Mol Sci. 2013; 14(8): 16087-16110.
12. Du C, Liu C, Kang J, Zhao G, Ye Z, Huang S, et al. MicroRNA miR-326 regulates T H-17 differentiation and is associated with the pathogenesis of multiple sclerosis. Nat Immunol. 2009; 10(12): 1252-1259.
13. Chen C, Zhou Y, Wang J, Yan Y, Peng L, Qiu W. Dysregulated MicroRNA involvement in multiple sclerosis by induction of T helper 17 cell differentiation. Front Immunol. 2018; 9: 1256.
14. Hecker M, Thamilarasan M, Koczan D, Schroder I, Flechtner K, Freiesleben S, et al. MicroRNA expression changes during interferon-beta treatment in the peripheral blood of multiple sclerosis patients. Int J Mol Sci. 2013; 14(8): 16087-16110.
15. Weinstock-Guttman B, Jacobs LD. What is new in the treatment of multiple sclerosis? Drugs. 2000; 59(3): 401-410.
16. Pereira VC, Malfetano FR, Meira ID, Souza LF, Liem AM, Maiolino A, et al. Clinical response to interferon beta and glatiramer acetate in multiple sclerosis patients: a Brazilian cohort. Arq Neuropsiquiatr. 2012; 70(10): 774-779.
17. Fangerau T, Schimrigk S, Haupts M, Kaeder M, Ahle G, Brune N, et al. Diagnosis of multiple sclerosis: comparison of the Poser criteria and the new McDonald criteria. Acta Neurol Scand. 2004; 109(6): 385-389.
18. Sormani MP, Rio J, Tintorè M, Signori A, Li D, Cornelisse P, et al. Scoring treatment response in patients with relapsing multiple sclerosis. Mult Scler. 2013; 19(5): 605-612.
19. Sormani MP, De Stefano N. Defining and scoring response to IFN-β in multiple sclerosis. Nat Rev Neurol. 2013; 9(9): 504-512.
20. Río J, Nos C, Tintoré M, Téllez N, Galán I, Pelayo R, et al. Defining the response to interferon-beta in relapsing-remitting multiple sclerosis patients. Ann Neurol. 2006; 59(2): 344-352.
21. Reboldi A, Coisne C, Baumjohann D, Benvenuto F, Bottinelli D, Lira S, et al. C-C chemokine receptor 6-regulated entry of TH-17 cells into the CNS through the choroid plexus is required for the initiation of EAE. Nat Immunol. 2009; 10(5): 514-523.
22. Compston A, Coles A. Multiple sclerosis. Lancet. 2002; 359(9313): 1221-1231.
23. Compston A, Coles A. Multiple sclerosis. Lancet. 2008; 372(9648): 1502-1517.
24. Ireland S, Monson N. Potential impact of B cells on T cell function in multiple sclerosis. Mult Scler Int. 2011; 2011: 423971.
25. Shi Y, Wang H, Su Z, Chen J, Xue Y, Wang S, et al. Differentiation imbalance of Th1/Th17 in peripheral blood mononuclear cells might contribute to pathogenesis of Hashimoto's thyroiditis. Scand J Immunol. 2010; 72(3): 250-255.
26. Honardoost MA, Naghavian R, Ahmadinejad F, Hosseini A, Ghaedi K. Integrative computational mRNA-miRNA interaction analyses of the autoimmune-deregulated miRNAs and well-known Th17 differentiation regulators: an attempt to discover new potential miRNAs involved in Th17 differentiation. Gene. 2015; 572(2): 153-162.
27. Ma X, Zhou J, Zhong Y, Jiang L, Mu P, Li Y, et al. Expression, regulation and function of microRNAs in multiple sclerosis. Int J Med Sci. 2014; 11(8): 810-818.
28. Ossege LM, Sindern E, Patzold T, Malin JP. Immunomodulatory effects of interferon-beta-1b in patients with multiple sclerosis. Int Immunopharmacol. 2001; 1(6): 1085-1100.
29. Bertolotto A, Gilli F. Interferon-beta responders and non-responders. A biological approach. Neurol Sci. 2008; 29 Suppl 2: S216-S217.

Original Article

Histone Modifications of H3K4me3, H3K9me3 and Lineage Gene Expressions in Chimeric Mouse Embryo

Maryam Salimi, Ph.D.[1], Abolfazl Shirazi, Ph.D.[2, 3*], Mohsen Norouzian, Ph.D.[1*], Mohammad Mehdi Mehrazar, M.Sc.[2], Mohammad Mehdi Naderi, Ph.D.[2], Mohammad Ali Shokrgozar, Ph.D.[4], Mirdavood Omrani, Ph.D.[5], Seyed Mahmoud Hashemi, Ph.D.[6]

1. Department of Biology and Anatomical Sciences, Faculty of Medicine, Shahid Beheshti University of Medical Sciences, Tehran, Iran
2. Reproductive Biotechnology Research Center, Avicenna Research Institute, ACECR, Tehran, Iran
3. Department of Gametes and Cloning, Research Institute of Animal Embryo Technology, Shahrekord University, Shahrekord, Iran
4. National Cell Bank of Iran, Pasteur Institute of Iran, Tehran, Iran
5. Department of Medical Genetics, Shahid Beheshti University of Medical Sciences, Tehran, Iran
6. Department of Immunology, School of Medicine, Shahid Beheshti University of Medical Sciences, Tehran, Iran

Corresponding Addresses: P.O.Box: 19615/1177, Reproductive Biotechnology Research Center, Avicenna Research Institute, ACECR, Tehran, Iran
P.O.Box: 1985717-443, Department of Biology and Anatomical Sciences, Faculty of Medicine, Shahid Beheshti University of Medical Sciences, Tehran, Iran
Emails: a.shirazi@ari.ir, norozian93@gmail.com

Received: 4/October/2018, Accepted: 18/February/2019

Abstract

Objective: Chimeric animal exhibits less viability and more fetal and placental abnormalities than normal animal. This study was aimed to determine the impact of mouse embryonic stem cells (mESCs) injection into the mouse embryos on H3K9me3 and H3K4me3 and cell lineage gene expressions in chimeric blastocysts.

Materials and Methods: In our experiment, at the first step, incorporation of the GFP positive mESCs (GFP-mESCs) 129/Sv into the inner cell mass (ICM) of pre-compacted and compacted morula stage embryos was compared. At the second and third steps, H3K4me3 and H3K9me3 status as well as the expression of *Oct4, Nanog, Tead4*, and *Cdx2* genes were determined in the following groups: i. *In vitro* blastocyst derived from *in vivo* morula subjected to mESCs injection (blast/chimeric), ii. *In vivo* derived blastocyst (blast/*in vivo*), iii. *In vitro* blastocyst derived from culture of morula *in vivo* (blast/morula), and iv. *In vitro* blastocyst derived from morula *in vivo* subjected to sham injection (blast/sham).

Results: Subzonal injection of GFP-mESCs at the pre-compacted embryos produced more chimeric blastocysts than compacted embryos (P<0.05). The number of trophectoderm (TE), ICM, ICM/TE and total cells in chimeric blastocysts were less than the corresponding numbers in blastocysts derived from other groups (P<0.05). In ICM and TE of chimeric blastocysts, the levels of H3K4me3 and H3K9me3 were respectively decreased and increased compared to the blastocysts of the other groups (P<0.05). Expressions of *Oct4*, *Nanog* and *Tead4* were decreased in chimeric blastocysts compared to the blastocysts of the other groups (P<0.05), while this was not observed for *Cdx2.*

Conclusion: In the present study, embryo compaction significantly reduced the rate of incorporation of injected mESCs into the ICM. Moreover, in chimeric blastocysts, the levels of H3K9me3 and H3K4me3 were altered. In addition, the expressions of pluripotency and cell fate genes were decreased compared to blastocysts of the other groups.

Keywords: Cell Lineage Genes, Chimera, H3Methylation

Cell Journal(Yakhteh), Vol 22, No 1, April-June (Spring) 2020, Pages: 96-105

Citation: **Salimi M, Shirazi A, Norouzian M, Mehrazar MM, Naderi MM, Shokrgozar MA, Omrani M, Hashemi SM. Histone modifications of H3K4me3, H3K9me3 and lineage gene expressions in chimeric mouse embryo. Cell J. 2020; 22(1): 96-105. doi: 10.22074/cellj.2020.6443.**

Introduction

Mouse chimeras have become a useful tool for studying the mammalian development processes, including formation of a specific cell lineage or tissue as well as gene function (1). Chimeras are the animals with two or more populations of genetically different cells or the recipient embryos with pluripotent stem cells from the same or different species (2). Previous studies showed that microinjection of embryonic stem cells (ESCs) is an efficient approach in producing good germ line-transmitted chimeras (3). It has been shown that injected ESCs into the 8-cell embryos or compacting morula can migrate into the inner cell mass (ICM) of resulting blastocysts (2, 4, 5) whose migration mechanisms has still remained to be elucidated (6).

On the other hand, chimeric animals are less viable and exhibit some abnormalities such as large offspring syndrome (LOS) and placental abruption. The abnormalities in early fetal and placental development may occur when embryos have been manipulated *in vitro* (7). Manipulation process and embryo culture condition can also change gene expression pattern and early embryo development by epigenetic factor modifications (8). Epigenetic changes, including modifications of DNA and histones without changing DNA sequence, are key regulatory factors in transcriptional activity and repression of genes in pre-implantation embryo (9). Recently the role of histone lysine methylation in embryo development has been noticed by many investigators

(10). Previous studies have shown that histone H3 tri-methylated at lysine 4 (H3K4me3) and histone H3 tri-methylated at lysine 9 (H3K9me3) are respectively associated with active and inactive chromatin compartments (11). H3K4me3 is generally detected at the 5′-end of proximal promoters and it is one of the essential factors required for transcription activity in ICM of embryo (12). In contrast, H3K9me3 is generally localized at the promoter of repressed genes and it is required for constitutive heterochromatin formation in pericentromeric and centromeric DNA (13). Previous study has shown that de-methylation of H3K9 at the regulatory regions of ESCs significantly up-regulated *Oct4* and *Nanog* gene expressions (14).

Gamete and embryo manipulations, such as oocytes *in vitro* maturation (IVM), *in vitro* embryo production through intracytoplasmic sperm injection (ICSI) or *in vitro* fertilization (IVF), have negative impacts on embryo quality and epigenetic modifications (9, 15, 16). Although many studies implicate the effects of *in vitro* manipulation on alterations of epigenetic modification, the pattern of these alterations (including histone methylations) in chimeric embryos is still unclear. Therefore, in our study we aimed to investigate the pattern of H3K4me3 and H3K9me3 modifications in mouse chimeric blastocysts as well as the effects of this modifications on the ICM lineage specific gene expression (*Oct4*, *Nanog*) and trophectoderm (TE) gene expressions (*Tead4*, *Cdx2*). Moreover, effect of embryo compaction at morula stage on incorporation of the injected mESCs into the ICM as well as the effects of embryo manipulation on blastocyst quality, ICM, TE numbers and ICM/TE ratio was investigated.

Materials and Methods

Animal care and chemicals

The study procedures were confirmed by the Research Ethics Committee of Avicenna Research Institute, Tehran, Iran (IR.SBMU.MSP.REC.1395.5.1). The chemical materials were obtained from Sigma-Aldrich (USA), unless otherwise mentioned in the text. The mice, C57BL/6, were procured from Pasteur institute of Iran and they were maintained in temperature- and humidity-controlled rooms at 12-hours dark/light cycles.

Experimental groups

This study is comprised of three experimental steps, including step 1: evaluating the effect of embryonic compaction on producing chimeric blastocyst following injection of GFP-mESCs into the subzonal space of mouse pre-compacted and compacted morula-stage embryos and step 2: determining the number of embryonic cells type, TE, ICM and total cells in blastocyst derived from different approaches including: i. *In vivo*-derived blastocyst (blastocyst/*in vivo*, control), ii. Blastocyst obtained from *in vivo*-derived morula (blastocyst/morula), iii. Blastocyst obtained from *in vivo*-derived morula which had been subjected to subzonal injection of the culture medium (blastocyst/sham), and iv. Blastocyst obtained from *in vivo*-derived morula which had been subjected to subzonal mESCs injection (blastocyst/chimeric). Step 3 is composed of assessment of the some lineage specific gene expressions in ICM (*Oct4*, *Nanog*) and TE (*Tead4*, *Cdx2*), in addition to the evaluation of H3K4me3 and H3K9me3 modification in the four above-mentioned groups of blastocysts (Fig.1).

Embryo collection

In this study, superovulation of 8-10 weeks old C57BL/6 female mice (n=53) was performed through intraperitoneal injections of 10 IU of pregnant mare serum gonadotropin (PMSG) followed by human chorionic gonadotropin (hCG) injection after 46-48 hours. In next step, the female mice were allowed to mate with C57BL/6 male. Females with vaginal plugs were sacrificed at 2.5 days post coitum (dpc) by cervical dislocation, to collect the embryos. The embryos were cultured in KSOM, supplemented with 4 mg/ml bovine serum albumin (BSA) and amino acids (KSOMaa) under mineral oil at 37˚C in a humidified atmosphere of 5% CO_2.

Subzonal injection of green fluorescent protein-embryonic stem cells (GFP-ESCs)

Mouse ESCs, 129/Sv, labelled with GFP (GFP-mESCs) were considered for subzonal injection. The cells were cultured in R2i-LIF medium consisting of 1:1 mixture of DMEM:F12 (Invitrogen Carlsbad, USA) containing 15% knockout serum replacement (KOSR), 2 mM L-glutamine, 1000 U/ml mouse leukemia inhibitory factor (LIF), 1% non-essential amino acids, 0.1 mM β-mercaptoethanol, 100 U/ml penicillin, 100 mg/ml streptomycin, 2% ESC qualified FBS (ES-FBS), 1 μM PD0325901 and 10 μM SB431542. SB431542 and PD0325901 are two chemicals that respectively inhibit transforming growth factor b (TGF-b) and MEK signalling pathways, which are named R2i. R2i enhance ground state of pluripotency in mESCs. In the absence of mouse embryonic fibroblasts (MEFs), the mESCs grew on 0.1% gelatin-coated wells. For preparation of single cell suspension, 79% confluent mESCs were trypsinized and kept at 4˚C in 1 ml of ESC medium supplemented with 0.2 m HEPES until use (5).

The injection of GFP-mESCs in subzonal space of pre-compacted (n=42) and compacted embryos (n=36) was carried out using a Narishige micromanipulator. A number of laser beams (150 FU, Prime Tech Ltd., Japan) were applied to thin the zona pellucida (ZP) before piercing the tip of injection needle. After rinsing the inner surface of injection needle (20 μm in diameter) with 10% polyvinylpyrrolidone (PVP)-PBS, about 15 GFP-mESCs were aspirated and then injected into the perivitelline space of embryos. For expansion of perivitelline space and in order to facilitate subzonal mESCs injection, the embryos were subjected to 0.2 M sucrose medium. The GFP-mESCs-injected embryos were cultured in KSOMaa at 37˚C for 24 hours in a humidified atmospheres to approach blastocyst stage (2).

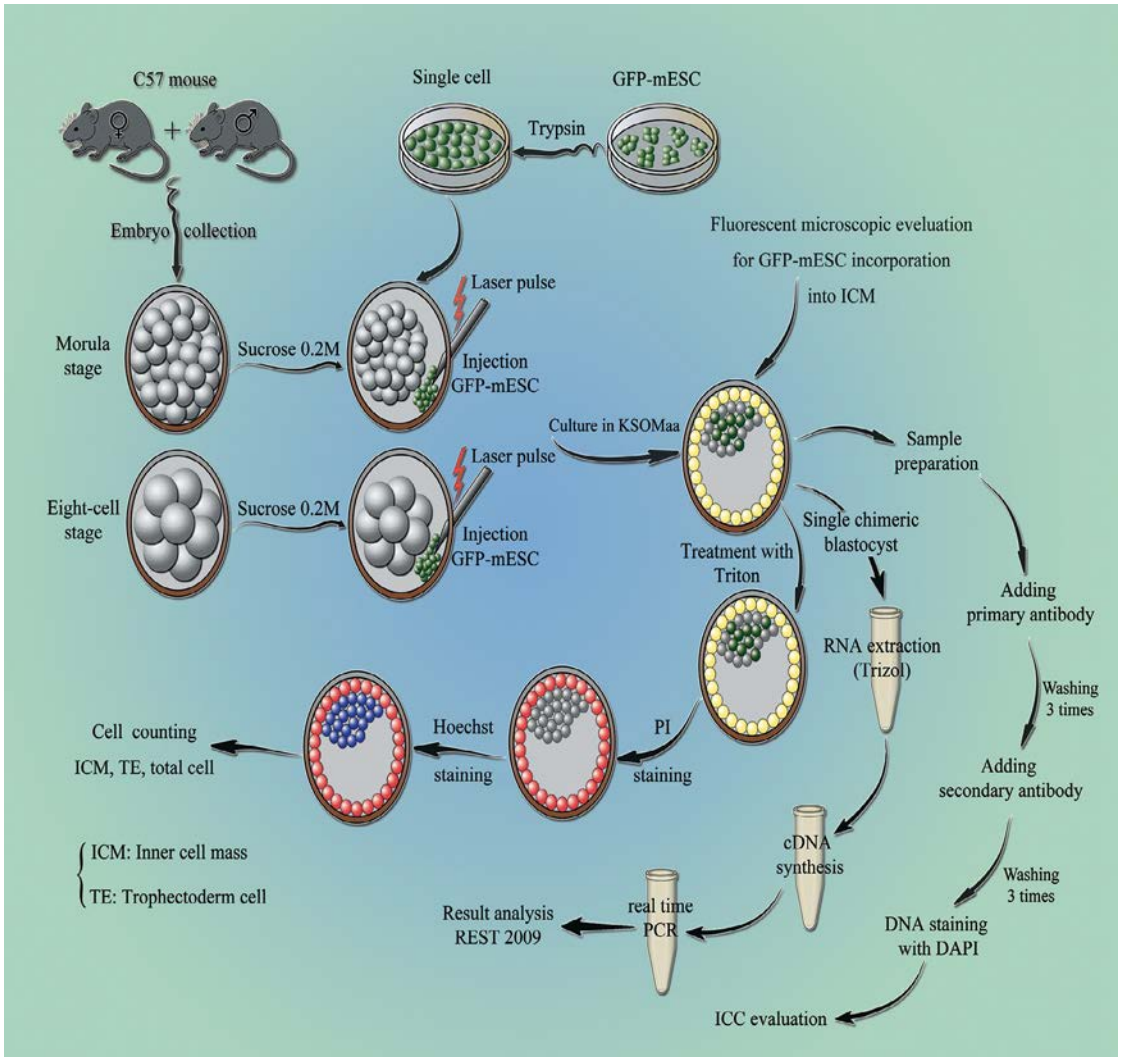

Fig.1: Workflow and study design for production of chimeric blastocysts. The procedure can be divided into four parts: i. Injection of GFP-mESCs, 129/Sv, into the *in vivo* derived pre-compacted and compacted mouse embryos, C57BL/6, ii. Differential staining to determine ICM and TE cells allocation of blastocysts, iii. The expression of lineage specific genes in the blastocysts derived from different approaches, using qRT-PCR, and iv. Histone methylation of H3K4me3 and H3K9me3 in blastocysts derived from different approaches using immunocytochemistry. ICM; Inner cell mass, TE; Trophectoderm, and qRT-PCR; Quantitative reverse transcription polymerase chain reaction.

Differential embryo staining

Differential staining of variant cell types of embryo, including TE, ICM and total cells number, was performed in each group by a previously described procedure (17). Briefly, blastocysts were permeabilized in 0.2% Triton X-100 in flushing holding medium (FHM) media for 20 seconds. They were then transferred into FHM media supplemented by 30 µg/ml propidium iodide (PI) for 60 seconds. This was followed by an incubation of blastocysts in cold ethanol supplemented by 10 µg/ml bisbenzimide (Hoechst 33342) for 15 minutes and immediately mounted on glass slides using glycerol. Finally, the stained blastocysts were observed and counted using an epifluorescent microscope (IX71 Olympus, Japan). In this study, 15 blastocysts were considered for each group.

Immunofluorescence staining of H3K9me3 and H3K4m3

In each group, the ZP of blastocysts was completely dissolved by incubating them with acidic Tyrode (pH=2.5) for 30 seconds. The embryos were washed three times by phosphate-buffered saline (PBS) added to 0.1% polyvinyl alcohol (PVA) and 0.1% Tween-20. They were then fixed in 4% paraformaldehyde (pH=7.4) for 30 minutes. Subsequently, the fixed embryos were treated by 0.3% Triton X-100 for one hour in PBS. For blocking, these blastocysts were kept in PBS, followed by adding 2% bovine serum albumin (BSA) to them for 40 minutes at 25˚C. They were next treated with primary anti-H3K4me3 (1:200, Abcam, USA) antibody for one hour at 25˚C and anti-H3K9me3 (1:200, Abcam, USA) antibody overnight at 4˚C. The embryos were then washed three times (10 minutes each) with 0.1% PVA+0.1% Tween-20 diluted in PBS, and they were then treated with the secondary antibody, goat IgG anti-mouse (PE/Cy5.5, 1:500, Abcam, USA) in blocking solution for 60 minutes at 37˚C, according to the manufacturer's instructions. After washing with PBS containing 0.1% PVA+0.1% Tween-20, for 10 minutes, DNA was stained

for 10 minutes with 15 µg/ml 6-diamidino-2-phenylindole (DAPI, Thermo Fisher Scientific, USA). The samples were then mounted on the slides by glycerol. Each experiment was biologically replicated three times and at least 20 blastocysts were evaluated in each group. In each experiment, embryos without primary antibody were stained, as negative controls. The slides were evaluated using an automated epifluorescent microscope (Nikon, Japan). The fluorescence intensity of blastocyst images was evaluated using ImageJ software (NIH Image, USA).

RNA isolation

Total RNA was isolated from single blastocyst using Trizol reagent (Life Technologies, Belgium) according to the manufacture's instruction. Briefly, to homogenate the samples, 50 µl Trizol and 25 µl chloroform were added to each sample. After precipitating with isopropanol, RNA was washed with 70% ethanol and total RNA was diluted in 10 µl RNase-free water. Total RNA was then kept at -80˚C. In our study, five blastocysts were considered in each group.

Before cDNA synthesis, the purity and concentration of isolated RNA was measured using a spectrophotometer (Picodrop Real-Life, UK). cDNA was produced using Prime Script QuantiTect Kit (Qiagen, Germany). Reactions were carried out in RNase-free tubes in a total volume of 20 µl, containing 2 µl gDNA, 6 µl total RNA, 4 µl RT buffer, 1 µl enzyme and 7 µl RNase-free water at the following condition: 42˚C for 2 minutes, 42˚C for 15 minutes and 95˚C for 3 minutes. For long term storage, cDNA were kept at -20˚C.

Quantitative reverse transcription polymerase chain reaction

In this study, quantitative reverse transcription polymerase chain reaction (qRT-PCR) was used to assess the expression of:

Oct4-
F: 5′-CGTGTGAGGTGGAGTCTGGA-3′,
R: 5′-GCTGATTGGCGATGTGAGTG-3′,

Nanog-
F: 5′-CTGAGGAGGAGGAGAACAAGGTC-3′,
R: 5′-CATCTGCTGGAGGCTGAGGTA-3′,

Tead4-
F: 5′-CGGAGGAAGGCAAGATGTATG-3′,
R: 5′-ACCTGGATGTGGCTGGAGAC-3′and

Cdx2-
F: 5′-GCTGCTGTAGGCGGAATGTAT-3′,
R: 5′-CTCCCGACTTCCCTTCACC-3′

using Rotor Gene Q instrument (Qiagen, Germany). qRT-PCR reactions were done in a final volume of 10 µl including 5 µl SYBR green (Takara, Japan), 0.2 µl of each forward and reverse primers (10 µM), 2 µl cDNA template (ten-fold diluted), and 2.6 µl nuclease free water. The thermal cycling was performed in 2 steps with following condition: one cycle of 95˚C for 30 seconds (holding time), followed by 50 cycles of 95˚C for 5 seconds and 60˚C for 30 seconds. High-resolution melting curve analysis was performed in a ramp rate of 0.2˚C from 72˚C up to 95˚C.

Gapdh-
F: 5′-TTCCAGTATGATTCCACCCAC-3′,
R: 5′-ACTCAGCACCAGCATCACC-3′ and
H2afz-
F: 5′-CTCGTCTCTTCCTCGCTCGT-3′,
R: 5′-CGTCCGTGGCTGGTTGTC-3′

were considered as internal endogenous housekeeping genes. At least, three replications from each cDNA sample were evaluated and the expression level of the gene was normalized against *H2afz* and *Gapdh*. Relative expression of the genes was determined by REST 2009 Software (Qiagen, Germany).The expression levels were reported as mean ± standard deviation (SD), while significant difference was reported as $P<0.05$.

Statistical analysis

The rates of development to the blastocyst in pre-compacted and compacted embryos following mESCs injection and the incorporation of injected mESCs into ICM were analysed by non-parametric analysis test (Mann Whitney) and expressed as mean ± standard error of the mean (SEM). The blastocyst cell number and fluorescent intensity of histone methylation were evaluated with one-way ANOVA post hoc tests and expressed as mean ± SD. Analyses were conducted using SPSS statistical program (SPSS Inc., USA). Comparisons were considered statistically different, if the p-value was less than 0.05. Gene expression of the each groups were evaluated by one-way ANOVA, REST 2009 Software (Qiagen, Germany).

Results

Generation of mouse chimeras

Integration of subzonal injected GFP-mESCs into the ICM of resulting blastocysts were significantly higher in pre-compacted (31/42) than compacted (13/36) morula-stage embryos ($P=0.012$, Table 1). As shown, the injected GFP-mESCs were incorporated into the ICM of resulting chimeric blastocysts using epifluorescent microscope. There was no difference in the blastocyst rate and developmental block between morula-stage embryos receiving mESCs at pre-compacted or compacted stages (Table 1).

Blastocyst cell count

As it has been shown in Table 2, the number of variant cell types of embryo, including total cell numbers, TE and ICM was measured in four groups to determine the blastocyst quality (Fig.2). Chimeric blastocysts had significantly fewer total cell, ICM and TE cell numbers compared to the other groups ($P<0.05$). The average number of ICM was respectively 9.7 ± 1.4 and 19.75 ± 1.3 in chimeric and derived blastocysts *in vivo*. The ration of ICM to TE cells (ICM/TE) was decreased in chimeric blastocysts compared to blastocyst/*in vivo* ($P<0.05$).

Table 1: Subzonal injection of mESCs in morula stage of pre-compacted as well as compacted mouse embryos, and incorporation of mESCs into ICM of resulting blastocysts

Injected morula	Produced blastocyst	Blastocyst		Blocked embryo
		Incorporated mESCs	Non-incorporated mESCs	
Compacted (n=36)	34 (94.4 ± 4.8)	13 (36.1 ± 7.5) [a]	23 (63.9 ± 10.6)[a]	2 (5.5 ± 2.8)
Pre-compacted (n=42)	40 (95.2 ± 2)	31(73.8 ± 4.5)[b]	11 (26.2 ± 3.1)[b]	2 (4.8 ± 1)
Total number: (n=78)	74 (94.67 ± 2.5)	44 (53.77 ± 7.17)	34 (40.90 ± 7.38)	4 (5.317 ± 1.56)

Data are presented as n (% ± SEM). [a, b]; The numbers with different uppercase letters at the same column are significantly different (P<0.05), mESC; Mouse embryonic stem cells, and ICM; Inner cell mass.

Table 2: The number of variant cell types of blastocysts obtained from different approaches

Groups	Number of ICM cells	Number of TE cells	Total cell number	ICM:TE Ratio
Blastocyst/*in vivo*	19.75 ± 1.3[a]	64.5 ± 14.1[a]	84.25 ± 17[a]	0.31 ± 0.09[a]
Blastocyst/morula	16.57 ± 1.5[b]	55.28 ± 8.9[a,b]	71.85 ± 9.5[a,b]	0.30 ± 0.1[a]
Blastocyst/sham	12.83 ± 0.8[c]	48.5 ± 6.5[b,c]	61.33 ± 8.5[b]	0.26 ± 0.12[b,c]
Blastocyst/ESCs injection	9.7 ± 1.4[d]	38 ± 9[c]	47.7 ± 9.6[d]	0.25 ± 0.15[c]

Data are presented as mean ± SD. [a-d]; The numbers with different uppercase letters at the same column differ significantly (P<0.05), TE; Trophectoderm, ICM; Inner cell mass, and EScs; Embryonic stem cells.

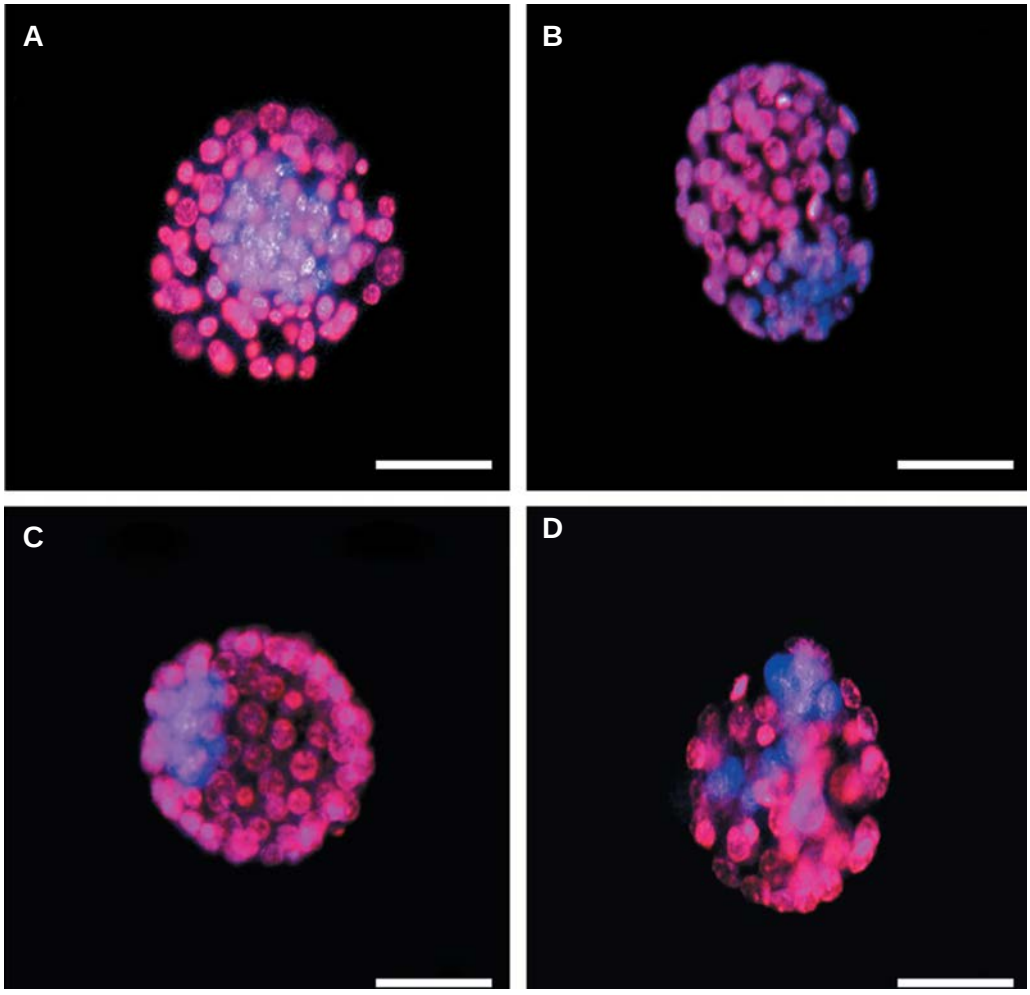

Fig.2: Epifluorescent microscopic imaging of mouse chimeric blastocysts produced by different approaches. ICM and TE nuclei were respectively stained with Hoechst 33342 (blue) and PI (red). **A.** Blastocyst/*in vivo*, **B.** Blastocyst/morula, **C.** Blastocyst/sham, and **D.** Blastocyst/ESCs injecton (scale bar: 50 µm). ICM; Inner cell mass, TE; Trophectoderm, and PI; Propidium iodide.

Immunocytochemistry analysis of H3K9me3 and H3K4me3

Methylation of H3K4 and H3K9 in the TE and ICM cells of blastocyst were measured by immunocytochemistry assay (Fig.3). As shown in Figure 4A, methylation of H3K4 in the ICM and TE of chimeric blastocysts was decreased in comparison with the other groups ($P<0.05$). Concerning tri-methylation of H3K9 in ICM, the highest rate was observed in chimeric embryos. Tri-methylation of H3K9 in ICM and TE was significantly higher in chimeric and sham groups compared to the other groups ($P<0.05$). On the other hand, there was no significant difference between expression of H3K9me3 in TE of sham groups and chimeric groups ($P> 0.05$, Fig.4B).

Inner cell mass and trophectoderm gene expressions

Relative expression analysis of particular lineage specific genes in the ICM and TE cells represented some differences. *Oct4, Nanog* and *Tead4* relative expressions in chimeric blastocysts was significantly lower than blastocysts in sham and control groups ($P<0.05$). However, no significant difference was observed for *Cdx2* between chimeric blastocysts and those derived from the other groups, except the sham group. Indeed, *Cdx2* expression in blastocysts derived from sham group was significantly lower than the other groups (Fig.4C, D, $P<0.05$).

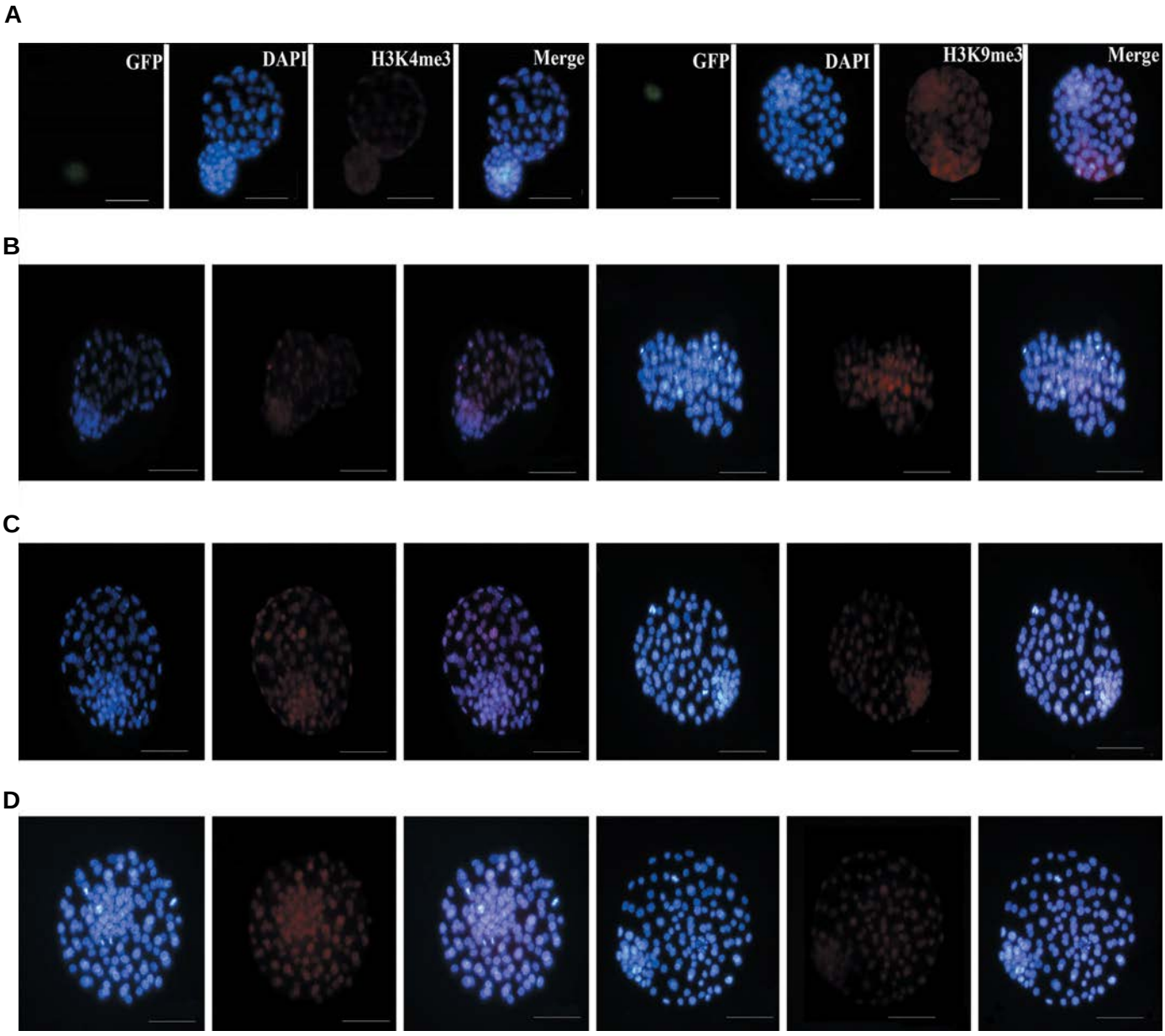

Fig.3: Immunostaining. Immunocytochemistry staining of H3K4me3 (left) and H3K9me3 (right) in chimeric blastocysts and blastocysts derived from the other groups: **A.** Blastocyst/embryonic stem cells (ESCs) injection, **B.** Blastocyst/sham, **C.** Blastocyst/morula, and **D.** Blastocyst/*in vivo*; control. The nuclei (blue) were stained with DAPI. The H3K4me3 and H3K9me3 were stained with anti-Mouse IgG (red). The merged images of H3K4me3 and H3K9me3 with DNA are purple (scale bars: 50 µm).

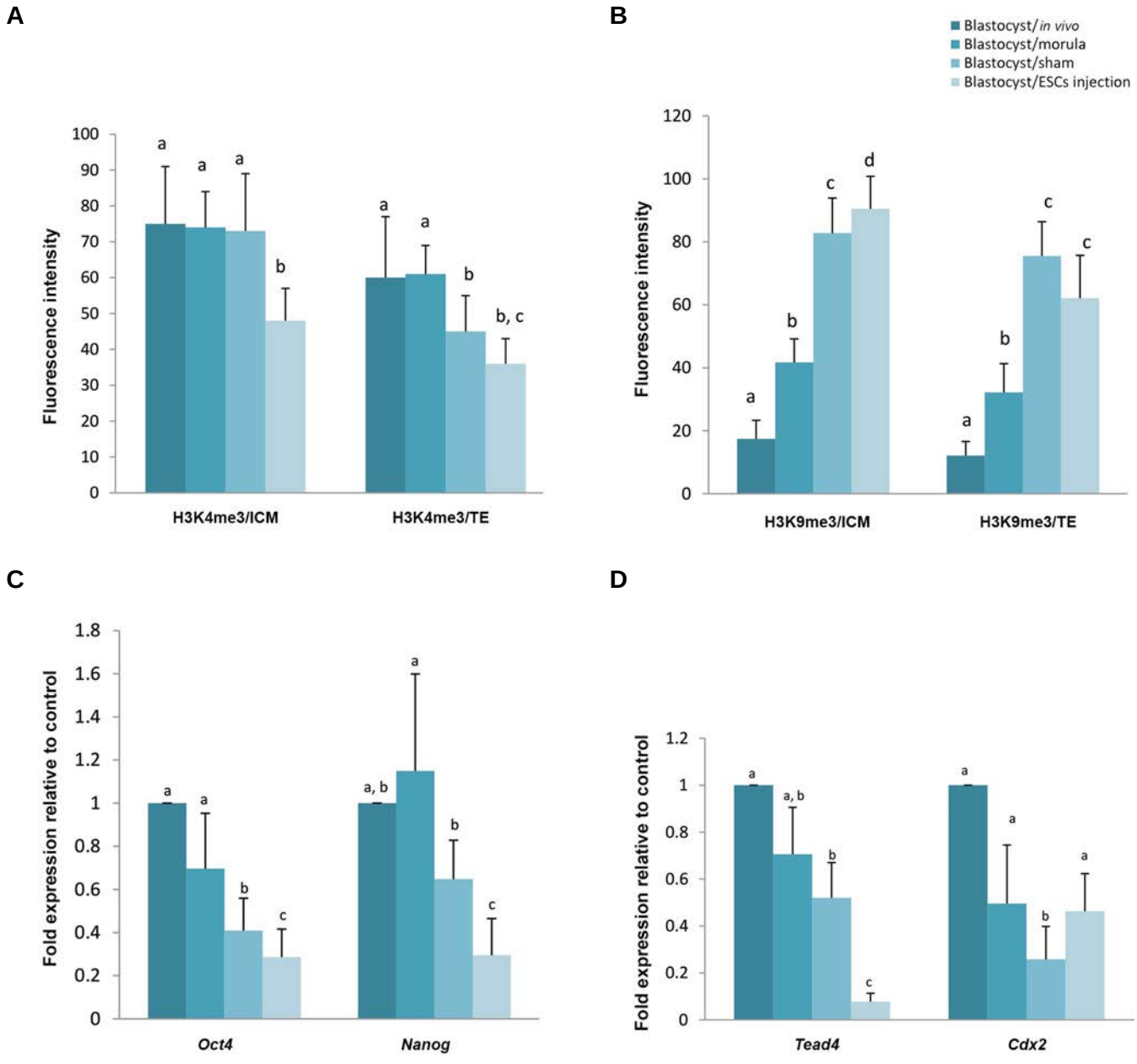

Fig.4: Three methylation of H3K4 and H3K9 as well as gene expressions in blastocysts produced by different approaches. **A.** H3K4me3 expression, **B.** H3K9me3 expression, **C.** Expression of the ICM genes, and **D.** Expression of the TE genes in mouse blastocysts produced by different approaches. a, b, c the columns with different type of the lowercase letters are significantly different (P<0.05). Data are shown as mean ± SD. ICM; Inner cell mass and TE; Trophectoderm.

Discussion

Currently, mESCs microinjection is a highly stable and reproducible technique which can produce full germ line-transmitted chimeras (1). In the present study, integration of mESCs into the ICM in pre-compacted embryos was significantly higher than compacted type. Our results was in agreement to the reports of Tokunaga and Tsunoda (18) indicating that mESCs injection into the 8-cell embryos, 2.5 dpc before formation of ICM, led to the higher incorporation of injected cells into the ICM. In our study, blastocysts were incubated in 0.2 M sucrose medium prior to mESCs injection into the subzonal cavity of morula-stage embryos. Our results were consistent with previous studies clearly showing that hypertonic microinjection method can generate the embryos with high percentages of chimerism. The precise cellular mechanism underlying this phenomenon is not yet clear (3, 19).

In our study, the number of variant cell types of embryo including total cells number, ICM and TE, as well as the ICM/TE ratio, was reduced in chimeric blastocysts compared to blastocysts *in vivo*. It seems that *in vitro* manipulation of the embryo can compromise the quality of produced blastocysts. So that, the number of ICM cells in the injected mESCs group was lower than that of the other groups. In other words, the number of ICM cells was reduced by increasing embryo manipulation. As expected, reducing the variant cell number of embryo, TE and ICM, as well as the abnormal changes in blastocyst

cells allocation, reduced the quality and post implantation development of blastocyst. It has also been shown that the rate of embryonic cell proliferation and the ICM/TE ratio in the blastocyst leads to placental abnormalities and LOS (20). In the cloned embryos with a small number of variant cell types, functional role of TE cells for successful implantation was reduced (21).

It has been demonstrated that mESCs-derived chimeras suffer from reduced viability and other anomalies such as altered growth rate and body weight (22). These abnormalities could be mainly due to the changes in gene expression of TE and ICM cells, causing by embryo manipulation and *in vitro* culture (23, 24). In this context, epigenetic modification has a profound effect on gene expression. Histone modification plays an important role in transcription activity via methylation of lysine and chromatin structure remodelling in pre-implanted embryo (25). Embryo manipulations, such as SCNT, ICSI and cryopreservation, modify somewhat the normal pattern of H3K9me3 and H3K4me3 methylation (16, 17, 26). However, there is no study to assess methylation of H3K4 and H3K9 in chimeric embryos and evaluate the role of this modification on gene expression.

It has been shown that H3K4me3 is enriched in transcription starting site of some transcription factors, including *Nanog*, *Oct4* and *Sox2* genes, which have regulatory role in gene expression (27). *Oct4* is one of the main genes, known to act as a master regulator of pluripotency (28). It belongs to POU family of transcription factor genes. It is found in the promoter and enhancer regions of many genes. *Oct4* also regulates expression of *Nanog*, *Sox2* and other genes modulating the cell fate during early embryo development (29, 30). In our study, H3K4me3 in ICM cells of chimeric blastocysts was decreased, in comparison with the other groups. It probably reduced the expression of certain specific genes, including *Oct4* and *Sox2* in ICM. This was in agreement with many studies indicating that *in vitro* derived embryos and embryo manipulation can alter methylation pattern, consequently leading to the change in expression of pluripotency genes, compared to the *in vivo* derived type (28, 31).

Our study shows that in chimeric embryos, duration and severity of the manipulation *in vitro* were more than the other groups. Based on that and in accordance with the previous studies (31, 32), duration and severity of the embryo manipulation may lead to more epigenetic alterations in H3K9me3 and H3K4me3, consequently reducing the ICM and TE gene expressions (32-34). According to the our results, because of difference in the type and duration of manipulation *in vitro*, there was a significant trend in reduction of the ICM cells H3K4me3 methylation, but not TE cells. Another possibility for decreasing H3K4 methylation in ICM cells of chimeric blastocysts, compared to the other groups, might be due to the possible interactions between injected mESC and ICM cells in chimeric blastocysts. Methylation of H3K4 in chimeric blastocysts was also reduced compared to other groups, although the difference between sham and chimeric groups was not significant.

In the normal process of blastocyst development, generating ICM and TE cells, there is a relationship between *Oct4* and *Cdx2* expressions. As such, the increase in *Oct4* expression leads to the reduction of *Cdx2* expression in ICM cells and vice versa in TE cells. *Cdx2* as a transcription factor is responsible for embryo compaction and TE lineage formation (35). In our study, despite the significant decrease in expression of *Oct4*, *Nanog* and *Tead4*, down-regulation of *Cdx2* expression was not significant in chimeric blastocysts under the impact of manipulation compared to *in vivo*-derived counterparts. Now, the question is why despite the reduced expression of other genes, expression of *Cdx2* has not been declined? Whether genes associated with cellular fate (*Tead4*) and pluripotency (*Oct4* and *Nanog*) are more sensitive than TE gene (*Cdx2*) in the face of inappropriate culture conditions or manipulation? However, there are studies indicating no significant difference in *Cdx2* expression between embryos with (cloned and ICSI embryos) and without manipulation (36).

H3K4me3 is generally associated with active chromatin, whereas H3K9me3 preferentially correlates with heterochromatin and transcription repression (37). Here, we found a converse relationship between H3K9me3 and gene expression in ICM and TE of chimeric embryos. In other words, increasing level of H3K9me3 leads to the reduction of *Nanog*, *Oct4* and *Tead*4 gene expressions in chimeric embryos, compared to *in vivo* derived blastocysts. It is hypothesized that reduction of H3K9me3 level by optimizing culture condition can improve epigenetic pattern in the chimeric embryos. Consistently, it has been shown in mouse and porcine cloned embryos (38, 39). In agreement with our study, H3K9me3 could down-regulate the pluripotency gene expressions in the cloned embryos (38). Regarding the *Cdx2* expression, despite decreasing trend of gene expression in the first three groups, the expression in test group (chimeric blstocysts) was increased in comparison with the sham group. One explanation for the significant decrease in *Cdx2* expression in the sham, compared to test group, might be due to the higher, though insignificant, level of H3K9me3 in sham group. Alder et al. (40) indicated that down-regulation of H3K9me3 in TE leads to the activation of *Cdx2* transcription. As expected, in our study, H3K9 histone methylation of the ICM cells was significantly increased in chimeric blastocysts compared to the sham group. It was in accordance to the general principle that further manipulation will cause more epigenetic alterations. In other words, more invasive operations, as with chimeric embryos, cause more epigenetic changes.

Concerning the level of H3K9me3 in TE cells, despite determining consistently increased level of methylation contrary to our expectations, there was no significant difference between the chimeric and sham groups. There are, however, other factors that can alter gene expressions, such as DNA methylation and histone modification,

which may affect the gene expression pattern in chimeric embryos, compared to the other groups. Apart from *Cdx2*, the expression of *Tead4* in TE cells was decreased, while it was increased in the embryo manipulation. Thus, the minimum expression level was shown in chimeric blastocysts, compared to the other groups. These alterations followed the pattern of H3K9me3 changes in TE cells.

Conclusion

In our study, the embryonic stage had a profound effect on production of chimeric blastocyst. Thus, embryo compaction significantly reduced the rate of mESCs incorporation to the ICM. Moreover, alterations in the levels of H3K9me3 and H3K4me3 could reduce the pluripotency and cell fate gene expressions, due to embryo *in vitro* culture and its manipulation.

Acknowledgements

The authors would like to thank the staff of Reproductive Biotechnology Research Center, Avicenna Research Institute, ACECR, Shahid Beheshti University (Tehran, Iran) to provide possibility of doing the study and their technical supports and Shahid Beheshti University of Medical Sciences for helpful assistance. This work did not receive any external funding. The authors declare no conflict of interest.

Authors' Contributions

A.S.; Participated in designing the experiments and critical revision of the manuscript. M.S; Writting the manuscript and performing the experiments. M.N; Participated in designing the experiments and processed the experimental data. M.M.M., M.M.N., M.A.Sh.; Facilities and reagents/materials/analytical preparation. S.M.H., M.D.O.; Data collection and analysis. All authors read and approved the final manuscript.

References

1. Tam PP, Rossant J. Mouse embryonic chimeras: tools for studying mammalian development. Development. 2003; 130(25): 6155-6163.
2. Poueymirou WT, Auerbach W, Frendewey D, Hickey JF, Escaravage JM, Esau L, et al. F0 generation mice fully derived from gene-targeted embryonic stem cells allowing immediate phenotypic analyses. Nature Biotechnol. 2007; 25(1): 91-99.
3. Saburi S, Azuma S, Sato E, Toyoda Y, Tachi C. Developmental fate of single embryonic stem cells microinjected into 8-cell-stage mouse embryos. Differentiation. 1997; 62(1): 1-11.
4. Chan YS, Göke J, Ng JH, Lu X, Gonzales KA, Tan CP, et al. Induction of a human pluripotent state with distinct regulatory circuitry that resembles preimplantation epiblast. Cell Stem Cell. 2013; 13(6): 663-675.
5. Guo J, Wu B, Li S, Bao S, Zhao L, Hu S, et al. Contribution of mouse embryonic stem cells and induced pluripotent stem cells to chimeras through injection and coculture of embryos. Stem Cells Int. 2014; 2014: 409021.
6. Johnson MH, Ziomek CA. Induction of polarity in mouse 8-cell blastomeres: specificity, geometry, and stability. J Cell Biol. 1981; 91(1): 303-308.
7. Farin CE, Farmer WT, Farin PW. Pregnancy recognition and abnormal offspring syndrome in cattle. Reprod Fertil Dev. 2010; 22(1): 75-87.
8. Ventura-Juncá P, Irarrázaval I, Rolle AJ, Gutiérrez JI, Moreno RD, Santos MJ. In vitro fertilization (IVF) in mammals: epigenetic and developmental alterations. Scientific and bioethical implications for IVF in humans. Biol Res. 2015; 48: 68.
9. Shi L, Wu J. Epigenetic regulation in mammalian preimplantation embryo development. Reprod Biol Endocrinol. 2009; 7(1): 59.
10. Fraser R, Lin C-J. Epigenetic reprogramming of the zygote in mice and men: on your marks, get set, go! Reproduction. 2016; 152(6): R211-R222.
11. Bogdanović O, van Heeringen SJ, Veenstra GJ. The epigenome in early vertebrate development. Genesis. 2012; 50(3): 192-206.
12. Paranjpe SS, Veenstra GJ. Establishing pluripotency in early development. Biochim Biophys Acta. 2015; 1849(6): 626-636.
13. Boland MJ, Nazor KL, Loring JF. Epigenetic regulation of pluripotency and differentiation. Circ Res. 2014; 115(2): 311-324.
14. Loh YH, Zhang W, Chen X, George J, Ng HH. Jmjd1a and Jmjd2c histone H3 Lys 9 demethylases regulate self-renewal in embryonic stem cells. Gene Dev. 2007; 21(20): 2545-2557.
15. Palermo GD, Neri QV, Takeuchi T, Squires J, Moy F, Rosenwaks Z. Genetic and epigenetic characteristics of ICSI children. Reprod Biomed Online. 2008; 17(6): 820-833.
16. Niemann H, Tian XC, King WA, Lee RS. Epigenetic reprogramming in embryonic and foetal development upon somatic cell nuclear transfer cloning. Reproduction. 2008; 135(2): 151-163.
17. Farahavar A, Shirazi A, Kohram H, Sarvari A, Borjian-Boroujeni S, Naderi M-M, et al. Improving the quality of ovine embryo produced in vitro by culturing zygote in isolated mouse oviduct. Small Ruminant Res. 2017.
18. Tokunaga T, Tsunoda Y. Efficacious production of viable germ-line chimeras between embryonic stem (ES) cells and 8-cell stage embryos. Dev Growth Differ. 1992; 34(5): 561-566.
19. Hillman N, Sherman MI, Graham C. The effect of spatial arrangement on cell determination during mouse development. J Embryol Exp Morphol. 1972; 28(2): 263-278.
20. Fouladi-Nashta AA, Alberio R, Kafi M, Nicholas B, Campbell KH, Webb R. Differential staining combined with TUNEL labelling to detect apoptosis in preimplantation bovine embryos. Reprod Biomed Online. 2005; 10(4): 497-502.
21. Dadi TD, Li MW, Lloyd KC. EGF and TGF-alpha supplementation enhances development of cloned mouse embryos. Cloning Stem Cells. 2007; 9(3): 315-326.
22. Eggan K, Jaenisch R. Differentiation of F1 embryonic stem cells into viable male and female mice by tetraploid embryo complementation. Method Enzymol. 2003; 365: 25-39.
23. Giritharan G, Delle Piane L, Donjacour A, Esteban FJ, Horcajadas JA, Maltepe E, et al. In vitro culture of mouse embryos reduces differential gene expression between inner cell mass and trophectoderm. Reprod Sci. 2012; 19(3): 243-252.
24. Giritharan G, Talbi S, Donjacour A, Di Sebastiano F, Dobson AT, Rinaudo PF. Effect of in vitro fertilization on gene expression and development of mouse preimplantation embryos. Reproduction. 2007; 134(1): 63-72.
25. Agrawal H, Selokar NL, Saini M, Singh MK, Chauhan MS, Palta P, et al. Epigenetic alteration of donor cells with histone deacetylase inhibitor m-carboxycinnamic acid bishydroxymide improves the in vitro developmental competence of buffalo (Bubalus bubalis) cloned embryos. Cell Reprogram. 2018; 20(1): 76-88.
26. Jahangiri M, Shahhoseini M, Movaghar B. H19 and MEST gene expression and histone modification in blastocysts cultured from vitrified and fresh two-cell mouse embryos. Reprod Biomed Online. 2014; 29(5): 559-566.
27. Bernstein BE, Mikkelsen TS, Xie X, Kamal M, Huebert DJ, Cuff J, et al. A bivalent chromatin structure marks key developmental genes in embryonic stem cells. Cell. 2006; 125(2): 315-326.
28. Nichols J, Zevnik B, Anastassiadis K, Niwa H, Klewe-Nebenius D, Chambers I, et al. Formation of pluripotent stem cells in the mammalian embryo depends on the POU transcription factor Oct4. Cell. 1998; 95(3): 379-391.
29. Yagi R, Kohn MJ, Karavanova I, Kaneko KJ, Vullhorst D, DePamphilis ML, et al. Transcription factor TEAD4 specifies the trophectoderm lineage at the beginning of mammalian development. Development. 2007; 134(21): 3827-3836.
30. Avilion AA, Nicolis SK, Pevny LH, Perez L, Vivian N, Lovell-Badge R. Multipotent cell lineages in early mouse development depend on SOX2 function. Gene Dev. 2003; 17(1): 126-140.
31. Lonergan P, Rizos D, Gutierrez-Adan A, Fair T, Boland MP. Oocyte and embryo quality: effect of origin, culture conditions and gene expression patterns. Reprod Domest Anim. 2003; 38(4): 259-267.
32. Kohda T. Effects of embryonic manipulation and epigenetics. J

Hum Genet. 2013; 58(7): 416-420.
33. Kohda T, Ishino F. Embryo manipulation via assisted reproductive technology and epigenetic asymmetry in mammalian early development. Philos Trans R Soc Lond B Biol Sci. 2013; 368(1609): 20120353.
34. Niwa H, Toyooka Y, Shimosato D, Strumpf D, Takahashi K, Yagi R, et al. Interaction between Oct3/4 and Cdx2 determines trophectoderm differentiation. Cell. 2005; 123(5): 917-929.
35. Jedrusik A, Bruce AW, Tan MH, Leong DE, Skamagki M, Yao M, et al. Maternally and zygotically provided Cdx2 have novel and critical roles for early development of the mouse embryo. Dev Biol. 2010; 344(1): 66-78.
36. Kishigami S, Hikichi T, Van Thuan N, Ohta H, Wakayama S, Bui H-T, et al. Normal specification of the extraembryonic lineage after somatic nuclear transfer. FEBS Lett. 2006; 580(7): 1801-1806.
37. Lee TI, Jenner RG, Boyer LA, Guenther MG, Levine SS, Kumar RM, et al. Control of developmental regulators by Polycomb in human embryonic stem cells. Cell. 2006; 125(2): 301-313.
38. Chen P, Yao JF, Huang RF, Zheng FF, Jiang XH, Chen X, et al. Effect of BIX-01294 on H3K9me2 levels and the imprinted gene Snrpnin mouse embryonic fibroblast cells. Biosci Rep. 2015; 35(5). pii: e00257.
39. Zhang Z, Zhai Y, Ma X, Zhang S, An X, Yu H, et al. Down-regulation of H3K4me3 by MM-102 facilitates epigenetic reprogramming of porcine somatic cell nuclear transfer embryos. Cell Phisiol Biochem. 2018; 45(4): 1529-1540.
40. Alder O, Lavial F, Helness A, Brookes E, Pinho S, Chandrashekran A, et al. Ring1B and Suv39h1 delineate distinct chromatin states at bivalent genes during early mouse lineage commitment. Development. 2010; 137(15): 2483-92.

Original Article

Alteration of Cytoskeleton Morphology and Gene Expression in Human Breast Cancer Cells under Simulated Microgravity

Florian Strube, M.D., Manfred Infanger, M.D., Markus Wehland, Ph.D., Xenia Delvinioti, M.D., Alexander Romswinkel, B.Sc., Carlo Dietz, B.Sc., Armin Kraus, M.D.*

Department of Plastic, Aesthetic and Hand Surgery, Otto-von-Guericke-University, Magdeburg, Germany

***Corresponding Address: Department of Plastic, Aesthetic and Hand Surgery, Otto-von-Guericke-University, Magdeburg, Germany**
Email: arminkraus@hotmail.com*

Received: 9/November/2018, Accepted: 16/February/2019

Abstract

Objective: Weightlessness simulation due to the simulated microgravity has been shown to considerably affect behavior of tumor cells. It is aim of this study to evaluate characteristics of human breast cancer cells in this scaffold-free 3D culture model.

Materials and Methods: In this experimental study, the cells were exposed to simulated microgravity in a random-positioning machine (RPM) for five days. Morphology was observed under phase-contrast and confocal microscopy. Cytofilament staining was performed and changes in expression level of cytofilament genes, proliferation/differentiation genes, oncogenes and tumor suppressor genes were detected by quantitative reverse transcription polymerase chain reaction (qRT-PCR), followed by western blot confirmation.

Results: After five days, distinct spheroid formation was observed. Rearrangement of the cytoskeleton into spherical shape was visible. *VIM* gene expression was significantly up-regulated for adherent cells and spheroids (3.3x and 3.6x respectively, P<0.05 each). *RHOA* also showed significant gene up-regulation for adherent cells and spheroids (3.2x and 3.9x respectively, P<0.05 each). *BRCA* showed significant gene up-regulation in adherent cells and spheroids (2.1x and 4.1x respectively, P<0.05 each). *ERBB2* showed significant gene up-regulation (2.4x, P<0.05) in the spheroids, but not in the adherent cells. *RAB27A* showed no significant alteration in gene expression. *MAPK*) showed significant gene up-regulation in adherent cells and spheroids (3.2x, 3.0x, P<0.05 each). *VEGF* gene expression was down-regulated under simulated microgravity, without significance. Alterations of gene expressions could be confirmed on protein level for vimentin and MAPK1. Protein production was not increased for BRCA1, human epidermal growth factor receptor 2 (HER2) and VEGF. Contradictory changes were determined for *RHOA* and its related protein.

Conclusion: Microgravity provides an easy-to handle, scaffold-free 3D-culture model for human breast cancer cells. There were considerable changes in morphology, cytoskeleton shape and gene expressions. Identification of the underlying mechanisms could provide new therapeutic options.

Keywords: Breast Neoplasms, Cytoskeleton, Proto-Oncogenes, Tumor Suppressor Genes, Weightlessness Simulation

Cell Journal(Yakhteh), Vol 22, No 1, April-June (Spring) 2020, Pages: 106-114

Citation: **Strube F, Infanger M, Wehland M, Delvinioti X, Romswinkel A, Dietz C, Kraus A. Alteration of cytoskeleton morphology and gene expression in human breast cancer cells under simulated microgravity. Cell J. 2020; 22(1): 106-114. doi: 10.22074/cellj.2020.6537.**

Introduction

Breast neoplasms are still a major cause of morbidity and mortality in the western world. To identify new mechanisms that could provide therapeutic targets, experiments in 2-dimensional (2D) cell culture struggle with various limitations. Phenotype alteration and loss in 2D cultures has been described for several cell types. It has been described for somatic cells such as tenocytes (1) and mesenchymal stem cells (2). Space flights have shown to impose significant alterations on human and animal organisms, as well as cell cultures. On the organism, various effects such as loss of bone mineralization or changes in blood pressure regulation are well known.

In different cell types, loss of attachment from the otherwise indispensable culture surface and transition to a state of 3-dimensional (3D) formations, so-called "spheroids", has been reported. This was observed during flights beyond the earth atmosphere (3), during parabolic flight maneuvers (4), in addition to the simulated microgravity on earth. Hereby, 2D rotating clinostats or 3D rotating random positioning machines (RPM) are in use. In both, simulated microgravity on earth and during space flights, several effects of microgravity on breast cancer cells have been reported, especially with regards to invasion, adhesion and metastasis formation (5).

Microgravity has also been reported to induce mitochondrial activity in breast cancer cells as a reaction to oxidative stress (6). Further studies by our group have shown alterations particularly with regard to the cytoskeleton arrangement (7). Microgravity therefore seems to be an attractive 3D cell culture model to study migration and invasiveness in breast cancer. We performed experiments where we exposed breast cancer cells to simulated microgravity. We studied cytoskeleton morphology as well as gene and protein expression levels related to tumor differentiation, proliferation and invasion. In this study, we aimed to provide new insights into these mechanisms in order to identify potential targets for new therapeutic strategies.

Materials and Methods

The present work was designed as an experimental laboratory study (level of evidence V).

Cell culture

Human breast cancer cells (adenocarcinoma, CRL-2351) were obtained from ATCC© (Wesel, Germany). All experiments were performed on this commercially available cell line, so no Ethical Committee approval was necessary. The cell line is negative estrogen receptor and it overexpresses the HER2/neu oncogene. The cells were firstly expanded under 2D-conditions in T125 flasks (Sarstedt, USA). Ham´s F12-media (Gibco, Germany) supplemented with 5% fetal calf serum (FCS, Biochrom AG, Germany) and 1% penicillin/streptomycin (Biochrom, Germany) was used. The medium was changed three times per week. For this experiment, 1×10^6 cells were counted by hemocytometer and added to six T125 flasks, as the experimental group in the RPM, and to the same number of flasks for the control group under 1g conditions. For cytoskeleton staining, the cells were seeded with a density of 1×10^5 per cm^2 to slide flasks (Thermo Scientific, Germany).

Random positioning machine

Weitghtlessness simulation was generated using an RPM. The RPM (developed by University of Applied Sciences, Northwestern Switzerland) was run with a commercially available incubator at 37˚C and 5% CO_2. The device was operated in a random walk modus using an angular velocity of 60°/seconds. The method was intensively investigated and published earlier (8). Six flasks of T125 cm^2 were attached as much as possible to the center of RPM machine, and the samples were rotated for the selected time period (five days). Static, non-rotated controls were exposed to the same environmental conditions nearby the device. The RPM machine was rebooted once per 24 hours to ensure proper operation. Interruption was kept as short as possible every time.

Phase contrast microscopy

Phase contrast microscopy was performed for visual observation of viability and morphology of the cells, and for detection of potential spheroids. A Leica microscope (Leica Microsystems GmbH, Germany) was used. Pictures were taken with a Canon EOS 60D (Canon GmbH, Germany).

Cytoskeleton staining

In terms of cytoskeleton analysis, the cells exposed to simulated microgravity in the RPM for five days were investigated in the slide flasks. Filamentous actin (F-actin) was analyzed by visualization of phalloidin-stained cells (PromoKine, USA). Both adherent cells and spheroids were fixed with 4% paraformaldehyde for 10 minutes and permeabilized with 1% Triton-X for 5 minutes. Nonspecific binding was blocked by incubation with 1% bovine serum albumin (BSA). Staining was performed by incubation of the slides with 6.6 µM solution of a phalloidin/Alexa Fluor 488 conjugate (Thermo Fisher Scientific, Germany) for 30 minutes at room temperature, followed by thorough washing with phosphate buffere saline (PBS) solution. Nuclei were counterstained with 4′,6-diamidine-2-phenylindol (DAPI, Thermo Fisher Scientific, Germany) at 0.1 µg/ml concentration for 1 minute. The samples were mounted with Vectashield mounting medium (Vector Laboratories, USA).

Confocal microscopy

Confocal microscopy of the slides stained for F-actin was performed with a Zeiss 510 META inverted confocal laser scanning microscope (Zeiss, Germany). Excitation and emission wavelengths were 485 nm/560 nm, respectively.

RNA and protein isolations, quantitative reverse transcription polymerase chain reaction and western blot

RNA isolation

An aliquot of cells was frozen in liquid nitrogen for subsequent lysis and protein isolation as described further below. RNA isolation and quantitative reverse transcription polymerase chain reaction (qRT-PCR) were done according to standard protocols following the manufacturer's manual. RNA isolation was performed with the AllPrep DNA/RNA/Protein Mini© Kit (Qiagen, Germany) according to the manual. The cells were brought into suspension from the culture plate surfaces by adding 0.025% trypsin (Sigma-Aldrich, Germany). The cell suspension was spun down in an RNase-free tube for five minutes at 300 g. Next, 350 µl of the lysis buffer RLT was added to the pellet to induce cell lysis. Remaining RNases were inactivated by 1% β-mercaptoethanol addition. The lysate was vortexed for 1 minute to obtain a homogenous lysate. Thereafter, it was stabilized by adding 100% ethanol in an equal volume to the lysate. The liquid was then transferred to an RNeasy Spin Column and centrifuged in a micro-centrifuge at 10,000 rpm for 15 seconds. The flow-through was put aside for further protein isolation as described below. Afterwards, 700 µl of the buffer RW1 (washing buffer) was given to the spin column, followed by centrifugation at 10,000 rpm for 15 seconds. The flow-through was discarded again. The washing buffer RPE© was added to the spin column at a volume of 500 µl and the column was centrifuged at 10,000 rpm for 15 seconds. This step was repeated after discarding the flow-through. The RNA was then eluted into an RNase-free collection tube by centrifugation with 30 µl of RNase-free water. The RNA was quantified photometrically by measuring the absorbance at 260 nm with a SpectraMax M2 device (Molecular Devices, USA).

Reverse transcription

Reverse transcription was done using the First Strand cDNA Synthesis Kit (Thermo Scientific, USA) according to the manual. Briefly, for each sample, 3 µg total RNA, random hexamer primers and nuclease-free water were mixed together to an overall volume of 11 µl. To this volume, reaction buffer, RNase inhibitor, oligonucleotides and reverse transcriptase were added to a total volume of 20 µl. All steps were performed under refrigeration on ice. The mix was kept

for five minutes at 25˚C, followed by 60 minutes at 42˚C. The reaction was stopped by incubation at 70˚C for five minutes. The complementary DNA (cDNA) was stored at -20˚C for less than one week before performing further experiments.

Quantitative reverse transcription polymerase chain reaction

qRT-PCR was utilized to determine relative expression of the target genes, such as proto-oncogenes and tumor suppressor genes, as shown in Table 1. The SYBR® Green PCR Master Mix (Applied Biosystems, Germany) and the 7500 Real-Time PCR System (Applied Biosystems, Germany) were used. 10 µl master mix, 1 µl of each forward and reverse primers at the concentration of 400 nM and 1-8 µl cDNA and RNase free water, in relation to the input-amount of RNA, were mixed together. Cycling steps were executed as follows after activation of uracil-DNA glycosylase (50˚C for two minutes) and DNA polymerase (95˚C for 2 minutes): 95˚C for 15 seconds and 60˚C for 1 minute (40 cycles). Absence of primer dimers was confirmed by checking dissociation curves. cDNA-selective primers were collected from Harvard primer database (https://pga.mgh.harvard.edu/primerbank) and were supplied by TIB Molbiol (Germany). All samples were measured as triplicates. 18S rRNA was used as housekeeping gene. The comparative C_T ($\Delta\Delta C_T$) method was used to calculate relative transcription levels of the target genes. The control group was defined as 100%. Primer sequences are as shown in Table 1. The experiments were performed in five replicates.

Table 1: Quantitative reverse transcription polymerase chain reaction (qRT-PCR) primer sequences. All primers were obtained from Harvard primer bank (https://pga.mgh.harvard.edu/primerbank/)

Gene	Primer sequence (5′-3′)
VIM	F: GACGCCATCAACACCGAGTT
	R: CTTTGTCGTTGGTTAGCTGGT
RHOA	F: CTCGCTCAGTGCGAAGACAA
	R: CATTCTCTGACGACATTTTCCCT
BRCA1	F: GCTCGTGGAAGATTTCGGTGT
	R: TCATCAATCACGGACGTATCATC
ERBB2	F: CCTCTGACGTCC ATCGTCTC
	R: CGGATCTTCTGCTGC CGTCG
RAB27A	F: GCTTTGGGAGACTCTGGTGTA
	R: TCAATGCCCACTGTTGTGATAAA
MAPK1	F: TACACCAACCTCTCGTACATCG
	R: CATGTCTGAAGCGCAGTAAGATT
VEGF	F: AGGGCAGAATCATCACGAAGT
	R: AGGGTCTCGATTGGATGGCA
18S rRNA	F: ATGGCGGCGTCTGTATTAAAC
	R: AGAACCATATCGCTCCTGGTAT

Western blotting

Protein and RNA isolations were simultaneously performed using the AllPrep DNA/RNA/Protein Mini© Kit, as described above. The flow-through preserved from the respective elution step, described above, was mixed with an equal volume of the buffer APP© from the extraction kit and kept for 10 minutes at room temperature after meticulous mixing for protein precipitation. The suspension was centrifuged for 10 minutes at maximum speed and the supernatant was carefully pipetted off to obtain a protein pellet. The pellet was dried at room temperature for 10 minutes. The pellet was next dissolved again in 100 µl of the buffer ALO© and heated to 95˚C for this purpose. The solution was centrifuged again at full speed for one minute to remove remaining precipitates and debris. The protein solution was frozen at -20˚C until further use. Gel electrophoresis, transblotting and densitometry were performed according to the standard protocols. Isolated protein was incubated for 10 minutes with sodium dodecyl sulfate (SDS)-gel loading buffer (consisting of 1 M Tris base, pH=6.8, 1% clycerol, 10% SDS, 0.1% bromophenol blue freshly added to 0.05% β-mercaptoethanol and 1% protease inhibitors, all purchased from Roche, Germany). The samples were denatured at 95˚C for five minutes. Afterwards, the probes were loaded together with the prestained page rule (Thermo Scientific, USA) onto a 10% SDS-polyacrylamide gel followed by electrophoresis and semi-dry blotting onto 0.45 µm nitrocellulose membranes (Whatman, Germany). Primary antibodies were used in blocking reagent with following dilutions: rabbit polyclonal anti-vimentin (1:2000), rabbit polyclonal anti-RhoA (1:500), rabbit polyclonal anti-Her2 (1:1000), rabbit polyclonal anti-RAB27A (1:1000), rabbit polyclonal anti-MAPK1 (1:1000), all obtained from Origene, USA, as well as rabbit polyclonal anti-BRCA1 (1:10000, Milipore, USA), rabbit polyclonal anti VEGF-A (1:1000, Thermo Fisher, USA). All antibodies were certified for western blot reactivity in human specimens by the suppliers.

The secondary antibody was included in the "BM Chemiluminescence Western Blotting Kit mouse/rabbit" (Roche, Germany). The blots were stripped at 50˚C for 30 minutes with stripping buffer (Restore Western blot stripping buffer, Thermo scientific, USA), washed and re-incubated with anti-GAPDH antibody (1:1000, Cell Signaling, Germany). Blots were analyzed by the Alpha-Ease® FC Imaging System (Alpha Innotech, Germany). The experiments were performed in three replicates.

Statistical analysis

All statistical analyses were done using SPSS 21.0 (SPSS, Inc., USA, 2012). The groups were tested with the Mann-Whitney U test. The data are shown as means ± standard deviation (SD). A $P<0.05$ was considered significant.

Results

A simulated average gravity value as low as 0.003 g was calculated by the RPM software.

Light microscopy

After 24 hours, formation of smaller spheroids, consisting of approximately 10-20 cells, was observed (Fig.1A). After five days, a considerable number of cells had detached from the culture surface, forming cluster shaped spheroids consisting of 30-50 cells (Fig.1B). Breast cancer cells showed rounded morphology with no obvious signs of impaired viability, according to preliminary trypan blue staining. This shows good cell viability without significant difference between the cells at 1g and those under simulated microgravity (data not shown). In the control group, under 1g conditions, the cells showed typical flat morphology with rectangular to hexagonal borders, attached to the culture surface (Fig.1C).

Confocal microscopy

After five days, the breast cancer cells showed under microgravity spherical rearrangement of actin filaments with accentuation of the filaments in the region of cell membrane (Fig.2A). In the adherent cells under simulated microgravity, a tendency towards spherical orientation of the actin filaments could be observed, while that is less pronounced than spheroids (Fig.2B). Under the condition of 1 g, actin filaments were arranged in a longitudinal manner with more uniform distribution of the filaments inside the cytoplasm (Fig.2C).

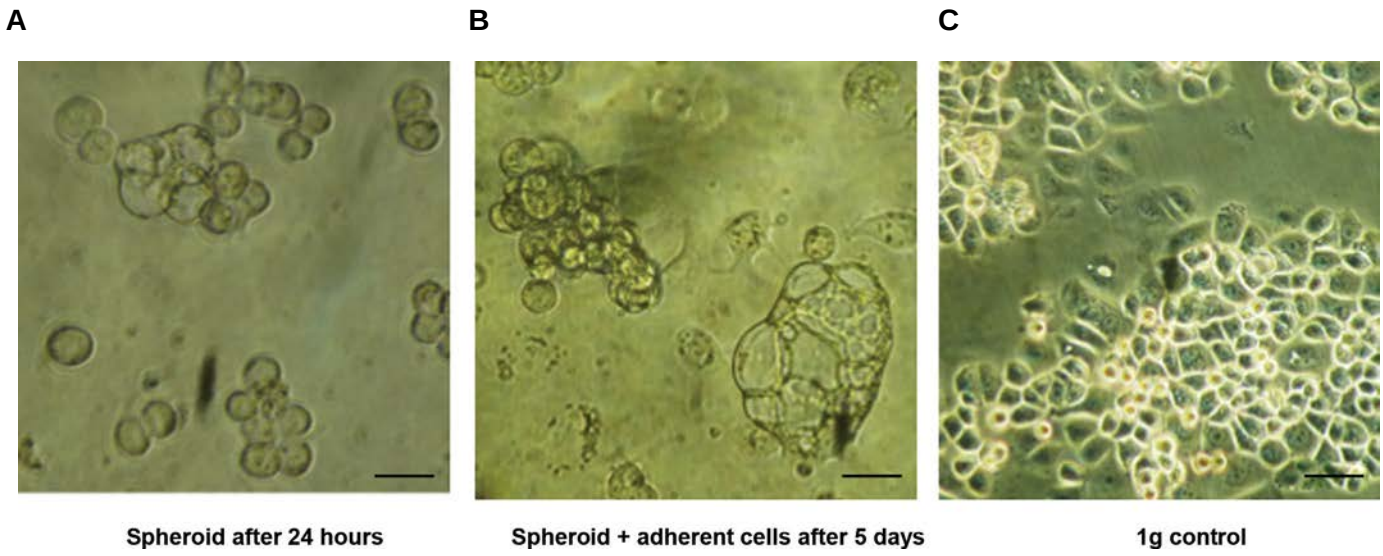

Fig.1: Analysis of spheroid formation of breast cancer cells under simulated microgravity (0.003 g) after one and five days, under light microscopy. **A.** Formation of small spheroids can be observed after 24 hours, **B.** After 5 days, size of the cluster to tubular shaped spheroids increased, while part of the cells remained attached to the culture flask surface, and **C.** In the control group under 1 g conditions, the cells showed typical shape with flat morphology and rectangular to hexagonal borders (scale bar: 50 µm).

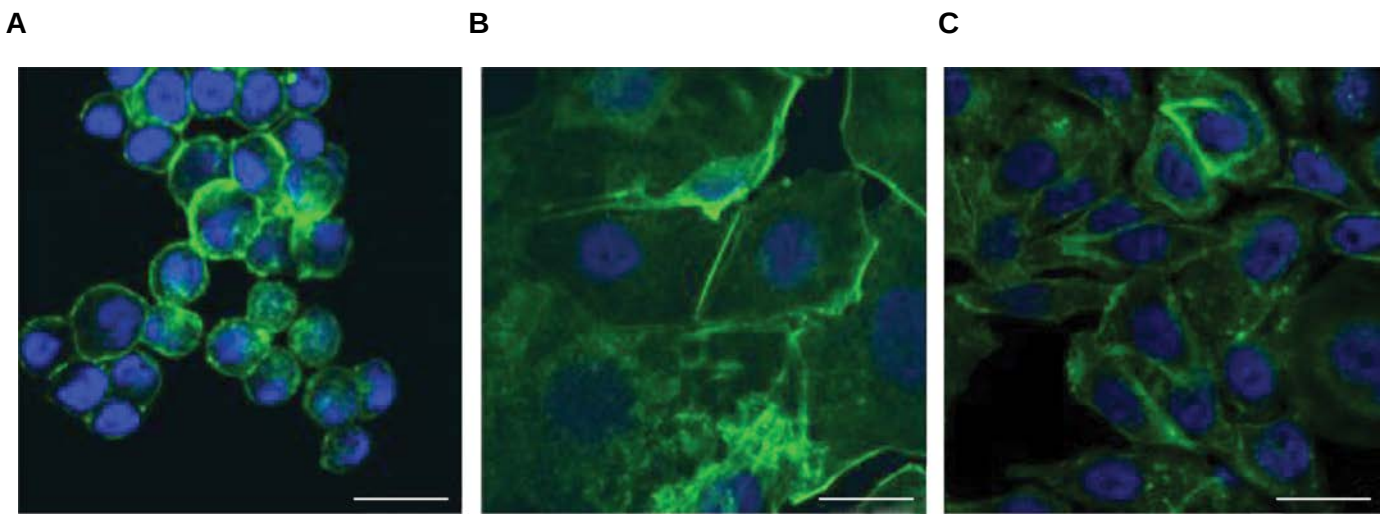

Fig.2: Actin staining of breast cancer cells. **A.** In the spheroids under simulated microgravity, actin filaments arranged in a spherical shape with accentuation in the area of the cell membrane, **B.** In the adherent cells under simulated microgravity, spherical orientation beginning of the actin filaments was observed, and **C.** In the 1 g control group, actin filaments were arranged in a longitudinal manner with uniform distribution among the cytoplasm (scale bar: 25 µm).

Quantitative reverse transcription polymerase chain reaction

After five days, *VIM* as a component of the cytoskeleton showed significantly up-regulated gene expression in the both attached cells and spheroids (3.3x and 3.6x respectively, P<0.05 each, Fig.3A). Correspondingly, *RHOA*, as a marker of cytoskeleton differentiation, also showed significant up-regulation in the both attached cells and spheroids under simulated microgravity (3.2x and 3.9x respectively, P<0.05 each, Fig.3B). *BRCA1* gene showed significant up-regulation in the both adherent cells and spheroids, compared to the control with 1 g (2.1x and 4.1x respectively, P<0.05, Fig.3C). *ERBB2* showed no significant up-regulation in the adherent cells under microgravity, while it was significantly up-regulated in the spheroids (2.4x, P<0.05, Fig.4A). *RAB27A*, as a KRAS-related control gene, showed no significant up-regulation in the both attached cells and spheroids under microgravity (Fig.4B). *MAPK1*, as a marker of proliferation and differentiation, showed significant up-regulation in the both adherent cells and spheroids under microgravity (3.2x and 3.0x respectively, P<0.05 each, Fig.5A). *VEGF* showed down-regulation in the both adherent cells (under simulated microgravity) and spheroids (0.67x and 0.60x respectively, Fig.5B), while it was not significant different (P=0.056 each).

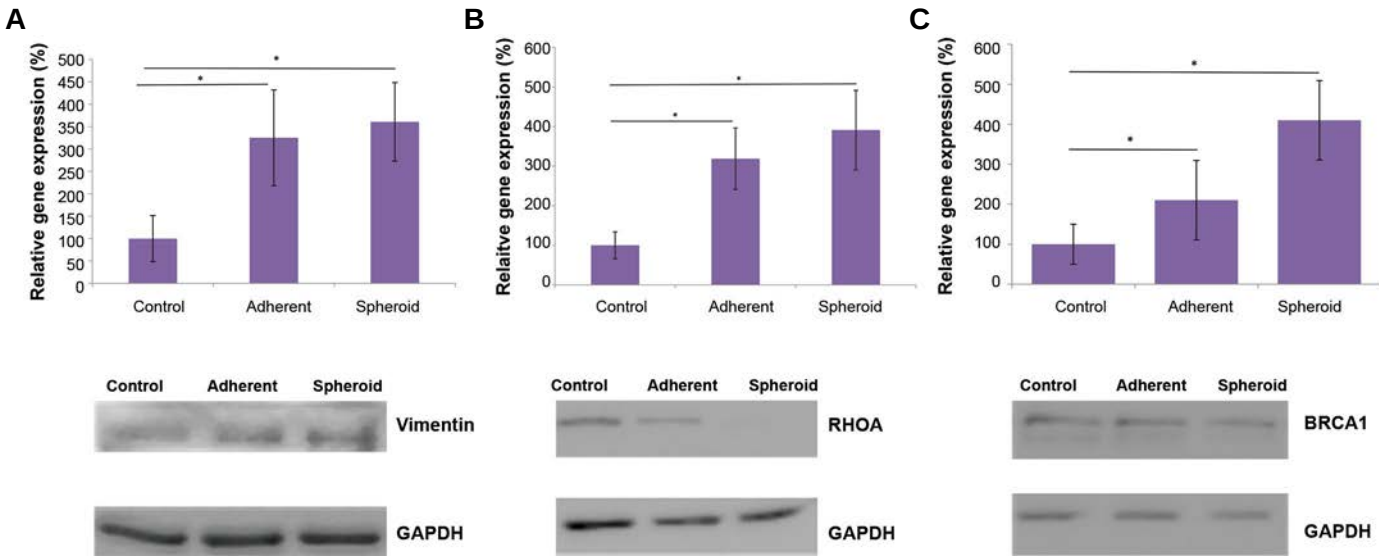

Fig.3: Alteration in gene expression and protein production under simulated microgravity**. A.** *VIM* as a component of the cytoskeleton showed significantly up-regulation in the both attached cells and spheroids, after five days (3.3x and 3.6x respectively, *P<0.05 each). *VIM* up-regulation was accompanied by increased vimentin protein production, **B.** *RHOA* also showed significant up-regulation in the both adherent cells and spheroids, under simulated microgravity (3.2x and 3.9x respectively, *P<0.05 each). In contrast, RhoA protein content was not increased under simulated microgravity, and **C.** *BRCA1* showed significant up-regulation in the both adherent cells and spheroids (2.1x and 4.1x respectively, *P<0.05 each). BRCA1 protein content was not significantly increased, as shown by western blot.

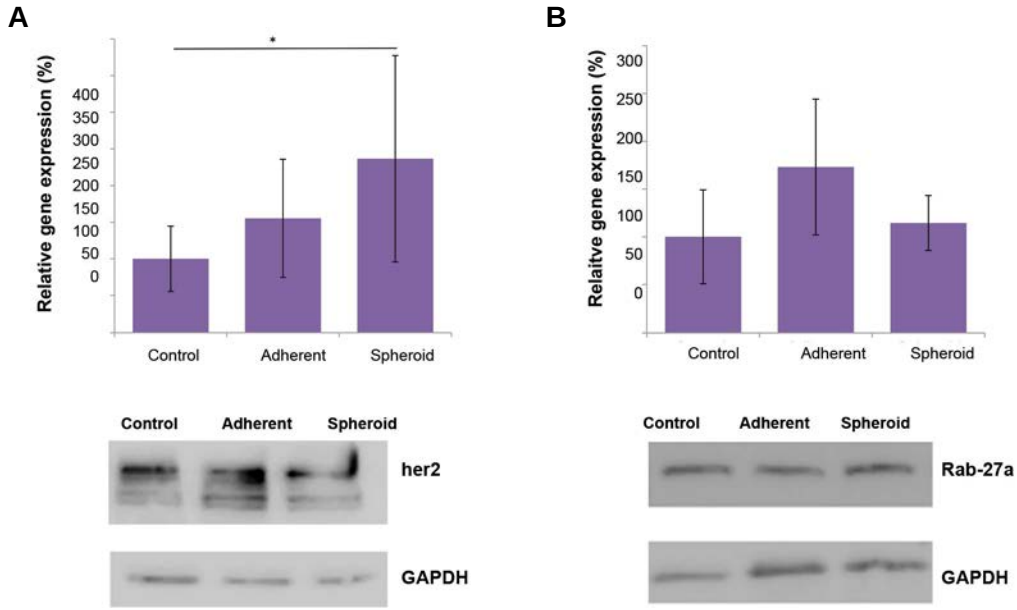

Fig.4: Alteration in gene expression and protein production under simulated microgravity. **A.** *ERBB2* showed significant gene up-regulation (2.4x, *P<0.05) in the spheroids, compared to the 1 g control group, while the corresponding protein production was not increased under microgravity and **B.** *RAB27A* showed no significant change in gene expression of the both adherent cells simulated under microgravity and spheroids. There was no change in Rab-27a protein content.

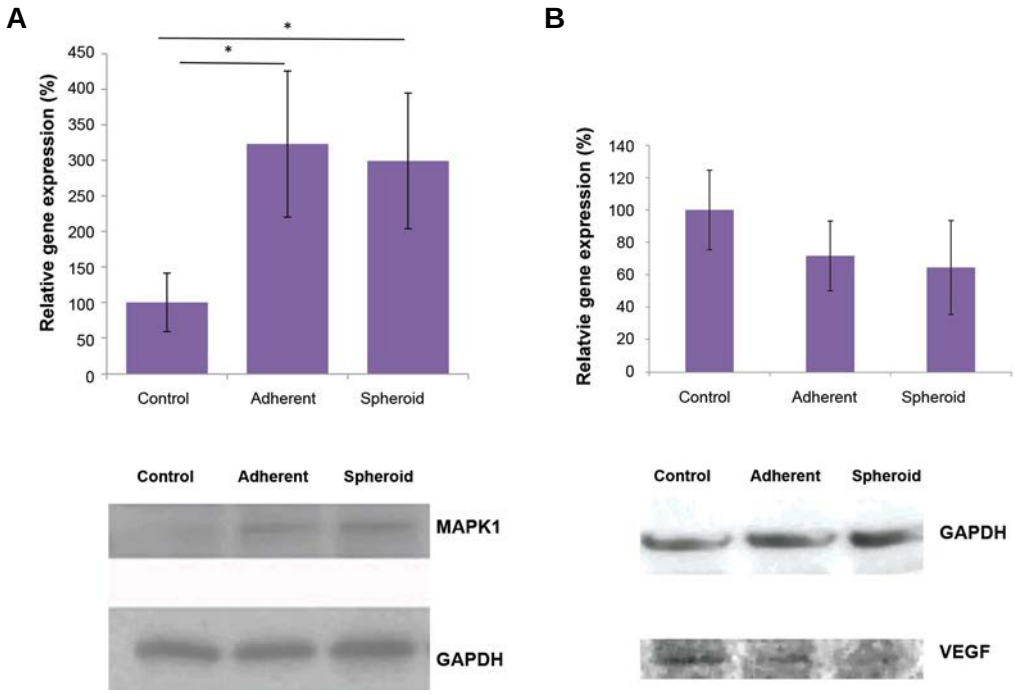

Fig.5: Alteration in gene expression and protein production under simulated microgravity. **A.** After five days, *MAPK1* showed significant up-regulation in the both adherent cells and spheroids under simulated microgravity (3.2x and 3.0 respectively, *P<0.05 each). Gene up-regulation was confirmed on protein level by western blot and **B.** *VEGF* was down-regulated under simulated microgravity in both gene expression and protein levels, but the values were not statistically significant.

Western blots

In line with *VIM* gene overexpression, analysis of western blot showed up-regulation of vimentin protein (Fig.3A). In the case of *RHOA,* protein expression level was attenuated under simulated microgravity gene (Fig.3B). Although *BRCA1* gene expression was significantly up-regulated in the adherent cells and spheroids, western blot analyses showed approximately similar protein levels for adherent cells, spheroids and the control (Fig.3C). *ERBB2* gene expression was significantly up-regulated in the spheroids, while the respective protein bands showed approximately equal intensities for all groups (Fig.4A). Rab-27a showed no changes in protein levels of the three groups, similar to the related gene expressions (Fig.4B). MAPK1 showed increased protein levels in the two simulated microgravity groups, which was consistent to the respective up-regulated gene expressions (Fig.5A). VEGF protein was decreased in both groups under simulated microgravity, compared to the control group (Fig.5B).

Discussion

Breast neoplasms are common malignancies. Thus, in terms of developing new treatments, researches on the cell culture level could be a valuable tool. It is well known that the cells tend to change their morphology, behavior and phenotype after being released from their *in vivo* environment and put into a 2D culture condition. By applying simulated microgravity, we could observe considerable changes in morphology, cytoskeleton arrangement, gene expression and protein synthesis compared to the 2D environment. For this study, five days investigation was selected, due to the following reason: preliminary experiments had shown that CRL-2351 cell line was relatively fast-growing and needed medium renewal after five days, according to the both vendor´s recommendations and our own observations. Furthermore, the cells showed almost complete confluence and the necessity of passaging after five days. We aimed to avoid medium change, because this maneuver would interrupt simulated microgravity and disturb its effects to particular degree. Therefore, five days was the longest period that this cell line could continuously be exposed to interruption-free simulated microgravity.

Compared to the several other studies utilizing 2D rotating clinostats, we used an RPM in this experiment, as a device simulating microgravity by 3D movements in space. Experiments, comparing the effects of simulated microgravity on an RPM with the space outside of earth atmosphere on cell cultures, have shown very good correlation between these two systems (9). Furthermore, we examined a cell line with unique characteristics which has not been exposed to microgravity so far, to our knowledge. In comparison with the MCF-7 cells, used in most of the studies dealing with breast cancer cells under simulated microgravity (5, 10, 11), the evaluated biologic features of CRL-2351 cell line in this study are controversial from many aspects: CRL-2351 cells are negative estrogen receptor, so the pathways usually associated with estrogen receptor signaling, like MAP kinase, will be influenced in a unique, hitherto unknown manner. Furthermore, HER2/neu is overexpressed in

CRL-2351 cells, in contrast to MCF-7 cells, particularly giving us the option to evaluate the effects of simulated microgravity on this important prognostic factor. Using light microscope, observations showed 3D constitution, round to tubular-shaped formations -known as spheroids- and reported already from various tumor and somatic cell types, such as from tenocytes (12), chondrocytes (13), or thyroid cancer cells (14) .

Another group of the cells under simulated microgravity remained adherent to the culture surface, but they showed various changes in morphology, gene expression and protein production. These cells could either represent a transitional state before spheroid formation, or remain in this adherent state for reasons still needing to be elucidated. In the MDA-MB-231 breast cancer cell line, Masiello et al. (15) could observe spheroid formation after 24 and 72 hours. In other studies, significant deceleration of breast cancer cell proliferation, while they are accumulated in the G2 phase, was reported under simulated microgravity (11). In the cytoskeleton, we observed a change from the longitudinal shape of actin filaments towards spherical distribution, accentuated in the region of cell membrane. This is in accordance with the results of Kopp *et al*. who reported similar findings for another line of breast cancer cells under simulated microgravity (10), and consistent to the results of Masiello et al. (15) cited above. To explain this phenomenon, a "gravity sensor" has been proposed inherited in the cytoskeleton, which is responsive to external forces (16). Particularly for the tumor cells, it has been reported that their metastatic potential is related to actin skeleton arrangement and remodeling (17). In addition, to investigate cytoskeleton changes in the molecular level, we examined gene expression of *VIM* and *RHOA*.

Vimentin is a cytoskeleton compound playing important role in the migration and invasion of breast cancer cells. Similar to the finding obtained in this experiment, an increased expression of *VIM* has been described as a epithelial to mesenchymal transition marker, leading to the enhanced invasion and metastasis in breast cancer cells. This may be one of the reasons why increased expression of *VIM* in breast cancer contributes to chemoresistance and poor prognosis (18). It is required to be furher elucidated whether *VIM* overexpression, under simulated microgravity, is indeed a marker of increased invasiveness. Thus metastatic potential is increased, or it rather reflects loss of surface attachment and spheroid formation without changes in metastatic ability. However, targeted and selective cytoskeleton derangement in cancer cells (e.g. by RNA-interference) could be a potential tool in future tumor therapy. As a therapeutic approach in this field, microRNA targeting against *VIM* was shown to decrease breast cancer invasion in animal studies (19). RhoA is another small GTPase with several functions, and it is known to be a key effector in the polymerization of actin filaments (20). Hence, we also examined *RhoA* gene and protein expressions.

In addition to these changes related to the cytoskeleton, we observed further various alterations in gene expression and corresponding protein synthesis. Firstly, we normalized qRT-PCR data to 18s rRNA and western blot data to GAPDH expression. Although it is not exactly known which gene or protein undergoes the least changes under simulated microgravity, the indicated housekeeping genes look the best option in this experiment, due to several reasons: 18s rRNA is known to be very stably expressed under many different circumstances and it has been used as a housekeeping gene in simulated microgravity research by the other groups before (10). GAPDH has also been previously used for normalization of western blot data in microgravity research by the other groups (21). Indeed, the corresponding bands of GAPDH protein showed very similar intensity in our experiments. In the endeavor to obtain information whether the breast cancer cells transform towards a more or less malignant phenotype under simulated microgravity, we measured a variety of genes known as proto-oncogenes, tumor suppressor genes, or those which are related to cell proliferation and differentiation. *BRCA1*, with no mutation and with normal function, is a well-known gene counteracting genome instability and acting as a tumor suppressor gene (22).

We observed significant overexpression of *BRCA1*, at least on the gene level, in the spheroids. This could be indicative of a transformation towards a phenotype with improved genomic repair and stability. Further experiments are required to evaluate this question in more detail. *BRCA1* gene expression was even higher in the spheroids than adherent cells, while this is not observed in the protein level. It is proposed that adherent cells under simulated microgravity might be a precursor of spheroids, turning into spheroids later. However, the adherent cells also could be an own entity for reasons unknown hitherto, remaining them adherent for a long period of time or even permanently. In a study, mouse embryonic stem cells (mESCs) were exposed to microgravity during spaceflight for 15 days. Analysis of this study showed down-regulation of *BRCA1* gene (23), Although it still need to evaluate whether *BRCA1* mimics similar tasks in mESCs and the breast cancer cells we examined. On the other hand, we observed significant up-regulation of *ERBB2* gene, but not HER2 protein, particularly in the spheroids. The cell line we used overexpresses HER2 anyway from the beginning. HER2 proteins consist of trans-membrane growth factor receptors activating intracellular signaling pathways. HER2 has been shown to play an important role in the pathogenesis of human breast cancer, and overexpression of this protein in human breast cancer cells is usually related to more aggressive behavior. Measurement of *ERBB2*/HER2 expression therefore seems of great interest to us, as this could give a hint towards transformation into a more aggressive phenotype induced by simulated microgravity.

As spheroid formation is associated with detachment of cells from a confluent 2D state, it is proposed that similar mechanisms to metastasis formation from a solid

tumor come into action. We therefore measured *RAB27A* gene expression and Rab-27a protein production, as it is known to play a crucial role not only in breast gland development, but also in breast cancer pathology, particularly in modulation of metastatic potential (24). As a small GTPase, Rab-27a controls various steps of exosome release, and exosome-mediated intercellular communication plays a crucial role in the above described processes. In our experiments, we could not detect any significant alteration in this gene and protein. The reasons still have to be elucidated, but a different exposure time to simulated microgravity possibly could show expression changes in future studies. To our knowledge, we chose a negative estrogen receptor cell line in our experiments and exposed it to simulated microgravity for the first. *MAPK1*/MAPK1 therefore seem particularly interesting measurement targets, as MAPK1 is one of the effectors in breast cancer cell estrogen signaling (25).

We observed significant up-regulation of *MAPK1*/MAPK1 on both gene and protein levels under simulated microgravity. It has been shown that inhibition of MAP kinase pathway can lead to conversion of negative estrogen receptor breast cancer cells, as with our experiments, to a positive estrogen receptor phenotype (26). Up-regulation of that could therefore be either interpreted in the sense of the negative estrogen receptor preservation, potentially more malignant phenotype, or the MAP kinase pathway take over further tasks in the microgravity setting which still needs to be elucidated. Despite not obtaining statistical significance, down-regulation of *VEGF* gene expression and protein production under simulated microgravity is another interesting finding. VEGF is known to be a potent endothelial growth factor regulating vascular permeability. Particularly, high VEGF expression is known to be associated with tumor progression and poor prognosis of breast neoplasms in the clinical setting (27). So that, *VEGF* gene and protein expression levels seem to be further important targets to evaluate. Anti-VEGF drugs (such as bevacizumab) are already administered in cancer therapy, and identification of the mechanisms responsible for *VEGF* down-regulation could help pave the way for new therapeutic strategies in this area.

Overall, we observed a variety of changes in gene and protein expressions. Most of these changes, particularly regarding the cytoskeleton, were indicative of a more invasive and aggressive phenotype. Up-regulation of *BRCA1*, as a tumor-suppressor gene in the non-mutated state, is contradictory to these findings to some extent, and significance of that needs to be further investigated. Utilizing western blot, a strong correlation was determined between alterations of gene expression and corresponding protein content in *VIM*/Vimentin, *RAB27A*/Rab-27a and *MAPK1*/MAPK1. BRCA1 and HER2 showed no detectable increase in protein content, despite up-regulation in gene expression level under microgravity. Surprisingly, there was decreased protein level of RhoA under simulated microgravity, despite up-regulation of gene expression. There are several possible explanations for this observation. One potential reason is the existence of several post-translational modifications. Different half-lives of proteins could be the other potential explanation. Rapid degradation of mRNA or delayed protein synthesis could also be conceived. RhoA protein, in particular, has been reported to undergo significant optional alteration in its half-life by post-translational methylation (28). Similar reasons my also account for the differences that we detected between western blot and qRT-PCR results for *BRCA1*/BRCA1 and *ERBB2*/HER2.

Interestingly, another study reported a general decrease of protein synthesis under microgravity for the yet unknown reasons (29). Simulated microgravity appears as an easy-to use and interesting 3D culture model for *in vitro* studies of breast cancer cells. Elongated shape of the spheroids resembles natural tumor structure better than conventional *in vitro* culture. Besides, both tumor-suppressor genes and proto-oncogenes were altered in their expressions. Better understanding of the underlying mechanisms could help develop new tools to selectively influence proliferation, differentiation and invasion of breast cancer cells and pave the way for new therapeutic options.

Conclusion

Simulated microgravity induces spheroid formation in human breast cancer cells. Here we observed substantial changes in cytoskeleton morphology, cytoskeleton related gene and protein expression. We also determined change in gene and protein expression levels of proto-oncogenes and tumor suppressor genes. Our experiments could be a step towards a versatile, easy-to handle 3D culture model of human breast cancer. It could provide new insights in the molecular mechanisms of breast cancer pathogenesis paving the way to new therapeutic strategies.

Acknowledgements

We are thankful to Andrea Kroeber and Sandra Vorwerk for technical assistance. The authors have no financial or other conflict of interest to disclose.

Authors' Contributions

F.S.; Conducted experiments and data evaluation. M.I.; Study design and draft evaluation. A.R., C.D.; Cell culture maintenance, draft evaluation. A.K.; Study design, draft preparation, study responsibility. M.W.; Study conception, critical review of the manuscript, conduction of part of the experiments. X.D.; Cell culture maintenance, critical review of the manuscript. The authors read and approved the final manuscript.

References

1. Yao L, Bestwick CS, Bestwick LA, Maffulli N, Aspden RM. Phenotypic drift in human tenocyte culture. Tissue Eng. 2006; 12(7): 1843-1849.
2. Li Y, Wu Q, Wang Y, Li L, Bu H, Bao J. Senescence of mesenchymal stem cells (Review). Int J Mol Med. 2017; 39(4): 775-782.
3. Pietsch J, Gass S, Nebuloni S, Echegoyen D, Riwaldt S, Baake

C, et al. Three-dimensional growth of human endothelial cells in an automated cell culture experiment container during the SpaceX CRS-8 ISS space mission - The SPHEROIDS project. Biomaterials. 2017; 124: 126-156.
4. Wehland M, Aleshcheva G, Schulz H, Saar K, Hubner N, Hemmersbach R, et al. Differential gene expression of human chondrocytes cultured under short-term altered gravity conditions during parabolic flight maneuvers. Cell Commun Signal. 2015; 13: 18.
5. Qian A, Zhang W, Xie L, Weng Y, Yang P, Wang Z, et al. Simulated weightlessness alters biological characteristics of human breast cancer cell line MCF. Acta Astronaut. 2008; 63(7): 947-958.
6. Zheng H, Tian W, Yan H, Jiang H, Liu S, Yue L, et al. Expression of estrogen receptor α in human breast cancer cells regulates mitochondrial oxidative stress under simulated microgravity. Adv Space Res. 2012; 49(10): 1432-1440.
7. Kopp S, Sahana J, Islam T, Petersen AG, Bauer J, Corydon TJ, et al. The role of NFkB in spheroid formation of human breast cancer cells cultured on the Random Positioning Machine. Sci Rep. 2018; 8(1): 921.
8. Wuest SL, Richard S, Kopp S, Grimm D, Egli M. Simulated microgravity: critical review on the use of random positioning machines for mammalian cell culture. Biomed Res Int. 2015; 2015: 971474.
9. Ulbrich C, Wehland M, Pietsch J, Aleshcheva G, Wise P, van Loon J, et al. The impact of simulated and real microgravity on bone cells and mesenchymal stem cells. Biomed Res Int. 2014; 2014: 928507.
10. Kopp S, Slumstrup L, Corydon TJ, Sahana J, Aleshcheva G, Islam T, et al. Identifications of novel mechanisms in breast cancer cells involving duct-like multicellular spheroid formation after exposure to the Random Positioning Machine. Sci Rep. 2016; 6: 26887.
11. Coinu R, Chiaviello A, Galleri G, Franconi F, Crescenzi E, Palumbo G. Exposure to modeled microgravity induces metabolic idleness in malignant human MCF-7 and normal murine VSMC cells. FEBS Lett. 2006; 580(10): 2465-2470.
12. Kraus A, Luetzenberg R, Abuagela N, Hollenberg S, Infanger M. Spheroid formation and modulation of tenocyte-specific gene expression under simulated microgravity. Muscles Ligaments Tendons J. 2017; 7(3): 411-417.
13. Aleshcheva G, Sahana J, Ma X, Hauslage J, Hemmersbach R, Egli M, et al. Changes in morphology, gene expression and protein content in chondrocytes cultured on a random positioning machine. PLoS One. 2013; 8(11): e79057.
14. Warnke E, Pietsch J, Wehland M, Bauer J, Infanger M, Gorog M, et al. Spheroid formation of human thyroid cancer cells under simulated microgravity: a possible role of CTGF and CAV1. Cell Commun Signal. 2014; 12: 32.
15. Masiello MG, Cucina A, Proietti S, Palombo A, Coluccia P, D'Anselmi F, et al. Phenotypic switch induced by simulated microgravity on MDA-MB-231 breast cancer cells. Biomed Res Int. 2014; 2014: 652434.
16. Vorselen D, Roos WH, MacKintosh FC, Wuite GJ, van Loon JJ. The role of the cytoskeleton in sensing changes in gravity by non-specialized cells. FASEB J. 2014; 28(2): 536-547.
17. Xu W, Mezencev R, Kim B, Wang L, McDonald J, Sulchek T. Cell stiffness is a biomarker of the metastatic potential of ovarian cancer cells. PLoS One. 2012; 7(10): e46609.
18. Li SS, Xu LZ, Zhou W, Yao S, Wang CL, Xia JL, et al. p62/SQSTM1 interacts with vimentin to enhance breast cancer metastasis. Carcinogenesis. 2017; 38(11): 1092-1103.
19. Bockhorn J, Yee K, Chang YF, Prat A, Huo D, Nwachukwu C, et al. MicroRNA-30c targets cytoskeleton genes involved in breast cancer cell invasion. Breast Cancer Res Treat. 2013; 137(2): 373-382.
20. O'Connor K, Chen M. Dynamic functions of RhoA in tumor cell migration and invasion. Small GTPases. 2013; 4(3): 141-147.
21. Cirelli E, De Domenico E, Botti F, Massoud R, Geremia R, Grimaldi P. Effect of microgravity on aromatase expression in sertoli cells. Sci Rep. 2017; 7(1): 3469.
22. Paul A, Paul S. The breast cancer susceptibility genes (BRCA) in breast and ovarian cancers. Front Biosci (Landmark Ed). 2014; 19: 605-618.
23. Blaber EA, Finkelstein H, Dvorochkin N, Sato KY, Yousuf R, Burns BP, et al. Microgravity reduces the differentiation and regenerative potential of embryonic stem cells. Stem Cells Dev. 2015; 24(22): 2605-2621.
24. Hendrix A, Hume AN. Exosome signaling in mammary gland development and cancer. Int J Dev Biol. 2011; 55(7-9): 879-887.
25. Maniyar R, Chakraborty S, Suriano R. Ethanol enhances estrogen mediated angiogenesis in breast cancer. J Cancer. 2018; 9(21): 3874-3885.
26. Bayliss J, Hilger A, Vishnu P, Diehl K, El-Ashry D. Reversal of the estrogen receptor negative phenotype in breast cancer and restoration of antiestrogen response. Clin Cancer Res. 2007; 13(23): 7029-7036.
27. Li S, Wang L, Meng Y, Chang Y, Xu J, Zhang Q. Increased levels of LAPTM4B, VEGF and survivin are correlated with tumor progression and poor prognosis in breast cancer patients. Oncotarget. 2017; 8(25): 41282-41293.
28. Backlund PS Jr. Post-translational processing of RhoA. carboxyl methylation of the carboxyl-terminal prenylcysteine increases the half-life of Rhoa. J Biol Chem. 1997; 272(52): 33175-33180.
29. Feger BJ, Thompson JW, Dubois LG, Kommaddi RP, Foster MW, Mishra R, et al. Microgravity induces proteomics changes involved in endoplasmic reticulum stress and mitochondrial protection. Sci Rep. 2016; 6: 34091.

Original Article

6-Formylindolo[3,2-b]carbazole (FICZ) Enhances The Expression of Tumor Suppressor miRNAs, miR-22, miR-515-5p, and miR-124-3p in MCF-7 Cells

Keivan Mobini, Ph.D.[1], Elham Banakar, Pharm.D.[1], Gholamhossein Tamaddon, Ph.D.[2], Afshin Mohammadi-Bardbori, Ph.D.[1*]

1. Department of Pharmacology and Toxicology, School of Pharmacy, Shiraz University of Medical Sciences, Shiraz, Iran
2. Diagnostic Laboratory Sciences and Technology Research Center, School of Paramedical Sciences, Shiraz University of Medical Sciences, Shiraz, Iran

**Corresponding Address: P.O.Box: 1583-71345, Department of Pharmacology and Toxicology, School of Pharmacy, Shiraz University of Medical Sciences, Shiraz, Iran*
Email: toxicology@sums.ac.ir

Received: 18/November/2018, Accepted: 21/February/2019

Abstract

Objective: microRNAs (miRNAs) play bifunctional roles in the initiation and progression of cancer, and recent evidence has confirmed that unusual expression of miRNAs is required for the progress of breast cancer. The regulatory role of aryl hydrocarbon receptor (AhR) and its endogenous ligand, 6-formylindolo[3,2-b]carbazole (FICZ) on the expression of tumor suppressor miRNAs, miR-22, miR-515-5p and miR-124-3p, as well as their association with the estrogen receptor alpha (ERα) were the aims of this study.

Materials and Methods: In this experimental study, the expression levels of *miR-22, miR-515-5p, miR-124-3p* and *miR-382-5p* in MCF-7 cells were determined using the quantificational real time polymerase chain reaction (qRT-PCR) assay.

Results: Our results revealed that *miR-22, miR-515-5p,* and *miR-124-3p* expressions were significantly increased in cells transfected with ERα siRNA. Our data also showed that *miR-22, miR 515-5p*, and *miR-124-3p* expression levels were significantly increased following FICZ treatment. Here, we found that AhR/ERα cross-talk plays a critical role in the expression of *miR-22, miR-515-5p* and *miR-124-3p* in MCF-7 cells.

Conclusion: Overall, our data demonstrated that FICZ, as an AhR agonist could induce the expression of tumor suppressor miRNAs, *miR-22, miR-515-5p*, and *miR-124-3p*; thus, FICZ might be regarded as a potential therapeutic agent for breast cancer treatment.

Keywords: Aryl Hydrocarbon Receptor, Estrogen Receptor Alpha, 6-formylindolo[3,2-b]carbazole, Tumor Suppressor miRNAs

Cell Journal(Yakhteh), Vol 22, No 1, April-June (Spring) 2020, Pages: 115-120

Citation: Mobini K, Banakar E, Tamaddon Gh, Mohammadi-Bardbori A. 6-Formylindolo[3,2-b]carbazole (FICZ) enhances the expression of tumor suppressor miRNAs, miR-22, miR-515-5p, and miR-124-3p in MCF-7 cells. Cell J. 2020; 22(1): 115-120. doi: 10.22074/cellj.2020.6549.

Introduction

Breast cancer as a malignant neoplasm originated from the breast tissues, is still the most common cause of women death worldwide despite advances made in both diagnosis and treatment (1).

microRNAs (miRNAs) are single-stranded non-coding RNAs with small size that regulate some of biological processes such as cell proliferation, differentiation, migration and apoptosis. miRNAs play roles in post-transcriptional modification of mRNAs by binding to the 3'-untranslated regions (3'-UTRs) through complementary base pairing (2), resulting in cleavage/degradation of the mRNA and consequently, translational repression (3). miRNAs can function as either oncomiRs or tumor suppressors (4). Owing to their potential ability to regulate numerous protein-encoding genes, miRNAs are regarded as a promising new target in the development of clinical treatments (5). miRNAs were found to be over-expressed in various human diseases including cancers (6). *miR-22* regulates estrogen receptor alpha (ERα) target genes by direct binding to ERα 3'-UTR region (7) through both destabilizing mRNA and inhibiting translation (8). *miR-22* increases the radiosensitivity of breast cancer cells and inhibits tumorgenesis by targeting Sirt 1 (silent information regulator 1) (9). Moreover, miR-22 down-regulates the proto-oncogene ATP citrate lyase which inhibits the growth and metastasis of breast cancer cells (10).

miR-515-5p controls cancer cell migration through modulation of MARK4 (microtubule affinity-regulating kinase 4) 3'-UTR region (11). The *miR-124* expression is significantly suppressed in breast cancer cells (12). *miR-124-3p* appears to be a tumor suppressor in breast cancer cells and it acts via targeting CBL (Cbl proto-oncogene, E3 ubiquitin protein ligase) (13). However, the molecular pathways underlying *miR-124* modulatory actions in breast cancer cells are not

fully understood. Cyclin-dependent kinase 4 (CDK4), a master regulator of the cell cycle belonging to the CDK family (14), is identified as a major oncogenic driver among the cell cycle components (15); also, CDK4 has been found in several tumor types including breast (16) and lung cancers (17). It was shown that CDK4 is a target of miR-124 (12).

Development of breast cancer is closely associated with estrogen levels in the body. UDP-glucuronosyltransferase (UGT) is an important class of phase 2 drug metabolizing enzymes that plays a pivotal role in detoxification of steroid compounds. UGTs eliminate estrogen hormones and influence estrogen signaling pathway (18). UGT2B isoforms are involved in regulating cell proliferation in human cancer cells. The UGT2B4, 2B7 and 2B15 isoforms are also involved in the glucuronidation of biologically active lipids (19). *miR-382-5p* regulates UGT2B15 and UGT2B17 isoforms (20). The Ras GTPase superfamily member RERG (Ras-related and estrogen-related growth inhibitor) reduces breast cancer cells proliferation and tumor formation. RERG was shown to play a regulatory role in the Ras/ERK pathway. *miR-382-5p* directly represses RERG; therefore, *miR-382-5p* promotes viability, survival, migration and invasion of breast cancer cells (21).

The aryl hydrocarbon receptor (AhR) belongs to the family of basic helix-loop-helix nuclear transcription factors (22). The AhR downstream targets, cytochrome P450 (CYP1) isoforms, play bifunctional roles in detoxification or bioactivation of carcinogens, xenobiotics, and physiological compounds such as benzo(a)pyrene and estradiol (23). At the cellular level, AhR has functional interactions with signaling pathways governing cell proliferation and cell cycle, cell morphology, cell adhesion and cell migration (24). 6-formylindolo[3,2-b]carbazole (FICZ), a derivative of tryptophan (Trp) amino acid, is an ideal substrate for CYP1A1, 1A2, and 1B1 (25). FICZ also binds the AhR with the highest affinity known to date and thus, it reveals the characteristics of an endogenous signaling molecule (26-28). FICZ stimulates AhR-mediated activation of drug metabolizing enzymes such as CYP1A1 that end up its activity by generating a negative feedback control of its action (22, 25, 27-29).

This study was designed to reveal effects of FICZ, as an endogenous AhR ligand, on the expression levels of *miR-22*, *miR-515-5p*, *miR-124-3p* and *miR-382-5p* in MCF-7 breast cancer cell line.

Materials and Methods

Chemicals

6-formylindolo[3,2-b]carbazole (FICZ) was purchased from Syntastic AB, Sweden. 1-methyl-N-[2-methyl-4-[2-(2-methylphenyl)diazenyl] phenyl]-1H-pyrazole-5-carboxamide (CH223191) and 17β-Estradiol (E2), dimethyl sulfoxide (DMSO) were bought from Sigma-Aldrich, Germany. All cell culture reagents and media were purchased from Invitrogen.

Cell culture and chemical treatments

In this experimental study, MCF-7 cells were maintained in 10% fetal bovine serum (FBS)-supplemented Dulbecco's modified Eagle's medium (DMEM) containing 100 µg/mL streptomycin, and 100 IU/mL penicillin under an atmosphere containing 5% CO_2 at 37˚C. Cells were treated with desired concentrations of chemicals, after replacing the growth medium with fresh medium without FBS. The final concentration of DMSO was 0.1% (v/v).

Small interfering RNA treatments

SiRNA against ERα (Santa Cruz Biotechnology, CA, USA) was used for the targeted knockdown of ERα protein expression. Non-targeting scrambled siRNA (Santa Cruz Biotechnology, USA) was used as a control. MCF-7 cells were seeded in 6-well plates and grown in an antibiotic-free medium containing 5% FBS. At 50-60% confluence, the cells were transfected with 100 nM ERα siRNA or scrambled siRNA using lipofectamine 2000 (Invitrogen, USA) in 1 ml of transfection medium (Santa Cruz Biotechnology, USA). After 5 hours, the medium was replaced with fresh medium and 3 hours later, the cells were treated with DMSO, FICZ (1 nM), E2 (10 nM), and CH223191 (10 nM) for 18 hours.

RNA extraction and cDNA synthesis of miRNAs

The TRizol reagent (Invitrogen, Carlsbad, CA, USA) was used for isolation of total RNA according to the manufacturer's instructions; then, total RNA was reversely transcribed into cDNA by using the RT microRNA Kit (EXIQON, Denmark). The ERα mRNA in the cells was quantified by using the following primers:

F: 5′-GTTCTTAGTGGCACATCTTCTG-3′
R: 5′-GAATCCTCACGCTTAGTAACATAG-3′.

Real-time reverse transcription polymerase chain reaction (RT-PCR) amplification consisted of 40 cycles (95˚C for 5 seconds, 63˚C for 20 seconds, and 72˚C for 30 seconds) after an initial denaturation done at 95˚C for 5 minutes in an ABI StepOne™ real-time quantitative PCR system. The fold change of the miRNA expression was calculated by using the $2^{-\Delta\Delta Ct}$ method after normalization against the 5S rRNA (used as internal control) expression.

Statistical analysis

Statistical significance was determined by one-way ANOVA and Tukey test. The results are expressed as means ± SD for at least three separate (replicate) experiments for

each treatment group in the *in vitro* studies. P<0.05 were considered statistically significant.

Results

Effect of ERα on the expression of *miR-22, mir-515-5p, miR-124-3p* and *miR-382-5p,* in MCF-7 cells

In this study, MCF-7 cells were treated with E2 (10 nM) and our results revealed that *miR-22, miR-515-5p,* and *miR-124-3p* expressions were significantly increased and miR-382-5p were decreased. The expression of *miR-22, miR-515-5p,* and *miR-124-3p* were respectively 8, 2.46, and 2.29 times higher in the ERα-silenced cells than scrambled ones (Fig.1).

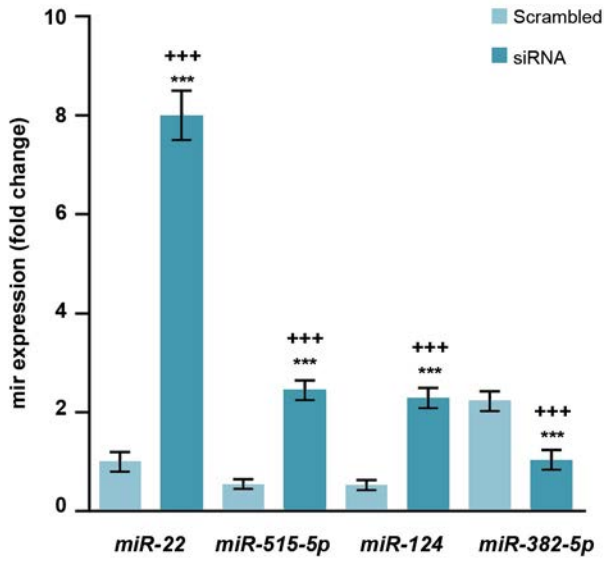

Fig.1: Expressions of *miR-22, miR-515-5p,* and *miR-124-3p* were inversely correlated with ERα in MCF-7. The cells were treated with E2 (10 nM) and the levels of *miR-22, miR-515-5p, miR-124-3p* and *miR-382-5P* were measured using real-time RT-PCR. Values are expressed as means ± SE. Asterisks denote significant differences (***; P<0.001) between control and other treated groups and significant differences (+++; P<0.001) between cells treated with siRNA and those treated with scrambled siRNA. ERα; Estrogen receptor alpha and RT-PCR; Real-time reverse transcription polymerase chain reaction.

Effect of AhR on the expression of *miR-22, mir-515-5p, miR-124-3p* and *miR-382-5p,* in MCF-7 cells

MCF-7 cells were treated with an AhR agonist, FICZ (1 nM) or an AhR antagonist, CH223191 (10 nM) either alone or in combinations, our data showed that the *miR-22, miR515-5p,* and *miR-124-3p* expression levels were significantly increased by FICZ and CH223191 treatments. The expression of *miR-22, miR515-5p,* and *miR-124-3p* in FICZ, CH223191 and FICZ+CH223191 treated groups were respectively 12.55, 7.94, 7.46; 4.75, 2.21, 3.7 and 8.69, 2.29, 5.27 times higher than the control group (Figs.2-4). *miR-382-5p* expression levels significantly decreased in cells treated with FICZ+ CH223191 (Fig.5).

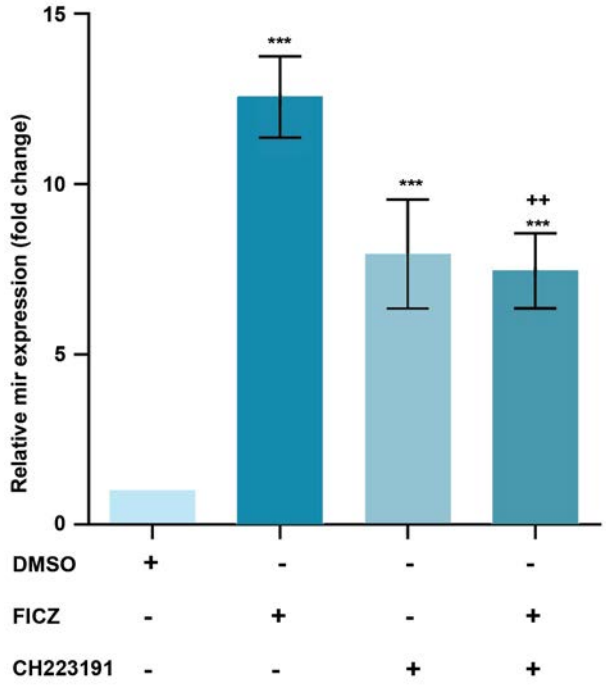

Fig.2: Expression of *miR-22* was AhR-dependent in MCF-7. The quantitative RT-PCR analysis showed that the expression level of *miR-22* was much higher in the cells treated with FICZ in comparison to control. Values are expressed as mean ± SE. Asterisks denote significant differences (***; P<0.001) between control and other treated groups and significant differences (++; P<0.001) between cells treated with FICZ and the cells treated with FICZ+ CH223191. AhR; Aryl hydrocarbon receptor, RT-PCR; Real-time reverse transcription polymerase chain reaction, and FICZ; 6-formylindolo[3,2-b]carbazole.

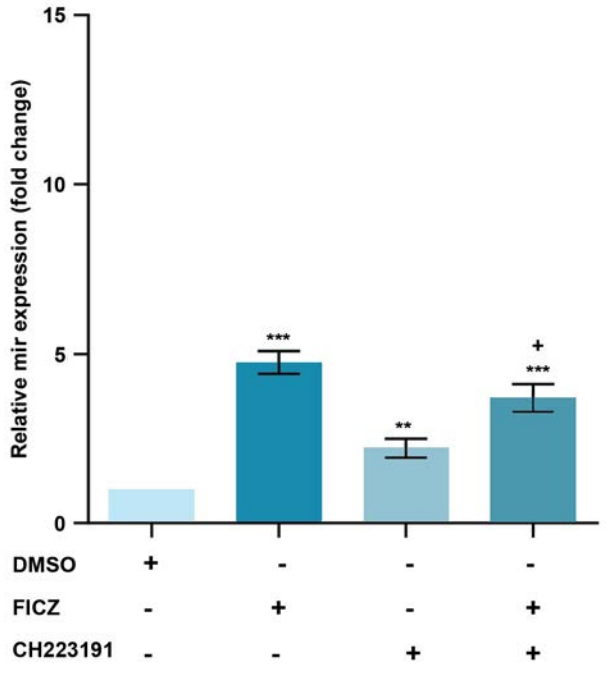

Fig.3: Expression of *miR-515-5p* was AhR-dependent in MCF-7. The quantitative RT-PCR analysis showed that the expression levels of *miR-515-5p* were much higher in the cells treated with FICZ in comparison to control. Values are expressed as mean ± SE. Asterisks denote significant differences (**; P<0.01 and ***; P<0.001) between control and other treated groups and significant differences (+; P<0.05) between cells treated with FICZ and the cells treated with FICZ+ CH223191. AhR; Aryl hydrocarbon receptor, RT-PCR; Real-time reverse transcription polymerase chain reaction, and FICZ; 6-formylindolo[3,2-b]carbazole.

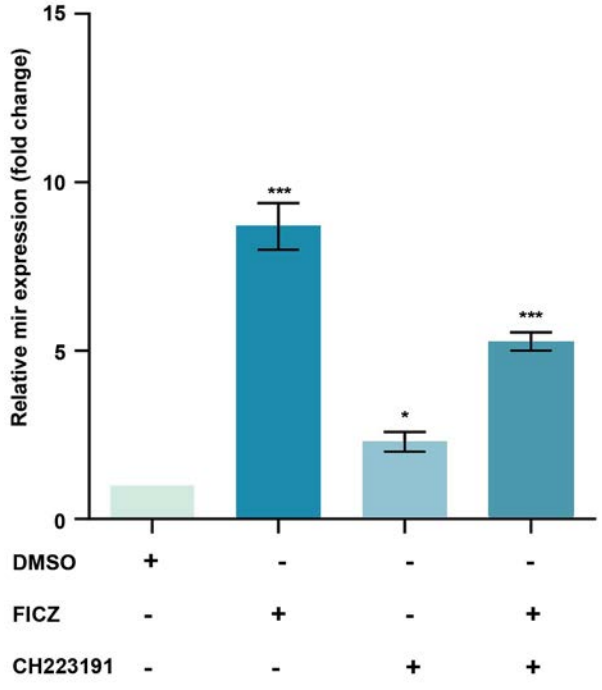

Fig.4: Expression of *miR-124-3p* was AhR-dependent in MCF-7. The quantitative RT-PCR analysis showed that the expression levels of *miR-124-3p* were much higher in the cells treated with FICZ in comparison to control. Values are expressed as mean ± SE. Asterisks denote significant differences (*; P<0.05 and ***; P<0.001) between control and other treated groups. AhR; Aryl hydrocarbon receptor, RT-PCR; Real-time reverse transcription polymerase chain reaction, and FICZ; 6-formylindolo[3,2-b] carbazole.

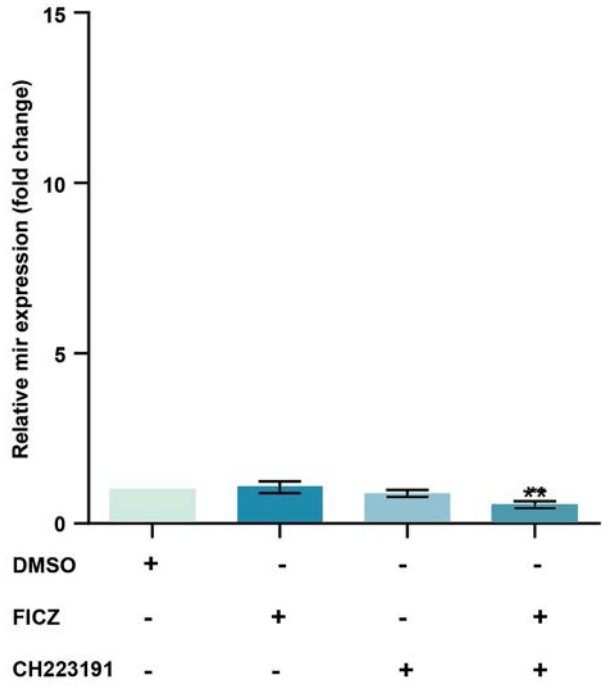

Fig.5: Expression of *miR-382-5p* was AhR-dependent in MCF-7. The quantitative RT-PCR analysis showed that the expression levels of *miR-382-5p* were much lower in the cells treated with FICZ+CH223191 in comparison to control.. Values are expressed as mean ± SE. Asterisks denote significant differences (**; P<0.01) between control and other treated groups. AhR; Aryl hydrocarbon receptor, RT-PCR; Real-time reverse transcription polymerase chain reaction, and FICZ; 6-formylindolo[3,2-b] carbazole.

Discussion

miRNAs are stable biomarkers as they have high stability in extreme conditions such as low pH and high temperatures (30) and are used as prognostic and therapeutic tools for breast cancer (31).

In ERα silencing cells, we observed significantly increased expression levels of *miR-22, miR-515-5p,* and *miR-124-3p*. Furthermore, FICZ treatments led to over-expression of *miR-22, miR-515-5p,* and *miR-124-3p*.

miR-22 regulates ERα target genes by direct binding to the ERα 3'-UTR region (7) through both destabilizing and inhibiting translation of mRNA (8). *miR-22* represses *CD147* expression by directly targeting the *CD147* 3'UTR site. *miR-22* also indirectly participates in the CD147 modulation by down-regulating Sp1. Indeed, *CD147* is overexpressed in breast cancer tissues, and its high expression is correlated with tumor invasion and metastasis (32). The transcription factors Sp1 could bind to the *CD147* promoter and enhance its expression as well. In addition, low miR22 levels are significantly associated with poor differentiation of breast cancer cells. Furthermore, *SIRT1* (Sirtuin1) expression levels are significantly up-regulated in breast cancer tissues. Since *miR22* has suppressive effects on breast cancer cells via targeting *SIRT1*, miR22/SIRT1 axis may be used as a novel and potential therapeutic target for breast cancer treatment (33).

Sphingo kinase-1 (SK1) mediates cell proliferation in cancer cells. *miR-515-5p* targets SK1 and inhibits breast cancer cells growth. Previous studies reported that SK1 mediates estrogen-dependent tumorigenesis in MCF-7 cells and estradiol down-regulates *miR-515-5p* expression but increases SK1 activity (34). *miR-124* targets Slug (SNAI2, transcriptional repressor of E-cadherin) and regulates epithelial-mesenchymal transition and metastasis of breast cancer cells (35). *miR-124* also suppresses breast cancer cells growth and motility by targeting CD151 (36). Moreover, *miR-124-3p* inhibits tumor metastasis by inhibiting *PDCD6* expression. In this regard, miR-124-3p/PDCD6 signaling axis may be a potential target for treatment of patients with advanced breast cancer.

Our results showed that ERα silencing significantly led to *miR-382-5p* down-regulation. *miR-382-5p* targets UDP-glucuronosyl transferases (UGTs) (20) which are involved in the detoxification of estrogen derivatives (18). Thus, *miR-382-5p* down-regulation may enhance estrogen detoxification. One of the new findings of the present study was that ERα silencing or FICZ treatment led to up-regulation of *miR-22, miR-515-5p,* and *miR-124-3p*. ERα suppresses Drosha (one of the main processing enzymes in miRNA biogenesis) activity in MCF-7 cells (37). Therefore, we suggest that silencing ERα may enhance tumor suppressor miRNAs such as *miR-22, miR-515-5p* and *miR-124-3p*.

A number of studies reported that AhR-ARNT complex

may reduce ERα-mediated transactivation (38) either directly by binding the inhibitory site of XRE (iXRE) or by employing shared coactivators (39).

Some reports also indicated that ERα can be activated by AhR agonists, but not by AhR antagonists (40). However, AhR antagonists may exhibit a partial effect.

Conclusion

Our data demonstrated that the overexpression of tumor suppressor miRNAs including *miR-22, miR-515-5p,* and *miR-124-3p* by FICZ, as an AhR agonist, might be considered a potential therapeutic approach against breast cancer.

Acknowledgements

The authors wish to express their appreciation to Shiraz University of Medical Sciences, Shiraz, Iran. Authors of this manuscript have no competing financial, professional or personal interests. This work was financially supported by Shiraz University of Medical Sciences [grant numbers: 11364; 15756; and 15383].

Authors' Contributions

K.M., E.B., Gh.T., A.M.-B.; Participated in study design, data collection and evaluation, manuscript drafting and statistical analysis. K.M., E.B.; Conducted molecular experiments and RT-qPCR analysis. All authors approved the final version of this paper for submission.

References

1. DeSantis C, Ma J, Bryan L, Jemal A. Breast cancer statistics, 2013. CA Cancer J Clin. 2014; 64(1): 52-62.
2. Bartel DP. MicroRNAs: genomics, biogenesis, mechanism, and function. Cell. 2004; 116(2): 281-297.
3. Chen SM, Chou WC, Hu LY ,Hsiung CN, Chu HW, Huang YL, et al. The effect of microRNA-124 overexpression on anti-tumor drug sensitivity. PLoS One. 2015; 10(6): e0128472.
4. Calin GA, Croce CM. MicroRNA signatures in human cancers. Nat Rev Cancer. 2006; 6(11): 857-866.
5. Greene SB, Herschkowitz JI, Rosen JM. Small players with big roles: microRNAs as targets to inhibit breast cancer progression. Curr Drug Targets. 2010; 11(9): 1059-1073.
6. Lu M, Zhang Q, Deng M, Miao J, Guo Y, Gao W, et al. An analysis of human microRNA and disease associations. PLoS One. 2008; 3(10): e3420.
7. Pandey DP, Picard D. miR-22 inhibits estrogen signaling by directly targeting the estrogen receptor α mRNA. Mol Cell Biol. 2009; 29(13): 3783-3790.
8. Xiong J, Yu D, Wei N, Fu H, Cai T, Huang Y, et al. An estrogen receptor alpha suppressor, microRNA-22, is downregulated in estrogen receptor alpha-positive human breast cancer cell lines and clinical samples. FEBS J. 2010; 277(7): 1684-1694.
9. Zhang X, Li Y, Wang D, Wei X. miR-22 suppresses tumorigenesis and improves radiosensitivity of breast cancer cells by targeting Sirt1. Biol Res. 2017; 50(1): 27.
10. Liu H, Huang X, Ye T. MiR-22 down-regulates the proto-oncogene ATP citrate lyase to inhibit the growth and metastasis of breast cancer. Am J Transl Res. 2018; 10(3): 659-669.
11. Pardo OE, Castellano L, Munro CE, Hu Y, Mauri F, Krell J, et al. miR-515-5p controls cancer cell migration through MARK4 regulation. EMBO Rep. 2016; 17(4): 570-584.
12. Feng T, Xu D, Tu C, Li W, Ning Y, Ding J, et al. MiR-124 inhibits cell proliferation in breast cancer through downregulation of CDK4. Tumour Biol. 2015; 36(8): 5987-5997.
13. Wang Y, Chen L, Wu Z, Wang M, Jin F, Wang N, et al. miR-124-3p functions as a tumor suppressor in breast cancer by targeting CBL. BMC Cancer. 2016; 16(1): 826.
14. Malínková V, Vylíčil J, Kryštof V. Cyclin-dependent kinase inhibitors for cancer therapy: a patent review (2009-2014). Expert Opin Ther Pat. 2015; 25(9): 953-970.
15. Choi HH, Phan L, Chou PC, Su CH, Yeung SC, Chen JS, et al. COP1 enhances ubiquitin-mediated degradation of p27Kip1 to promote cancer cell growth. Oncotarget. 2015; 6(23): 19721-19734.
16. Lu J. Palbociclib: a first-in-class CDK4/CDK6 inhibitor for the treatment of hormone-receptor positive advanced breast cancer. J Hematol Oncol. 2015; 8: 98.
17. Guo F, Yu F, Wang J, Li Y, Li Y, Li Z, et al. Expression of MALAT1 in the peripheral whole blood of patients with lung cancer. Biomed Rep. 2015; 3(3): 309-312.
18. Zhou X, Zheng Z, Xu C, Wang J, Min M, Zhao Y, et al. Disturbance of mammary UDP-glucuronosyltransferase represses estrogen metabolism and exacerbates experimental breast cancer. J Pharm Sci. 2017; 106(8): 2152-2162.
19. Dates CR, Fahmi T, Pyrek SJ, Yao-Borengasser A, Borowa-Mazgaj B, Bratton SM, et al. Human UDP-glucuronosyltransferases: effects of altered expression in breast and pancreatic cancer cell lines. Cancer Biol Ther. 2015; 16(5): 714-723.
20. Wijayakumara DD ,Hu DG, Meech R, McKinnon RA, Mackenzie PI. Regulation of human UGT2B15 and UGT2B17 by miR-376c in prostate cancer cell lines. J Pharmacol Exp Ther. 2015; 354(3): 417-425.
21. Ho J-Y, Hsu R-J, Liu J-M, Chen S-C, Liao G-S, Gao H-W, et al. MicroRNA-382-5p aggravates breast cancer progression by regulating the RERG/Ras/ERK signaling axis. Oncotarget. 2017; 8(14): 22443-22459.
22. Wincent E, Amini N, Luecke S, Glatt H, Bergman J, Crescenzi C, et al. The suggested physiologic aryl hydrocarbon receptor activator and cytochrome P4501 substrate 6-formylindolo [3, 2-b] carbazole is present in humans. J Biol Chem. 2009; 284(5): 2690-2696.
23. Nebert DW, Dalton TP. The role of cytochrome P450 enzymes in endogenous signalling pathways and environmental carcinogenesis. Nat Rev Cancer. 2006; 6(12): 947-960.
24. Mohammadi-Bardbori A, Bastan F, Akbarizadeh AR. The highly bioactive molecule and signal substance 6-formylindolo[3,2-b]carbazole (FICZ) plays bi-functional roles in cell growth and apoptosis in vitro. Arch Toxicol. 2017; 91(10): 3365-3372.
25. Wincent E, Bengtsson J, Mohammadi Bardbori A, Alsberg T, Luecke S, Rannug U, et al. Inhibition of cytochrome P4501-dependent clearance of the endogenous agonist FICZ as a mechanism for activation of the aryl hydrocarbon receptor. Proc Natl Acad Sci USA. 2012; 109(12): 4479-4484.
26. Mohammadi-Bardbori A, Vikstrom Bergander L, Rannug U, Rannug A. NADPH oxidase-dependent mechanism explains how arsenic and other oxidants can activate aryl hydrocarbon receptor signaling. Chem Res Toxicol. 2015; 28(12): 2278-2286.
27. Mohammadi-Bardbori A, Bengtsson J, Rannug U, Rannug A, Wincent E. Quercetin, resveratrol, and curcumin are indirect activators of the aryl hydrocarbon receptor (AHR). Chem Res Toxicol. 2012; 25(9): 1878-1884.
28. Omidi M, Ghafarian-Bahraman A, Mohammadi-Bardbori A. GSH/GSSG redox couple plays central role in aryl hydrocarbon receptor-dependent modulation of cytochrome P450 1A1. J Biochem Mol Toxicol. 2018: e22164.
29. Mohammadi-Bardbori A, Akbarizadeh AR, Delju F, Rannug A. Chromatin remodeling by curcumin alters endogenous aryl hydrocarbon receptor signaling. Chem Biol Interact. 2016; 252: 19-27.
30. Mitchell PS, Parkin RK, Kroh EM, Fritz BR, Wyman SK, Pogosova-Agadjanyan EL, et al. Circulating microRNAs as stable blood-based markers for cancer detection. Proc Natl Acad Sci USA. 2008; 105(30): 10513-10518.
31. Koufaris C, Valbuena GN, Pomyen Y, Tredwell GD, Nevedomskaya E, Lau CH, et al. Systematic integration of molecular profiles identifies miR-22 as a regulator of lipid and folate metabolism in breast cancer cells. Oncogene. 2016; 35(21): 2766-2776.
32. Kong LM, Liao CG, Zhang Y, Xu J, Li Y, Huang W, et al. A regulatory loop involving miR-22, Sp1 and c-Myc modulates CD147 expression in breast cancer invasion and metastasis. Cancer Res. 2014; 74(14): 3764-3778.
33. Zou Q, Tang Q, Pan Y, Wang X, Dong X, Liang Z, et al. MicroRNA-22 inhibits cell growth and metastasis in breast cancer via targeting of SIRT1. Exp Ther Med. 2017; 14(2): 1009-1016.
34. Sukocheva OA, Wang L, Albanese N, Pitson SM, Vadas MA, Xia P.

Sphingosine kinase transmits estrogen signaling in human breast cancer cells. Mol Endocrinol. 2003; 17(10): 2002-2012.
35. Liang YJ, Wang QY, Zhou CX, Yin QQ, He M, Yu XT, et al. MiR-124 targets Slug to regulate epithelial–mesenchymal transition and metastasis of breast cancer. Carcinogenesis. 2012; 34(3): 713-722.
36. Han Z-B, Yang Z, Chi Y, Zhang L, Wang Y ,Ji Y, et al. MicroRNA-124 suppresses breast cancer cell growth and motility by targeting CD151. Cell Physiol Biochem. 2013; 31(6): 823-832.
37. Yamagata K, Fujiyama S, Ito S, Ueda T, Murata T, Naitou M, et al. Maturation of microRNA is hormonally regulated by a nuclear receptor. Mol Cell. 2009; 36(2): 340-347.
38. Rüegg J, Swedenborg E, Wahlström D, Escande A, Balaguer P, Pettersson K, et al. The transcription factor aryl hydrocarbon receptor nuclear translocator functions as an estrogen receptor β-selective coactivator, and its recruitment to alternative pathways mediates antiestrogenic effects of dioxin. Mol Endocrinol. 2008; 22(2): 304-316.
39. Matthews J, Gustafsson J-Å. Estrogen receptor and aryl hydrocarbon receptor signaling pathways. Nucl Recept Signal. 2006; 4: e016.
40. Beischlag TV, Perdew GH. ER alpha-AHR-ARNT protein-protein interactions mediate estradiol-dependent transrepression of dioxin-inducible gene transcription. J Biol Chem. 2005; 280(22): 21607-21611.

Ethics, Legal, Social, Counseling Article

Investigation of Stem cells Technology in The Light of Jurisprudential Documents

Ahmad Pourebrahim, Ph.D.[1], Iraj Goldouzian, Ph.D.[2]*, Ahmad Ramezani, Ph.D.[3]

1. Department of Law, Qeshm Branch, Islamic Azad University, Qeshm, Iran
2. Department of Law, Tehran University, Tehran, Iran
3. Department of Law, University of Knowledge and Culture, Tehran, Iran

Corresponding Address: P.O.Box: 7953163135, Department of Law, Tehran University, Tehran, Iran
Email: igoldoz@ut.ac.ir

Received: 16/May/2018, Accepted: 13/March/2019

Abstract

Objective: The aim of this study is investigation of Stem cells Technology in The Light of Jurisprudential Documents.

Materials and Methods: In this analytical-descriptive research, we collected the relevant data through a literature search. We have used PubMed, ScienceDirect, Google Scholar, Iranian databases like SID, Iran doc, Iranian law and also Islamic resources for this study.

Results: There are so many controversies about safety of these cells and possible dangers for human body. As in Iran, laws of stem cells are not clear. Elimination of barriers requires drafting laws compatible with regional and cultural beliefs of Iranian people. Unfortunately, available laws could not keep up with the advances.

Conclusion: Iran juridical system should conduct and restrict actions in the area of stem cells technology by gathering experts of different political, science, medicine, social and mindful who are familiar with law, according to notions of intellectual jurists and legislators, Islam and Shia religious.

Keywords: Embryo, Jurisprudential, Law, Stem Cell

Cell Journal(Yakhteh), Vol 22, No 1, April-June (Spring) 2020, Pages: 121-127

Citation: **Pourebrahim A, Goldouzian I, Ramezani A. Investigation of stem cells technology in the light of jurisprudential documents. Cell J. 2020; 22(1): 121-127. doi: 10.22074/cellj.2020.5694.**

Introduction

Today, stem cells technology is considered a new approach in treatment of diseases and it has brought hope for production and recovery of body tissues and organs by tissue engineering and regenerative medicine. The world's great tendency for this technology is because it is promising approach for treatment of diseases. It is predicted that the countries which have this technology are going to be internationally rated as powerful countries. In parallel with the development of this technology, many ethical and religious issues have been raised. Scientific developments, usually encounter moral and religious issues. The research involving embryo stem cells has similar matters in question. Performing experiments on human embryo is still a matter of debate. Since the status of jurisprudence in Iran in the field of stem cells is not obvious and unfortunately the existing regulations could not go along with these developments, the development of legal and institutional infrastructures is considered as the main priority. In order to develop this technology, it is necessary to review the rules of the leading countries in the field of cell therapy technology to draft new laws (1). In this regard, although Shia jurisprudence does not ban these studies, jurisprudential views must be taken serious in this regard (2). Although manipulation of human embryo is a matter of discussion from Shia jurisprudence point of view. In this paper we discussed ethical, legal and religious issues about stem cell research and usage along with pointing to the research on human embryos according to Shia jurisprudence.

Materials and Methods

This analytical-descriptive research gathered the relevant data through a literature search. In this study, we described the relationship between the human being and his own stem cells based on the Islamic point on permission and reverence of stem cells technology. We have used PubMed, ScienceDirect, Google Scholar, Iranian databases like SID and Iran doc and also Iranian law and Islamic resources for this review.

Stem cells

Stem cells are undifferentiated cells that have the ability of proliferation and differentiation into other cells of the body and can be obtained from four sources: i. Human embryo, ii. Adult tissues, iii. Cord blood and iv. Induced pluri-potential stem cells (IPS) which are produced from skin cells (fibroblasts) and adult. In 1998, scientists successfully extracted these cells from the human spare embryos remaining unused from *in vitro* fertilization (IVF). Adult stem cells can be found in many specialized tissues including the brain, bone marrow, liver, skin, digestive system cord blood can be obtained from umbilical cord of new born and IPSs are produced by inserting genes in fibroblast cells (3). But as these cells have different potencies of proliferation and differentiation, some of them may not exhibit the

expected performance. Embryonic stem cells have the highest power among them that cannot be ignored

Stem cells are expected to be used for repairing the damaged cells of heart, repairing the bone tissues, treatment of nerve diseases and lesions, repairing burn and skin lesions, improving the pancreas and insulin secretion, testing the effectiveness of new medicines, practicing transplantation, producing sperm and ovum, etc… (4).

Stem cells research in Islamic societies

According to Islam, scientists are not only responsible for medical research for treatment of untreatable diseases, but they are also responsible for proving the benefits of research on embryo for treatment of diseases. Thus, related documents proving that justifies researches on stem cells according to corresponds with moral-religious and functional theory in Islamic world, should be provided. So, Islamic jurists should evaluate the advantages and disadvantages of stem cell research by considering Islamic values in relation with the importance of moral status of human embryo. There are some debates among religious scholars whether embryo possesses personhood and moral and legal dignity or not. According to moral-divine considerations of the catholic religion, the developmental stages of embryo's growth pass till reaching the personality; in this regard transmigration of the soul and shaping the personality of the embryo happen just after fertilization (5).

Criminal justice system determines the blood money *(DIAA)* of the embryo based on the age of it and the cause of abortion. Under some conditions, law considers the embryo as a part of the mother's body (please refer to therapeutic abortion law). In the field of IVF technology, scholars spiritually discriminate between an implanted embryo and supernumerary embryos. In this regard, an implanted embryo has the life rights but the supernumerary embryo is regarded as an aborted embryo, because it is out of the womb and transmigration of the soul did not occur. Thus, there is no punishment for discarding of this kind of embryo before being placed in womb, using these embryos for stem cell researches is allowed because they are potential sources of treatment (6).

Islamic jurists don't permit all aspects of using supernumerary embryo because in such permission it seems to treat human beings as a product. Human embryo contains potential life power and it deserves respect but not dignity from the beginning. If the previous statement was not right, why should Islamic criminal laws assign penalty for intentional abortion in its early stages of development but after implantation? The Quran description of the development of embryo till ensoulment and reaching human dignity is an emphasis on the gradualness of establishment of human personhood in human embryo (6).

This mysterious issue in Islam is shown by terms used for different stages of embryo development from the fertilized egg, blastocyst, and embryo in the womb till birth that are exactly noted in various religious texts. These texts also discuss ensoulment. Checking the majority of religious terms used for "abortion" shows related spiritual and legal dignity issues with more details. In Shia rules, similar to catholic rules, abortion of the embryo is a sin, but in contrary to Catholics' beliefs, some Shia jurists believe that human life begins at the implantation time. Some people based on the Holly prophet's statements, believe that ensoulment happens at the end of the 4 months (i.e. 120 days) of pregnancy.

So it can be said that the Quran's silence about the embryo's dignity has given the jurists the possibility to distinguish between the bio and spiritual personality. Definition of levels of the embryo development, at least in the first 3 months of pregnancy, Jurists consider the punishment for abortion of implanted embryos but not for laboratory embryos in the IVF clinics and allow the use of the supernumerary embryos for stem cells researches. Also, as beliefs approve the possibility of the embryo's life in the last stages of embryo development and since there is no discussion over the development of spiritual capacity of the embryo at first stages, the Islamic jurists require moral justification about using embryos for extracting stem cells (6). Therefore, according to Islam and some scholars, study and research on the embryo for therapeutic purposes can be accepted if done before ensoulment.

Stem cells research in Christianity

Roman and Orthodox Catholics believe that there is a connection between humanity and fertilization and development continues till human being reach the stage at which he could physically and spiritually have a picture of God, so all stages of development must be regarded as "HOLY". The Roman Catholic Church opposes the use of fetus in research and treatment. According to the Catholics, human comes to life from the moment of fertilization. Therefore, the human embryo is considered as a complete human and has the right to live, and all embryos must have a chance of development to a complete human and be born. Therefore, it is unacceptable to deliberately eliminate an embryo, even for medical purposes. The IVF process, which normally generates surplus embryos with the potency for becoming humans and making them a fetal source for research, is not a legitimate procedure in the view of Catholic Church. Protestants believe in pluralism and they do not have single source for making decisions and releasing the divine commands to be referred by Christians. Protestant beliefs about stem cells should be judged by the conscience of each individual. According to them, different people can have different ideas on a common topic, and these beliefs must be consistent with Christian beliefs. Some protestant branches believe that a perfect human is gradually created; so, this person may not exist in that primary cell mass and some others believe that ensoulment happens after day 14 of gestational age (7).

Stem cells researches in Judaism

Based on the Bible and the Jewish legal rules (Talmud), the human identity does not establish at the moment of fertilization, but during the growth in the mother's womb. The fetus is a part of mother's body as long as it is inside the mother's body. Also, at the birth, the fetus is regarded as a complete human being similar to his mother. Before the first forty days, even as long as the fetus is in the womb, it does not have the moral and legal status of a person, because according to the Jews, the fetus remains as water until the forty days after fertilization (7).

The type of relationship between the human being and his own stem cells based on Islamic point of view

At the first glance, the relationship between human being and his own tissues and stem cells was not exclusively discussed in juridical texts alone but in attachments to this topic, organ transplants have been discussed. Since tissues and adult stem cells are found in the organs, the religious view about the relationship between man and his body, is applicable for tissues and stem cells (8).

Stem cells transplantation, is a new phenomenon; so, in juridical texts and traditional laws, it has not been discussed; but, contemporary scholars have discussed and many of them accept organ transplantation from living donor, cadaver and brain dead. Using body organs for organs transplants has two ways: auto graft which is transplantation of humans own tissue to himself or heterograft which is grafting the tissue from a person to someone. From jurists' point of view, transplantation is allowed following receiving donor's consent and in the case of living donor permitted if complications of organs transplantation are compensated (9).

To answer the question that whether a man is the owner of his body and he can sell his body organs, tissues, and cells, the Muslim jurists have discussed and it was concluded that human body does not have a price thus it cannot be sold. If the part of the human body is sold as goods, in fact the dignity of human has been compromised (10) based on the holy Quran (11). In this respect, selling human parts and sale contract is not allowed. Unlike paying a price for human part to the donor which is banned, expenses of organ transplantation process including the physician, hospital, etc. can be paid with no problem but just for organ donor who is volunteer of this process, receiving money is banned. Late supreme leader of Iran, Emam Khomeini (peace be upon him) regarded the person as the owner of his body but the ownership was different from ownership of properties. However, from this difference he does not conclude that the human cannot decide for his body, but he believes that a person can decide for his body for treatment as he wishes except for the cases in which there is a legal or religious prevention (12).

It is obvious that the relationship between the man and organs or tissues of the body cannot be in the form of benefit rights (13) because the profit right is for the lands and properties, thus the profit right cannot be used for body organs. Also, according to the definition of profit right (14), it cannot be applied for the relationship between the man and his organs because for proving this, one must be able to transfer the right to use of his organs to another person by a contract (usufruct right) so, recipient person would be the owner based on transfer the usufruct right to him, in fact, everyone from the birth is the natural owner of his body organs and this kind of relationship indicates that nobody else can be the owner of another person's body organs (13). Concerning the relationship between the man and his body organs and cells, there are three ideas in Islam that whether the man is able to donate his tissue, cells, and organs to somebody else or has the permission to sell/buy tissues, cells, and organs.

The relationship of domination and capture

Some jurists indicated that the human has absolute power over his body (monarchy) (13, 15). In this way, "monarchy" can be used, like people's absolute power on their body which is a logical phenomenon. Like the way that human has power over his properties, he also has power over his self from any aspect, but based on this view point, organ donation can be permitted (16). Also, the Islamic rule that says: the people are predominant on their properties and lives (17) as a juridical rule describes the human "monarchy" on his body. According to the monarchy and the effects it has, the term natural ownership is better for this relationship (8).

Trust relationship

Some jurists believe humans are the God's properties trustee and they believe human lacks any ownership of his body organs and they believe he does not have any ownership even benefits or shared ownership (18). Based on the above idea, humans are protectors of their body and soul which is against the human freedom authority. Additionally, we are allowed to seize body organs to the extent that the religion permits while the trustee cannot seize but for protection.

Ownership relationship

But most of the jurists have called the relationship between the human and his body organs an "ownership relationship". Based on this idea, some jurists believe that in punishment amputation (for example in nemesis or theft), the amputated organ belongs to the person whose organ has been amputated (19). Overall, from the juridical view, human ownership of his body organs is a matter of controversy; these debates are expressed and explained below:

Formative ownership relationship

Some jurists believe that the existence of something depends directly upon the existence of human beings; in this regard, if we do not exist they could not exist either, they are not separate from us, and so they are our properties. Like body organs and five senses that because

of the formative ownership that we have on our body, we are the real owners of them (20). But it seems that we cannot accept this kind of relationship between the human and his body organs because human does not have this kind of complete ownership and authority on his body, while human in religious and juridical sources is banned from harming his body (16).

The relation of credit possession

The credit possession established by a clergy jurist or common law is determined for the person who is credited and its area is also determined. Therefore, the source of this kind of possession is wisdom and common law given by the jurist's signature. Due to the person possession on his/her own body organs is a rational thing that is discovered through the intellectuals unanimous and their practical collusion, and it is not rejected or is defined by the jurist who is the one of the intellectuals, so this kind of possession agrees the religious law (21). Furthermore, unlike the previous statements that says the body organs had no fiscal value, today, common law considers a great value for it and according to the common law, a kind of possession is credited for it. Of course, this problem is acceptable by the intellectual just in special situation that it does not involve some of harmful possessions, so this credit possession lacks free will and unconditional authority which primarily is one of the features of the right possession.

At the same time, the credit possession is the result of state and forging. So, a forging should be done by a jurist or it is created according to the rational basis when there is no prevention by the jurist. While it cannot be said that this kind of ownership is absolutely accepted by intellectuals, although the intellectuals preferred donation of organ to another person and they accepted saving the life even payment as compensation, from the point of view of intellectuals, these are not important reasons for accepting the personal ownership of body organs like properties; also, it can be the only reason for the personal dominance over her/his body organs (16).

Concerning credit possession of people on their body organs, it can be said that: first, the source of this it, is not issued by clergy scholars but is the rational deduction, and in religious contexts this rational basis is not improved yet or at least it is uncertain; second, it is assumed that acceptance of this idea faces a lot of limitations that turns its situation into "dominance right and possession" (8).

The relation of innate possession

Personal ownership of organs can be defined as "the relation, dominance or any permanent right that arranged between mankind and his/her organs and the legislator validated it and with such right, the person can have authority of his/her own organs legally, in a way that they can benefit from all possible profits and no one can prevent them" (13). Most religious scholars approve the idea that the human an original ownership of his own organs (21, 22).

Intuitional and rational approaches also approve such kind of ownership and authority, as the religious scholars and law. Many phrases are common in the language of religious scholars and law that validate the presented relation and significance discussions including "protection of the human body integrity" that indicate that the legislator respect such dominance and mastery (8).

The religious view on permission of stem cells technology

Legit rule and the legitimate law

Legit rule *"ESALAT al EBAHA"* means everything is acceptable and lawful unless there is a clear order against it in Islamic texts. In case there is no reason for the permission or prohibition, the law considers it "permissible" (23). The law or legitimate rule is also equipoised as the legit rule. Based on this rule, human has a right of any involvement and occupation of things nearby (24).

Legit rule and the legitimate law are the bases for clergy scholars to permit new topics of life technology.

The human ownership of their organs and cells

A) With reference to the prophetic tradition "people have dominance over their body and property" (25). This rule shows the authority of people over their own properties and body; thus, people must legally have this authority different organs of their body.

B) Sacrifice is praised: "is there anyone who sells his life just for God sake? (it resembles Imam Ali (peace be upon him) who slept in prophet's bed in the night of prophet's migration to Madina), and God is compassionate and kind with his servants" (26). This verse indicates that God gives the option of personhood to human and it is for this reason that he takes action of sacrificing for a good reason like altruism (27).

According to the first rule, people rightfully own their body organs and cells, so they have the right to sacrifice it. Based on this view, there is no difference between sacrificing and donation of an organ or cells for saving the life of a Muslim (22). Concerning this argument, it should be said that it is correct according to dominance law that everyone has the complete authority on oneself and owns properties and they are free; however, the holly religion Islam has defined some limit and boundaries for this freedom that must have benefit and no harm from this freedom, it should be within religious rules framework and does not interfere with others rights. The ownership of body is limited to the any harm to wealth. Although, the person will be recognized with dizziness or dementia or any situation that decreases the capacity of the person for making decision, this person will be banned from any ownership to the body. Furthermore, human authority on himself is limited up to wasting his life or making harm to an organ and no one is allowed to make harm to

himself, but some harms can be tolerated and can help others to live better for example blood donation or kidney donation. In such cases, this can be considered as sacrifice and is accepted (27).

C) Another proof that can be noted for the person's authority over himself in Islam, is the ability of the person to converts nemesis punishment to blood money.

Thus, altruism is appreciated and advised in Islam mostly in properties like food and drink. However, the "altruism" can be increased to the level of sacrifice for the Muslims. Therefore, a Muslim can donate an organ of his body for transplantation for saving another Muslim's life.

Together, if the reason of transplantation of an organ, tissue and cell is that these are person's properties, after cutting them off, they are still his properties and he can sell it as he likes; but, selling an organ is not acceptable if we believe that organs and cells are not one's properties, but he has the right to use them, and donate them for altruistic reasons.

The principle of innocence

The most Shia jurists believe that whenever after gathering justifications and juridical documents, there is still doubt in some actions, that action cannot be acceptable and should be avoided. Of course, when there are no valid reasons for religious scholars on permission or banning the usage of stem cells technologies, they approve it. It means that, although the jurist may not find a reason from the real juridical law and Islamic texts, due to necessity of the topic based on scientific documents, the statement is given in the absence of an existent cause for forbidding it, it becomes permissible (26).

The juridical view on accepting the stem cells technology

Changing the divine creation

Mainly, the jurists of Sunni point to changing the creation of GOD with the reference to Holy Quran Sura Nesa (4th) verses 117-119, which reminded that the devil will misguide people and instruct them to change God creations: "instruct them to change people" (28). In addition to this verse, in another source, it is said that: "do not change the people" (29). From both of these two verses, the changing God's creations is forbidden *(HARAM)* (24). By this argument, some Sunni clergy scholars state that many new technologies can be obvious proofs for changing the God's creation, so, it is forbidden (30).

In response to this argument, it can be said that first, the meaning of changing creation in the notable verse is shifting and distortion in the right religion and God's world not the absolute changing in creatures (31); second, the belief in this argument in general, prevents many normal actions that are allowed in Islam religion (32). So, there is no benefit in this argument for justification of biological or medical issues.

Human does not own his organs

Legislators believe that a person is not the absolute owner of his body and this body is just a god-given gift and every ownership in this gift needs the owner's permission and the person has the authority to use body parts except in some special cases. This reason is disputable from different aspects; first, the purpose of the absence of man ownership on his own body is not explicitly clear. If the meaning of this reason is to prevent commercial organ donation, it would be acceptable; but this meaning cannot be a respect for body parts; second, does "deposit and safekeeping of the body", have the same meaning as authority? If it is so, the body of no one is not a deposit for them. The last word is that the ownership of the body does not prohibit the safekeeping (24).

Argument of "No harm"

The rule of "no harm in Islam" declares that, there is no harmful law in Islam meaning that Islamic statements have only benefits. The harm is defined as "a defect in property and life" and the meaning of loss is "exacerbation, restriction, severity and difficulty". This argument is along with both ownership and gift argument and a person must not harm his body even if he is absolute owner of it (27).

Precaution rule

Precaution rule maybe is the reason for banning stem cell technology; it is justifiable that other reasons and religious proofs relevant to this issue, are not sufficient for this purpose. Precaution rule, also known as (practical rule), is the statement of the jurist or legislature about the necessity of considering all possible tasks in cases that the task could be trusted and in the source of the task but there are doubts about its application in the life (23). On this basis, a scholar should act in a way that he was sure about application of the task along with the source of it. This is opposite of legit rule that says the task is OK when there is nothing absolutely against it.

Discussion

The jurists by considering process of embryo growth and evolution, at least in the first three-month of pregnancy, study the rules that deny the personhood of "supernumerary" embryo before implantation in I.V.F clinics and they allowed using the unneeded embryos in stem cells research (5).

From Islamic jurisprudence point of view, there are three theories for the relationship between man and his organs and body cells: dominance and ownership relation, safekeeping and ownership; according to the meaning of dominion, it is clear that between the meaning of dominion and the meaning that is presented for the ownership, there is not a difference from the nature aspect, so it seems that using the ownership word is better for this relationship, because dominion is a result or a statement of possession commands (8). On the basis of ownership theory, also people are just changed to conservators of their own soul

and body and this order is against the freedom and person authority. Furthermore, we are allowed to take authority of our body parts in juridical limitations while a trustee does not have the ownership right, except for protection. Most jurists that expressed their opinion in this area regard the human relationship and his body as a kind of owning relation (19) that briefly includes originating ownership, credit and innate; according to the originating ownership while God is the owner of all the world, we also have a kind of originating ownership about organs and parts of body. But, the man does not have total authorization over his body; also, based on religious and juridical texts, causing injury and harm to the body is prohibited (16). About the credit possession of the person on body organ, it can be said that first, the basis and source of it is thinking because that does not have rational basis about the ownership on body organs is not proved or it is in doubt; second supposing that it is accepted, this kind of ownership faces many limitations making it "dominance and possession" (8). But, most of jurists agreed innate authority of human being on his own body. Intuitional approach and rational basis confirmed this kind of ownership and dominance, as the jurists and scholars confirmed it (8).

Most of Shia jurists believe in permission and legit. The main reference reason toward recognizing a task statement for applying these technologies is "legit rule" and the "legitimate law". Referring to these rules beside rejecting of forbidden reasons and responding to them, make permission and legit application for these technologies. The statement that relies on the "legitimate law" and "legit rule" in new topics in biomedical and biotechnological fields, are the first reasoning of Shia scholars leading to the permission. Regarding the person ownership over his body parts and cells, it can be said that being praised of sacrifice cannot be the reason of donation of cells or organs. Importantly, in typical affairs, the person has a right to prefer others right to oneself. So, a Muslim can separate a part of his body and gives it to save another Muslim's life. As a result, if the reason for justification of transplanting an organ, tissue and cell is that those body parts are donor's properties, after removing them, they are still his properties, and he can sell it in any way he likes; but if we don't consider body parts as properties, and he has only the right of using it, there is no right for selling body parts for money (31).

Reasons indicating the absence of permission and reverence of this technology include the changing reverence in God creation, the absence of human possession on his organs, referring to the profitable and harmless law and following the precaution rule. In response to the argument of change in divine creation, it was said that change in creation has been meant distortion in the divine religion and nature, and only it has been considered as absolute change (31). Second promise to this word in general and total is in conflict by many permission of actions that are allowed in Islamic religion (32). As a result, it cannot be used for confirming reverence and prohibition in this topic. Permission in taking authority is enough, even if it issued by the real owner. The evidence for this is that human being can naturally and continually make several changes in his body and organs by jurists' permission and none of these kinds of possession are illegal (24). Reasoning to the usage of stem cells technologies makes it acceptable, when it is performed carefully and safely. These technologies in special situations, maybe are harmful and dangerous for people life and society. The topic is a matter of discussion that even though from the point of view of others, do not contain in jurists tasks; however, seeking the religious statement relevant to the topic will be different by multidirectional cognition of that topic even by using the external knowledge of jurists. To sum up, causing harm to the body, is illegal and forbidden according to the scholars' point of view. Besides, statements about the need for prevention of harm in some juridical subdivisions are also referred by Shia juridical. Since it should be considered that the stem cells technologies maybe are not safe to use for human, can lead to prevent harm argument. Also, resort to precaution rule, it is advisable to calculate risk and benefit and consider safety of using these technologies before approving them although this consideration is not religious (23).

Conclusion

It can be concluded that as currently there are so many controversies about safety of these cells and possible dangers for human body, till getting new advances and clearness of risks and benefits, also discovering prevention ways with these dangers and securing the usage of these technologies, we should follow precaution rule.

As delay in accepting the stem cells technologies deprive human from potential treatments for incurable diseases, Islamic scholars and governments should assess risks and benefits of stem cells researches to approve them. On the basis of Islamic values related to the moral status of embryo, and according to the superior moral, cultural and religious values of the Islamic society of Iran accepted the action towards development of these researches. Iran juridical system should, according to notions of intellectual jurists and legislators, Islam and Shia religious, conduct and restrict actions in the area of stem cells technology by gathering experts of different political, science, medicine, social and mindful who are familiar with law, philosophy and divinity, also express the existence challenges and exit methods, and try to pass codes and design guidelines to fill legal and ethical gaps.

Acknowledgements

There is no financial support and conflict of interest in this study.

Authors' Contributions

A.P.; Participated in study design, data collection and evaluation, drafting. A.R.; Contributed to analysis, participated in study design. I.G; Were responsible for overall supervision, contributed extensively in

interpretation of the data and the conclusion. All authors read and approved the final manuscript.

References

1. Goldozian I, PourEbrahim A. Third Conference on Cellular and Molecular Freshness, and the First International Symposium on Genomics and Proteomics; Univercity Azad Islamic Ardebil. 2017.
2. Goldozian I, PourEbrahim A. International Law Congress of Iran with the Citizenship Rights Approach; Tehran; 2017.
3. Baharvand H, Kazemi Ashtiani S. Embryonic stem cells: concepts and potentials. Quarterly Journal of Clinical Medicine. 2004; 7(4:) 177-178.
4. Royan Stem Cell technology Company participates in the 2nd Symposium on Skin Heal, Stem Cells and Regenerative Medicine. Available from: http://www.rsct.ir/benefits-stem-cells.
5. Sashadina A. Islamic views on ethics in stem cell research. Medical Law Quarterly. 2007; 1(2): 55-84.
6. Ibn Abidin M. Durr al-Mukhtar and Hahaythah. Beirut: Dar Al Fikr; 1992; 591.
7. Mahmoudian H, Pak Nit Jahromi B, Sadeghpour N, Nabi'I P. A review of the ethical and legal considerations of embryonic stem cell research. Journal of Biomedical Ethics. 2016; 5(18): 69-101.
8. Rahmani Menshadi H, Abbasi M, Jelodari Bardastan D. Comparative study of human relations with laboratories and tissues. Medical Law Quarterly. 2014; 8(30): 65-98.
9. Makarem Shirazi N. Resale of tozih Al-Masaleel. Qom: Purpose; 1998.
10. Goldozian I, PourEbrahim A. Trafficking in human beings with an approach to internal rights and international documents. 1st ed. Tehran: Khorsandi; 2016.
11. Quran. 17: 70.
12. Moosavi Khomeini R. Translation of the tahrir al-vasileh. Tehran: The Institute for the Setting up and Publishing of Imam Khomeini Works; 2006; 661.
13. Rajaee F, Mohaghegh Damad SM, Mousavi SM. Islamic jurisprudence and Right. 2011; 1(2):45-62 .
14. Shahid Thani Z. Al-Rousha Al-Behayee Fei Al-Lama'a Al- Damascus. Qom: Davoudi; 1989; 196.
15. Albar MA. Al-Mukhouf al-Fegh'hi and the moral of the organ transplantation. Damascus: Dar Al-Shamieh; 1994; 187.
16. Asghari Aghmashhadi F, Kazemi Afshar. How to connect human beings with their organs from the point of view of jurisprudence and law. Islamic Jurisprudence and Right Studies. 2009; 1(1): 33-45.
17. Bojnourdi SH. Al-Qawaed Al-Faghih. 1st ed. al-Hadi; 1998; 242.
18. Javadi Amoli A. The right in Islam. Center for the Publishing of the esra; 2007; 96.
19. Jurisprudence Research Center of the Judiciary. Informing the jurisprudential views (2). Organ transplantation. Serie C. in an effort: Aziz Feyzi Talib. Qom: The Judicial Research Center of the Imam Khomeini Judiciary; 1999; 13-53.
20. Tabatabaei SM. Al-Mizan commentary. Islamiyah; 1990; 35.
21. Mohseni MA. Al-Fiqah and Al-Masale Al-Tabaye. 1st ed. Qom; 1999; 217.
22. Mu'men Qumi M. Al-Sadeedeh Fi-Massael-e-Jadideh. Qom: Al-Nashr al-Islami Institute; 1994; 178.
23. Welaeei I. An exploratory dictionary of terms principles. 4th ed. Tehran: Ney; 2005; 72-73.
24. RahbarPour MR. The juridical foundations of prohibition and criminalization in the domain of bioethics. Islamic Law: 42(11); 2015; 41-59.
25. Majlesi MB. Baharalanvar. Dar al-Kabul Islamiyah. 272.
26. Quran. 2: 207.
27. Mousavi Bojnourdi SM. Evaluation of organ transplantation using stem cells with an approach to Imam Khomeini's viewpoint. Matin Research. 23-36: 14(56); 2012.
28. Quran. 4: 119.
29. Quran. 30: 30.
30. Al-Ash'ghar MS. Ijtihad research in medical Jurisprudence. Beirut: Alrsaleh Institute; 2001; 23.
31. Ayyashi Samarqandi, MBM. Al-Ayyashi's commentary. Tehran: Almiyah Islamiyah; 1976; 276.
32. Nazari Tavakoli S. Organ transplantation in Islamic jurisprudence. Mashhad: Islamic Research Foundation of Astan Quds Razavi; 2002.

Case Report

A Homozygous 1.16 Megabases Microdeletion at 8p22 Including The Whole *TUSC3* in A Three Years Old Girl with Intellectual Disability and Speech Delay

Evren Gumus, M.D.[1, 2*]

1. Department of Medical Genetics, Faculty of Medicine, University of Harran, Sanliurfa, Turkey
2. Department of Medical Genetics, Faculty of Medicine, University of Mugla Sitki Kocman, Mugla, Turkey

**Corresponding Address: Department of Medical Genetics, Faculty of Medicine, University of Harran, Sanliurfa, Turkey*
Email: evreng@harran.edu.tr

Received: 11/December/2018, Accepted: 23/February/2019

Abstract

Intellectual disability (ID) is defined as an intelligence quotient (IQ) level below than 70. In the present paper, a 1.16 megabases (Mb) homozygous deletion in the 8p22 region was identified in a three years old girl with ID, speech and developmental delays. This is the first report from Turkey with this form of ID. The present paper demonstrates that application of microarray technique to help clinicians, especially when clinical diagnosis includes a complex group of disorders (such as ID) and differential diagnostic list is broad.

Keywords: Deletion, Intellectual Disability, Microarray, *TUSC3*

Cell Journal(Yakhteh), Vol 22, No 1, April-June (Spring) 2020, Pages: 128-132

Citation: **Gumus E. A homozygous 1.16 megabases microdeletion at 8p22 including the whole TUSC3 in a three years old girl with intellectual disability and speech delay. Cell J. 2020; 22(1): 128-132. doi: 10.22074/cellj.2020.6606.**

Introduction

Intellectual disability (ID) is an important indicator in the differential diagnosis of genetic diseases. ID comprises two types: syndromic ID (S-ID) and nonsyndromic ID (NS-ID). In S-ID, individuals show one/variousmajor dysmorphic finding(s) or co-morbidities in addition to ID. In NS-ID, an isolated ID is observed. However, it is not always possible to make a clear distinction between these two forms (1)also referred to as mental retardation (MR. According to the inheritance pattern, it is possible to distinguish NS-ID into three main groups: non-syndromic X-linked ID (NS-XLID), non-syndromic autosomal dominant ID (NS-ADID) and non-syndromic autosomal recessive ID (NS-ARID). Regarding NS-ARID, up to 2004, four genes had been identified and up to 2011 they extended to eight genes. Currently, about 40 genes have been recognized corresponding to this group of abnormalities. One of these genes is the Tumor Suppressor Candidate 3 (*TUSC3*) gene. *TUSC3* plays a key role in the N-linked glycosylation process, which is located at the p arm of chromosome 8, containing 11 exons and it is approximately 0.22 megabase (Mb) length. The *TUSC3* gene-associated NS-ARID has been described to date in less than 10 families and less than 30 patients (2-4).

Case Report

The study was performed in accordance with the Declaration of Helsinki 2013, the principles of Good Clinical Practice and Local Ethic Regulation (code: 28617). Informed consent was obtained for genetic analysis of the patient, the publication of patient data and photos.

A three years old child born to healthy 21-years-old mother and 23-years-old father with Turkish origin. The parents are first degree cousins (Fig.1A). Her birth weight was 2950 g (10-25 percentile) and birth length was 49 cm (25-50 percentile). Occipitofrontal circumference (OFC) at birth was not recorded. The patient was referred to our department with intellectual disability, developmental delay, speech delay and minor dysmorphic features. On the examination, her weight, length and OFC is respectively 11.7 kg (3-10 percentile), 96 cm (50-75 percentile) and 47 cm (10-25 percentile). She sat at 22 months, while she is not yet able to walk independently and her speech skills had not been developed. Minor dysmorphic features, such as epicanthus, broad nasal base and thin upper lipare were noted (Fig.1B, C). The creatine kinase level of the patient was 98 U/L (N: 22-198 U/L). Copy number variation of *SMN1*gene is normal. ID was estimated as severe to profound.

Electroencephalography (EEG), electromyography (EMG) and brain magnetic resonance imaging (MRI) were normal. Ophthalmological examination revealed strabismus. Conventional karyotype analysis shows normal female: 46, XX. Chromosomal microarray studies were performed with the Affymetrix CytoScan Optima (315k; Thermo Fisher Scientific, USA) chips from the DNA obtained from her peripheral blood. All data were analyzed in the ChAS 3.1 program (Thermo Fisher Scientific). Microarray result showed a 1.16 Mb homozygous deletion, namely arr[hg19] 8p22(14,701,241-15,869,703)x0. This region contains the whole *TUSC3*, *miR-383* and a portion of the sarcoglycan, zeta (*SGCZ*) gene (Fig.2). Genetic analysis of her mother and father showed arr[hg19] 8p22 (14,701,241-15,869,703) x1, indicating both parents are heterozygous for this deletion.

For confirmation of this deletion in the index patient, fluorescence in situ hybridization (FISH) analysis was performed with the locus specific probe RP11-165A17 (Empire Genomics LLC, USA), mapping to 8p22, and for the control Vysis CEP 8 (D8Z2) Spectrum Green Probe (Abbott Molecular, USA) (Fig.3). These findings also validated the heterozygous deletion in the individual parents. No similar deletion was observed in any healthy woman or man originated from the local population (Fig.4).

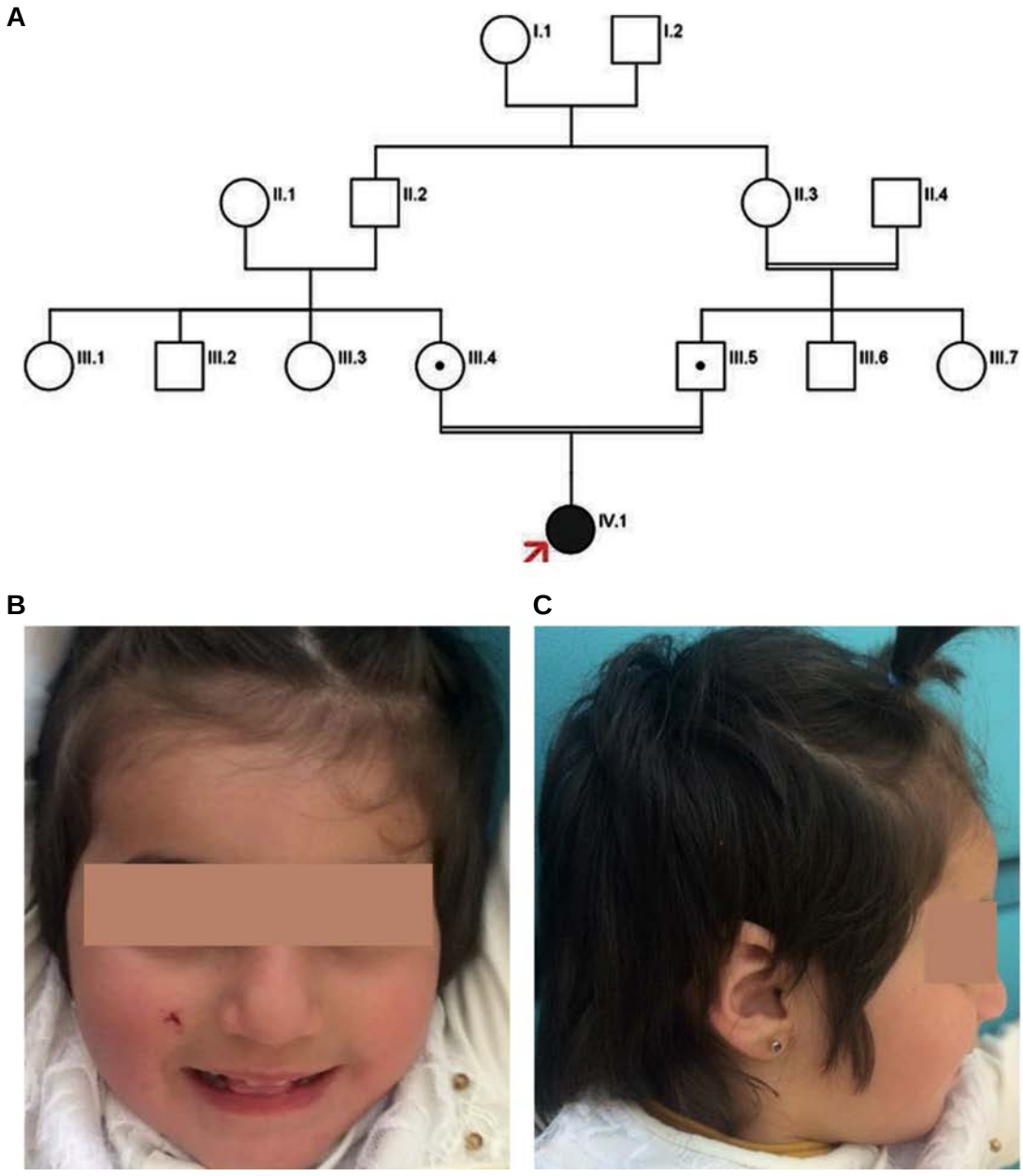

Fig.1: The patient's pedigree and observed dysmorphic features are indicated. **A.** The pedigree, **B,** and **C.** Front and lateral views of the patient at age 2 years and 8 months shows epicanthus, broad nasal base and thin upper lip.

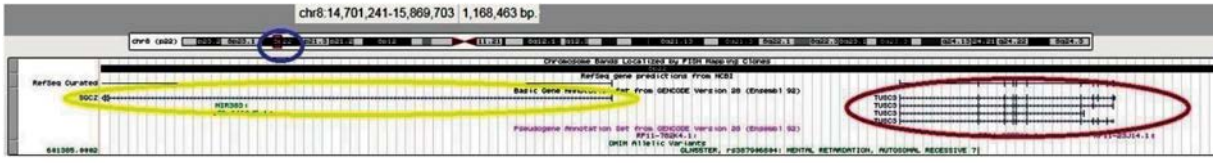

Fig.2: Homozygous deletion of 8p22 region, composed of the whole *TUSC3*, *miR-383* and a portion of *SGCZ* gene (Adapted from *UCSC* Genome Browser).

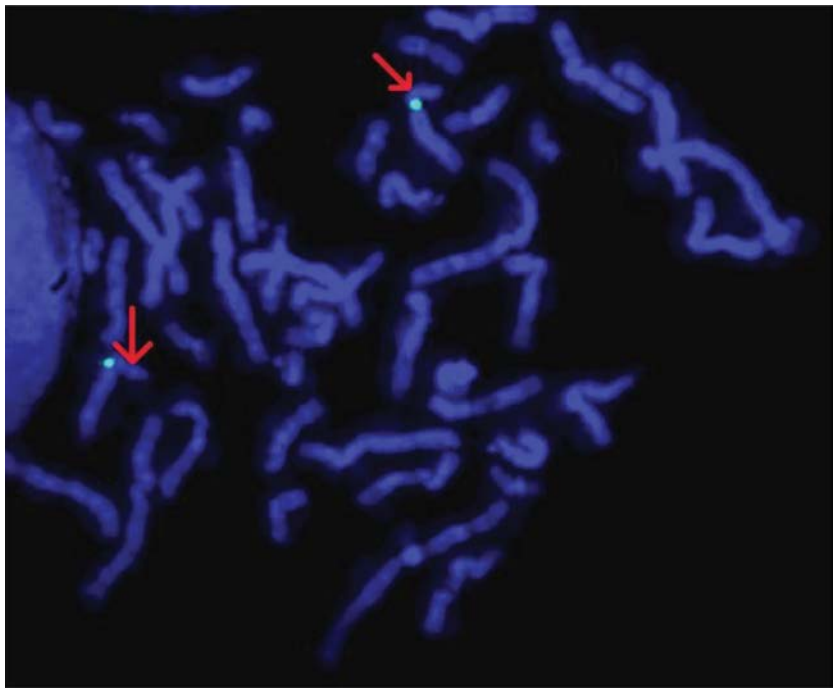

Fig.3: FISH technique analysis was performed by the locus specific probe RP11-165A17, designing to 8p22 and demonstrating no signal (red arrows). A specific probe for the centromeric region of chromosome 8 was utilized as control (green signals).

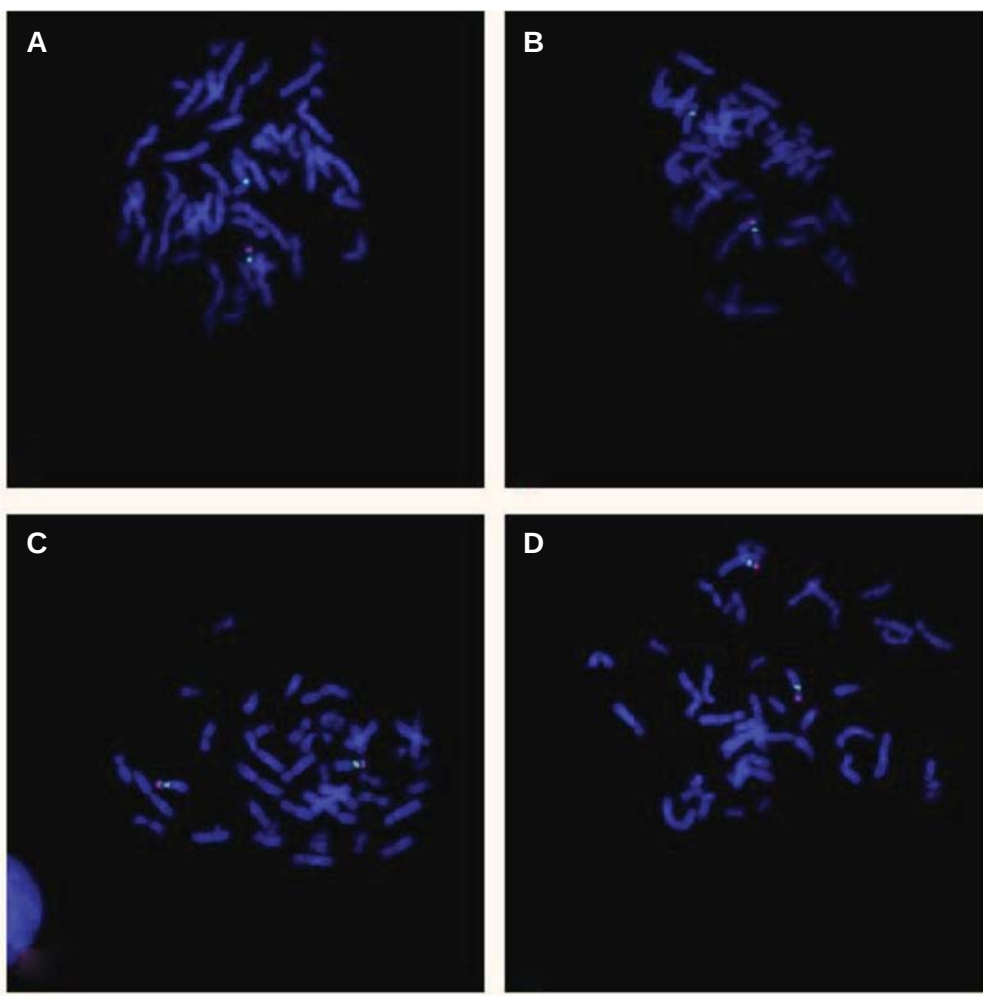

Fig.4: FISH technique analysis was performed with the locus specific probe RP11-165A17, designing to 8p22 (red signals), and a specific probe for the centromeric region of chromosome 8 was utilized as control (green signals). **A.** Mother, **B.** Father, **C.** Healthy woman, and **D.** Healthy man.

Discussion

In the present paper, a 1.16 Mb homozygous deletion within the 8p22 region was identified in a three years old girl with ID, speech and developmental delays. This is the first report from Turkey, presenting this form of ID.

microRNAs are small (containing about 22 nucleotides) and extremely preserved non-coding RNA molecules involved in the arrangement of gene expression (5). There is no evidence that *miR-383* plays role in neurodevelopmental processes, but it has been shown to play a role in the etiopathogenesis of ovarian, stomach, colon, prostate and thyroid cancers (6). No malignancy was identified by Piovani et al. (4) in the patient with an 8p22 deletion including *TUSC3*, *SGCZ* and *miR-383* regions. Although at the time of assessment, there is no evidence of malignancy in our patient, we recommend that this case should be followed-up in later stages of her life. Since this effect is only observed in the homozygous case, other family members do not need to be included in the follow-up program (2).

Mutations in β, γ, δ and α sarcoglycans have been associated with limb-girdle muscular dystrophy, myoclonic dystonia and dilated cardiomyopathy, but no phenotype relation has yet been reported for *SGCZ* (7) in a proportion of cases, by mutations of the maternally imprinted epsilon-sarcoglycan gene (SGCE. This has also been implicated by Piovani et al. (4).

The present paper is the first case with deletion of whole *TUSC3* gene. Mouse studies have shown that Tusc3 protein is related to synaptic plasticity, learning continuum and memory (8, 9). There are publications reporting that this interaction is performed via magnesium membrane transport system (10). Reduction of TUSC3 functional expression in zebrafish embryos results in the early developmental arrest (9). The underlying mechanism of ID associated with the *TUSC3* is mainly attributed to this phenomenon. While low TUSC3 protein expression levels are observed in the adult brain, high expression levels are detected in the fetal brain and cerebellum (2). This effect is manifested by ID and developmental delay, observing at an early age. Copy number and single nucleotide variations in the *TUSC3* have been associated with the autosomal recessive syndromic or non-syndromic ID. Previous clinical studies have presented moderate to severe ID, as a common feature in all of these patients. Additionally, speech problems, minor dysmorphic features and developmental delay was also observed in most of these patients (Table 1). Congenital anomalies, including syndactyly and undescended testis, were also found in less than five patients. Similar to our patient, no congenital anomaly was observed in the other patients (3, 4, 8, 11, 12). Although many of these patients are non-syndromic, presence of the syndromic features in a few patients is an indication that this distinction is not certain in autosomal recessive ID.

Conclusion

Current paper indicate the extensive implementation of microarray technique to assist clinicians, particularly in the case of complex disease groups and wide list of differential diagnosis.

Table 1: Major clinical features of the previously reported patients and the present case

Findings	Garshasbi et al. (8)	Loddo et al. (3)	El Chehadeh et al. (11)	Piovani et al. (4)	Al-Amri et al. (12)	Present case
Number of patients	7	1	2	1	4	1
Intellectual disability	+	+	+	+	+	+
Speech delay	+	+	+	+	+	+
Microcephaly	1/7	-	-	NA	3/4	-
Consanguinity	Yes	No	Yes	No	Yes	Yes
Height (length)	NA	50p	50p	50p	3-10p	50-75p
Weight	NA	25-50p	50p	50p	3-50p	3-10p
Sat with no support	NA	18 M	15 M	Delayed	NA	22 M
Independent walking	NA	2 Y	2 Y	Delayed	19 M	Not yet
Speech	NA	Delayed	Delayed	Delayed	Delayed	No speech

NA; Not available, M; Month, Y; Year, and P; Percentile.

Acknowledgements

We cordially thank parents contributing in this study. I would like to thank Dr. Zafer Yuksel, M.D. for his contribution and critical review. The author declare no conflicting interest in this work. No fund was received on this experiment.

Authors' Contributions

All design and evaluations were made by E.G.

References

1. Kaufman L, Ayub M, Vincent JB. The genetic basis of non-syndromic intellectual disability: a review. J Neurodev Disord. 2010;2(4): 182-209.
2. Vašíčková K, Horak P, Vaňhara P. TUSC3: the functional duality of a cancer gene. Cell Mol Life Sci. 2018;75(5):849-857.
3. Loddo S, Parisi V, Doccini V, Filippi T, Bernardini L, Brovedani P, et al. Homozygous deletion in TUSC3 causing syndromic intellectual disability: a new patient. Am J Med Genet A. 2013;161A(8):2084-2087.
4. Piovani G, Savio G, Traversa M, Pilotta A, De Petro G, Barlati S, et al. De novo 1Mb interstitial deletion of 8p22 in a patient with slight mental retardation and speech delay. Mol Cytogenet. 2014; 7:25.
5. Perron MP, Provost P. Protein interactions and complexes in human microRNA biogenesis and function. Front Biosci. 2008;13: 2537-2547.
6. Cui Y, Chen LG, Yao HB, Zhang J, Ding KF. Upregulation of microRNA-383 inhibits the proliferation, migration and invasion of colon cancer cells. Oncol Lett. 2018;15(1):1184-1190.
7. Peall KJ, Ritz K, Waite AJ, Groen JL, Morris HR, Baas F, et al. SGCZ mutations are unlikely to be associated with myoclonus dystonia. Neuroscience. 2014;272: 88-91.
8. Garshasbi M, Hadavi V, Habibi H, Kahrizi K, Kariminejad R, Behjati F, et al. A defect in the TUSC3 gene is associated with autosomal recessive mental retardation. Am J Hum Genet. 2008;82(5): 1158-1164.
9. Yu X, Zhai C, Fan Y, Zhang J, Liang N, Liu F, et al. TUSC3: a novel tumour suppressor gene and its functional implications. J Cell Mol Med. 2017;21(9): 1711-1718.
10. Zhou H, Clapham DE. Mammalian MagT1 and TUSC3 are required for cellular magnesium uptake and vertebrate embryonic development. Proc Natl Acad Sci USA. 2009;106(37): 15750-15755.
11. El Chehadeh S, Bonnet C, Callier P, Béri M, Dupré T, Payet M, et al. Homozygous truncating intragenic duplication in TUSC3 responsible for rare autosomal recessive nonsyndromic intellectual disability with no clinical or biochemical metabolic markers. JIMD Rep. 2015;20: 45-55.
12. Al-Amri A, Saegh AA, Al-Mamari W, El-Asrag ME, Ivorra JL, Cardno AG, et al. Homozygous single base deletion in TUSC3 causes intellectual disability with developmental delay in an Omani family. Am J Med Genet Part A. 2016;170(7): 1826-1831.